DESIGN AND SYNTHESIS OF NOVEL CHIRAL DIRHODIUM(II) CARBOXYLATE COMPLEXES FOR ASYMMETRIC CYCLOPROPANATION REACTIONS

FRADY GAMAL ADLY GOUANY

B.Sc. (Hons.), M.Sc.

A thesis submitted in fulfilment of the requirements for the degree of

DOCTOR OF PHILOSOPHY

(APPLIED SCIENCE)

UNIVERSITY OF CANBERRA

Australian Capital Territory, Australia

May 2015

“THE GOD OF HEAVEN WILL PROSPER US THEREFORE WE, HIS SERVANTS, WILL ARISE AND BUILD” (Nehemiah 2:20)

"إِلهَ السَّمَاءِ يُعْطِينَا النَّجَاحَ، وَنَحْنُ عَبِيدُهُ نَقُومُ وَنَبْنِي"

(نحميا 2: 20)

FORM B: CERTIFICATE OF AUTHORSHIP OF THESIS

Except where clearly acknowledged in footnotes, quotations and bibliography, I certify that I am the sole author of the thesis submitted today entitled:

"DESIGN AND SYNTHESIS OF NOVEL CHIRAL DIRHODIUM(II) CARBOXYLATE COMPLEXES FOR ASYMMETRIC CYCLOPROPANATION REACTIONS"

I further certify that, to the best of my knowledge, the thesis contains no material previously published or written by another person except where due reference is made in the text of the thesis.

The material in the thesis has not been the basis of an award of any other degree or diploma except where due reference is made in the text of the thesis. The thesis complies with University requirements for a thesis as set out in *Higher Degree by Research Examination Policy, Schedule Two (S2).* Refer to http://www.canberra.edu.au/research/hdr-policy-and-procedures.

Signature of the candidate

Signature of the supervisory panel

Date

12 May 2015

ACKNOWLEDGMENTS

First and foremost, I would like to thank my Lord and Master, *Jesus Christ*, for giving me the strength, power, support, wisdom and finally success throughout my Ph.D. trip. It has been one of the toughest challenges of my life and I am entirely sure I would have never been able to pass through without him. Thanks for being always there for me.

Next, I want to express my sincere gratitude to all my supervisory panel members and to thank them for giving me the opportunity to research under their guidance and supervision.

First, I would like to thank my primary advisor, *A/Prof. Dr. Ashraf Ghanem*, for letting me experience and being the gateway to get into the field of asymmetric catalysis research. I am really so grateful for putting me on such high quality research track. Dr. Ghanem's comments and criticism at all different stages of my research were though provoking and helped me improving my research. I also would like to thank him for using his precious time to read my thesis and giving his valuable suggestions and comments. Dr. Ghanem's suggestions regarding each version greatly helped in improving the thesis more and more.

Further, I would like to express my sincere gratitude to *Prof. Dr. Bill Maher* for believing in me and for the so many discussions and advices. I admire very much his efficient way of giving feedback, along with his endless encouragement and support. Without his continuous support, I would not have reached this stage of my thesis. Further, I would like to thank him for using his precious time to carefully read this thesis and for his valuable suggestions and comments.

I am also so grateful to *A/Prof. Dr. Michael Gardiner* from the University of Tasmania for his contribution in this work. Dr. Gardiner assisted in X-ray crystal structure determination of some of the prepared dirhodium(II) complexes. Dr. Gardiner's efforts were so important for the successful realization of this research and so to this thesis.

I would like to extend my thankfulness to the *University of Canberra* for offering the W. J. Weeden postgraduate research scholarship for pursuing my Ph.D. research. I

must confess that I have gained an extraordinary life experience studying at this university.

Special thanks must go to my senior colleagues, *Dr. Vijaybabu Madadapu* and *Dr. Marwa Ahmed*, for their continuous support and encouragement. It has been really a great fortune to be able to go through this postgraduate experience with both of you guys. Also, I have been blessed with a friendly and cheerful group of fellow students; *Robert Healey*, *Johncarlo Maddalena*, *Nana Antwi*, *Tamotsu Kanazawa*, *Haysem Alhassen* and *Marina Gawargi*. I would like to thank them for their care, friendship and for the overall laboratory atmosphere. I really wish them all the best in their future postgraduate studies.

Sincere thanks are also due to the Australian Synchrotron scientists for the given access to the MX1 and MX2 beamlines. Getting regular access to such a facility contributed to considerable extent in the success of the current project.

I would like to thank *Chris Blake* and *Peta Simmonds* from the NMR department, Australian National University (ANU). My research could not have been performed without their really valuable assistance and support.

I would like to thank my friend, *Ahmed Magdy*, who has always been excellent in expediting my MS samples when I have requested it. I really wish him all the best in completing his current study.

I would like to thank *Dr. Tony Willis*, ANU, for obtaining the X-ray crystal structures for some cyclopropane products reported in this thesis.

I would like to express a special acknowledgment to *A/Prof. Dr. Simon Foster* for his generous assistance. Dr. Foster was always willing to help and he already did a lot, especially, in getting the ICP-MS analysis done.

Once again, I would like to thank all of them for their assistance as performing experiments is not of much use if you cannot get data out of it.

Above all, I am forever indebted to my small family for all the feelings, support and encouragement they have given to me. My dear wife, *Mona Beshai*, who supported me through all the years of this work with her continuous love, patience and understanding regardless of my mood. My little hero, *Philopateer Gouany*, whose

smile was like a magic wand that introduced a lot of happiness into my life when I needed it.

No words can also express my gratitude for my bigger family overseas. My father, *Mr. Gamal Gouany*, who departed without experiencing the joy seeing me graduating with a Ph.D. degree. This thesis is dedicated to him to express how much I am grateful for being a life time supporter. My mother and my two younger brothers whose support has been always unconditional. I am quite sure that without the support I received from both my small and big families, I wouldn't be who or where I am today. Thanks for believing in me.

Last but not least, I would like to thank everybody who was important to the success of this thesis. I also apologize to anyone who was not mentioned personally here. Thank you.

The Author

Frady G. A. Gouany

This dissertation is dedicated to my Father, Mr. Gamal Gouany

CITATIONS

PUBLICATIONS

1. Frady G. Adly and Ashraf Ghanem, Chiral Dirhodium(II) Carboxylates and Carboxamidates as Effective Chemzymes in Asymmetric Synthesis of Three Membered Carbocycles, *Chirality*, 26(11), **2014**, 692-711.
2. Frady G. Adly, Johncarlo Maddalena and Ashraf Ghanem, Rh_2(*S*-1,2-NTTL)$_4$: A Novel Rh_2(*S*-PTTL)$_4$ Analogue with Reduced Ligand Symmetry for Asymmetric Synthesis of Chiral Cyclopropylphosphonates, 26(11), *Chirality*, **2014**, 764-774.
3. Moteaa El-Deftar, Frady G. Adly, Michael G. Gardiner and Ashraf Ghanem, Chiral Dirhodium Catalysts: A New Era for Asymmetric Catalysis, *Curr. Org. Chem.*, 16(15), **2012**, 1808-1836.
4. Frady G. Adly and Ashraf Ghanem (in preparation for submission).
5. Frady G. Adly, Michael Gardiner and Ashraf Ghanem (in preparation for submission).

CONFERENCE PRESENTATIONS

1. POSTER: F. G. Adly, Michael Gardiner, A. Ghanem; Novel chiral dirhodium(II) complexes for highly enantioselective cyclopropanations: Design, synthesis and crystal structure; Chirality Conference, **2015**, *Boston, USA.*
2. POSTER: F. G. Adly, A. Ghanem; Rh_2(*S*-1,2-NTTL)$_4$: A new chiral dirhodium(II) carboxylate catalyst for asymmetric synthesis of chiral cyclopropylphosphonates; Chirality Conference, **2015**, *Boston, USA.*
3. POSTER: F. G. Adly, A. Ghanem; Polymer monolith-supported dirhodium(II)-catalyzed asymmetric cyclopropanations in capillary format; Chirality Conference, **2015**, *Boston, USA.*
4. POSTER: F. G. Adly and A. Ghanem; Rh_2(*S*-1,2-NTTL)$_4$: A novel Rh_2(*S*-PTTL)$_4$ analogue with lower ligand symmetry for asymmetric synthesis of

chiral cyclopropylphosphonates; 15th Tetrahedron Symposium - Asia Edition, **2014**, *Singapore*.

5. POSTER: F. G. Adly and A. Ghanem; New dirhodium(II) carboxylate catalysts derived from imides of amino acids with asymmetric *N*-protecting groups for asymmetric synthesis of chiral cyclopropylphosphonates; Chirality Conference, **2014**, *Prague, Czech Republic*.

6. POSTER: F. G. Adly and A. Ghanem; Chiral chromatographic evaluation of the enantiomeric purity of *N*-1,2-naphthaloyl amino acids as ligands for the enantioselective access to cyclopropane derivatives; R&D Topics Conference, **2013**, *ANU, Canberra, Australia.*

ABSTRACT

A novel approach for the design of dirhodium(II) tetracarboxylates derived from (*S*)-amino acid ligands is outlined. The new approach is founded on modifying the catalyst sterics through reducing the symmetry of the ligand's *N*-heterocyclic tether. Investigations towards the new approach led to the preparation of Rh_2(*S*-1,2-NTTL)$_4$ and analogues, Rh_2(*S*-1-Ph-BPTTL)$_4$, Rh_2(*S*-^{tert}PTTL)$_4$, Rh_2(*S*-BHTL)$_4$, Rh_2(*S*-BOTL)$_4$ and Rh_2(β-D-TAGA)$_4$. The screening of the new complexes led to the uncovering of Rh_2(*S*-^{tert}PTTL)$_4$ as a new member to the dirhodium(II) complexes family with an extraordinary selectivity. The stereoselectivity of Rh_2(*S*-^{tert}PTTL)$_4$ was found to be comparable to Rh_2(*S*-PTAD)$_4$ (up to >99% *ee*), while being much more synthetically accessible catalyst. X-ray structure-based correlations justifying the observed enantioinduction enhancement are also discussed.

The process of preparation and characterization of a Rh_2(*S*-^{tert}PTTL)$_4$-catalyzed cyclopropanation capillary microreactor is also presented. The continuous flow Rh_2(*S*-^{tert}PTTL)$_4$-catalyzed cyclopropanation microreaction is carried out to generate the cyclopropane product in moderate yield (44%) and excellent diastereoselectivity (>20:1 *E*:*Z* dr). The microreaction enantioselectivity, however, did not exceed 10% *ee*.

Finally, the results are concluded and an outlook regarding the current field of research is outlined highlighting potential investigations that might be necessary for future development.

KEYWORDS: Chiral catalysis, Asymmetric synthesis, Cyclopropanation, Rh_2(*S*-NTTL)$_4$, Rh_2(*S*-PTTL)$_4$, Rh_2(*S*-^{tert}PTTL)$_4$, Carbenoids, Paddlewheel complexes, Dirhodium.

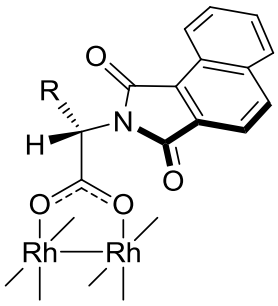

Rh_2(*S*-1,2-NTTL)$_4$, R = *t*-Bu
Rh_2(*S*-1,2-NTPA)$_4$, R = Bn
Rh_2(*S*-1,2-NTLU)$_4$, R = *i*-Bu
Rh_2(*S*-1,2-NTTR)$_4$, R = (3-Indolyl)methyl
Rh_2(*S*-1,2-NTTY)$_4$, R = *p*-Hydroxybenzyl

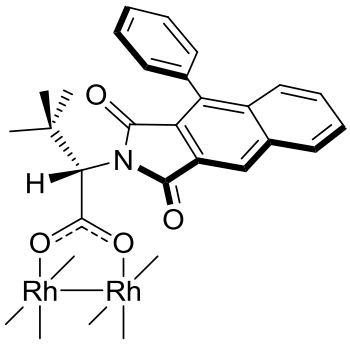

Rh_2(*S*-1-Ph-BPTTL)$_4$

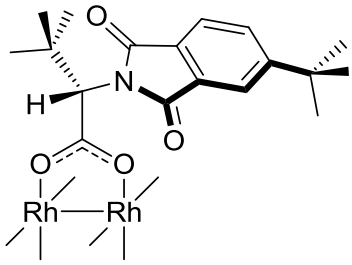

Rh_2(*S*-^{tert}PTTL)$_4$

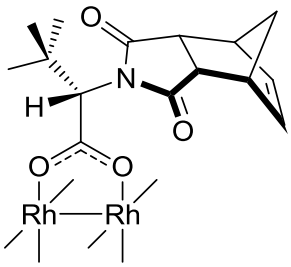

Rh_2(*S*-BHTL)$_4$

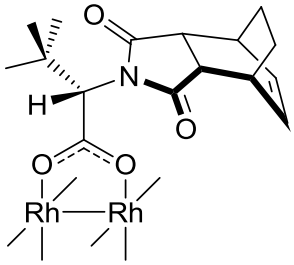

Rh_2(*S*-BOTL)$_4$

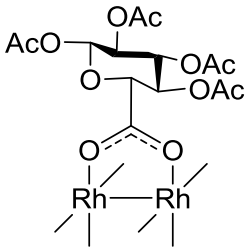

Rh_2(β-D-TAGA)$_4$

*All new dirhodium(II) complexes have been patented by the University of Canberra (*DIRHODIUM COMPOUNDS AND METHODS OF USE*, Provisional Patent AU2014903620, 2014).

TABLE OF CONTENTS

FORM B: CERTIFICATE OF AUTHORSHIP OF THESIS i

ACKNOWLEDGMENTS iii

CITATIONS ix

ABSTRACT xi

TABLE OF CONTENTS xiii

TABLE OF FIGURES xvii

TABLE OF SCHEMES xxv

TABLE OF TABLES xxix

ABBREVIATIONS xxxiii

CHAPTER 1: CHIRAL DIRHODIUM(II) CARBOXYLATES AND CARBOXAMIDATES AS EFFECTIVE CHEMZYMES IN ASYMMETRIC SYNTHESIS OF CYCLOPROPANE DERIVATIVES 1

1.1. INTRODUCTION 1

1.2. HISTORY 1

1.3. DIRHODIUM(II)-CATALYZED CYCLOPROPANATION REACTIONS 3

1.3.1. Types of carbenoid intermediates 6

1.3.2. Modes of interaction between the rhodium complex and the carbene 8

1.3.3. Approach of the alkene 10

1.4. MODIFICATIONS IN THE DIRHODIUM(II) FRAMEWORK 11

1.4.1. Electronic modifications 11

1.4.2. Steric modifications 13

1.5. DIRHODIUM(II) CARBOXYLATES 14

1.5.1. Conformations in dirhodium(II) carboxylate complexes 14

1.5.2. Dirhodium(II) catalysts derived from prolinate ligands 15

1.5.3. Dirhodium(II) catalysts derived from chiral *N*-protected amino acid ligands 25

1.5.3.1. Homoleptic complexes 25

1.5.3.2. Heteroleptic complexes 43

1.5.4. Dirhodium(II) catalysts derived from substituted cyclopropanecarboxylate ligands 46

1.6. DIRHODIUM(II) CARBOXAMIDATES 49

1.6.1. Homoleptic complexes 49

1.6.2. Heteroleptic complexes 65

1.7. EFFECT OF AXIAL LIGANDS ON ENANTIOSELECTIVITY 69

1.8. CONCLUSION AND AIM OF WORK 72

1.9. REFERENCES 76

CHAPTER 2: DESIGN AND SYNTHESIS OF NOVEL CHIRAL DIRHODIUM(II) CARBOXYLATES FOR APPLICATION IN ASYMMETRIC INTERMOLECULAR CYCLOPROPANATION REACTIONS 91

2.1. INTRODUCTION 91

2.2. RESULTS AND DISCUSSION 95

2.2.1. Preparation of chiral dirhodium(II) carboxylate complexes 95

2.2.1.1. Synthesis of chiral carboxylate ligands 95

2.2.1.2. Synthesis of dirhodium(II) carboxylate complexes 109

2.2.2. Screening for asymmetric cyclopropanation with *donor-acceptor* substrates 111

2.2.2.1. Enantioselective synthesis of chiral cyclopropylphosphonate derivatives . 111

2.2.2.2. Hypothetical model for the observed asymmetric induction 118

2.2.3. Screening for asymmetric cyclopropanation with *diacceptor* substrates 124

2.3. RE-EVALUATION OF CONCEPT AND PREPARATION OF MORE DIRHODIUM(II) CATALYSTS WITH LOWER SYMMETRY *N*-PROTECTING GROUPS 128

2.3.1. Screening in enantioselective synthesis of phosphonate-substituted cyclopropanes 135

2.3.1.1. Scope of catalysts with respect to the olefin 139

2.3.1.2. Effect of phosphonate ester group size on the enantioselectivity of catalysts142

2.3.2. Single crystal X-ray diffraction analysis 144

2.3.3. Screening in enantioselective synthesis of trifluoromethyl-substituted cyclopropanes 154

2.3.4. Screening in enantioselective synthesis of carboxylate-substituted cyclopropanes 156

2.3.4.1. Using methyl *α*-diazo-*p*-methoxyphenyldiazoacetate and styrene 156

2.3.4.2. Using methyl *α*-diazo-2-phenylacetate and styrene 160

2.3.4.3. Using (*E*)-methyl *α*-diazo-4-phenylbut-3-enoate and styrene 163

2.3.5. Screening in enantioselective synthesis of nitrile-substituted cyclopropanes 166

2.3.6. Screening in enantioselective synthesis of sulfonate-substituted cyclopropanes 169

2.4. PRELIMINARY RESULTS FOR A SECOND GENERATION CATALYST WITH LIGANDS CARRYING LOWER SYMMETRY *N*-PROTECTING GROUPS WITH BULKIER SUBSTITUENTS 170

2.4.1. Endeavours for the preparation of *N*-(4-adamantylphthaloyl)-(*S*)-*tert*-leucine170

2.5. OTHER INVESTIGATED DIRHODIUM(II) COMPLEXES WITH LOWER SYMMETRY LIGANDS..... 173

2.5.1. Complexes derived from D-glucuronic acid ligands..... 173

2.6. CONCLUSION 178

2.7. EXPERIMENTAL SECTION 179

2.8. REFERENCES 220

CHAPTER 3: POLYMER MONOLITH-SUPPORTED DIRHODIUM(II)-CATALYZED CYCLOPROPANATIONS IN CAPILLARY FORMAT 233

3.1. INTRODUCTION 233

3.1.1. Immobilization of dirhodium(II) catalysts 238

3.1.1.1. Immobilization by axial coordination 239

3.2. RESULTS AND DISCUSSION 241

3.2.1. Preparation of porous polymer monolith 241

3.2.2. Dirhodium(II) catalyst immobilisation on porous polymer monolith 243

3.2.3. Flow-through dirhodium(II)-catalyzed cyclopropanation microreaction 245

3.3. CONCLUSION 249

3.4. EXPERIMENTAL SECTION 249

3.5. REFERENCES 257

CHAPTER 4: GENERAL DISCUSSION, CONCLUSION AND FUTURE PERSPECTIVE 261

4.1. REFERENCES 267

APPENDICES S1

TABLE OF FIGURES

Figure 1.1. Lantern structure of dirhodium(II) tetraformate ($Rh_2(O_2CH)_4$)..... 2

Figure 1.2. Selected examples of cyclopropane containing naturally occurring and synthetic compounds. 4

Figure 1.3. Carbenoid resonance structure and back-bonding from the metal atom.[35] 6

Figure 1.4. Metastable dirhodium(II)-carbene complex.[77] 6

Figure 1.5. Classification of diazo compounds.[78,18] 7

Figure 1.6. Relationship between reactivity and selectivity of rhodium-carbenoids.[33] 8

Figure 1.7. Alignment of carbene on rhodium complex.[80,14] 9

Figure 1.8. Calculated structures for a) methyl *α*-phenyldiazoacetate as *donor-acceptor* system and b) methyl diazoacetate as *acceptor* system, top and side views; C = grey, H = white, O = red, N = blue and Rh = purple.[71] (Reprinted with permission from Hansen, J.; Autschbach, J.; Davies, H. M. L. *J. Org. Chem.* **2009**, *74*, 6555. Copyright 2009). 10

Figure 1.9. Transition states of $Rh_2(O_2CH)_4$-catalyzed cyclopropanation of styrene with ethyl bromodiazoacetate: I and III represent end-on trajectory transition states, II and IV represent side-on trajectory transition states.[82] (Reprinted with permission from Bonge, H. T.; Hansen, T. *J. Org. Chem.* **2010**, 75, 2309. Copyright 2010)..... 11

Figure 1.10. Models for different ligand arrangements (the sterically blocking groups around the rhodium active sites are depicted as ovals).[9] 15

Figure 1.11. Dirhodium(II) carboxylates derived from chiral prolinate ligands (Mckervey complex **9**[92] and Davies complexes **10**-**20**[80]). 16

Figure 1.12. A 3D model for Rh_2(*S*-DOSP)$_4$ (top view).[9] (Reprinted from Hansen, J.; Davies, H. M. L. *Coord. Chem. Rev.* **2008**, *252*, 545, Copyright 2008, with permission from Elsevier). 17

Figure 1.13. Second generation prolinate complexes.[108,109] 24

Figure 1.14. Structures of reported chiral dirhodium(II) carboxylates derived from chiral *N*-protected amino acid ligands (Hashimoto complexes **21**-**39**,[119-121,115,112

Dauban complex **40**,[122] Müller and Ghanem complexes[123] **41-52** and Davies complexes **53-54**[124-126]). 26

Figure 1.15. a) Rh(II)-catalyzed cyclopropanation transition states of diazomalonates as carbene precursors; b) The proposed strategy with carbenoids possessing two different groups with different *trans*-directing abilities.[138,139] 34

Figure 1.16. Structure of Rh_2(*S*-PTTL)$_3$(TPA).[147] 43

Figure 1.17. *α,α,α,β*-Structure of Rh_2(*S*-TCPTTL)$_3$(PTAiB).[148] 46

Figure 1.18. Structures of reported chiral dirhodium(II) carboxylates derived from cyclopropane carboxylate ligands.[149-151] 47

Figure 1.19. D_2-symmetry of Rh_2(*R*-BTPCP)$_4$ according to its X-ray structure.[149] ... 47

Figure 1.20. a) Lowest-energy conformation of *s*-trans carbene, top view (left) and side view (right). b) Predictive stereochemical model for Rh_2(*R*-BTPCP)$_4$-catalyzed transformations.[149] (Reprinted with permission from Qin, C.; Boyarskikh, V.; Hansen, J. H.; Hardcastle, K. I.; Musaev, D. G.; Davies, H. M. L. *J. Am. Chem. Soc.* **2011**, *133*, 19198. Copyright 2011). 49

Figure 1.21. Favoured and dis-Favoured amide forms for ligand exchange.[154] 50

Figure 1.22. Reported structures of different classes of chiral dirhodium(II) carboxamidates (cont.).[16,161,162] 51

Figure 1.23. Reported structures of different classes of chiral dirhodium(II) carboxamidates.[16,163,164] 52

Figure 1.24. Possible geometrical isomers of dirhodium(II) carboxamidates.[16] 53

Figure 1.25. CO_2Me (E) entity is occupying two adjacent quadrants around the dirhodium core (top view).[166,164] 54

Figure 1.26. Configurational differences between matched and mismatched catalysts.[16,167] (Part a: Reprinted with permission from Doyle, M. P.; Duffy, R.; Ratnikov, M.; Zhou, L. *Chem. Rev.* **2010**, *110*, 704. Copyright 2010. Part b: Reprinted from Doyle, M. P.; Morgan, J. P.; Colyer, J. T. *J. Organomet. Chem.* **2005**, *690*, 5525, Copyright 2005, with permission from Elsevier). 57

Figure 1.27. Spatial orientations in the transition state of intramolecular cyclopropanations using dirhodium(II) carboxamidates.[164] 61

Figure 1.28. Structure of Hashimoto's Rh_2(*S*-PTPI)$_4$ and Rh_2(*S*-BPTPI)$_4$ catalysts.[181-183,43,42] 65

Figure 1.29. Structure of Rh_2(DPTI)$_3$(OAc) and Rh_2(DTBTI)$_2$(OAc)$_2$.[184,185] 66

Figure 1.30. Structure of 1,6-BPGlyc and Rh_2(1,6-BPGlyc)$_2$(OAc)$_2$.[186] 66

Figure 1.31. Possible geometrical isomers for Rh_2(1,6-BPGlyc)$_2$(OAc)$_2$.[186] 67

Figure 1.32. Enantiotopic binding of 1,6-BPGlyc on Rh_2(1,6-BPGlyc)$_2$(OAc)$_2$.[186] .. 68

Figure 1.33. a) Trend of stereoselectivity in dirhodium(II) carboxylate-catalyzed cyclopropanations. b) The main focus of the current research. 75

Figure 2.1. Structures of lower symmetry bis(oxazoline) ligands studied by Garcia *et al.*[1] 92

Figure 2.2. Ligands backbone structure comparison. 93

Figure 2.3. X-ray structure of Rh_2(*S*-NTTL)$_4$[9] (Reprinted from Ghanem, A.; Gardiner, M. G.; Williamson, R. M.; Müller, P. *Chem.-Eur. J.* **2010**, *16*, 3291, Copyright 2010, with permission from John Wiley and Sons). 95

Figure 2.4. Structure of the new hybrid ligands derived from *N*-1,2-napthaloyl-(*S*)-amino acids. 96

Figure 2.5. Enantiomer separation of *N*-(1,2-naphthaloyl)-(*S*)-*tert*-leucine (**1a**). Conditions for chiral HPLC trace: a) Chiralpak® ID column, 10% 2-propanol in *n*-hexane (*v/v*%) with 0.1% TFA, 0.25 mL/min, 254 nm. b) Chiralpak® IB column, 10% 2-propanol in *n*-hexane (*v/v*%) with 0.1% TFA, 0.25 mL/min, 254 nm. 101

Figure 2.6. Effect of changing the reaction solvent on enantiomeric purity of the obtained ligands. 103

Figure 2.7. Enantiomer separation of *N*-(1,2-naphthaloyl)-(*S*)-*tert*-leucine (**1a**) prepared using a) acetic acid, b) DMF or c) toluene/TEA as reaction solvents. Conditions for chiral HPLC trace: Chiralpak® IB column, 10% 2-propanol in *n*-hexane (*v/v*%) with 0.1% TFA, 0.25 mL/min, 254 nm. 104

Figure 2.8. Enantiomer separation of *N*-(1,2-naphthaloyl)-(*S*)-phenylalanine (**1b**) prepared using a) acetic acid, b) DMF or c) toluene/TEA as reaction solvents. Conditions for chiral HPLC trace: Chiralpak® ID column, 10% 2-propanol in *n*-hexane (*v/v*%) with 0.1% TFA, 0.5 mL/min, 254 nm. 105

Figure 2.9. Enantiomer separation of *N*-(1,2-naphthaloyl)-(*S*)-leucine (**1c**) prepared using a) acetic acid, b) DMF or c) toluene/TEA as reaction solvents. Conditions for chiral HPLC trace: Chiralpak® ID column, 10% 2-propanol in *n*-hexane (*v/v*%) with 0.1% TFA; 0.25 mL/min, 254 nm. 106

Figure 2.10. Enantiomer separation of *N*-(1,2-naphthaloyl)-(*S*)-tryptophan (**1d**) prepared using a) acetic acid, b) DMF or c) toluene/TEA as reaction solvents. Conditions for chiral HPLC trace: Chiralpak® ID column; 10% 2-propanol in *n*-hexane (*v/v*%) with 0.1% TFA, 0.5 mL/min, 254 nm. 107

Figure 2.11. Enantiomer separation of *N*-(1,2-naphthaloyl)-(*S*)-tyrosine (**1e**) prepared using a) acetic acid, b) DMF or c) toluene/TEA as reaction solvents. Conditions for chiral HPLC trace: Chiralpak® ID column, 10% 2-propanol in *n*-hexane (*v/v*%) with 0.1% TFA, 0.5 mL/min, 254 nm. 108

Figure 2.12. Structure of Rh_2(*S*-1,2-NTHS)$_4$ complex (**3f**)..... 111

Figure 2.13. Model applications of cyclopropylphosphonate and cyclopropylphosphonic acid derivatives. 112

Figure 2.14. Illustration to justify the observed high levels of diastereoselectivities a) dis-Favoured, blockage of the approach of the substrate over the phosphonate group, b) Favoured, attractive π-stacking attractions between the aryl rings. 117

Figure 2.15. Chiral HPLC trace of (1*S*, 2*R*)-dimethyl 1,2-diphenylcyclopropylphosphonate (**5**) a) prepared using $Rh_2(OAc)_4$ (Racemic sample), b) prepared using Rh_2(*S*-1,2-NTTL)$_4$. Chromatographic conditions: Chiralcel® OJ column, 2% 2-propanol in *n*-hexane (*v/v*%), 1 mL/min, 220 nm. ... 118

Figure 2.16. 3D models for the distinct ligand orientations used to rationalize the observed enantioselectivity of dirhodium(II) carboxylates derived from *N*-protected amino acid ligands.[68] (Reprinted with permission from Qin, C.; Boyarskikh, V.; Hansen, J. H.; Hardcastle, K. I.; Musaev, D. G.; Davies, H. M. L. *J. Am. Chem. Soc.* **2011**, *133*, 19198. Copyright 2011)..... 120

Figure 2.17. 2D-Heteronuclear NOESY experiments on Rh_2(*S*-PTTL)$_4$ and related complexes.[66,11] 121

Figure 2.18. X-ray structure of bis(ACN) adduct of Rh_2(*S*-1,2-NTPA)$_4$ (**3b**) (side view). As shown, not all ligand atoms could be located in the structure refinement.122

Figure 2.19. Predictive model for the observed asymmetric Rh_2(*S*-1,2-NTTL)$_4$-catalyzed cyclopropanation. 123

Figure 2.20. Application of Fox's predictive model for the asymmetric cyclopropanation catalyzed by Rh_2(*S*-1,2-NTTL)$_4$ (**3a**). 124

Figure 2.21. Examples for reactivity and application of 1,1-cyclopropane diesters.[91] 125

Figure 2.22. Structures of prepared catalysts. 130

Figure 2.23. Suitable positions for substituent introduction; favoured substitution positions are represented in black arrows. 131

Figure 2.24. The two possible orientations of the *N*-protecting group in Rh_2(*S*-BHTL)$_4$ (**13**) and Rh_2(*S*-BOTL)$_4$ (**14**). 132

Figure 2.25. Structure of dirhodium(II,II) tetrakis[(1*S*, 3*R*, 4*R*)-2-(*p-tert*-butylphenylsulphonyl)-2-aza-bicyclo[2.2.1]heptane-3-carboxylate]. 133

Figure 2.26. ORTEP for (1*S*, 2*R*)-dimethyl 1-pheny-2-(*p*-methylphenyl)-cyclopropylphosphonate (**21**) product. 142

Figure 2.27. a) Features that gives the nature of chirality to the binding pocket of Rh_2(*S*-PTTL)$_4$ and analogues, b) and c) Schematic illustration of the daisy chain manner in which the rectangular binding pocket of Rh_2(*S*-PTTL)$_4$ is built up. 145

Figure 2.28. Molecular structure of bis(THF) adduct of Rh_2(*S*-^{tert}PTTL)$_4$ (**12**). Space filling representation; a) top view, b) bottom view, c) and d) side views (A second similar molecule, as well as axial ligands were omitted for clarity). 146

Figure 2.29. Space filling structure comparison between mono(EtOAc) adduct of Rh_2(*S*-PTTL)$_4$ and bis(THF) adduct of Rh_2(*S*-^{tert}PTTL)$_4$ (**12**); a) and c) top views of Rh_2(*S*-PTTL)$_4$ and Rh_2(*S*-^{tert}PTTL)$_4$, respectively, b) and d) side views of Rh_2(*S*-PTTL)$_4$ and Rh_2(*S*-^{tert}PTTL)$_4$, respectively. 147

Figure 2.30. Molecular structure of bis(EtOAc) adduct of Rh_2(*S*-PTAD)$_4$; a) viewed into the chiral crown cavity, b) general view (All hydrogen atoms, a second similar molecule and lattice solvent were omitted for clarity). Space filling representation viewed along the Rh-Rh axis c) into the chiral crown cavity, d) onto the axial Rh coordination site shrouded by the adamantyl groups. 148

Figure 2.31. Molecular structure of bis(EtOAc) adduct of Rh_2(*S*-1-Ph-BPTTL)$_4$ (**11**) collected on MX1 beamline at the Australian Synchrotron, Victoria. The structure suffers from a severe disorder of the axial EtOAc ligands. 149

Figure 2.32. Molecular structure of bis(EtOAc) adduct of Rh_2(*S*-1-Ph-BPTTL)$_4$ (**11**); a) viewed into the chiral crown cavity, b) general view (All hydrogen atoms, a second similar molecule and lattice solvent were omitted for clarity). Space filling representation viewed along the Rh-Rh axis c) into the chiral crown cavity, d) onto the axial Rh coordination site shrouded by the *tert*-butyl groups. 151

Figure 2.33. Molecular structure of bis(ACN) adduct of Rh_2(*S*-BHTL)$_4$ (**13**). Space filling representation; a) top view, b) prolate shaped ACN axial ligand entirely shrouded by cavity walls, c) bottom view, d) and e) side views. 152

Figure 2.34. Molecular Structure of bis(MeOH) adduct of Rh_2(*S*-BOTL)$_4$ (**14**). Space filling structure representation; a), b) and c) three pictures of the complex in various states of "undressing" the MeOH ligands around the cavity. 154

Figure 2.35. ORTEP for (1*S*, 2*R*)-1-trifluoromethyl-1,2-diphenylcyclopropane product. 155

Figure 2.36. Structures of ligands containing *tert*-butyl and adamantyl substituents.170

Figure 2.37. First chiral ligands prepared from carbohydrates. 173

Figure 3.1. Schematic setup for Hashimoto's millilitre continuous flow reactor.[13] (Reprinted from Takeda, K.; Oohara, T.; Shimada, N.; Nambu, H.; Hashimoto, S. *Chem.-Eur. J.* **2011**, *17*, 13992, Copyright 2011, with permission from John Wiley and Sons). 236

Figure 3.2. A monolith standing at the entrance of the Summer Palace Park, Beijing, China.[26] (Reprinted from Guiochon, G. *J Chromatogr A* **2007**, *1168*, 101, Copyright 2007, with permssion from Elsevier). 237

Figure 3.3. Channel of dirhodium(II) immobilized amine-SBA-15 non-porous catalyst.[39] (Reprinted from Dikarev, E. V.; Kumar, D. K.; Filatov, A. S.; Anan, A.; Xie, Y.; Asefa, T.; Petrukhina, M. A. *ChemCatChem* **2010**, *2*, 1461, Copyright 2010, with permission from John Wiley and Sons). 240

Figure 3.4. SEM image for the prepared poly(AA-*co*-VP-*co*-Bis) monolithic column cross-sections. 243

Figure 3.5. Structure of bis(4-vinylpyridine) adduct of Rh_2(*S*-PTTL)$_4$. 244

Figure 3.6. SEM imaging for the prepared poly(AA-*co*-VP-*co*-Bis) monolithic column cross section with Rh_2(*S*-PTTL)$_4$ added to the initial pre-polymerization mixture. 245

Figure 3.7. Typical flow-through dirhodium(II)-catalyzed cyclopropanation microreaction setup. 247

Figure 3.8. Chiral HPLC trace of (1*S*, 2*R*)-dimethyl 1,2-diphenylcyclopropylphosphonate prepared using a) homogenous Rh_2(*S*-^{tert}PTTL)$_4$-catalyzed flask reaction, b) polymer-supported Rh_2(*S*-^{tert}PTTL)$_4$-catalyzed microreaction. Chromatographic conditions: Chiralcel® OJ column, 2% 2-propanol in *n*-hexane (*v*/*v*%), 1 mL/min, 220 nm. 248

Figure 3.9. Microreactors capillary sections mounted perpendicularly on pin-type aluminium stub using double face epoxy resin tape for high resolution SEM imaging..... 251

Figure 3.10. Standard calibration curves for both enantiomers of dimethyl 1,2-diphenylcyclopropylphosphonate generated by injecting different concentrations of a standard sample through the HPLC. 256

Figure 4.1. The two possible electronically equivalent and sterically different substrate orientations within the chiral cavity (represented in grey and white areas).262

Figure S1. Molecular structure of polymeric Rh_2(*R*,*R*,*S*,*S*-1,2-NTTY)$_4$ (side view). As shown, not all ligand atoms could be located in the structure refinement..... S5

TABLE OF SCHEMES

Scheme 1.1. Reaction mechanistic pathway for carbenoid formation and cyclopropanation.[69-75,7] 5

Scheme 1.2. Asymmetric total synthesis of cyclopropyl analogue of Tamoxifen.[99] . 18

Scheme 1.3. Solid-phase cyclopropanation between phenyldiazoacetate and a resin bounded olefin.[101] 19

Scheme 1.4. Asymmetric cyclopropanations using heteroaryldiazoacetates.[97] 19

Scheme 1.5. Example for Rh_2(*S*-DOSP)$_4$-catalyzed decomposition of alkynyldiazoacetates.[102] 20

Scheme 1.6. Rh_2(*R*-DOSP)$_4$-catalyzed decompositions of aryldiazoacetates in the presence of pyrroles or furans.[104] 21

Scheme 1.7. Hypothetical model for asymmetric induction by dirhodium(II) (*S*)-prolinate catalysts. 22

Scheme 1.8. Rh_2(*S*-biTISP)$_2$-catalyzed cyclopropanation.[109] 24

Scheme 1.9. Rh_2(*S*-DOSP)$_4$-catalyzed cyclopropanation of allyl vinyldiazoacetate.[110] 25

Scheme 1.10. Rh_2(*S*-NTTL)$_4$-catalyzed cyclopropanation of (silanyloxyvinyl)-diazoacetates.[134-136] 32

Scheme 1.11. Rh_2(*S*-NTTL)$_4$-catalyzed enantioselective formation of 1,1-cyclopropane diesters (*trans*-directing group concept).[138-141] 33

Scheme 1.12. Enantioselective cyclopropanation with 1,2,3-triazoles.[143] 37

Scheme 1.13. Synthesis of Rh_2(*S*-PTAD)$_4$ catalyst (**53**).[124] 38

Scheme 1.14. Rh_2(*S*-PTAD)$_4$-catalyzed cyclopropanation of diazo ketones.[146] 41

Scheme 1.15. Rh_2(*S*-PTAD)$_4$-catalyzed enantioselective cyclopropanation of styrene with 2-chlorophenyl aryldiazoacetate derivative.[98] 41

Scheme 1.16. Rh_2(*S*-TCPTAD)$_4$-catalyzed reaction of aryldiazoacetates and vinyldiazoacetates with electron deficient alkenes.[126] 42

Scheme 1.17. Schematic presentation of the cyclopropanation, ylide formation and epoxidation pathways.[126] 43

Scheme 1.18. Rh_2(*R*-BTPCP)$_4$-catalyzed asymmetric cyclopropanation. 48

Scheme 1.19. Divergent synthesis of **55** and **56**.[152] 49

Scheme 1.20. Rh_2(4*S*-MEAZ)$_4$-catalyzed asymmetric preparation of **92**.[172] 58

Scheme 1.21. Total synthesis of cyclopropane-configured phenylethylthiazoyl-thiourea (PETT) analogue **93**.[171] 59

Scheme 1.22. Rh_2(4*S*, *R*-MenthAZ)$_4$-catalyzed cyclopropanation of vinyl diazolactone **94** with different olefins.[173] 60

Scheme 1.23. Intramolecular cyclopropanation of substituted allylic *α*-cyano-*α*-diazoacetates.[174] 60

Scheme 1.24. Rh_2(4*S*-MPPIM)$_4$-catalyzed intermolecular cyclopropanation of 2-methallyl diazoacetate.[175,176] 61

Scheme 1.25. Decomposition of *N*-allyl diazoacetamide in the presence of catalytic amount of Rh_2(4S-MEOX)$_4$.[164] 62

Scheme 1.26. Rh_2(4*S*, 2*S*-BSPIM)$_4$-catalyzed double intramolecular cyclopropanation.[177] 62

Scheme 1.27. Rh_2(*S*-IBAZ)$_4$-catalyzed cyclopropan(en)ation.[178] 63

Scheme 1.28. Example for Rh_2(*S*-PTPI)$_4$-catalyzed enantioselective cyclopropanation of styrene with 2,4-dimethyl-3-pentyl diazoacetate.[182] 65

Scheme 1.29. Solvent effect on the enantioselectivity of Rh_2(*S*-TBSP)$_4$-catalyzed cyclopropanation of styrene.[189] 70

Scheme 1.30. Additive effect on the activity of Rh_2(*S*-biTISP)$_2$ in cyclopropanation reaction of Styrene with methyl *α*-phenyldiazoacetate.[21] 71

Scheme 2.1. Preparation of chiral ligands; HMBC correlations are represented in blue arrows. 98

Scheme 2.2. Preparation and structure of the new catalytic series. 110

Scheme 2.3. Ruthenium-porphyrin-catalyzed cyclopropanation of styrene derivatives with di*iso*propyl diazomethylphosphonate.[52] 113

Scheme 2.4. Ru(II)-Pheox-catalyzed asymmetric cyclopropanation of various classes of alkenes with diethyl diazomethylphosphonate.[54] 114

Scheme 2.5. Rh_2(*S*-IBAZ)$_4$-catalyzed cyclopropanations of alkenes with di*iso*propyl *α*-cyano-*α*-diazophosphonates.[56] 115

Scheme 2.6. Preparation of chiral ligands **7**, **8**, **9** and **10**. 129

Scheme 2.7. The attempt to use *exo*-3,6-epoxy-1,2,3,6-tetrahydrophthalic anhydride **15** as a protecting group for L-*tert*-leucine amino acid. 133

Scheme 2.8. The attempt to use *N*-phthaloyl-L-glutamic anhydride as a protecting group for L-*tert*-leucine amino acid. 134

Scheme 2.9. Attempt for the preparation of 4-*tert*-butyl-1,8-naphthalic anhydride; HMBC correlations are represented in blue arrows. 135

Scheme 2.10. Attempts for the preparation of methyl *α*-diazobenzylsulfonate. 169

Scheme 2.11. Endeavours for the synthesis of 4-(1-adamantyl)phthalic acid **39**. ... 171

Scheme 2.12. a) Reaction of **40** with L-*tert*-leucine and b) ^{1}H NMR of reaction product **41**. 172

Scheme 2.13. Preparation of Rh_2(*β*-D-TAGA)$_4$ complex (**47**). 174

Scheme 2.14. Rh_2(*β*-D-TAGA)$_4$-catalyzed cyclopropanation of styrene with Meldrum's acid. 176

Scheme 2.15. Endeavours for the preparation of **49**. 177

Scheme 3.1. Preparation of polymer-supported Rh_2(*S*-PTTL)$_4$ beads.[13] 235

Scheme 3.2. Structure of the PIB-supported dirhodium(II) complex. 238

Scheme 3.3. Davies universal strategy for immobilization of dirhodium(II) complexes. 239

Scheme 3.4. Internal surface modification of glass capillaries.[40] 241

Scheme 3.5. The approach for the preparation of the pyridine-functionalized polymer monolithic support inside the capillary microreactor. 242

Scheme 3.6. Schematic illustration for the developed flow-through Rh_2(*S*-^{tert}PTTL)$_4$-catalyzed cyclopropanation microreactor. 246

Scheme 3.7. Flask Rh_2(*S*-^{tert}PTTL)$_4$-catalyzed cyclopropanation of styrene and dimethyl *α*-diazobenzylphosphonate in toluene at room temperature. 247

Scheme 4.1. Suggested retro-synthetic route for the preparation of *N*-(4-*tert*-butylnaphthaloyl)-(*S*)-*tert*-leucine ligand, ^{tert}NTTL. 265

TABLE OF TABLES

Table 1.1. Selected example for the effect of catalyst electrophilic profile on reaction pathway.[83] 13

Table 1.2. Selected example for the effect of catalyst steric profile on reaction chemoselectivity.[91] 14

Table 1.3. Chiral catalysis approach for asymmetric *donor-acceptor* carbenoid cyclopropanation[14] 18

Table 1.4. Cyclopropanation of allenes with *p*-bromophenyldiazoacetate.[106,107] 23

Table 1.5. Rh_2(*S*-PTTL)$_4$-catalyzed intermolecular cyclopropanation reactions of *α*-alkyldiazo compounds.[127] 27

Table 1.6. Rh_2(*S*-PTTL)$_4$-catalyzed asymmetric cyclopropanation of diazooxindole with various olefins.[128] 28

Table 1.7. Rh_2(*S*-TCPTTL)$_4$-catalyzed cyclopropanation of styrene with *α*-nitro-*α*-diazo-*p*-methoxyacetophenone.[121] 29

Table 1.8. Rh_2(*S*-TCPTTL)$_4$-catalyzed cyclopropanation of several *α*-EWG-diazoacetophenones bearing an *α*-*p*-methoxyphenyl (PMP)-ketone group.[129] 30

Table 1.9. Rh_2(*S*-TBPTTL)$_4$-catalyzed cyclopropanation of styrene with *α*-diazopropionates.[130] 31

Table 1.10. Intramolecular cyclopropanation of 1-phenyl-1-propenyl 2-diazo-3-silanyloxybut-3-enoates.[142] 36

Table 1.11. Enantioselective preparation of dimethyl 1,2-diphenylcyclopropylphosphonate.[124] 39

Table 1.12. Dirhodium(II)-catalyzed enantioselective synthesis of trifluoromethyl-substituted cyclopropanes.[125] 40

Table 1.13. Dirhodium(II)-catalyzed enantioselective synthesis of nitrile-substituted cyclopropanes.[145] 40

Table 1.14. Rh_2(*S*-PTTL)$_3$(TPA)-catalyzed cyclopropanation of ethyl *α*-diazobutanoate.[147] 44

Table 1.15. Evaluation of chiral heteroleptic Rh_2(*S*-TCPTV)$_3$(PTAiB) and Rh_2(*S*-TCPTTL)$_3$(PTAiB) complexes as catalysts in asymmetric cyclopropanation.[148] 45

Table 1.16. Results for intramolecular C–H insertion.[167] 55

Table 1.17. Dirhodium(II) carboxamidates-catalyzed cyclopropanation of styrene with methyl phenyldiazoacetate.[163] 64

Table 1.18. *cis*/*trans*-Selectivity of Rh_2(1,6-BPGlyc)$_2$(OAc)$_2$ in the formation of **96** and **97**.[186] 69

Table 2.1. Enantioselective cyclopropanation of styrene with dimethyl malonate *via* the *in situ* generated phenyliodonium ylide method.[8] 94

Table 2.2. Enantiomer separation of *N*-1,2-naphthaloyl-(*S*)-amino acids on Chiralpak® ID. 100

Table 2.3. Effect of changing the reaction solvent on yield and enantiomeric purity of the prepared ligands. 103

Table 2.4. Asymmetric cyclopropanation of styrene with dimethyl *α*-diazobenzylphosphonate. 116

Table 2.5. Asymmetric cyclopropanation with Meldrum's acid (*diacceptor* substrate). 126

Table 2.6. Asymmetric cyclopropanation of styrene with dimethyl *α*-diazobenzylphosphonate. 137

Table 2.7. Scope of the catalysts investigations with respect to the alkene. 140

Table 2.8. Effect of the *α*-diazophosphonate ester group size on the enantioselectivity of the catalysts. 143

Table 2.9. Asymmetric cyclopropanation of styrene with 1-phenyl-2,2,2-trifluromethyldiazoethane (*donor-acceptor* substrate). 156

Table 2.10. Asymmetric cyclopropanation of styrene with *p*-methoxyphenyldiazoacetate (*donor-acceptor* substrate). 158

Table 2.11. Asymmetric cyclopropanation with phenyldiazoacetate (*donor-acceptor* substrate). 161

Table 2.12. Effect of solvent and temperature on the stereoselectivity of Rh_2(*S*-1,2-NTTL)$_4$ (**3a**) with phenyldiazoacetate substrate. 162

Table 2.13. Asymmetric cyclopropanation with styryldiazoacetate (*donor-acceptor* substrate). 164

Table 2.14. Asymmetric cyclopropanation of styrene with *α*-diazo-2-phenylacetonitrile. 167

Table 2.15. Rh_2(*β*-D-TAGA)$_4$-catalyzed asymmetric cyclopropanation of styrene. 176

Table 3.1. ICP-MS optimised conditions for rhodium analysis in synthetic samples.254

Table S1. Effect of ligand enantiopurity on the enantioselectivity of the final catalyst. S3

Table S2. Rh_2(1,2-NTTY)$_4$-catalyzed cyclopropanation of various olefins with Meldrum's acid. S6

ABBREVIATIONS

The following abbreviations are used in this work:

4Å MS	4Å Molecular sieves
AA	Acrylamide
Ac	Acetyl
ACN	Acetonitrile
AIBN	Azobis*iso*butyronitrile
Ar	Aryl
Bis	*N*,*N*-Methylenebisacrylamide
Bn	Benzyl ($PhCH_2$)
BOC	*tert*-Butyloxycarbonyl
Bz	Benzoyl
COSY	Correlation spectroscopy
CSP	Chiral stationary phase
DBU	1,8-Diazabicyclo[5.4.0]undec-7-ene
DCE	1,2-Dichloroethane
de	Diastereomeric excess
DCM	Methylene chloride (CH_2Cl_2)
DFT	Density functional theory
DIPEA	*N*,*N*-Di*iso*propylethylamine

2,2-DMB	2,2-Dimethylbutane
DMAP	Dimethylaminopyridine
DMF	Dimethylformamide
DMSO	Dimethylsulfoxide
dr	Diastereomeric ratio
EDG	Electron donating group
ee	Enantiomeric excess
equiv.	Equivalents
ESI	Electrospray ionization
Et	Ethyl
EWG	Electron withdrawing group
h	Hours
HCl	Hydrochloric acid
HF	Hydrofluoric acid
HMBC	Heteronuclear multiple-bond correlation spectroscopy
HPLC	High performance liquid chromatography
HSQC	Heteronuclear single-quantum correlation spectroscopy
Hz	Hertz
i-Bu	*iso*Butyl
ICP	Inductively coupled plasma
IPA	*iso*Propanol

i-Pr	*iso*Propyl
IR	Infrared spectroscopy
J	Coupling constant
MALDI	Matrix assisted laser desorption ionization
Me	Methyl
MeOH	Methanol
mp	Melting point
ND	Not determined
NMR	Nuclear magnetic resonance
MS	Mass spectrometry
nOe	Nuclear overhauser effect
NOESY	Nuclear overhauser effect spectroscopy
Oct	Octyl
ORTEP	Oak ridge thermal ellipsoid plot
p-ABSA	4-Acetamidobenzenesulfonyl azide
Ph	Phenyl
PMP	*p*-Methoxyphenyl
ppm	Parts per million
PTAiB	*N*-Phthalimido-*α*-amino*iso*butyric acid
R_f	Retention factor
Rh	Rhodium

rt	Room temperature
SEM	Scanning electron microscopy
t-Bu	*tert*-Butyl
TEA	Triethylamine
Tf	Triflyl
TFA	Trifluoroacetic acid
TFT	*α*,*α*,*α*-Trifluorotoluene
THF	Tetrahydrofuran
TIPS	Tri*iso*propylsilyl
TLC	Thin layer chromatography
TMS	Trimethylsilyl
TMU	Tetramethylurea
TOF	Time of flight
UV	Ultraviolet absorption
VP	4-Vinylpyridine

CHAPTER 1: CHIRAL DIRHODIUM(II) CARBOXYLATES AND CARBOXAMIDATES AS EFFECTIVE CHEMZYMES IN ASYMMETRIC SYNTHESIS OF CYCLOPROPANE DERIVATIVES

1.1. INTRODUCTION

The term "Chemzyme" was first introduced by Corey in 1989 to describe an oxazaborolidene derivative used as a catalyst for highly enantioselective reduction of a variety of achiral ketones to chiral secondary alcohols.[1] Corey defined a chemzyme to be a small soluble organic molecules that can catalyze certain chemical reactions in similar way that natural enzymes catalyze biochemical reactions while being able to tell left from right.[2] In other words, a chemzyme sequesters the reactants molecules out of the surrounding, twists them into position, welds them together with a precise three dimensional structure and then releases the product away to free itself for the next catalytic cycle.[2] Nowadays, the "chemzyme" description has been applied to a number of catalysts including multifunctional heterobimetallic complexes for catalytic asymmetric Michael additions,[3] chiral Lewis acid catalysts for hetero-Diels-Alder reactions,[4] cyclodextrin based artificial enzymes,[5] achiral aluminium phenoxide derivatives as catalysts for conjugate allylation reactions[6] and dirhodium(II) paddlewheel complexes for metal carbenes transformation reactions.[7]

Although many transition metal compounds have been recently developed, dirhodium(II) paddlewheel complexes are among the most attractive catalysts because of their activity, efficiency and selectivity.[8-19] The ability of such complexes to effectively catalyze a variety of reactions at low catalyst loading has demonstrated their synthetic potential, particularly, in the context of chiral catalysis. Dirhodium(II) catalysts with very high turnover numbers have been reported.[20,21] Therefore, the toxicity and cost of rhodium was enormously overcast by the capability of very small amounts of the catalyst to return large quantities of value-added chemicals.

1.2. HISTORY

The story of dirhodium(II) complexes begun in 1960 when Chernyaev and co-workers[22] uncovered a fruitful area of rhodium chemistry. They reported an air stable green crystalline complex that was obtained by refluxing rhodium(III) chloride in

formic acid. They initially formulated this product as being the rhodium(I) species, $H[Rh(O_2CH)_2.0.5H_2O]$. However, it was quickly found that this compound lacks acid character. The product was subsequently identified as dirhodium(II) tetraformate monohydrate $[Rh_2(O_2CH)_4.H_2O]$ by X-ray diffraction.[23] This was the first example of a binuclear rhodium(II) carboxylate complex that possesses the now known ‘‘lantern’’ structure illustrated in Figure 1.1.

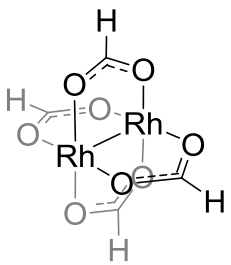

$Rh_2(O_2CH)_4$

Figure 1.1. Lantern structure of dirhodium(II) tetraformate ($Rh_2(O_2CH)_4$).

Later in the 1970’s, dirhodium(II) tetraacetate ($Rh_2(OAc)_4$), which was prepared in mid-1960’s,[24,25] was reported as an exceptionally effective catalyst for a wide variety of catalytic transformations involving diazo compounds.[26,27] This discovery by Teyssie and co-workers holds a unique importance in the history of this methodology development.[26-28] In fact, $Rh_2(OAc)_4$ is not susceptible to redox transformations with diazo compounds, does not form π-complexes with olefins and is resistant to ligand exchange under ordinary catalytic conditions. Besides, It was found that product yields from $Rh_2(OAc)_4$-catalyzed cyclopropanations were not diminished even when catalyst to diazo compound molar ratios as low as 0.0005 were employed.[29] $Rh_2(OAc)_4$ also serves as the parent compound for the synthesis of other dirhodium(II) complexes. The introduction of ligand exchange procedures gave access to a wide variety of other dirhodium(II) complexes with similar paddlewheel frameworks.[8] In addition to achiral ligands, the introduction of chiral ligands allowed opportunities to explore, design and synthesize of various classes of chiral dirhodium(II) complexes. Furthermore, the study of their catalytic activity promoted the rhodium-carbenoid chemistry to unprecedented levels of chemo-, regio- and stereoselectivity.

Currently, chiral dirhodium(II) complexes are considered exceptional catalysts for a wide range of chemical transformations, particularly, in metal-nitrenoid and -carbenoid chemistry.[10] These chemical transformations involves aziridinations,[30-32] C-H insertions,[11,33] ylide transformations,[34-38] Lewis acid-catalyzed processes,[39-43,34] cross-coupling reactions[44] and cyclopropanation and cyclopropenation reactions.[45-48] In this chapter, an overview is provided on the development in dirhodium(II) carboxylates and carboxamidates as two of the most important classes of dirhodium(II) paddlewheel complexes. The discussion will be further extended to their utilization as effective chemzymes in inter- and intramolecular asymmetric cyclopropanation reactions.

1.3. DIRHODIUM(II)-CATALYZED CYCLOPROPANATION REACTIONS

Cyclopropane derivatives played an important role in organic chemistry for decades. They emerged as important building blocks in organic synthesis allowing access to complex molecules with defined orientation of functional groups.[49-53] Also, the cyclopropyl group is a well-known structure motif in nature, even though it is a highly strained entity.[54,55] Naturally occurring and synthetic chiral cyclopropanes are endowed with a large spectrum of biological properties including enzyme inhibition, insecticidal, herbicidal, antibacterial, antifungal, antiviral and antitumor activities (Figure 1.2).[55-57] For example, they have been found as structural moieties in cyclopropane-based peptidomimetics,[58,59] Pyrethroids insecticides,[60,61] antipsychotic agents,[62] selective inhibitors for papain and cystein proteases,[63] the antidepressant and anxiolytic agent; Tranylcypromine,[64] the antimitotic agent; (+)-Curacin[65] and the anticancer agent; (+)-Ptaquiloside.[66] This is in addition to a number of best-selling pharmaceuticals containing the cyclopropyl group which render the cyclopropane chemistry more economic importance.[67]

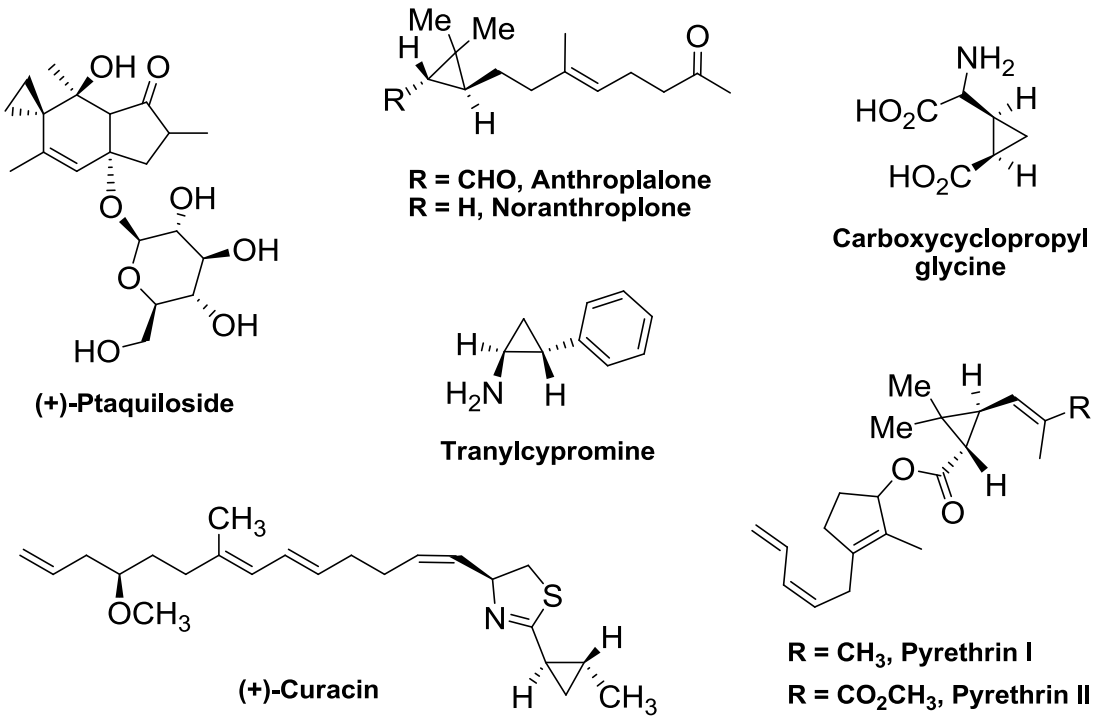

Figure 1.2. Selected examples of cyclopropane containing naturally occurring and synthetic compounds.

The cyclopropyl group can be efficiently constructed through the reaction of a dirhodium(II)-carbenoid species (formed when a diazo compound reacts with a dirhodium(II) catalyst) and an alkene (Scheme 1.1a). The current generally accepted mechanism for this reaction was originally proposed by Yates[68] in 1952 for copper-catalyzed diazo decomposition. This mechanism involves the initial complexation of the negatively polarized carbon of the diazo compound to the axial site of the Rh(II) catalyst, which is coordinatively unsaturated (Scheme 1.1b). Subsequent irreversible extrusion of N_2 from the intermediate **2** generates the Rh(II)-carbene complex **4**. In this mechanism, the extrusion of N_2 is considered to be the rate-limiting step and a number of kinetic studies have provided some support for this mechanism.[69-75,7] Computational, as well as kinetic studies of dirhodium(II) carboxylate-catalyzed carbenoid reactions indicated that carbene binding occurs only at one of the two rhodium active sites at a time.[7,69,76]

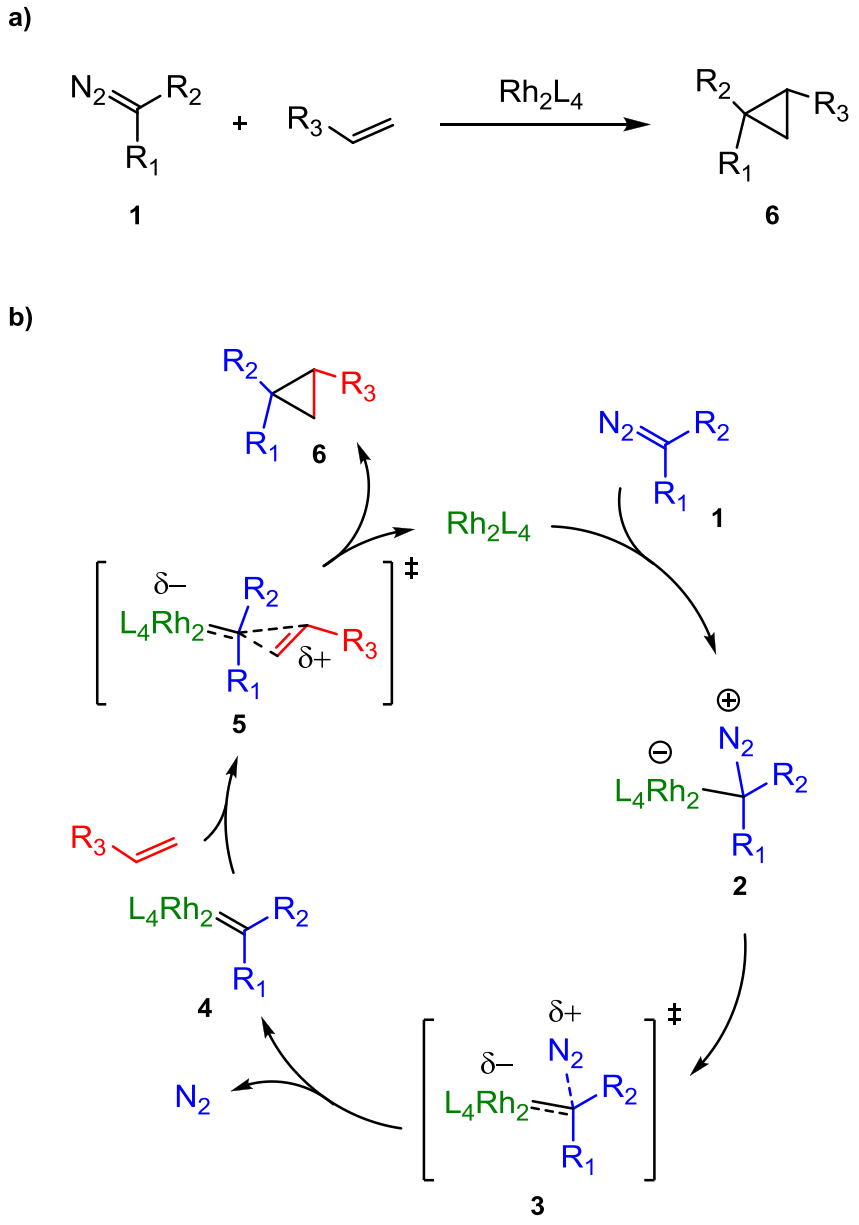

Scheme 1.1. Reaction mechanistic pathway for carbenoid formation and cyclopropanation.[69-75,7]

Dirhodium-carbenoid intermediate **4** can be represented by either a double bond to the metal catalyst (**7a**), or as a charge separated structure (**7b**). Although representation of **4** as a charge separated structure de-emphasizes the back-bonding stabilization from the rhodium atom (Figure 1.3),[35] it does emphasize the electrophilic nature of the carbenoid carbon.

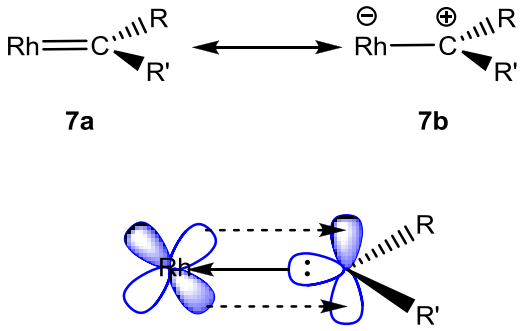

Figure 1.3. Carbenoid resonance structure and back-bonding from the metal atom.[35]

In fact, the formation of this intermediate in dirhodium(II)-catalyzed carbenoid transformations remained elusive until, very recently, Davies, Berry and co-workers[77] provided a direct evidence for being a genuine dirhodium(II)-carbene complex. They reported the generation of the metastable dirhodium(II)-carbenoid intermediate **8** (Figure 1.4) which was stable for a period of ~20 h in chloroform kept at 0 ^{o}C. This discovery opened the door for the exploration of its physical and chemical properties. The authors were able to characterize the Rh=C bond by vibrational and NMR spectroscopy, extended X-ray absorption, fine structure analysis and quantum chemical calculations.[77]

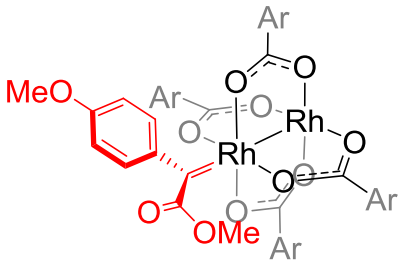

Ar = Triphenylmethyl

8

Figure 1.4. Metastable dirhodium(II)-carbene complex.[77]

1.3.1. Types of carbenoid intermediates

The electrophilicity of the metal-carbenoid intermediates is a very important feature that set the chemo-, regio- and stereoselectivity of the reaction at which; low electrophilicity can lead to less reactivity, while too much electrophilicity causes

side-reaction. Away from the structure of the dirhodium(II) catalyst, varying the substituents linked to the carbene carbon is a different way to change the electronic properties of the carbenoid intermediates. Typically, diazo substrates can be classified into three groups based on the electron donating/withdrawing characteristics of their substituents; *monoacceptor*, *diacceptor* and *donor-acceptor*.[78,18] The terms "*donor*" and "*acceptor*" refers to electron donating or electron withdrawing groups, respectively. Typical *acceptor* groups can be keto, cyano, trifluoromethyl, phosphonate or sulfonate, while typical *donor* groups are vinyl, alkynyl, aryl or heteroaryl (Figure 1.5).

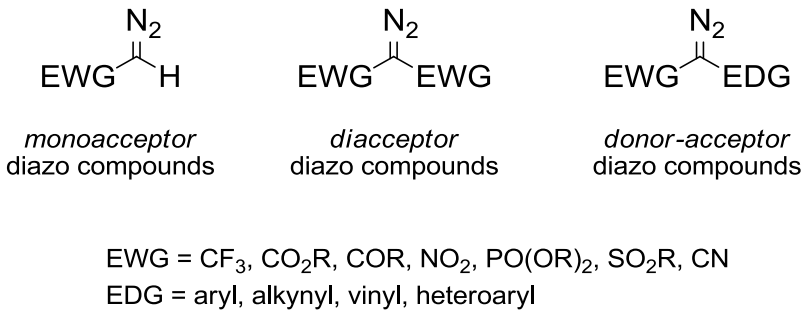

Figure 1.5. Classification of diazo compounds.[78,18]

Generally, an *acceptor* substituent will force the diazo substrate to be less reactive towards carbenoid generation. However once the corresponding carbenoid intermediate is generated, it will display a more electrophilic and reactive nature, while being less stable and selective. On the contrary, introducing a *donor* substituent will make the diazo substrate more reactive towards carbenoid generation. But once the carbenoid is formed, it tend to be less electrophilic and reactive, while being more stable and selective (Figure 1.6).[33]

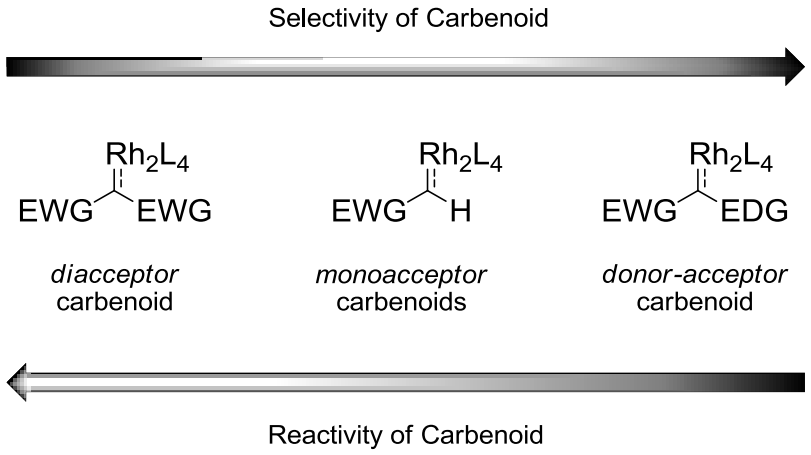

Figure 1.6. Relationship between reactivity and selectivity of rhodium-carbenoids.[33]

An emerging area in asymmetric synthesis involves the utilization of *donor-acceptor* carbenoids due to their enhanced levels of selectivity compared to other carbenoid classes. In a number of cases, the reactivity and stability observed with *donor-acceptor* carbenoids differs substantially from those *monoacceptor* and *diacceptor* ones. Due to the enhanced stability of this class of intermediates, they have potential capability towards a variety of highly regio- and stereoselective reactions, especially when combined with chiral dirhodium(II) carboxylate catalysts. Their unique selectivities have already facilitated in the efficient construction of complex molecular architectures.[79]

1.3.2. Modes of interaction between the rhodium complex and the carbene

The preferred mode of interaction between the rhodium complex and the carbene was already explained using MM2 followed by extended Hückel calculations focusing on the interaction between dirhodium(II) tetraacetate and vinyl carbene.[80] The results revealed that the carbene favourably align staggered to the oxygen of the carboxylates rather than an eclipsed alignment (Figure 1.7). The staggered orientation is, not only realistic on steric basis, but also is required for metal back-bonding stabilization of the carbenoid as the d_{yz} and d_{xz} orbitals of rhodium are hybridized to generate two new orbitals that lie in this staggered positions.[81]

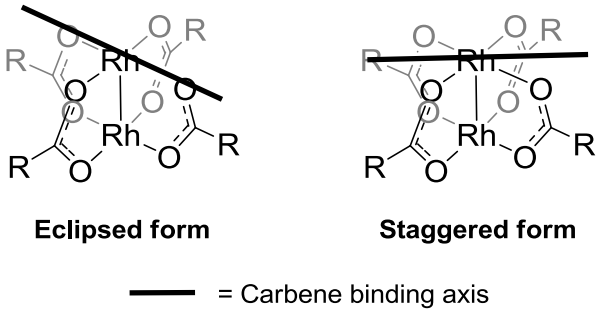

Figure 1.7. Alignment of carbene on rhodium complex.[80,14]

Later, Singleton, Davies and co-workers[72] analyzed both methyl diazoacetate and methyl vinyldiazoacetate as models for *acceptor* and *donor-acceptor* systems, respectively, to justify the greater chemoselectivity displayed by the later. However, in 2009, these models were re-evaluated by the same research group[71] as the calculated small potential energy barrier was not consistent with a large amount of experimental data which suggests that *donor-acceptor* are highly selective species. The authors recognized that the previously used calculations weren't appropriately describing rhodium in the system. The new models revealed that an *acceptor* carbenoid (e.g. methyl diazoacetate) prefers the eclipsed conformation, while a *donor-acceptor* carbenoid (e.g. methyl *α*-phenyldiazoacetate) adopts the staggered conformation as the more sterically bulky nature of the phenyl group does not permit the eclipsed conformation (Figure 1.8). The authors communicated that, this observation might have major implications on the developed models to describe the enantioinduction of chiral dirhodium(II) complexes since the two carbenoids will orient themselves differently relative to the given chiral ligand environment.[71]

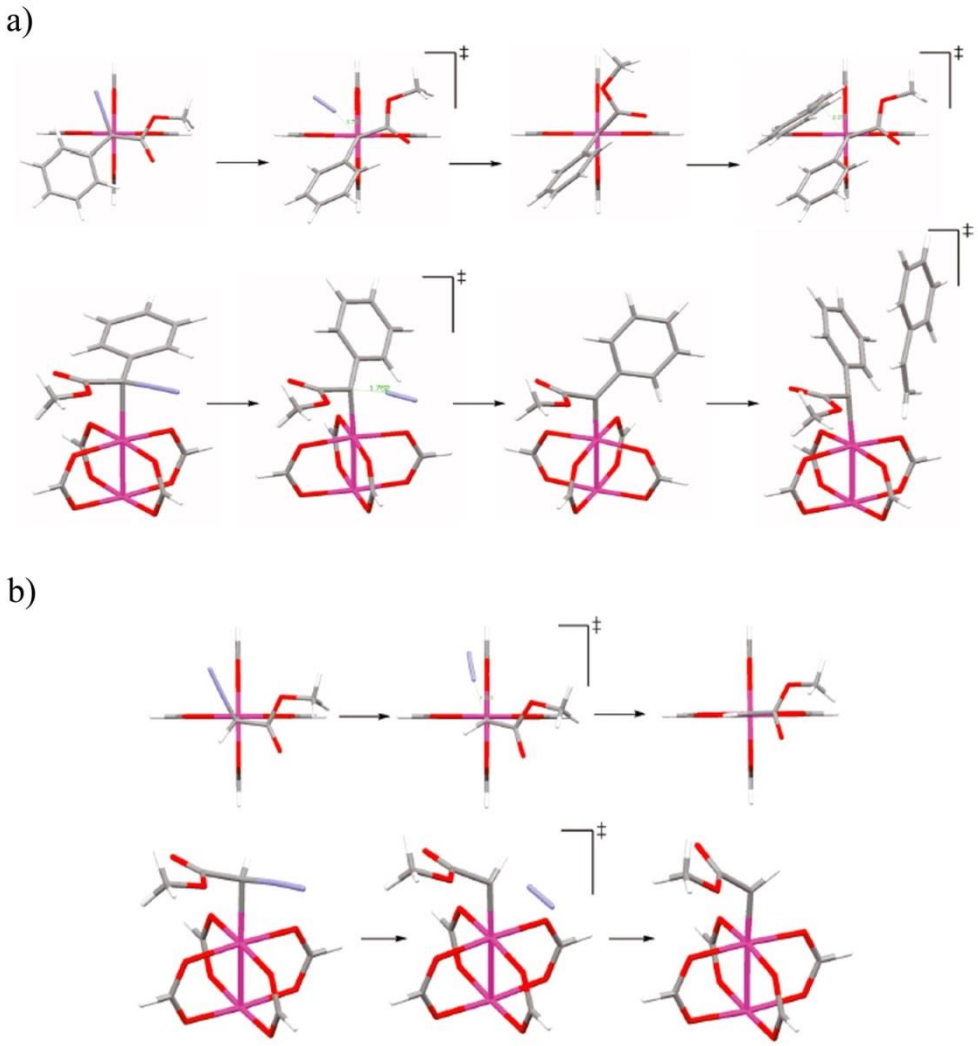

Figure 1.8. Calculated structures for a) methyl *α*-phenyldiazoacetate as *donor-acceptor* system and b) methyl diazoacetate as *acceptor* system, top and side views; C = grey, H = white, O = red, N = blue and Rh = purple.[71] (Reprinted with permission from Hansen, J.; Autschbach, J.; Davies, H. M. L. *J. Org. Chem.* **2009**, *74*, 6555. Copyright 2009).

1.3.3. Approach of the alkene

The final step in the dirhodium(II)-catalyzed cyclopropanations mechanism involves the approach of the alkene and generation of cyclopropane final product **6** (Scheme 1.1b). Bonge and Hansen[82] studied the mechanism of dirhodium(II)-catalyzed cyclopropanations with ethyl bromo-, chloro- and iododiazoacetate through density functional theory (DFT) calculations. They found that, in addition to transition states

in which the alkene approaches the carbenoid in an end-on manner, side-on trajectory states were also found to be of importance (Figure 1.9). The relative energies of the side-on trajectory transition states compared to the end-on trajectory transition states are shown to be affected by the alkene substrate, as well as the carbenoid substituents.

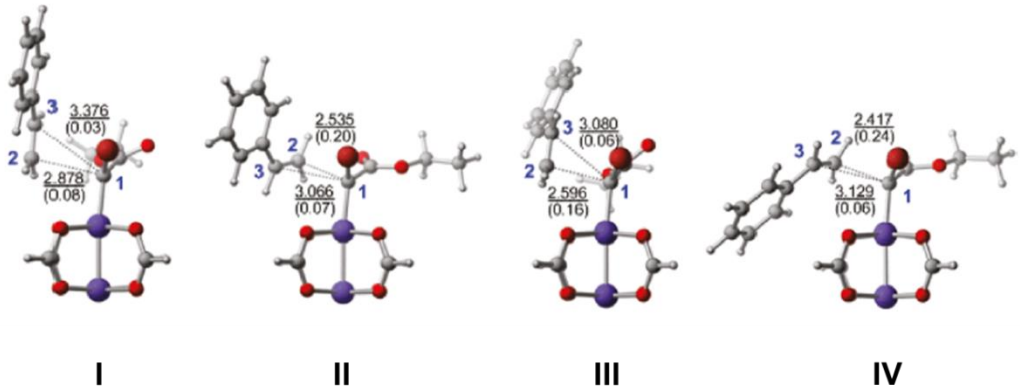

Figure 1.9. Transition states of $Rh_2(O_2CH)_4$-catalyzed cyclopropanation of styrene with ethyl bromodiazoacetate: I and III represent end-on trajectory transition states, II and IV represent side-on trajectory transition states.[82] (Reprinted with permission from Bonge, H. T.; Hansen, T. *J. Org. Chem.* **2010**, 75, 2309. Copyright 2010).

1.4. MODIFICATIONS IN THE DIRHODIUM(II) FRAMEWORK

All dirhodium(II) complexes are structurally characterized by a bimetallic core with a Rh-Rh single bond, bridged by four μ_2-carboxylate, carboxamidate, phosphonate or other ligands. Reported modifications in the dirhodium(II) framework is mostly related to either electronic (Section 1.4.1) or steric modifications (Section 1.4.2) within its ligands.

1.4.1. Electronic modifications

Altering the electronic profile of ligands mainly affects the reactivity of the dirhodium(II) catalyst as electronically different bridging ligands coordinated to the Rh-Rh axes donate distinct degrees of charge to the metal changing the overall electronic profile of the complex. This in turn, will impact on the electrophilicity of the carbenoid generated during catalysis to significantly influence the reaction mechanistic pathway.[83,19] For example, the competition reaction between

cyclopropanation and aryl C-H insertion illustrated in Table 1.1 clearly demonstrated the role of the catalyst electronic profile on reactivity.[83] A completely opposite reactivity was observed at which the more electron rich catalyst, $Rh_2(cap)_4$, returned exclusively the cyclopropanation product (Table 1.1, entry 3), while the highly electrophilic catalyst, $Rh_2(pfb)_4$, merely led to the generation of the C-H insertion product (Table 1.1, entry 1).

Examples to electronic modifications within the rhodium scaffold included employing mixed valence dirhodium(II,III) species,[32,84] complexes with Bi-Rh heterobimetallic species,[85-88] complexes with axially coordinated *N*-heterocyclic carbenes[89,90] and applying reaction additives. The latter will be discussed in detail in Section 1.7. Although several examples have been reported, the use of the electronic modifications pathway is generally limited to the fine tuning of the selectivity of a particular catalyst in a particular reaction for the preparation of a particular product.[19]

Table 1.1. Selected example for the effect of catalyst electrophilic profile on reaction pathway.[83]

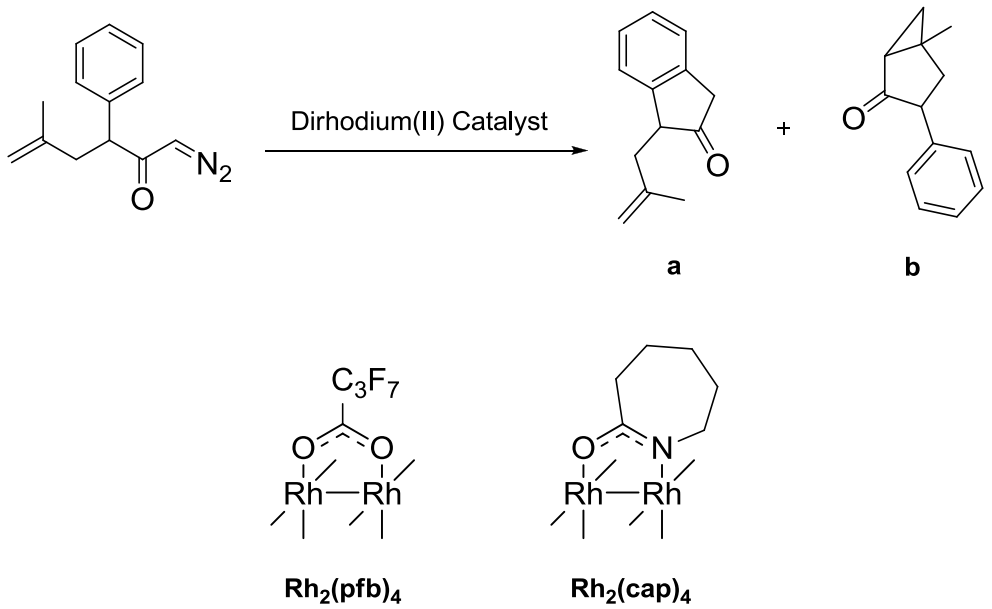

Entry	Catalyst	Yield (%)	a:b
1	$Rh_2(pfb)_4$	86	100:0
2	$Rh_2(OAc)_4$	92	52:48
3	$Rh_2(cap)_4$	75	0:100

1.4.2. Steric modifications

On the other hand, the importance of the ligand sterics has been confirmed through multiple reports not only on chemo- and regioselectivity, but also on the enantioselectivity of the catalyst.[19] In the example illustrated in Table 1.2, a completely opposite reactivity was observed when ligand sterics was altered from methyl in $Rh_2(OAc)_4$ to triphenylmethyl in $Rh_2(tpa)_4$.[91] Aryl C-H insertion was the exclusive pathway observed with $Rh_2(tpa)_4$ (Table 1.2, entry 2). This was opposite to cyclopropanation being the preferred mode of reactivity in competition with aryl C-H insertion in the $Rh_2(OAc)_4$-catalyzed reaction (Table 1.2, entry 1).

Using the ligand's steric profile for controlling, predicting and justifying the observed selectivity of a dirhodium(II) catalyst is essentially the fundamental

pathway employed in the field of dirhodium(II) development.[9,19] The importance related to the exploration and manipulation of ligand sterics in chiral dirhodium(II) development will be manifested within the upcoming sections.

Table 1.2. Selected example for the effect of catalyst steric profile on reaction chemoselectivity.[91]

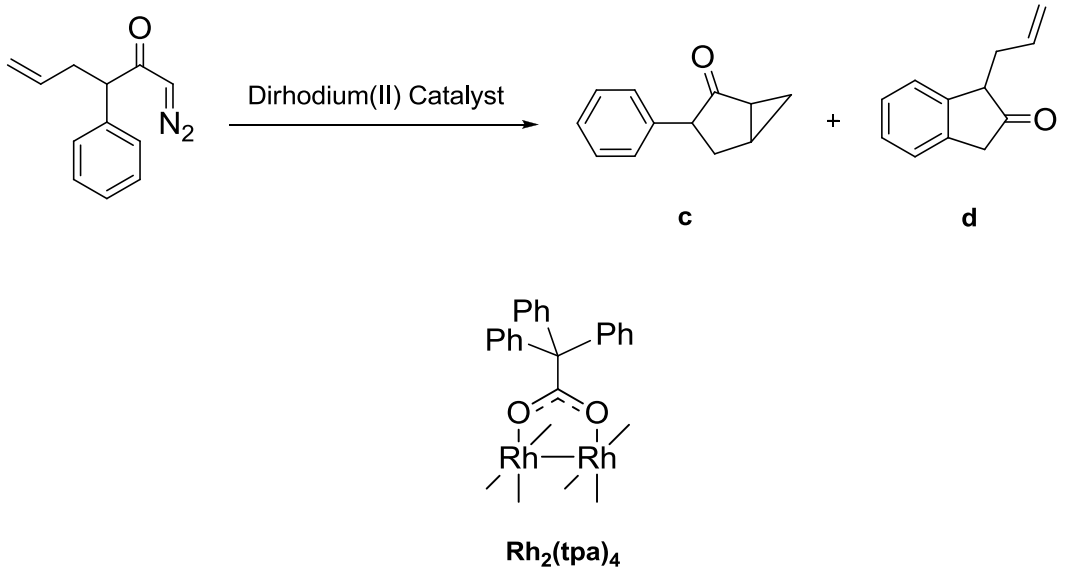

Entry	Catalyst	Yield (%)	c:d
1	$Rh_2(OAc)_4$	63	71:29
2	$Rh_2(tpa)_4$	83	0:100

1.5. DIRHODIUM(II) CARBOXYLATES

1.5.1. Conformations in dirhodium(II) carboxylate complexes

In general, conformation of chiral dirhodium(II) paddlewheel complexes is believed to be a critical factor in their chemistry and this topic was previously reviewed by Hansen and Davies.[9] In most dirhodium(II) catalysts, the ligand blocking groups would have a considerable conformational mobility. However, due to steric constraints, these blocking groups either adapt an "up (α)" or "down (β)" conformation (Figure 1.10). The blocking groups cannot lie in the periphery of the catalyst as it would bump into the adjacent ligand. Based on this and by considering

the α- and β-arrangement for all four ligands, four possible conformations may be generated: $\alpha,\alpha,\alpha,\alpha$ (C_4-symmetry), $\alpha,\alpha,\alpha,\beta$ (C_1-symmetry), $\alpha,\alpha,\beta,\beta$ (C_2-symmetry) and $\alpha,\beta,\alpha,\beta$ (D_2-symmetry)[80,14,9] (Figure 1.10).

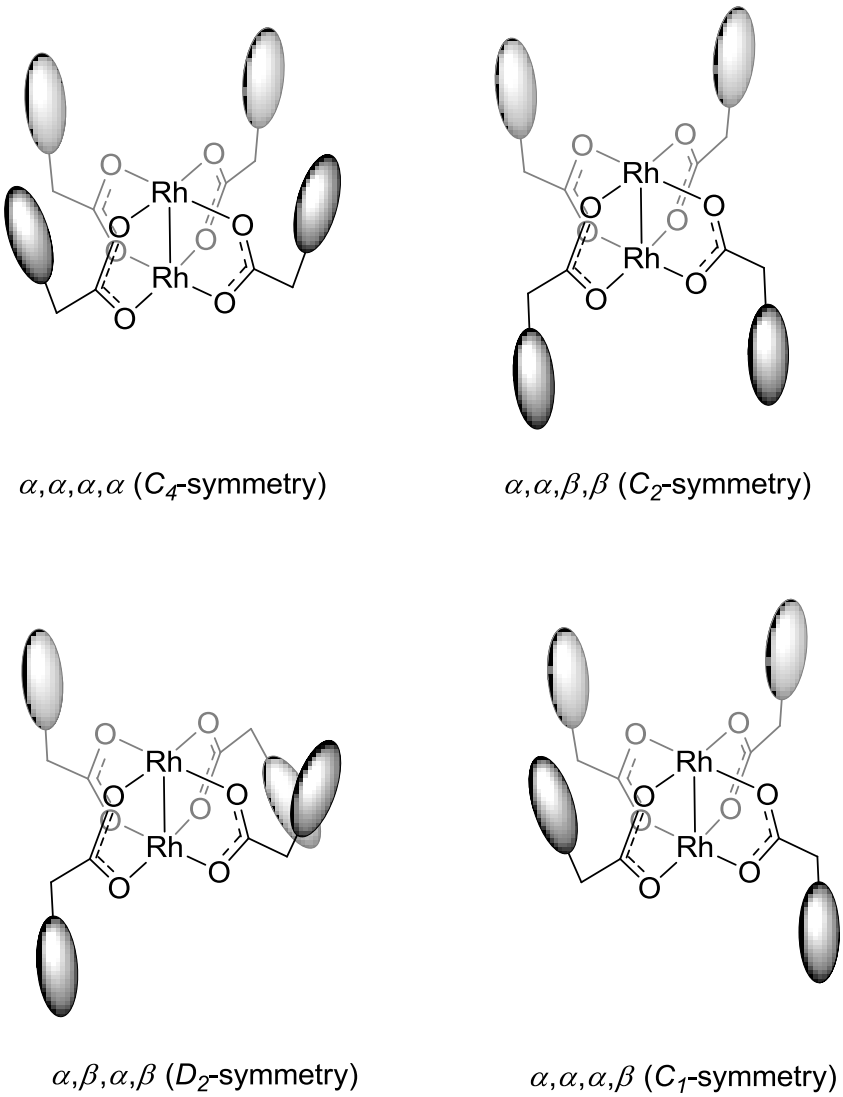

Figure 1.10. Models for different ligand arrangements (the sterically blocking groups around the rhodium active sites are depicted as ovals).[9]

1.5.2. Dirhodium(II) catalysts derived from prolinate ligands

Mckervey and co-workers[92-94] were the first to explore *N*-protected proline derivatives as carboxylate ligands (**9**, Figure 1.11). However, the importance of this kind of ligands was not recognized until Davies *et al.*[80,14] synthesized a series of

prolinate based chiral catalysts (**10-20**, Figure 1.11) and discovered that the long aliphatic chain variant, Rh_2(*S*-DOSP)$_4$ (**11**), was an exceptional chiral catalyst among the prepared series.

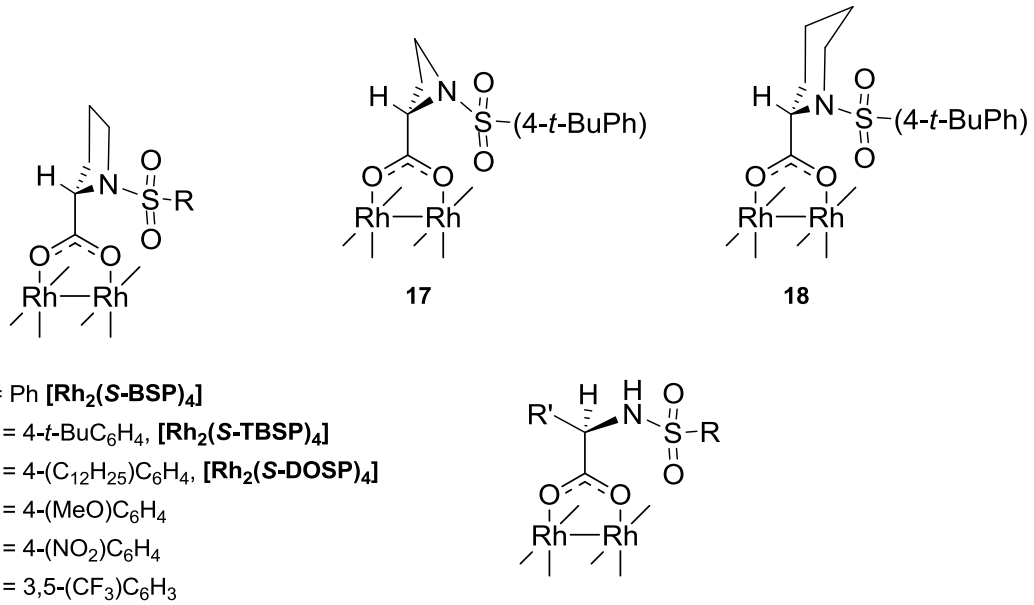

9 R = Ph **[Rh_2(*S*-BSP)$_4$]**
10 R = 4-*t*-BuC_6H_4, **[Rh_2(*S*-TBSP)$_4$]**
11 R = 4-($C_{12}H_{25}$)C_6H_4, **[Rh_2(*S*-DOSP)$_4$]**
12 R = 4-(MeO)C_6H_4
13 R = 4-(NO_2)C_6H_4
14 R = 3,5-(CF_3)C_6H_3
15 R = 2,4,6-(*i*-Pr)C_6H_2
16 R = *i*-Pr

19 R = 4-*t*-BuC_6H_4, R' = *i*-Pr
20 R = 4-(Me)C_6H_4, R' = $PhCH_2$

Figure 1.11. Dirhodium(II) carboxylates derived from chiral prolinate ligands (Mckervey complex **9**[92] and Davies complexes **10-20**[80]).

The high levels of asymmetric induction exhibited by dirhodium(II) prolinate complexes, especially Rh_2(*S*-DOSP)$_4$, has been suggested to originate from their favoured D_2-symmetrical arrangement in solution. As I will illustrate later in this chapter, the *N*-dodecylarylsulfonyl groups are stretched out and aligned in an $\alpha,\beta,\alpha,\beta$ arrangement. This generates a catalyst with two equivalent rhodium active sites with adequate sterically overburden groups to limit the trajectories approaching the axial carbene ligand (Figure 1.12).[9,14,80]

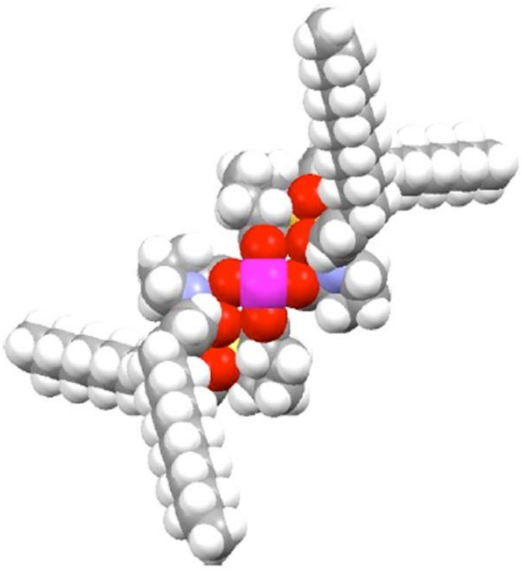

Figure 1.12. A 3D model for Rh_2(*S*-DOSP)$_4$ (top view).[9] (Reprinted from Hansen, J.; Davies, H. M. L. *Coord. Chem. Rev.* **2008**, *252*, 545, Copyright 2008, with permission from Elsevier).

Rh_2(*S*-DOSP)$_4$ has shown to be an excellent chiral catalyst for asymmetric cyclopropanations. Its utilization was expanded by the discovery that it is an exceptional catalyst for reactions involving *donor-acceptor* substituted carbenoids.[20,80,95-99] In the standard cyclopropanation reaction between styryldiazoacetate and styrene, Rh_2(*S*-DOSP)$_4$ was the optimum catalyst (Table 1.3). Even at -78 ^{o}C, Rh_2(*S*-DOSP)$_4$ is still an active catalyst leading to the formation of the cyclopropane product in 98% *ee*. This chemistry was successfully applied in the asymmetric total synthesis of (+)-Sertraline[100] and cyclopropyl amino acids.[80] But unfortunately, high asymmetric induction of Rh_2(*S*-DOSP)$_4$ is limited to *donor-acceptor* carbenoid systems.[14]

Rh_2(*S*-DOSP)$_4$-catalyzed decomposition of methyl phenylacetate in the presence of 1,1-diarylethylenes resulted in cyclopropane products with high enantioselectivity (up to 99% *ee*) and moderate diastereoselectivity (up to 80% *de*). This cyclopropanation reaction was utilized in the asymmetric total synthesis of a cyclopropyl analogue of Tamoxifen (Scheme 1.2).[99]

Table 1.3. Chiral catalysis approach for asymmetric *donor-acceptor* carbenoid cyclopropanation[14]

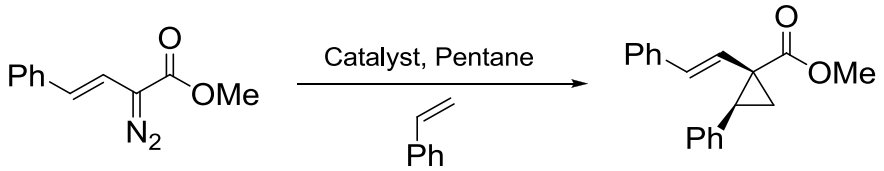

Entry	Catalyst	Temperature (°C)	*ee* (%)
1	Rh_2(*S*-TBSP)$_4$ (**10**)	25	90
2	Rh_2(*S*-DOSP)$_4$ (**11**)	25	92
3	Rh_2(*S*-DOSP)$_4$ (**11**)	-78	98

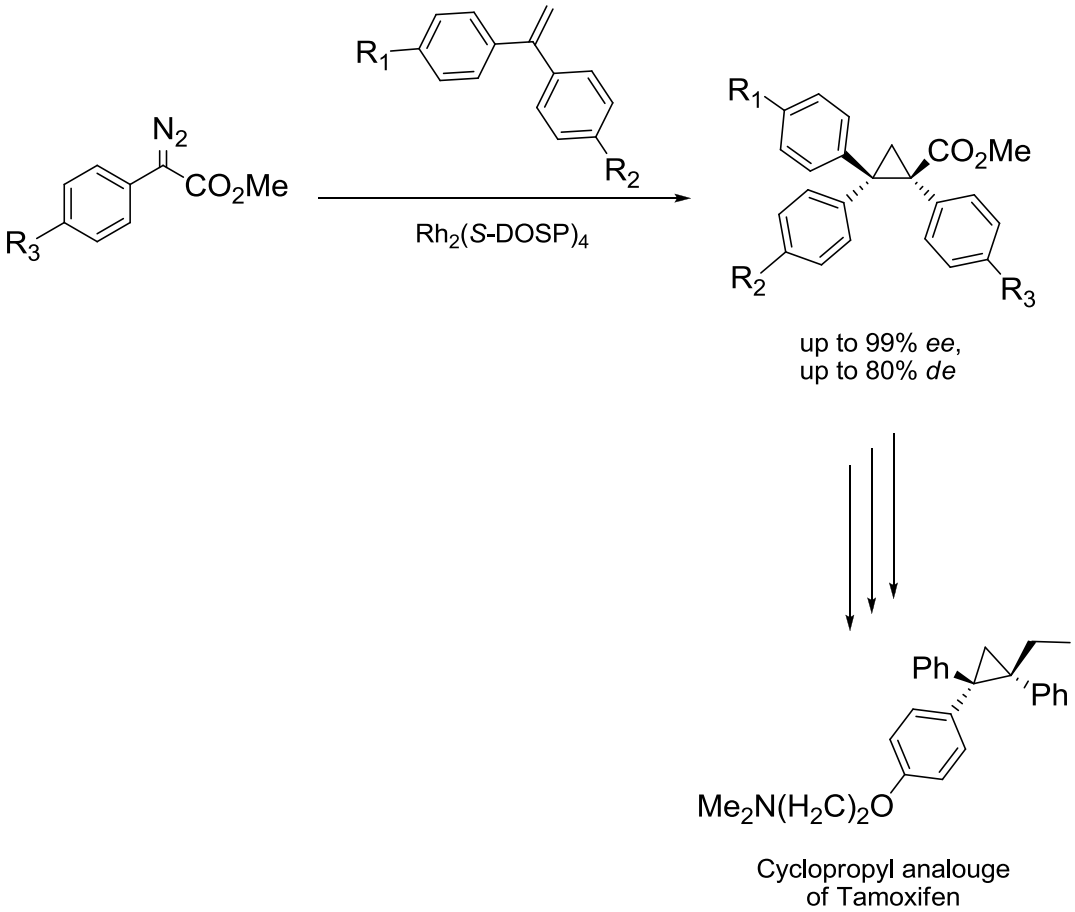

Scheme 1.2. Asymmetric total synthesis of cyclopropyl analogue of Tamoxifen.[99]

A solid-phase cyclopropanation version of the same reaction was also reported and it involved the reaction between phenyldiazoacetate and a resin-bonded alkene. Stereoselectivities were almost identical to those observed for the solution-phase reactions (Scheme 1.3).[101]

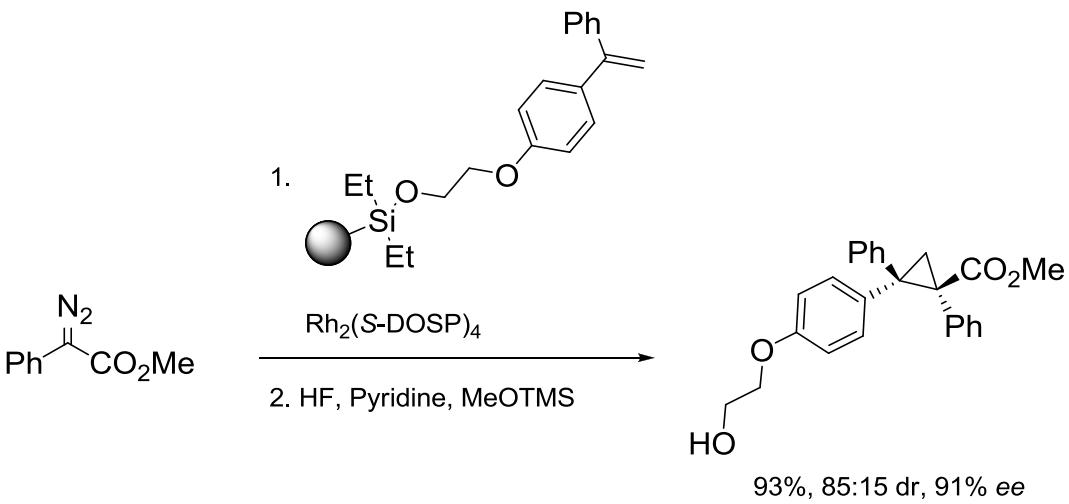

Scheme 1.3. Solid-phase cyclopropanation between phenyldiazoacetate and a resin bounded olefin.[101]

The scope of this chemistry was broadened when Rh_2(*S*-DOSP)$_4$-catalyzed decomposition of heteroaryldiazoacetates resulted in highly diastereoselective and enantioselective cyclopropanations (up to 97% *ee*). Heteroaryldiazoacetates containing both electron-rich and electron-deficient heterocycles, such as thiophene, furan, pyridine, indole, oxazole, isoxazole and benzoxazole, were effective for this reaction (Scheme 1.4).[97]

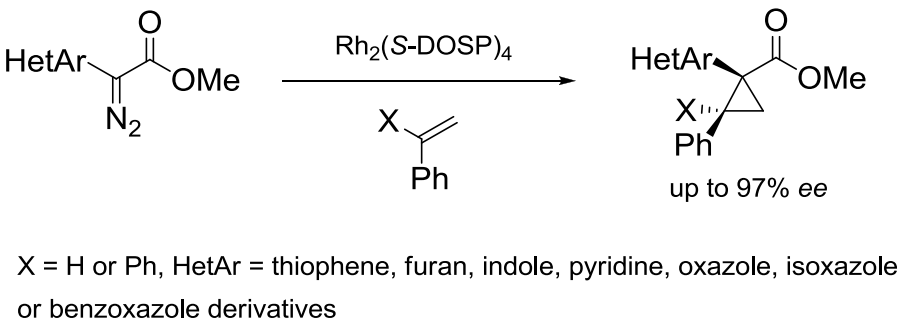

Scheme 1.4. Asymmetric cyclopropanations using heteroaryldiazoacetates.[97]

This chemistry was extended to include Rh_2(*S*-DOSP)$_4$-catalyzed decomposition of alkynyldiazoacetates. It led to alkynyl-substituted cyclopropanes with good to excellent enantiomeric induction (Scheme 1.5).[102]

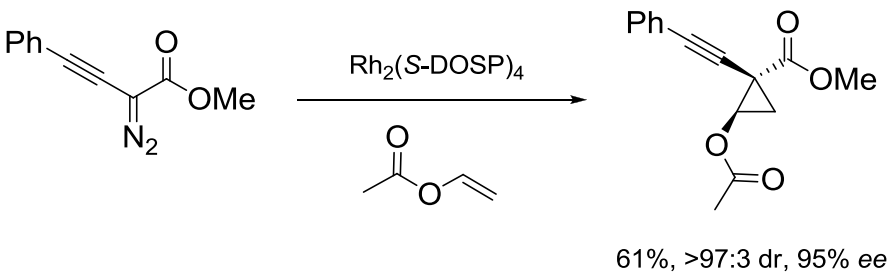

Scheme 1.5. Example for Rh_2(*S*-DOSP)$_4$-catalyzed decomposition of alkynyldiazoacetates.[102]

In 2006, the complementary nature of Rh(II)- and Pd(II)-catalyzed reactions was highlighted. Aryldiazoacetates containing reactive functionality for Palladium(II) cross-coupling reactions (iodide, triflate, organoboron and organostannane) are capable of effective rhodium-catalyzed enantioselective cyclopropanations without interference from the additional functionality.[103]

It was also reported that Rh_2(*R*-DOSP)$_4$ (the enantiomer of **11**, Figure 1.11) can be used to induce the decomposition of aryldiazoacetates in the presence of pyrroles or furans resulting in the formation of mono- or bis-cyclopropanes of the heterocycle, but with opposite enantioinduction (Scheme 1.6).[104] The enantioinduction was markedly influenced by the structure of the heterocyclic substrate. This methodology was applied to the total synthesis of the natural product, (+)-Erogorgiaene, on the basis of Rh_2(*S*-DOSP)$_4$-catalyzed cyclopropanation of dihydronaphthalene.[105]

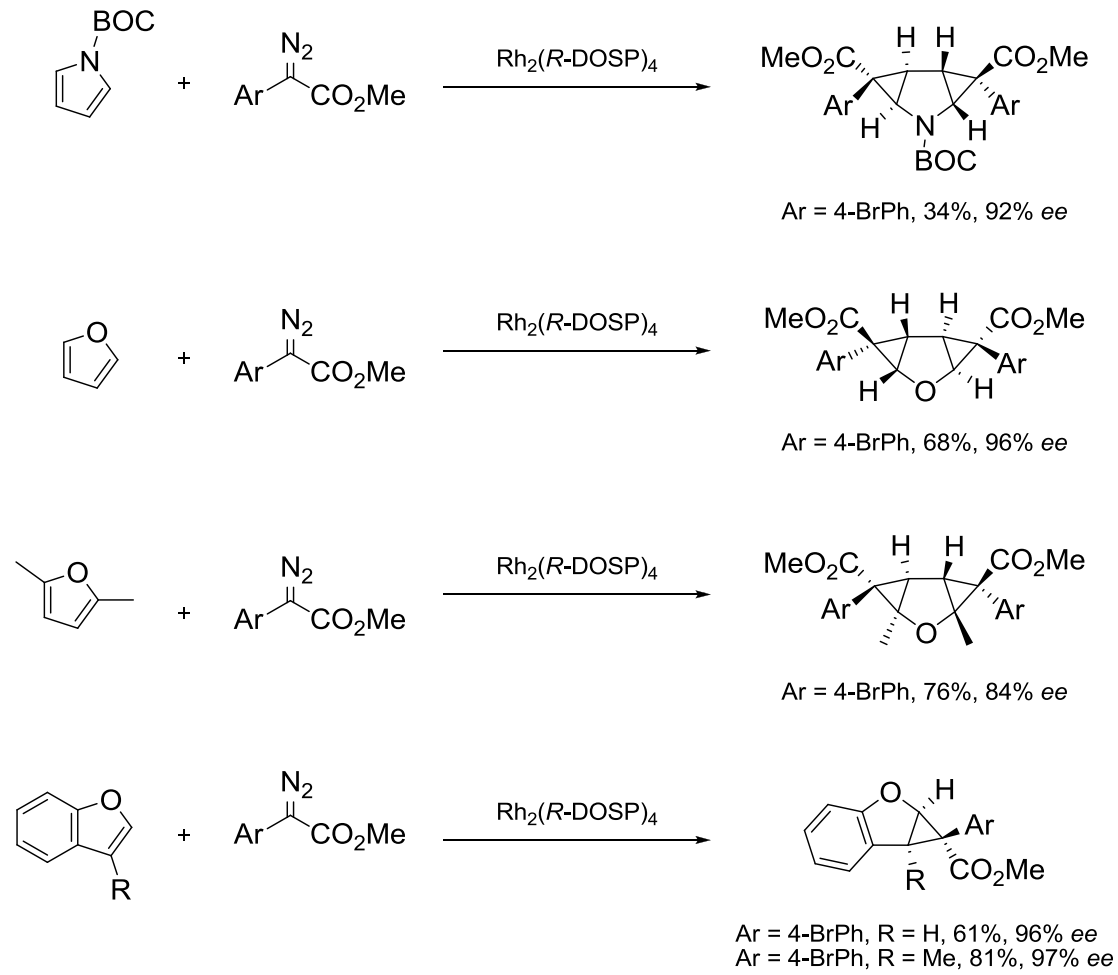

Scheme 1.6. Rh_2(*R*-DOSP)$_4$-catalyzed decompositions of aryldiazoacetates in the presence of pyrroles or furans.[104]

Recently, a study that provided guidelines for choosing the optimal chiral dirhodium(II) catalyst for cyclopropanation of substituted aryldiazoacetates was carried out. It confirmed that the expectation that Rh_2(*S*-DOSP)$_4$ would give high asymmetric induction for all aryldiazoacetates is not true. However, Rh_2(*S*-DOSP)$_4$ was found to be the most effective catalyst for the broadest range of substituted methyl aryldiazoacetates.[98]

A general hypothetical model has been proposed to explain the outcomes of dirhodium(II) prolinates-catalyzed asymmetric cyclopropanations (Scheme 1.7).

In this model, the most stable conformation of these catalysts is believed to have a D_2-symmetry. Once the carbenoid is formed, its *si*-face is protected by a sulfonyl ligand behaving as a blocking group. Approach of the alkene takes place over the electron withdrawing group (EWG) from the *re*-face, resulting in the formation of the observed diastereomer configuration.[14,80,97,99]

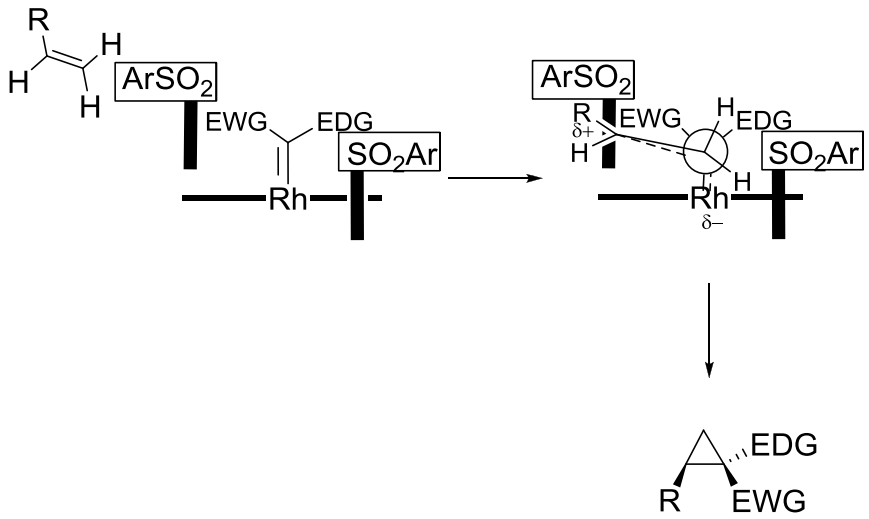

Scheme 1.7. Hypothetical model for asymmetric induction by dirhodium(II) (*S*)-prolinate catalysts.

Gregg *et al.*[106,107] investigated the enantioselective cyclopropanation of allenes using aryldiazoacetate esters mediated by Rh_2(*S*-DOSP)$_4$ as a catalyst. The reaction led to the generation of alkylidene cyclopropane products in 80 to 90% *ee* (Table 1.4).

Table 1.4. Cyclopropanation of allenes with *p*-bromophenyldiazoacetate.[106,107]

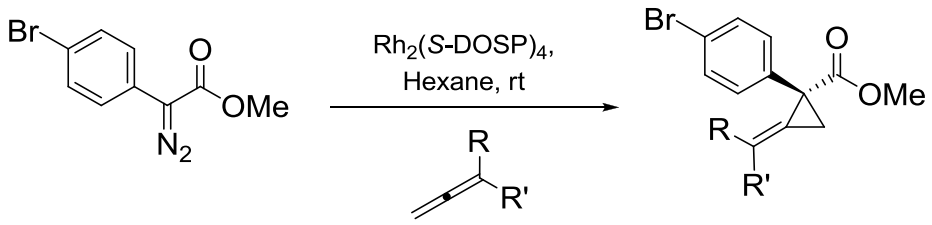

Entry	R	R’	Yield (%)	*ee* (%)
1	Ph	H	76	90
2	*p*-ClC_6H_4	H	61	84
3	C_5H_{11}	H	60	88
4	Bn	H	54	>80
5	Ph	Me	33	86
6	Me	Me	30	90
7	TMS	Me	79	85

Based on the D_2-symmetry hypothesis, second generation prolinate complexes were designed (Figure 1.13). In these complexes, the arylsulfonyl groups were conformationaly locked in the $\alpha,\beta,\alpha,\beta$ arrangement.[108,109] This was achieved by the synthesis of bidentate C_2-symmetric ligands with two sulphonylprolinates linked together. As the ligands themselves are possessing a C_2-symmetry, a higher D_2-symmetry was accessible affording a more rigid version of the $\alpha,\beta,\alpha,\beta$-complexes carrying the C_1-symmetric ligands. In the new complexes, not only both rhodium faces are equivalent, but also all staggered binding orientations of the axial substituent involved in the asymmetric reaction are identical with respect to the approaching substrate.[109,9]

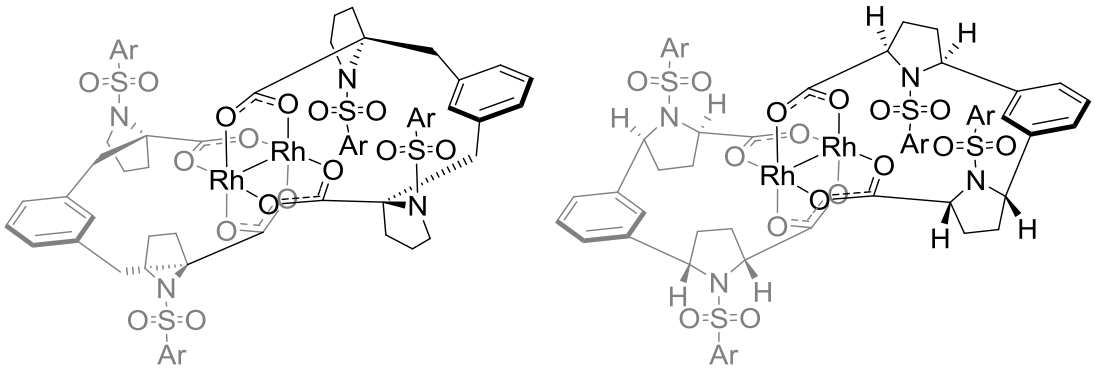

Ar = 4-*t*-BuC$_6$H$_4$

Ar = 4-*t*-BuC$_6$H$_4$ **[Rh$_2$(*S*-biTBSP)$_2$]**
Ar = 4-C$_{12}$H$_{25}$C$_6$H$_4$ **[Rh$_2$(*S*-biDOSP)$_2$]**
Ar = 2,4,6-tri*i*-prC$_6$H$_4$ **[Rh$_2$(*S*-biTISP)$_2$]**

Figure 1.13. Second generation prolinate complexes.[108,109]

The demonstration that the rigid bridged prolinate Rh$_2$(*S*-biTISP)$_2$ is an excellent catalyst for asymmetric cyclopropanation (Scheme 1.8) added further support to the proposed concept that the efficiency of Rh$_2$(*S*-DOSP)$_4$ as a chiral catalyst is due to the arrangement of the ligands in a D_2-symmetry.[109]

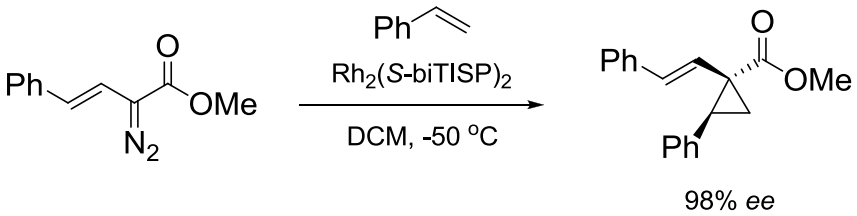

Scheme 1.8. Rh$_2$(*S*-biTISP)$_2$-catalyzed cyclopropanation.[109]

In contrast to intermolecular cyclopropanation, dirhodium(II) prolinates result in modest enantioselectivities for intramolecular cyclopropanation reactions with *donor-acceptor* carbenoids. For example, Rh$_2$(*S*-DOSP)$_4$-catalyzed cyclopropanation of allyl vinyldiazoacetate afforded the corresponding fused cyclopropyl lactone in 72% *ee* (Scheme 1.9).[110]

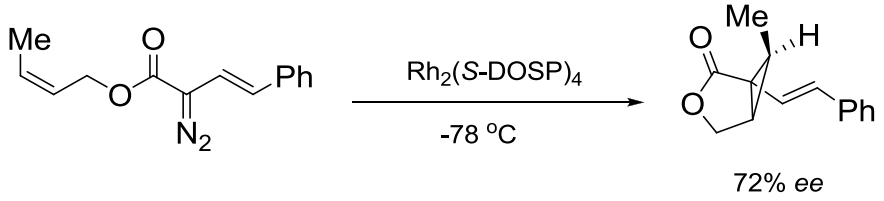

Scheme 1.9. Rh_2(*S*-DOSP)$_4$-catalyzed cyclopropanation of allyl vinyldiazoacetate.[110]

1.5.3. Dirhodium(II) catalysts derived from chiral *N*-protected amino acid ligands

1.5.3.1. Homoleptic complexes

Hashimoto, Ikegami and co-workers[111-118] have developed a series of homochiral dirhodium(II) carboxylate complexes derived from enantiomerically pure *N*-phthalimido protected L-amino acids as ligands (**21-35**, Figure 1.14). The optimum group at the *α*-carbon groups can vary depending on the reaction,[9] but, in general, the *tert*-butyl derivative, Rh_2(*S*-PTTL)$_4$ (**32**), is the catalyst with the broadest application in asymmetric cyclopropanations. Other catalysts were also introduced by vertically extending the length of the *N*-phthalimide moiety (**36-39**, Figure 1.14).[112,8]

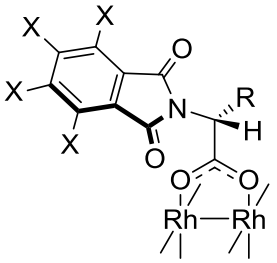

21 R = $PhCH_2$, X =H **[Rh_2(*R*-PTPA)$_4$]**
22 R = *t*-Bu, X= H, **[Rh_2(*R*-PTTL)$_4$]**
23 R = *t*-Bu, X= Cl, **[Rh_2(*R*-TCPTTL)$_4$]**

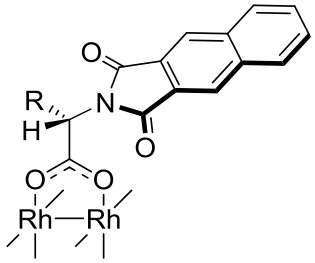

36 R = $PhCH_2$, **[Rh_2(*S*-BPTPA)$_4$]**
37 R = Me, **[Rh_2(*S*-BPTA)$_4$]**
38 R = *i*-Pr, **[Rh_2(*S*-BPTV)$_4$]**
39 R = *t*-Bu, **[Rh_2(*S*-BPTTL)$_4$]**

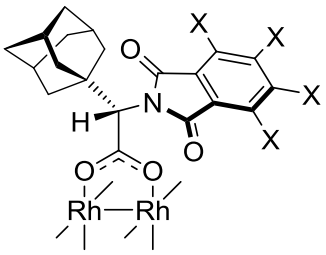

53 X= H, **[Rh_2(*S*-PTAD)$_4$]**
54 X= Cl, **[Rh_2(*S*-TCPTAD)$_4$]**

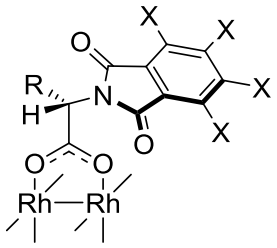

24 R = $PhCH_2$, X= H, **[Rh_2(*S*-PTPA)$_4$]**
25 R = $PhCH_2$, X= Cl, **[Rh_2(*S*-TCPTPA)$_4$]**
26 R = Me, X= H, **[Rh_2(*S*-PTA)$_4$]**
27 R = Me, X= Cl, **[Rh_2(*S*-TCPTA)$_4$]**
28 R = Et, X= H, **[Rh_2(*S*-PTTEA)$_4$]**
29 R = *i*-Pr, X= H, **[Rh_2(*S*-PTV)$_4$]**
30 R = *i*-Pr, X= Cl, **[Rh_2(*S*-TCPTV)$_4$]**
31 R = *i*-Pr, X= Br, **[Rh_2(*S*-TBPTV)$_4$]**
32 R = *t*-Bu, X= H, **[Rh_2(*S*-PTTL)$_4$]**
33 R = *t*-Bu, X= Cl, **[Rh_2(*S*-TCPTTL)$_4$]**
34 R = *t*-Bu, X= F, **[Rh_2(*S*-TFPTTL)$_4$]**
35 R = *t*-Bu, X= Br, **[Rh_2(*S*-TBPTTL)$_4$]**

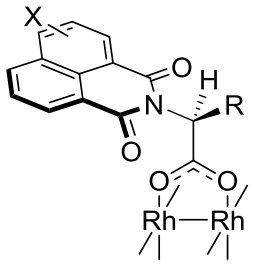

40 R = Me, X = H; **[Rh_2(*S*-NTV)$_4$]**
41 R = *t*-Bu, X = H; **[Rh_2(*S*-NTTL)$_4$]**
42 R = *t*-Bu, X = 4-Cl; **[Rh_2(*S*- 4-Cl-NTTL)$_4$]**
43 R = *t*-Bu, X = 3-Cl; **[Rh_2(*S*-3-Cl-NTTL)$_4$]**
44 R = *t*-Bu, X = 4-Br; **[Rh_2(*S*-4-Br-NTTL)$_4$]**
45 R = *t*-Bu, X = 4-NO_2; **[Rh_2(*S*-4-NO_2-NTTL)$_4$]**
46 R = *t*-Bu, X = 3-NO_2; **[Rh_2(*S*-3-NO_2-NTTL)$_4$]**
47 R = $PhCH_2$, X = H; **[Rh_2(*S*-NTPA)$_4$]**
48 R = $PhCH_2$, X = 4-Cl; **[Rh_2(*S*- 4-Cl-NTPA)$_4$]**
49 R = $PhCH_2$, X = 3-Cl; **[Rh_2(*S*- 3-Cl-NTPA)$_4$]**
50 R = $PhCH_2$, X = 4-Br; **[Rh_2(*S*-4-Br-NTPA)$_4$]**
51 R = $PhCH_2$, X = 4-NO_2; **[Rh_2(*S*-4-NO_2-NTPA)$_4$]**
52 R = $PhCH_2$, X = 3-NO_2; **[Rh_2(*S*-3-NO_2-NTPA)$_4$]**

Figure 1.14. Structures of reported chiral dirhodium(II) carboxylates derived from chiral *N*-protected amino acid ligands (Hashimoto complexes **21**-**39**,[119-121,115,112] Dauban complex **40**,[122] Müller and Ghanem complexes[123] **41**-**52** and Davies complexes **53**-**54**[124-126]).

Fox *et al.*[127] investigated if Rh_2(*S*-PTTL)$_4$ could be useful for intermolecular cyclopropanation reactions of *α*-alkyldiazo compounds that originally gives products of *β*-hydride elimination. The catalyst led to cyclopropane products with high diastereoselectivity and yield, while the enantioselectivity was highly sensitive to the structure of the diazoester and larger *α*-alkyl substituents led to increasingly higher *ee* (Table 1.5).

Table 1.5. Rh_2(*S*-PTTL)$_4$-catalyzed intermolecular cyclopropanation reactions of *α*-alkyldiazo compounds.[127]

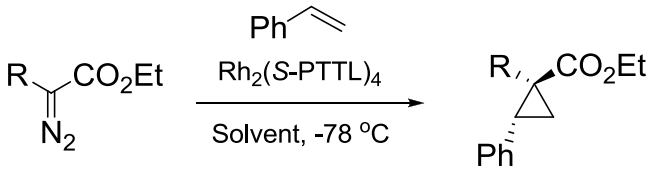

Entry	R	Yield (%)	dr	*ee* (%)
1	Me	95	91:9	3
2	Et	95	92:8	79
3	*n*-Pr	100	>95:5	94
4	*n*-Bu	96	>95:5	96
5	*i*-Bu	92	>95:5	99

Awatta and Arai[128] further reported the Rh_2(*S*-PTTL)$_4$-catalyzed asymmetric cyclopropanation of diazooxindole generating the corresponding spiro-cyclopropyloxindole products with high levels of diastereoselectivity and moderate to good enantioselectivity (Table 1.6).

Table 1.6. Rh_2(*S*-PTTL)$_4$-catalyzed asymmetric cyclopropanation of diazooxindole with various olefins.[128]

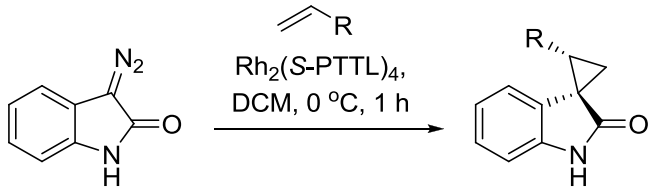

Entry	R	Yield (%)	dr	*ee* (%)
1	Ph	>99	98:2	66
2	4-ClC_6H_4	>99	97:3	65
3	3-ClC_6H_4	98	98:2	60
4	2-ClC_6H_4	92	96:4	66
5	4-FC_6H_4	>99	96:4	64
6	4-MeC_6H_4	>99	96:4	62
7	4-$MeOC_6H_4$	>99	93:7	48
8	*n*-C_3H_5	65	88:12	74

Likewise, Charette[121] reported the first catalytic enantioselective cyclopropanation of alkenes with *α*-nitro diazoacetophenones as part of their *trans*-directing group investigations. Rh_2(*S*-TCPTTL)$_4$ (**33**, Figure 1.14) proved to be the most suitable catalyst for this kind of asymmetric cyclopropanations. For example, the Rh_2(*S*-TCPTTL)$_4$-catalyzed cyclopropanation of styrene with *α*-nitro-*α*-diazo-*p*-methoxyacetophenone gave the product in 93% *ee* (Table 1.7). The corresponding products obtained from this reaction were used as precursors for the synthesis of optically active *cis*-cyclopropane *α*-amino acids.

Table 1.7. Rh_2(*S*-TCPTTL)$_4$-catalyzed cyclopropanation of styrene with *α*-nitro-*α*-diazo-*p*-methoxyacetophenone.[121]

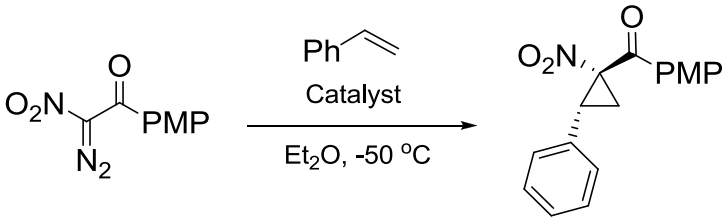

Entry	Catalyst	Yield (%)	dr	*ee* (%)
1	Rh_2(*S*-PTA)$_4$ (**26**)	55	53:47	22
2	Rh_2(*S*-PTPA)$_4$ (**24**)	56	55:45	43
3	Rh_2(*S*-PTV)$_4$ (**29**)	76	72:28	16
4	Rh_2(*S*-PTTL)$_4$ (**32**)	80	33:67	2
5	Rh_2(*S*-TCPTA)$_4$ (**27**)	81	97:3	92
6	Rh_2(*S*-TCPTPA)$_4$ (**25**)	72	94:6	91
7	Rh_2(*S*-TCPTV)$_4$ (**30**)	82	98:2	91
8	Rh_2(*S*-TCPTTL)$_4$ (**33**)	81	98:2	93
9	Rh_2(*S*-TBPTV)$_4$ (**31**)	89	96:4	80
10	Rh_2(*S*-TCPTTL)$_4$ (**33**)	70	99:1	92
11	Rh_2(*S*-TCPTTL)$_4$ (**33**)	80	98:2	93

This method was further extended to different *diacceptor* *α*-EWG-diazoacetophenones bearing an *α*-PMP-ketone group, as diastereo- and enantioselectivity control group. They were found to be effective carbene precursors for Rh_2(*S*-TCPTTL)$_4$-catalyzed highly stereoselective cyclopropanation of alkenes (Table 1.8).[129]

Table 1.8. Rh_2(*S*-TCPTTL)$_4$-catalyzed cyclopropanation of several *α*-EWG-diazoacetophenones bearing an *α*-*p*-methoxyphenyl (PMP)-ketone group.[129]

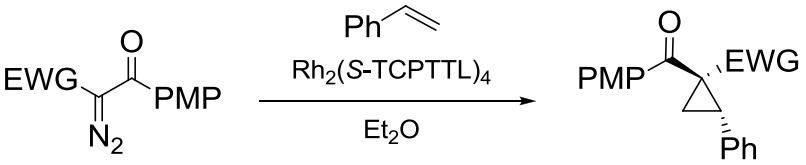

Entry	EWG	Temp. (^{o}C)	Yield (%)	dr	*ee* (%)
1	NO_2	-50	81	98:2	93
2	CN	-35	98	95:5	84
3	CO_2Me	-40	60	99:1	88
4	Ph	-50	9	>95:5	98

Rh_2(*S*-TBPTTL)$_4$ (**35**, Figure 1.14) was also reported as an exceptionally effective catalyst for asymmetric cyclopropanation reactions of 1-aryl-substituted and related conjugated alkenes with *tert*-butyl *α*-diazopropionate.[130] High levels of enantioselectivity (up to 93% *ee*), as well as virtually complete *trans*-diastereoselectivity were successfully achieved (Table 1.9). According to the authors, this protocol represented the first example of catalytic asymmetric cyclopropanation of alkenes with *α*-diazopropionates and partially complements the above discussed Fox cyclopropanation methodology.

Table 1.9. Rh_2(*S*-TBPTTL)$_4$-catalyzed cyclopropanation of styrene with *α*-diazopropionates.[130]

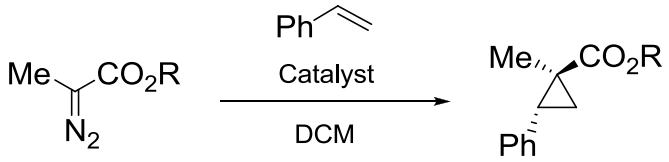

Entry	R	Catalyst	Temp. (°C)	Yield (%)	dr	*ee* (%)
1	CH(*i*-Pr)$_2$	Rh_2(*S*-PTTL)$_4$ (**32**)	-60	89	94:6	47
2	CH(*i*-Pr)$_2$	Rh_2(*S*-TFPTTL)$_4$ (**34**)	-60	86	92:8	33
3	CH(*i*-Pr)$_2$	Rh_2(*S*-TCPTTL)$_4$ (**33**)	-60	89	95:5	69
4	CH(*i*-Pr)$_2$	Rh_2(*S*-TBPTTL)$_4$ (**35**)	-78	86	>99:1	86
5	Et	Rh_2(*S*-TBPTTL)$_4$ (**35**)	-60	80	91:9	35
6	*t*-Bu	Rh_2(*S*-TBPTTL)$_4$ (**35**)	-78	87	>99:1	92

Similar types of catalysts using *N*-1,8-naphthaloyl-L-amino acids were developed by Müller and co-workers[131-133] (**41-52**, Figure 1.14). They demonstrated the suitability of Rh_2(*S*-NTTL)$_4$ catalyst (**41**, Figure 1.14) for Rh-catalyzed cyclopropanation of styrene with (silanyloxyvinyl)diazoacetates producing exceptional diastereo- and enantioselectivities (Scheme 1.10a).[134] The scope of the catalyst was extended with respect to the alkene to include dihydrofuran and dihydropyran (Scheme 1.10b,c).[135,136] When this methodology was applied to ethyl diazo(triethylsilyl)acetate, it gave the corresponding cyclopropane in a good yield (69%), but with modest diastereoselectivity (64% *de*) and enantioselectivity (54% *ee*).[137]

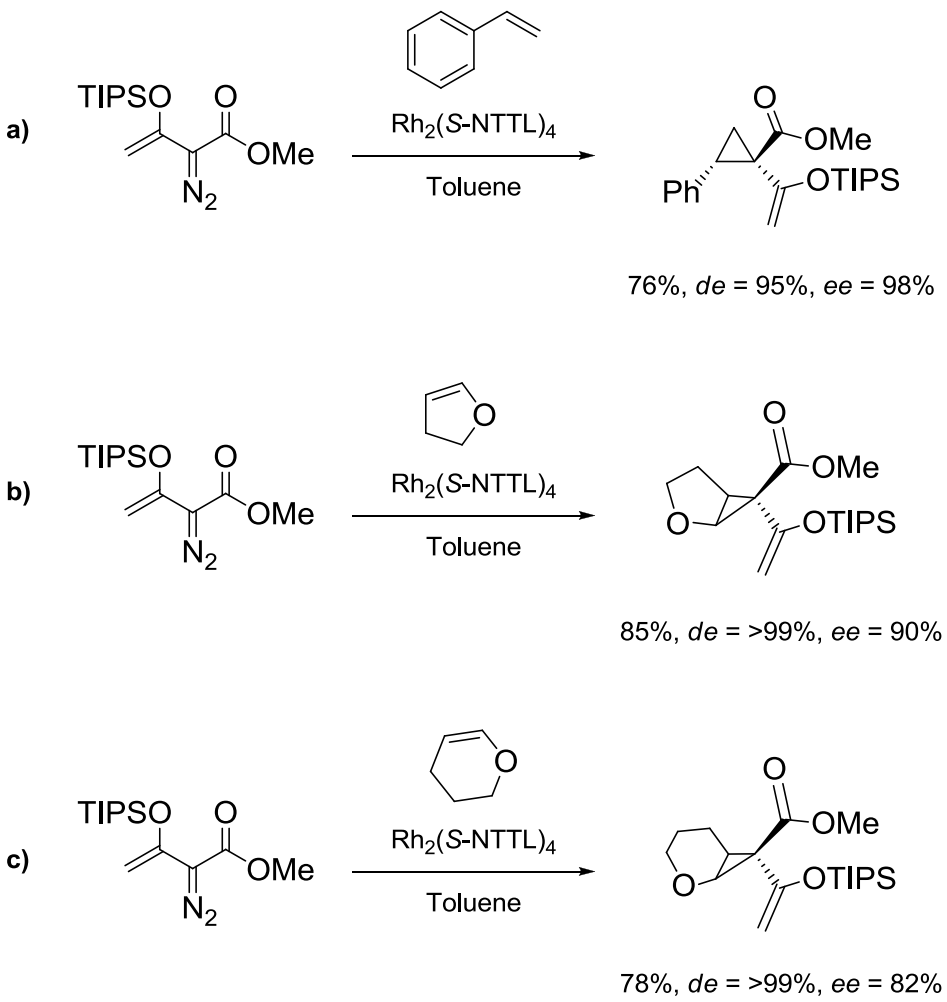

Scheme 1.10. Rh_2(*S*-NTTL)$_4$-catalyzed cyclopropanation of (silanyloxyvinyl)-diazoacetates.[134-136]

Charette *et al.*[138-141] described the enantioselective formation of 1,1-cyclopropane diesters *via* Rh_2(*S*-NTTL)$_4$-catalyzed cyclopropanation of olefins (Scheme 1.11). They were the first to elaborate the concept of the *trans*-directing ability of amide groups in Rh(II)-catalyzed cyclopropanation reactions. This concept provided a solution for the stereoselective synthesis of 1,1-dicarboxycyclopropane derivatives.

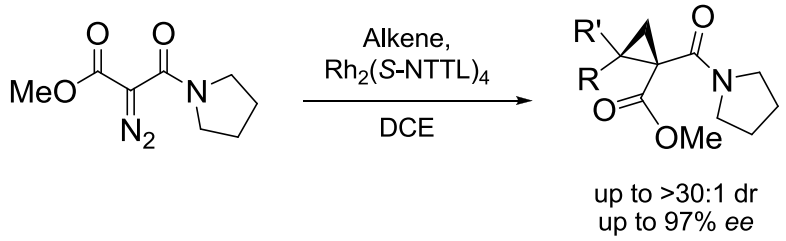

Scheme 1.11. Rh_2(*S*-NTTL)$_4$-catalyzed enantioselective formation of 1,1-cyclopropane diesters (*trans*-directing group concept).[138-141]

The authors hypothesized that the in-out conformation for a carbene derived from malonates is operative. Placing one group in the same plane of the metal carbene liberates space for an alkene to approach and enhances the electrophilicity of the carbenoid.[138,139] The out-of-plane substituent can act as a *trans*-directing group and transition states I-IV (Figure 1.15a) would be plausible. Assuming that the use of a chiral catalyst would be effective at blocking the pro-(*S*)-face, they found that the four possible transition state structures would lead to a pair of enantiomers. These postulations may explain the low enantiocontrol obtained to date with Rh(II)-catalyzed cyclopropanation of malonates.

One of the proposed strategies was using a carbene that possesses two different groups with different *trans*-directing abilities, in combination with, a catalyst that would be effective at blocking one of the two prochiral faces. Transition states VII and IX (Figure 1.15b) would not be accessible due to the greater *trans*-directing ability of the COR group. By applying this strategy and by using Rh_2(*S*-NTTL)$_4$ as a catalyst, the authors succeeded in obtaining the cyclopropane products with enantioselectivities up to 97% *ee* and diastereoselectivities up to >30:1 dr.[138,139]

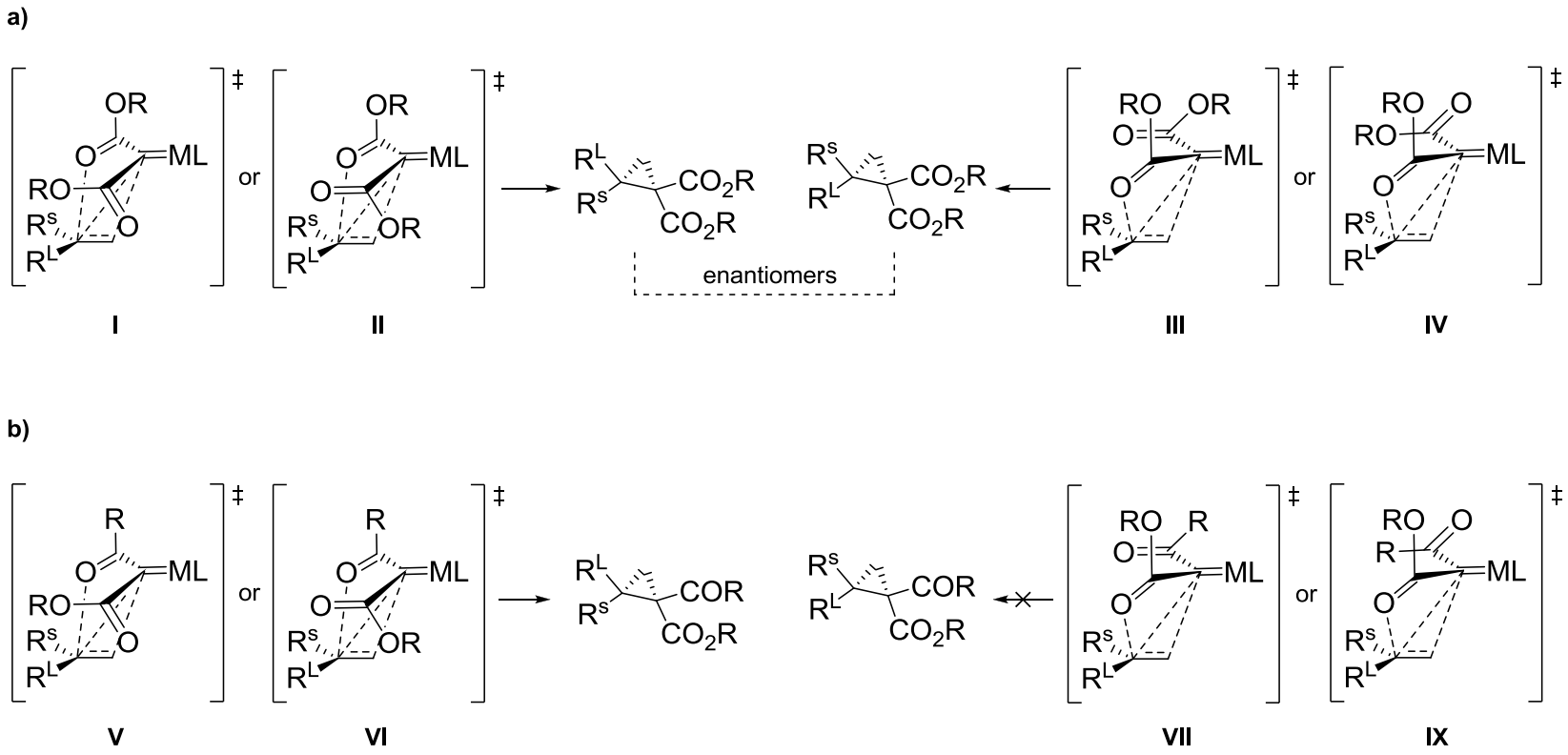

Figure 1.15. a) Rh(II)-catalyzed cyclopropanation transition states of diazomalonates as carbene precursors; b) The proposed strategy with carbenoids possessing two different groups with different *trans*-directing abilities.[138,139]

The potential utility of this property was further illustrated in several functional group transformations and in the stereoselective synthesis of (*S*)-(+)-Curcumene, (*S*)-(+)-Nuciferal, (*S*)-(+)-Nuciferol, (+)-Erogorgiaene, (±)-Xanthorrhizol and (±)-2-Hydroxycalamenene.[138]

The performance of Rh_2(*S*-NTTL)$_4$, Rh_2(*S*-PTTL)$_4$ and Rh_2(*S*-DOSP)$_4$ catalysts in intramolecular cyclopropanation of allyl 2-diazo-3-silanyloxybut-3-enoates was also examined by Müller *et al.*[142,136] (Table 1.10). The best results were obtained with Rh_2(*S*-PTTL)$_4$, where 89% *ee* was observed at -78 ^{o}C. Rh_2(*S*-NTTL)$_4$ was slightly less selective, while Rh_2(*S*-DOSP)$_4$ was found not suitable for these substrates.

Table 1.10. Intramolecular cyclopropanation of 1-phenyl-1-propenyl 2-diazo-3-silanyloxybut-3-enoates.[142]

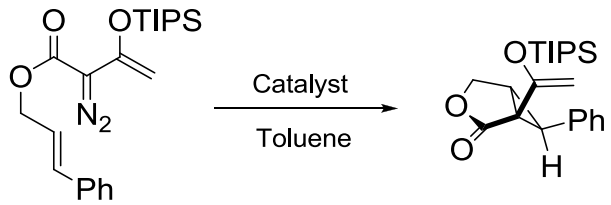

Entry	Catalyst	Temp. (^{o}C)	Yield (%)	*ee* (%)
1	Rh_2(*S*-NTTL)$_4$ (**41**)	rt	77	73
2	Rh_2(*S*-PTTL)$_4$ (**32**)	rt	93	77
3	Rh_2(*S*-PTTL)$_4$ (**32**)	-78	66	89
4	Rh_2(*S*-DOSP)$_4$ (**11**)	rt	69	5

Fokin *et al.*[143] reported a novel Rh_2(*S*-NTTL)$_4$-catalyzed asymmetric cyclopropanation methodology that utilizes *N*-sulfonyl-1,2,3-triazoles as azavinyl carbene precursors. The azavinyl carbenes readily reacted with various olefins providing cyclopropane carboxaldehydes in very high levels of enantioselectivity (Scheme 1.12a). Examination of the scope of the reaction with respect to the 1-sulfonyltriazole revealed that substrates possessing both electron-rich and electron-deficient aryl groups at C4 reacted smoothly to produce the cyclopropane products with excellent enantioselectivity (up to 98% *ee*). Moreover, the authors recognized that reduction of imine product with $LiAlH_4$ immediately after their synthesis had the ability to provide an easy access to aminocyclopropanes in good yields and excellent enantioselectivity (Scheme 1.12b).

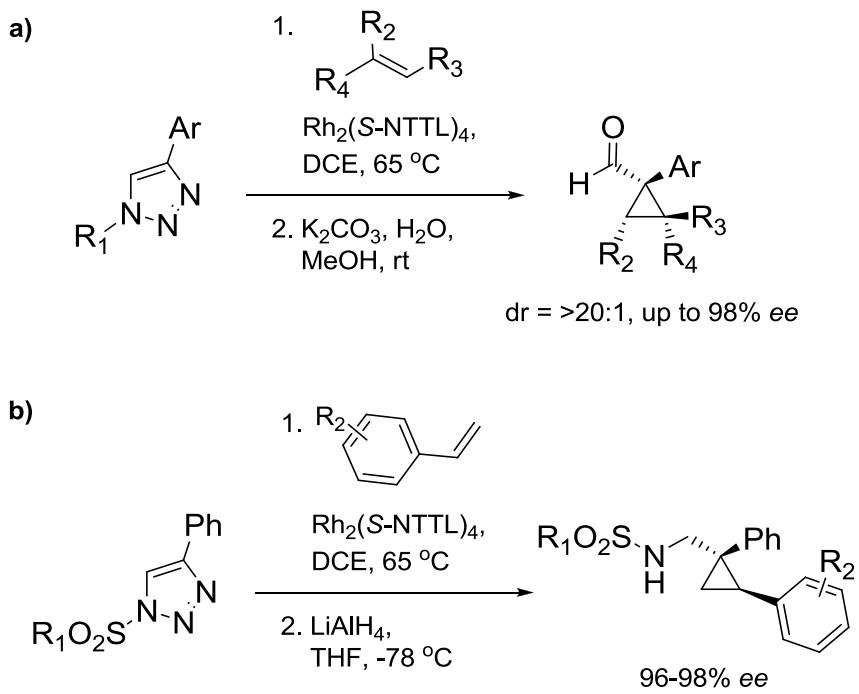

Scheme 1.12. Enantioselective cyclopropanation with 1,2,3-triazoles.[143]

Müller, Ghanem and co-workers[144,123] reported a number of substituted Rh_2(*S*-NTTL)$_4$ analogues (**42-52**, Figure 1.14) with Rh_2(*S*-4-Br-NTTL)$_4$ (**44**) giving the best enantioselectivity. This catalyst will be discussed in details in Chapter 2, Section 2.1.

In 2006, Davies *et al.*[124] suggested that the logical way for further improvement of the Rh_2(*S*-PTTL)$_4$ catalyst and analogues was to have a much bulkier hydrocarbon than the *tert*-butyl group at the *α*-carbon. They used their own developed C-H activation chemistry to access the synthetic amino acid, L-adamantylglycine, in enantiomerically pure form[124] for the preparation of Rh_2(*S*-PTAD)$_4$ (Scheme 1.13).

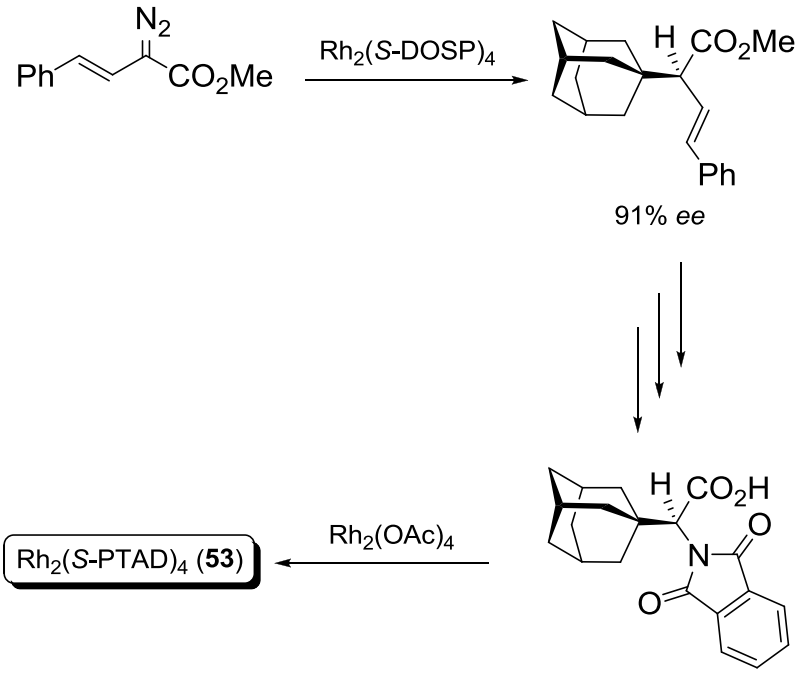

Scheme 1.13. Synthesis of Rh_2(*S*-PTAD)$_4$ catalyst (**53**).[124]

Rh_2(*S*-PTAD)$_4$ catalyst was applied to the stereoselective synthesis of dimethyl 1,2-diphenylcyclopropylphosphonate containing quaternary stereocenters. The results demonstrated that Rh_2(*S*-PTAD)$_4$ was a very effective catalyst, at which the cyclopropylphosphonate product was obtained in high levels of enantioselectivity (99% *ee*) compared to Rh_2(*S*-DOSP)$_4$ (34% *ee*), Rh_2(*S*-biTISP)$_2$ (88% *ee*) and Rh_2(*S*-PTTL)$_4$ (97% *ee*) (Table 1.11).[124]

Table 1.11. Enantioselective preparation of dimethyl 1,2-diphenylcyclopropylphosphonate.[124]

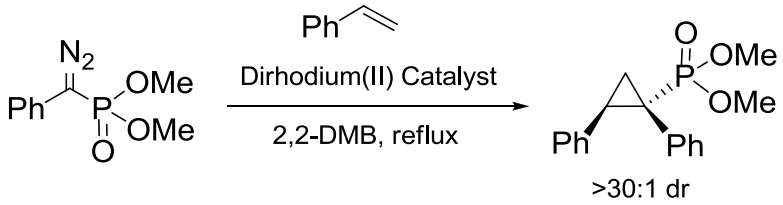

Entry	Catalyst	Yield (%)	*ee* (%)
1	Rh_2(*S*-DOSP)$_4$ (**11**)	69	34
2	Rh_2(*S*-biTISP)$_2$	89	88
3	Rh_2(*S*-PTTL)$_4$ (**32**)	85	97
4	Rh_2(*S*-PTAD)$_4$ (**53**)	86	99

In the same context, the Rh_2(*S*-PTAD)$_4$-catalyzed reaction of 1-aryl-2,2,2-trifluorodiazoethanes or α-diazo-2-phenylacetonitrile with electron rich alkenes generated the corresponding trifluoromethyl-substituted or nitrile-substituted cyclopropanes, respectively, with high levels of diastereoselectivity and enantioselectivity (Tables 1.12 and 1.13).[125,145]

Table 1.12. Dirhodium(II)-catalyzed enantioselective synthesis of trifluoromethyl-substituted cyclopropanes.[125]

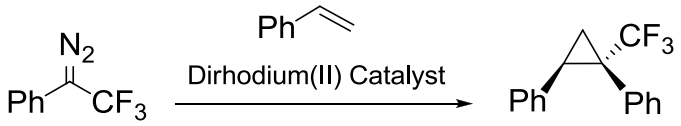

Entry	Catalyst	Solvent	Yield (%)	*de* (%)	*ee* (%)
1	Rh_2(*S*-DOSP)$_4$ (**11**)	Hexanes	80	94	40[a]
2	Rh_2(*S*-DOSP)$_4$ (**11**)	TFT	60	90	37[a]
3	Rh_2(*S*-PTTL)$_4$ (**32**)	TFT	95	>94	97
4	Rh_2(*S*-PTTL)$_4$ (**32**)	CH_2Cl_2	96	>94	86
5	Rh_2(*S*-PTAD)$_4$ (**53**)	TFT	94	>94	>98

[a]Opposite enantiomer preferentially formed.

Table 1.13. Dirhodium(II)-catalyzed enantioselective synthesis of nitrile-substituted cyclopropanes.[145]

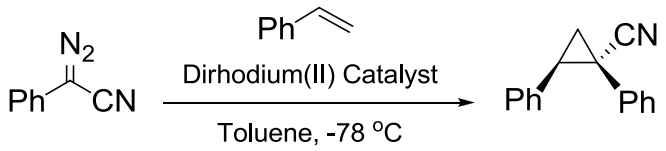

Entry	Catalyst	Loading (mol%)	Yield (%)	dr	*ee* (%)
1	Rh_2(*S*-DOSP)$_4$ (**11**)	2	85	95:5	34
2	Rh_2(*S*-PTTL)$_4$ (**32**)	2	84	96:4	90
3	Rh_2(*S*-PTAD)$_4$ (**53**)	2	86	97:3	90
4	Rh_2(*S*-PTAD)$_4$ (**53**)	1	80	97:3	85

Furthermore, the reaction of a variety of α-aryl-α-diazoketones with activated olefins catalyzed by Rh_2(*S*-PTAD)$_4$ was reported to generate cyclopropyl ketones with high diastereoselectivity (up to >95:5 dr) and enantioselectivity (up to 98% *ee*) (Scheme 1.14).[146]

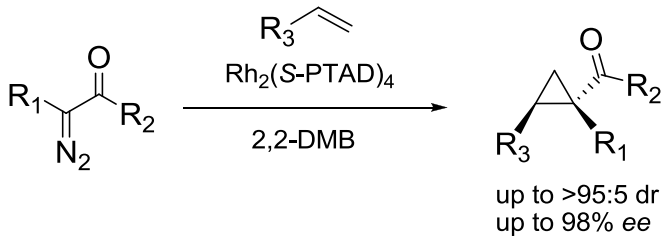

Scheme 1.14. Rh_2(*S*-PTAD)$_4$-catalyzed cyclopropanation of diazo ketones.[146]

Rh_2(*S*-PTAD)$_4$ was also defined as the optimal catalyst that provides high levels of enantioinduction for cyclopropanations with *ortho*-substituted aryldiazoacetates. In particular, Rh_2(*S*-PTAD)$_4$ was very effective with 2-chlorophenyl aryldiazoacetate derivative (97% *ee*) (Scheme 1.15).[98]

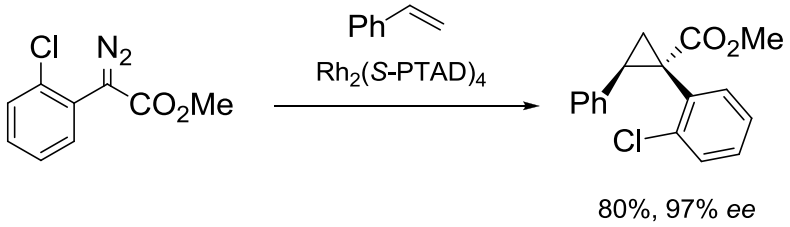

Scheme 1.15. Rh_2(*S*-PTAD)$_4$-catalyzed enantioselective cyclopropanation of styrene with 2-chlorophenyl aryldiazoacetate derivative.[98]

Also recently, it was demonstrated that aryldiazoacetates and vinyldiazoacetates are capable of undergoing high enantioselective cyclopropanations with electron deficient alkenes (Scheme 1.16). The optimal catalyst for this high enantioselective transformation was the tetrachloro variant, Rh_2(*S*-TCPTAD)$_4$ (**54**, Figure 1.14).[126]

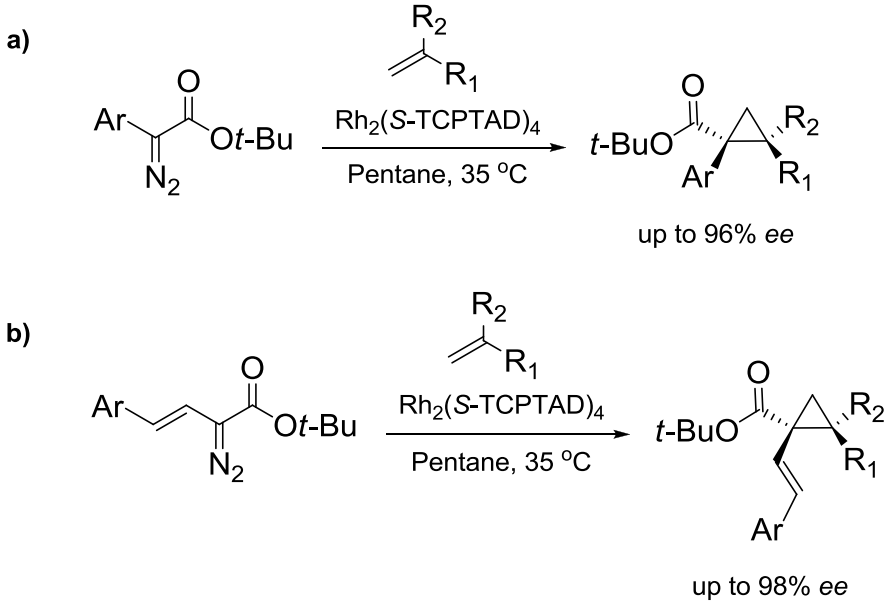

Scheme 1.16. Rh_2(*S*-TCPTAD)$_4$-catalyzed reaction of aryldiazoacetates and vinyldiazoacetates with electron deficient alkenes.[126]

The reaction involves the initial generation of a pre-reaction complex between the carbene intermediates and the carbonyl group of the substrate. But the final reaction product is dependent on the nature of the carbonyl group. Acrylates and acrylamides result in the formation of cyclopropanation products, while unsaturated aldehydes and ketones lead to the formation of epoxide products (Scheme 1.17).[126] Computational studies revealed that with acrylates and acrylamides, the ylide is favourably formed but its formation is reversible and so a cyclopropane is eventually observed. With methyl vinyl ketone, however, ylide formation is not reversible due to its rapid transformation into epoxide (Scheme 1.17).

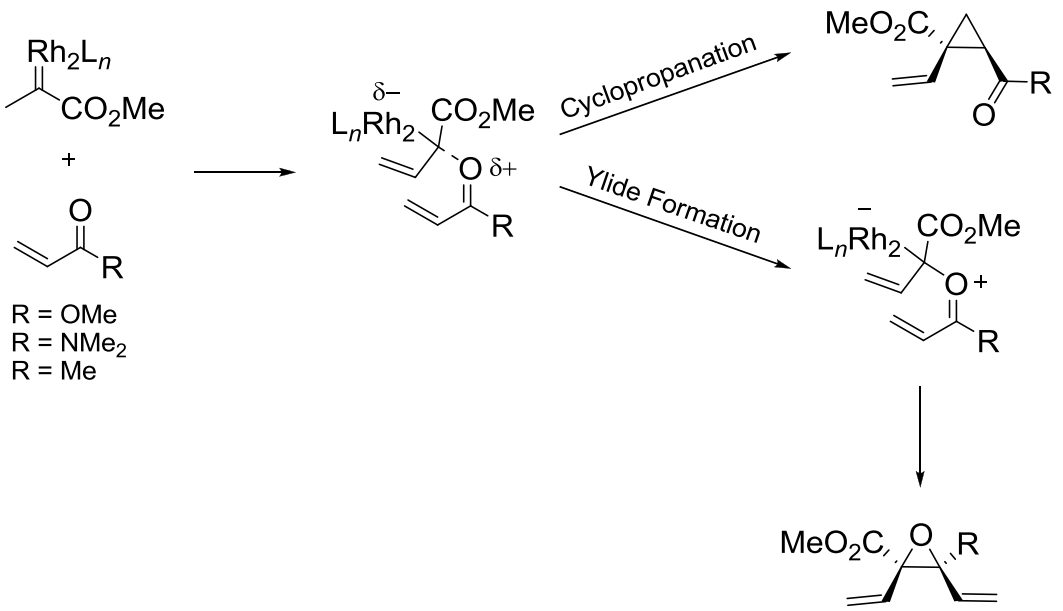

Scheme 1.17. Schematic presentation of the cyclopropanation, ylide formation and epoxidation pathways.[126]

1.5.3.2. Heteroleptic complexes

In 2012, Fox reported the synthesis of the mixed ligand complex dirhodium(II) tris[*N*-phthaloyl-(*S*)-*tert*-leucinate]triphenylacetate, Rh_2(*S*-PTTL)$_3$(TPA) (Figure 1.16). It displays all of the *N*-phthalimide groups on one face in structural similarity to the chiral crown complex, Rh_2(*S*-PTTL)$_4$.[147]

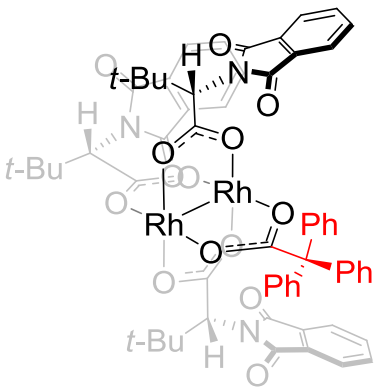

Rh_2(S-PTTL)$_3$(TPA)

Figure 1.16. Structure of Rh_2(*S*-PTTL)$_3$(TPA).[147]

From the Rh-catalysts surveyed, Rh_2(*S*-PTTL)$_3$(TPA) gave the best enantioselectivity in the cyclopropanation of styrene with ethyl *α*-diazobutanoate (88% *ee*) (Table 1.14). The scope of the catalyst was extended to include various substrate classes (aliphatic alkynes, silylacetylenes, *α*-olefins) that were especially challenging in intermolecular reactions of *α*-alkyl-*α*-diazoesters. Generally, Rh_2(*S*-PTTL)$_3$(TPA) was able to catalyze enantioselective cyclopropanation with yields and enantioselectivities that were comparable and sometimes superior to Rh_2(*S*-PTTL)$_4$.[147]

Table 1.14. Rh_2(*S*-PTTL)$_3$(TPA)-catalyzed cyclopropanation of ethyl *α*-diazobutanoate.[147]

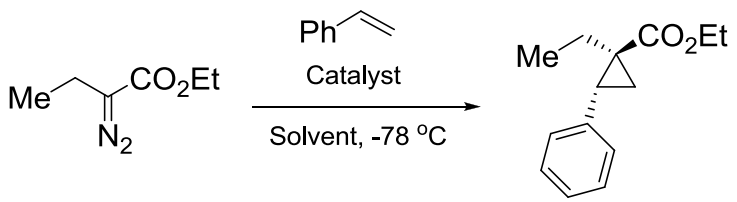

Entry	Catalyst	Solvent	Yield (%)	dr	*ee* (%)
1	Rh_2(*S*-PTTL)$_4$ (**32**)	Hexanes	95	92:8	79
2	Rh_2(*S*-BPTTL)$_4$ (**39**)	Toluene	80	88:12	73
3	Rh_2(*S*-NTTL)$_4$ (**41**)	Toluene	61	75:25	45
4	Rh_2(*S*-TBPTTL)$_4$ (**35**)	CH_2Cl_2	6	97:3	11
5	Rh_2(*S*-TBPTTL)$_4$ (**35**)	Toluene	10	88:12	16
6	Rh_2(*S*-TBPTTL)$_4$ (**35**)	Hexanes	23	84:16	16
7	Rh_2(*S*-PTTL)$_3$(TPA)	Toluene	66	95:5	81
8	Rh_2(*S*-PTTL)$_3$(TPA)	Hexanes	91	96:4	88

In the same context, Charette *et al.*[148] reported a comprehensive study for the synthesis of chiral heteroleptic dirhodium(II) tetracarboxylate catalysts. The major

observation was that replacing one of the chlorinated ligands in Rh_2(*S*-TCPTV)$_4$ or Rh_2(*S*-TCPTTL)$_4$ with achiral nonchlorinated PTAiB had a beneficial impact on the asymmetric induction (Table 1.15).

Table 1.15. Evaluation of chiral heteroleptic Rh_2(*S*-TCPTV)$_3$(PTAiB) and Rh_2(*S*-TCPTTL)$_3$(PTAiB) complexes as catalysts in asymmetric cyclopropanation.[148]

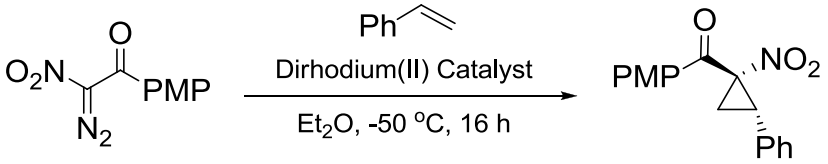

Entry	Catalyst	Yield (%)	dr	*ee* (%)
1	Rh_2(*S*-TCPTV)$_4$ (**30**)	82	98:2	91.1
2	Rh_2(*S*-TCPTTL)$_4$ (**33**)	81	98:2	92.9
3	Rh_2(*S*-TCPTV)$_3$(PTAiB)	76	93:7	95.0
4	Rh_2(*S*-TCPTTL)$_3$(PTAiB)	84	92:8	96.4

The X-ray structure of Rh_2(*S*-TCPTTL)$_3$(PTAiB) revealed that the achiral PTAiB points toward the opposite direction relative to the three *N*-phthalimido groups in the complex in solid state (Figure 1.17). The reason why this $\alpha,\alpha,\alpha,\beta$ conformation resulted in an enhancement in enantioinduction is still ambiguous. However, Charette's report is considered the first report of a successful enantioselective transformation using a catalyst with such conformation, as this kind of no symmetry conformation has long been overlooked as non-operative for enantioselection.[80,9]

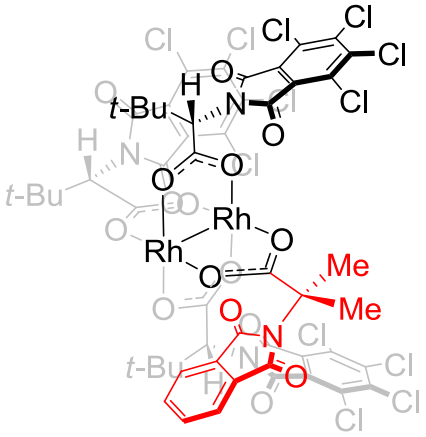

Rh_2(*S*-TCPTTL)$_3$(PTAiB)

Figure 1.17. *α,α,α,β*-Structure of Rh_2(*S*-TCPTTL)$_3$(PTAiB).[148]

1.5.4. Dirhodium(II) catalysts derived from substituted cyclopropanecarboxylate ligands

In 2011, Davies *et al.* explored the usefulness of using chiral cyclopropane carboxylic acids as ligands for dirhodium(II) catalysts. They patented dirhodium(II) tetrakis[(*R*)-1-(4-bromophenyl)-2,2-diphenylcyclopropane carboxylate], Rh_2(*R*-BTPCP)$_4$ (Figure 1.18), as the first member of a new class of chiral dirhodium(II) carboxylates.[149,150] Later, the same research group introduced another four catalysts that belongs to the same dirhodium(II) family, Rh_2(*R*-NPCP)$_4$, Rh_2(*R*-BPCP)$_4$, Rh_2(*S*-BNPCP)$_4$ and Rh_2(*R*-TPCP)$_4$, as efficient catalysts for enantioselective [3+2]-cycloaddition between nitrones and vinyldiazoacetates (Figure 1.18).[151]

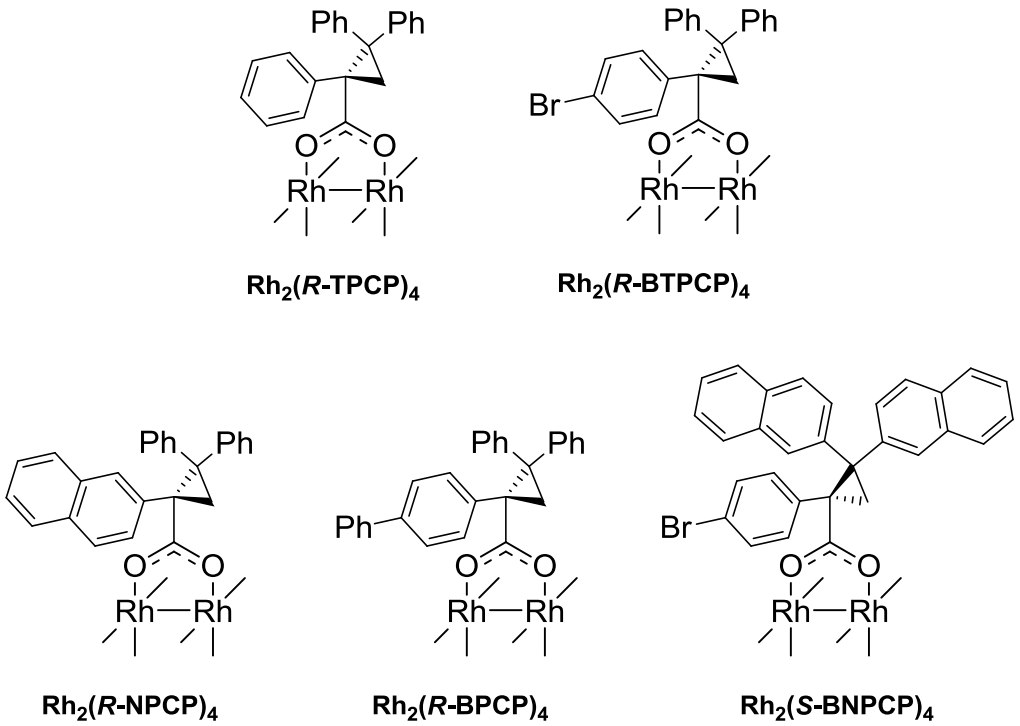

Figure 1.18. Structures of reported chiral dirhodium(II) carboxylates derived from cyclopropane carboxylate ligands.[149-151]

The single crystal X-ray structure of Rh_2(*R*-BTPCP)$_4$ revealed that the ligands are organized in an overall D_2-symmetry with two identical binding cavities of C_2-symmetry (Figure 1.19).[149] The rectangular binding cavity of Rh_2(*R*-BTPCP)$_4$ (8.5 x 10.5 Å) was significantly smaller than the cavity of Rh_2(*S*-PTTL)$_4$ (12.8 x 14.1 Å).

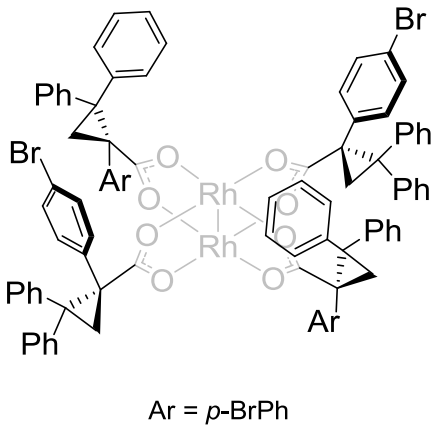

Figure 1.19. D_2-symmetry of Rh_2(*R*-BTPCP)$_4$ according to its X-ray structure.[149]

The introduction of Rh_2(*R*-BTPCP)$_4$ offered several advantages in *donor-acceptor* carbenoid cyclopropanations. In addition to its compatibility with DCM as reaction solvent, Rh_2(*R*-BTPCP)$_4$ exhibited excellent tolerance to carbenoid ester group size. Rh_2(*R*-BTPCP)$_4$-catalyzed *donor-acceptor* carbenoid cyclopropanations with various alkenes resulted in the cyclopropane products in high yields, diastereo- and enantioselectivity (up to 97% *ee*) (Scheme 1.18).[149]

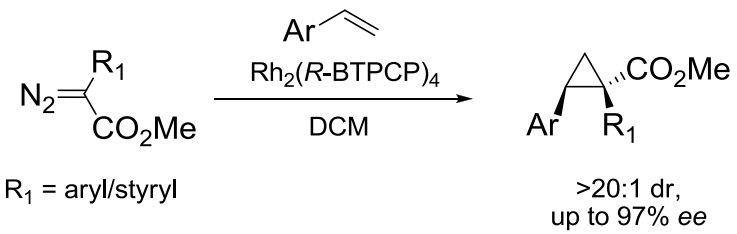

Scheme 1.18. Rh_2(*R*-BTPCP)$_4$-catalyzed asymmetric cyclopropanation.

DFT calculations of the lowest energy carbenoid conformation revealed a conformer that is having two ligands rotated in conrotary fashion to minimize steric interactions with the carbene. Whereas, the other two ligands remained in an upward position to reduce steric interaction with neighbouring ligands (Figure 1.20a). This arrangement resulted in a C_2-symmetric environment at the carbene site cavity containing two phenyl rings and two *p*-bromophenyl rings. One of the phenyl rings is blocking the *donor* aryl/styryl group, while the other ring is positioned next to the *acceptor* ester group (Figure 1.20b).[149]

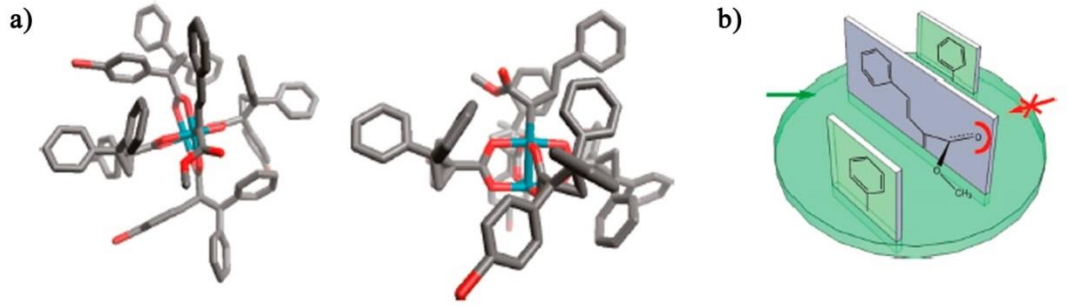

Figure 1.20. a) Lowest-energy conformation of *s*-trans carbene, top view (left) and side view (right). b) Predictive stereochemical model for Rh_2(*R*-BTPCP)$_4$-catalyzed transformations.[149] (Reprinted with permission from Qin, C.; Boyarskikh, V.; Hansen, J. H.; Hardcastle, K. I.; Musaev, D. G.; Davies, H. M. L. *J. Am. Chem. Soc.* **2011**, *133*, 19198. Copyright 2011).

They also reported the Rh_2(*R*-BTPCP)$_4$-catalyzed preparation of a variety of 2-arylbicyclo[1.1.0]butane carboxylate derivatives **55** under low catalyst loading (0.01 mol%) with high levels enantioselectivity (70-94% *ee*). Whereas the same reaction catalyzed by higher catalyst loading of $Rh_2(tpa)_4$ (1.0 mol%) gave the cyclohexene carboxylate derivatives **56** (Scheme 1.19).[152]

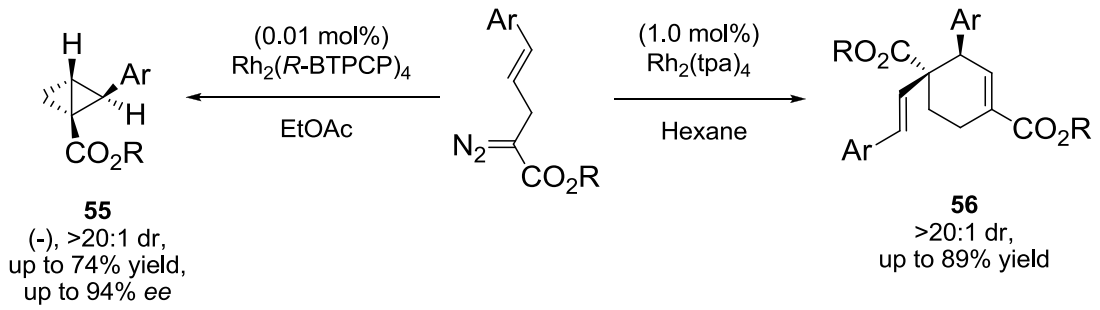

Scheme 1.19. Divergent synthesis of **55** and **56**.[152]

1.6. DIRHODIUM(II) CARBOXAMIDATES

1.6.1. Homoleptic complexes

The first synthesis of a dirhodium(II) carboxamidate occurred in the 1980's, when dirhodium(II) tetraacetamidate was isolated from a melt of acetamide and

$Rh_2(OAc)_4$.[153] Chiral dirhodium(II) carboxamidates were initially developed by Doyle and co-workers.[154,35] The chiral carboxamidate ligands are comprised of bridging lactams derived from amino acids with an ester group at the carbon position adjacent to the nitrogen (Figures 1.22 and 1.23). Early investigations in carboxamidate ligands design established the usefulness of esters as the optimum stereodirecting group (introduces the (*R*)- or (*S*)-configuration to the ligand). The utilization of alkyl or aryl attachments resulted in significant deterioration in enantioselectivity.[155,156] In fact, the influence of the catalyst's ester group size on enantiocontrol is substantial and can delicately balance the catalyst steric factors.[157] Moreover, initial attempts led to the realization that acyclic amides were not generally suitable because ligand exchange requires access to the *cis* (*E*) amide form rather than the *trans* (*Z*) form (Figure 1.21).[154] Modifications of the lactam ring have given rise to four classes of carboxamidate ligands: pyrrolidinates,[155] oxazolidinates,[158] imidazolidinates[159] and azetidinates[160] (Figures 1.22 and 1.23). Again, they differ in reactivity and selectivity on the basis of their steric and/or electronic influences.

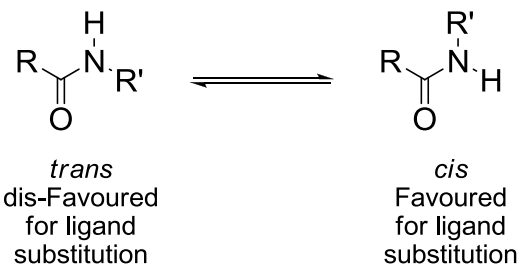

Figure 1.21. Favoured and dis-Favoured amide forms for ligand exchange.[154]

Dirhodium(II) carboxamidates derived from chiral pyrrolidinates

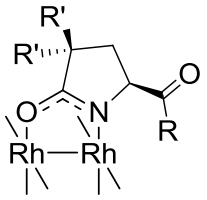

57 R = OMe, R' = H **[Rh_2(5*S*-MEPY)$_4$]**
58 R = OCH_2CMe_3, R' = H **[Rh_2(5*S*-NEPY)$_4$]**
59 R = $O(CH_2)_{17}CH_3$, R' =H **[Rh_2(5*S*-ODPY)$_4$]**
60 R = NMe_2, R' = H **[Rh_2(5*S*-DMAP)$_4$]**
61 R = OMe, R' = F **[Rh_2(5*S*-dFMEPY)$_4$]**

Dirhodium(II) carboxamidates derived from chiral oxazolidinates

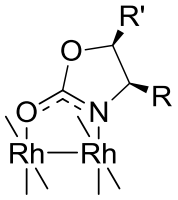

62 R = R' = H **[Rh_2(4*S*-MEOX)$_4$]**
63 R = H, R' = Me **[Rh_2(4*S*-THREOX)$_4$]**
64 R = $PhCH_2$, R' = H **[Rh_2(4*S*-BNOX)$_4$]**
65 R = *i*-Pr, R' = H **[Rh_2(4*S*-IPOX)$_4$]**
66 R = Ph, R' = H **[Rh_2(4*S*-PHOX)$_4$]**
67 R = Me, R' = Ph **[Rh_2(4*S*-MPOX)$_4$]**

Dirhodium(II) carboxamidates derived from chiral azetidinates

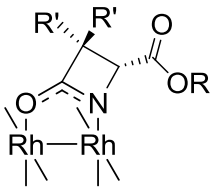

68 R = Me, R' = H **[Rh_2(4*S*-MEAZ)$_4$]**
69 R = $PhCH_2$, R' = H **[Rh_2(4*S*-BNAZ)$_4$]**
70 R = CH_2CMe_3, R' = H **[Rh_2(4*S*-NEPAZ)$_4$]**
71 R = *t*-Bu, R' = H **[Rh_2(4*S*-IBAZ)$_4$]**
72 R = $^cC_6H_{11}$, R' = H **[Rh_2(4*S*-CHAZ)$_4$]**
73 R = $^cC_6H_{11}$, R' = F **[Rh_2(4*R*-dFCHAZ)$_4$]**
74 R = *i*-Pr, R' = F **[Rh_2(4*R*-dFIBAZ)$_4$]**
75 R = *S*/*R*-menthyl, R' = H **[Rh_2(4*S*, *S*/*R*-MenthAZ)$_4$]**
76 R = 4-$FC_6H_4CH_2$, R' = H **[Rh_2(4*S*-(4')-FBNAZ)$_4$]**

Figure 1.22. Reported structures of different classes of chiral dirhodium(II) carboxamidates (cont.).[16,161,162]

Dirhodium(II) carboxamidates derived from chiral imidazolidinates

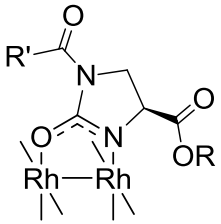

77 R = R' = Me **[Rh_2(4*S*-MACIM)$_4$]**
78 R = Me, R' = C_6H_4-*t*-Bu **[Rh_2(4*S*-TBOIM)$_4$]**
79 R = Me, R' = $^cC_6H_{11}CH_2$ **[Rh_2(4*S*-MCHIM)$_4$]**
80 R = Me, R' = Ph **[Rh_2(4*S*-MBOIM)$_4$]**
81 R = Me, R' = $PhCH_2$ **[Rh_2(4*S*-MPAIM)$_4$]**
82 R = Me, R' = $PhCH_2CH_2$ **[Rh_2(4*S*-MPPIM)$_4$]**
83 R = Et, R' = $PhCH_2CH_2$ **[Rh_2(4*S*-EPPIM)$_4$]**
84 R = *i*-Bu, R' = $PhCH_2CH_2$ **[Rh_2(4*S*-BPPIM)$_4$]**

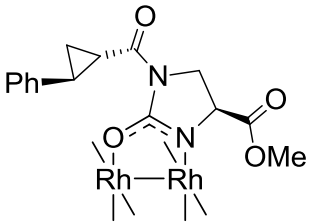

85 Rh_2(4*S*, 2'*S*, 3'*S*-MCPIM)$_4$

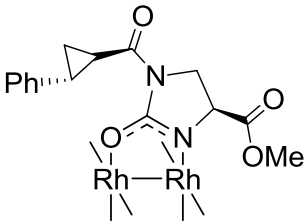

86 Rh_2(4*S*, 2'*R*, 3'*R*-MCPIM)$_4$

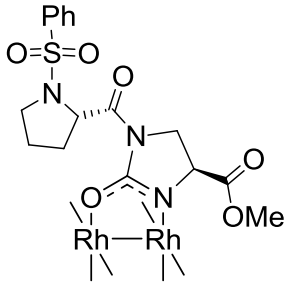

87 Rh_2(4*S*, 2'*R*-BSPIM)$_4$

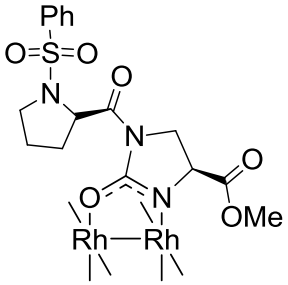

88 Rh_2(4*S*, 2'*S*-BSPIM)$_4$

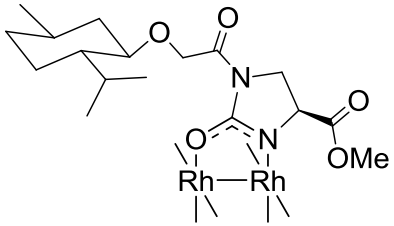

89 Rh_2(4*S*-MLMIM)$_4$

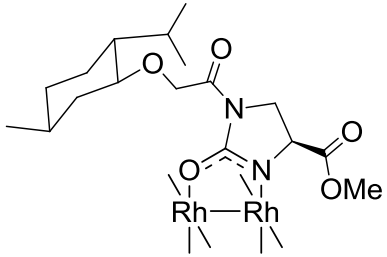

90 Rh_2(4*S*-MDMIM)$_4$

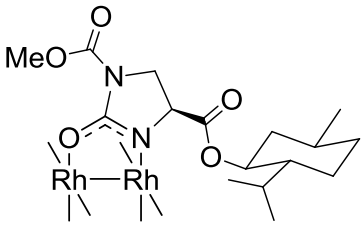

91 Rh_2(1'*S*, 2'*R*, 5'*S*, 4*S*-MNACIM)$_4$

Figure 1.23. Reported structures of different classes of chiral dirhodium(II) carboxamidates.[16,163,164]

Dirhodium(II) carboxamides have a more complicated paddlewheel structure if compared to dirhodium(II) carboxylates. Since the carboxamidate ligand type bridges the Rh-Rh core *via* both an oxygen and a nitrogen atoms and because of the unsymmetrical bridging ligands, there are four possible geometrical isomers based on the positions of nitrogens and oxygens on each rhodium: (2,2)-*cis*, (2,2)-*trans*, (3,1) and (4,0) (Figure 1.24).[16]

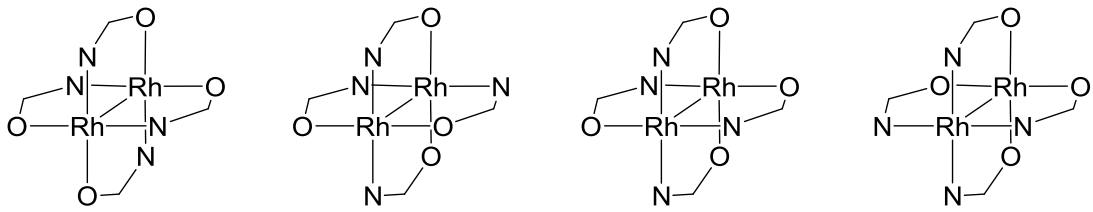

Figure 1.24. Possible geometrical isomers of dirhodium(II) carboxamidates.[16]

Examples of each geometrical isomer, except for the (2,2)-*trans* isomer, have been isolated and characterized.[165,16] However, monitoring the ligand exchange process with HPLC-ICP-MS indicated that the complex with (2,2)-*cis* geometry is the dominant isomer (>85%). Also, all of the other isomers isomerizes into this major isomer upon heating.[165,155,158]

The (2,2)-*cis* configuration defines that each rhodium is bound to two nitrogen atoms and two oxygen atoms in a *cis*-fashion. As a consequence, these complexes can only adapt C_2-symmetry due to this substantial ligand binding tendency.[9] The (2,2)-*cis* geometry was also consistently found in the X-ray structures of different dirhodium(II) carboxamidate complexes, such as $Rh_2(5R\text{-MEPY})_4$[155] (The enantiomer of **57**, Figure 1.22) and $Rh_2(4S\text{-MEOX})_4$ (**62**, Figure 1.22). In these two complexes, the two ester groups in the ligands oriented in counter clockwise fashion and can effectively block one side of the carbenoid intermediate (Figure 1.25).[166,164]

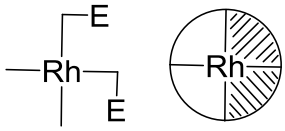

Figure 1.25. CO_2Me (E) entity is occupying two adjacent quadrants around the dirhodium core (top view).[166,164]

The evolution of this (2,2)-*cis* geometry led to the emergence of imidazolidinone carboxylate-ligated catalysts carrying chiral *N*-acyl groups (**77**-**91**, Figure 1.23). The chiral *N*-acyl attachments of the imidazolidinone carboxylate catalysts were designed to potentially reinforce the inherent stereocontrol provided by the core ligand system (Figure 1.26). For example, use of ligand diastereomers to form Rh_2(1'*S*, 2'*R*, 5'*S*, 4*S*-MNACIM)$_4$ (**91**) and its diastereomer, Rh_2(1'*R*, 2'*S*, 5'*R*, 4*S*-MNACIM)$_4$, revealed remarkable difference in diastereo- and enantioselectivity. The highest diastereocontrol achieved was with **91** (Table 1.16, entry 3 *vs.* 4).[167]

Table 1.16. Results for intramolecular C–H insertion.[167]

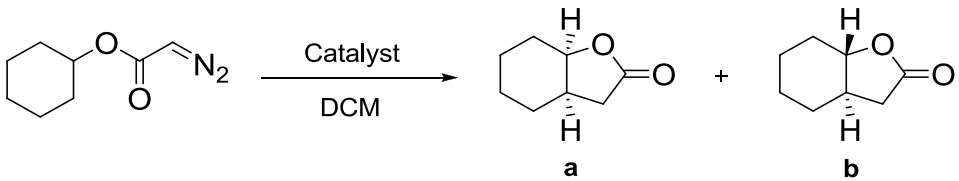

Entry	Catalyst	Yield (%)	dr (a:b)	*ee* of a (%)	*ee* of b (%)
1	Rh_2(1'*S*, 2'*R*, 5'*S*, 4*S*-MNACIM)$_4$ (**91**)	80	100:0	95	-
2	Rh_2(1'*R*, 2'*S*, 5'*R*, 4*S*-MNACIM)$_4$	71	79:21	84	68
3	Rh_2(4*S*, 2'*S*, 3'*S*-MCPIM)$_4$ (**85**)	78	99:1	97	-
4	Rh_2(4*S*, 2'*R*, 3'*R*-MCPIM)$_4$ (**86**)	63	80:20	72	13
5	Rh_2(4*S*, 2'*S*-BSPIM)$_4$ (**88**)	88	97:3	>99	>99
6	Rh_2(4*S*, 2'*R*-BSPIM)$_4$ (**87**)	89	98:2	74	33

Viewing the diastereomers of $Rh_2(MCPIM)_4$ and $Rh_2(BSPIM)_4$ catalysts down the Rh-Rh bond axis revealed that these catalysts are configured as shown in Figure 1.26a. Rh_2(4*S*, 2'*S*, 3'*S*-MCPIM)$_4$ (**85**) and Rh_2(4*S*, 2'*S*-BSPIM)$_4$ (**88**) have the pendent ester and *N*-acyl side chains oriented in the same direction following a counter clockwise spiral (matched complexes) (Figure 1.26a). This orientation is particularly well suited to intramolecular reactions in which the active site for reaction is tethered to the dirhodium(II) axial coordination site. In contrast, the ester and *N*-acyl side chains are in configurational opposition in Rh_2(4*S*, 2'*R*, 3'*R*-MCPIM)$_4$ (**86**) and Rh_2(4*S*, 2'*R*-BSPIM)$_4$ (**87**) (mismatched complexes) which provides a barrier to stereoselectivity enhancement in intramolecular transformations.[16,168]

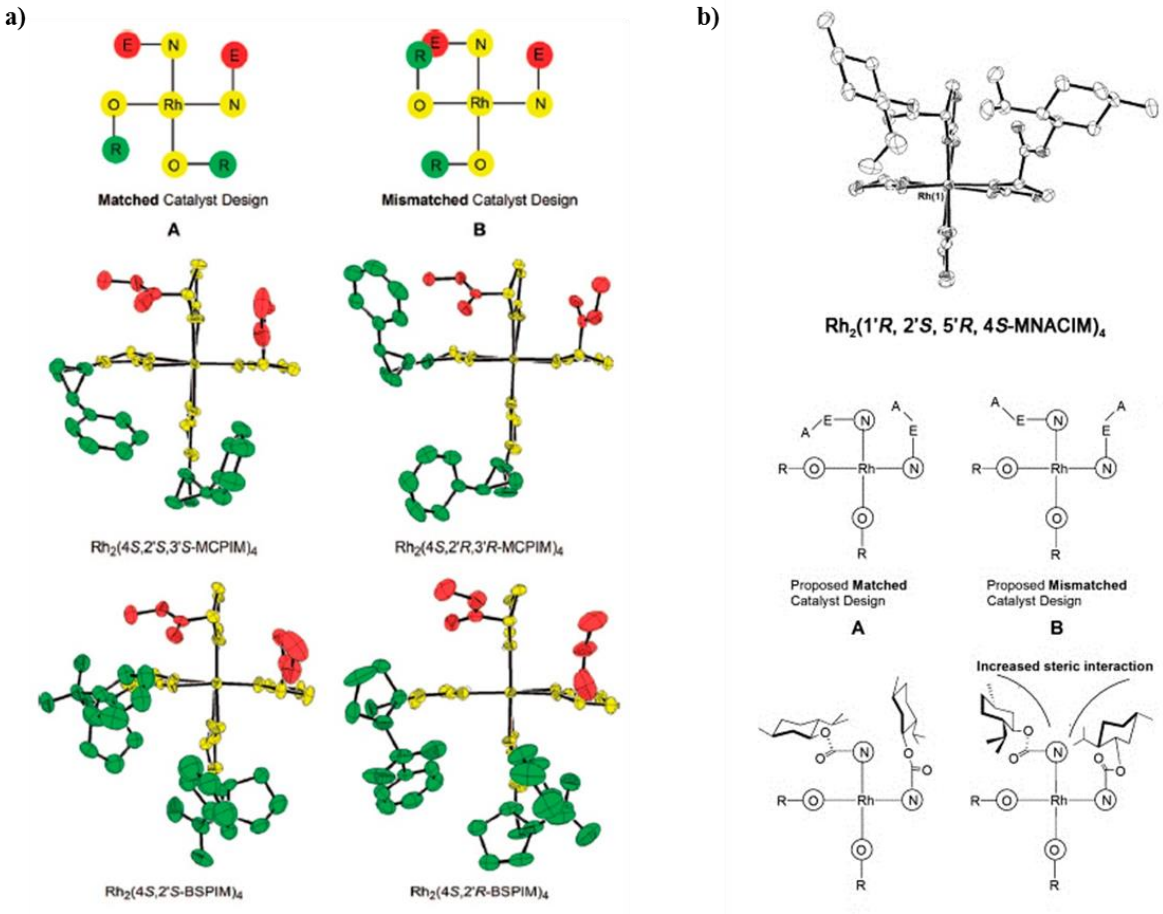

Figure 1.26. Configurational differences between matched and mismatched catalysts.[16,167] (Part a: Reprinted with permission from Doyle, M. P.; Duffy, R.; Ratnikov, M.; Zhou, L. *Chem. Rev.* **2010**, *110*, 704. Copyright 2010. Part b: Reprinted from Doyle, M. P.; Morgan, J. P.; Colyer, J. T. *J. Organomet. Chem*. **2005**, *690*, 5525, Copyright 2005, with permission from Elsevier).

As a result of the electron-rich character of dirhodium(II) carboxamidates, they are catalytically less active than dirhodium(II) carboxylates. However, they are very effective catalysts in the decomposition of diazoacetates derivatives and widely used for intramolecular cyclopropanation,[164] intermolecular cyclopropenation[169] and intramolecular C-H insertion reactions,[16] often resulting in reactions proceeding in >90% *ee*.

Among the different classes of dirhodium(II) carboxamidates, azetidinate based catalysts (**68-76**, Figure 1.22)[170,160,171] are considered the most reactive chiral dirhodium(II) carboxamidates toward diazo compounds. They are capable to react with diazoacetates that are unstable toward pyrrolidinate-, oxazolidinate- and immidazolidinate-ligated catalysts.[160] For example, $Rh_2(4S\text{-MEAZ})_4$ (**68**, Figure 1.22) offered distinct advantages for rapid diazo decomposition and achieving the highest levels of enantioselectivity in the preparation of **92** (95% *ee*) which is a key intermediate in the total synthesis of Milnacipran and its analogues (Scheme 1.20).[172]

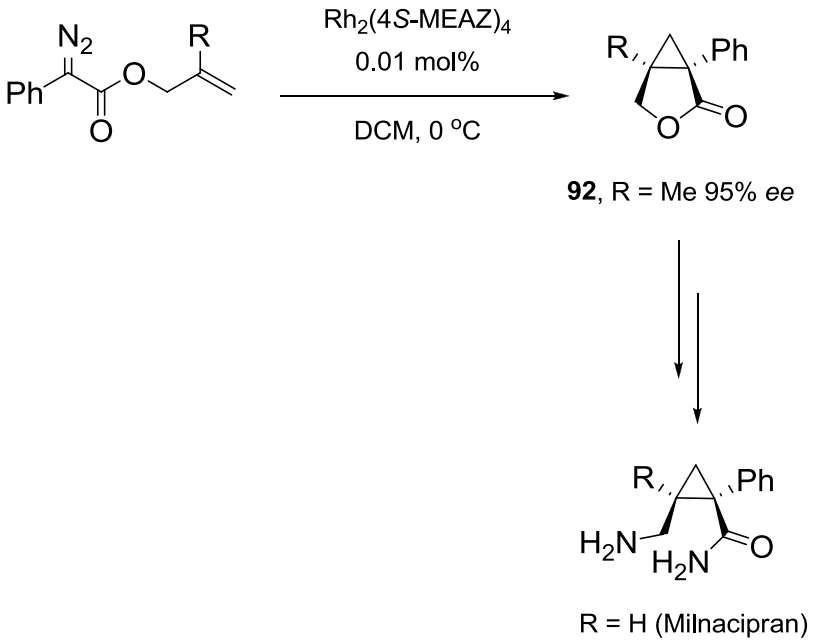

Scheme 1.20. $Rh_2(4S\text{-MEAZ})_4$-catalyzed asymmetric preparation of **92**.[172]

Also, azetidinate-ligated $Rh_2(4S,R\text{-MenthAZ})_4$ (**75**, Figure 1.22) provided significant diastereocontrol and high enantiocontrol for the formation of *cis*-cyclopropane products in reactions of substituted styrenes with diazoesters. This was in preference

to the thermodynamically favoured *trans*-isomer. The usefulness of this reaction was demonstrated by the total synthesis of cyclopropane-configured phenylethylthiazoylthiourea (PETT) analogue **93** (Scheme 1.21).[171]

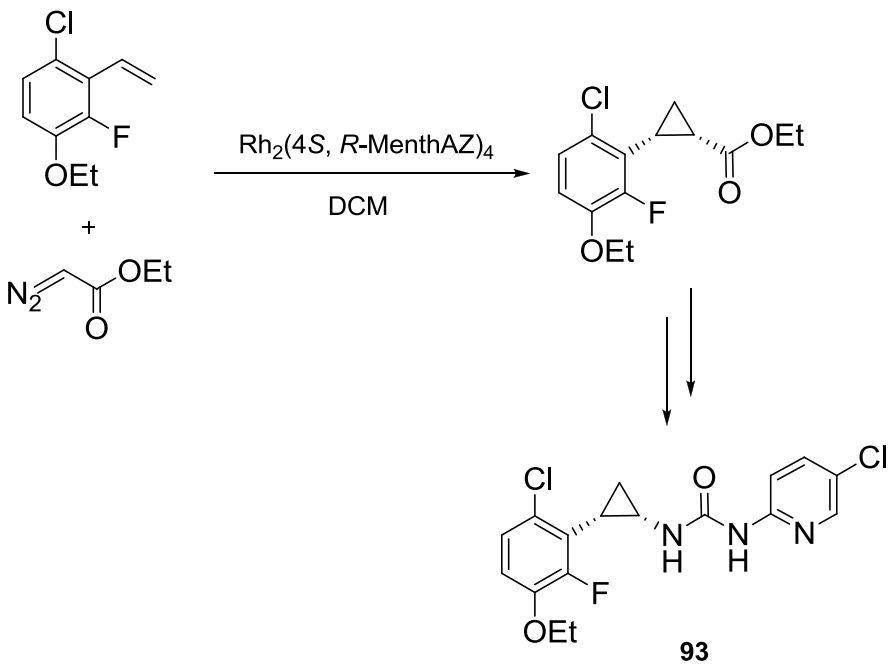

Scheme 1.21. Total synthesis of cyclopropane-configured phenylethylthiazoyl-thiourea (PETT) analogue **93**.[171]

Similarly, Doyle *et al.*[173] reported the cyclopropanation reaction of vinyl diazolactone **94** with various alkenes in the presence of $Rh_2(4S, R\text{-MenthAZ})_4$ (Scheme 1.22). The corresponding cyclopropanes were obtained in high yields with notable diastereo- and enantioselectivities (up to 86% *ee*).

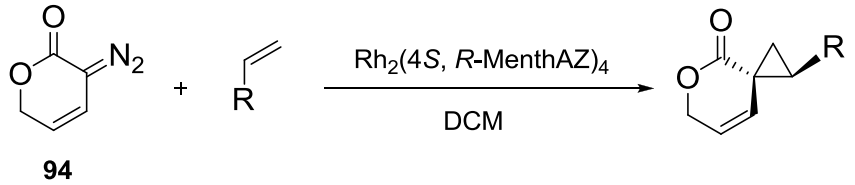

R = Ph	74%, *de* = >90%, *ee* = 84%
R = (Me)C=CHPh	81%, *de* = 78%, *ee* = 86%
R = CH=CHPh	86%, *de* = 66%, *ee* = 73%

Scheme 1.22. Rh_2(4*S*, *R*-MenthAZ)$_4$-catalyzed cyclopropanation of vinyl diazolactone **94** with different olefins.[173]

Later, Charette *et al.*[174] introduced the azetidinate-based catalyst, Rh_2(4*S*-(4')-FBNAZ)$_4$ (**76**, Figure 1.22). This catalyst was found to be effective for intramolecular cyclopropanation of substituted allylic *α*-cyano-*α*-diazoacetates with up to 91% *ee* (Scheme 1.23).

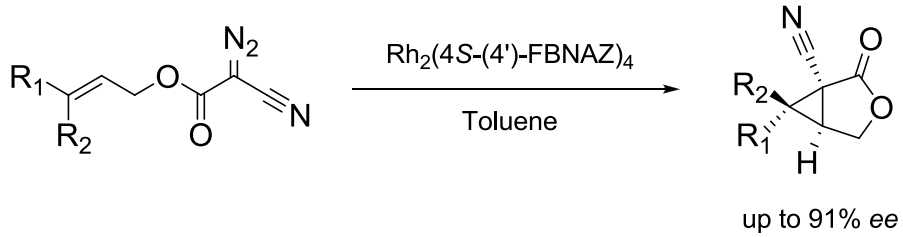

Scheme 1.23. Intramolecular cyclopropanation of substituted allylic *α*-cyano-*α*-diazoacetates.[174]

Doyle *et al.*[164] utilized Rh_2(5*S*-MEPY)$_4$ (**57**, Figure 1.22) and its enantiomer, Rh_2(5*R*-MEPY)$_4$, in intramolecular cyclopropanations through diazo decomposition of several trisubstitiuted and *cis*-disubstituted allylic diazoacetates. He succeeded in producing the chiral cyclopropane fused lactone products in good to excellent yields and with exceptional enantioselectivity. However, when similar reactions were carried out using the *trans*-disubstituted isomers, the products were observed with moderate *ee* values. The use of Rh_2(4*S*-MPPIM)$_4$ catalyst (**82**, Figure 1.23) resulted in 89-96% *ee*,[175] emphasizing the importance of the steric bulk and positioning of the ligand on enantioselectivity control. For example, the Rh_2(5*S*-MEPY)$_4$-catalyzed

intermolecular cyclopropanation of 2-methallyl diazoacetate afforded the cyclopropane product with only 7% *ee*. Alternatively, Rh_2(4*S*-MPPIM)$_4$ was employed to increase the level of enantiocontrol to 89% *ee* (Scheme 1.24).[175,176] In the same context, a comparative study using Doyle's catalysts and Cu(I) and Ru(II) catalysts indicated that dirhodium(II) carboxamidates are far superior in producing enantiomerically pure products.[176]

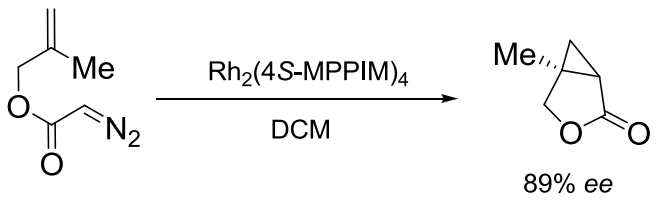

Scheme 1.24. Rh_2(4*S*-MPPIM)$_4$-catalyzed intermolecular cyclopropanation of 2-methallyl diazoacetate.[175,176]

Doyle succeeded to interpret the observed absolute configuration and the high level of enantiocontrol in these intramolecular cyclopropanations through the transition state model illustrated in Figure 1.27.[164]

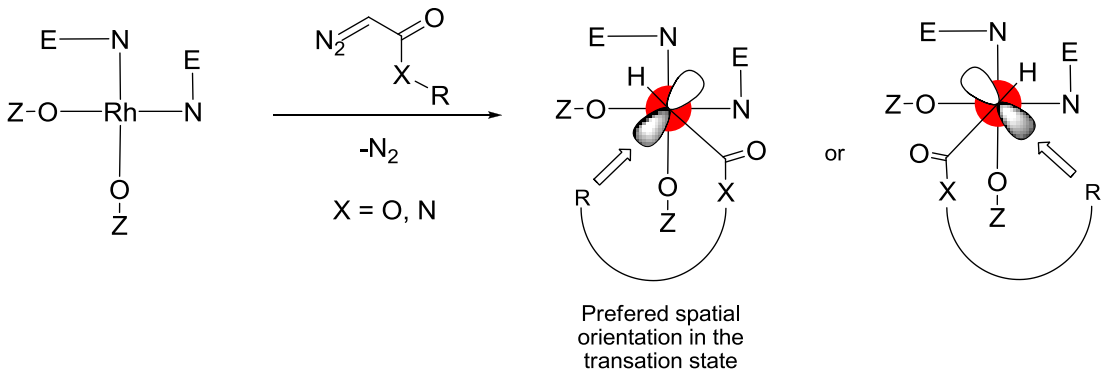

Figure 1.27. Spatial orientations in the transition state of intramolecular cyclopropanations using dirhodium(II) carboxamidates.[164]

Likewise, he extended this intramolecular cyclopropanation to include cyclization of allylic diazoacetamides to give the corresponding cyclopropane fused lactams. For

example, the decomposition of *N*-allyl diazoacetamide in the presence of catalytic amount of $Rh_2(4S\text{-MEOX})_4$ (**62**, Figure 1.22) gave the 3-azabicylo[3.1.0]hex-2-one product in 98% *ee* (Scheme 1.25).[164] When using the allylic diazoacetamides as substrates, substitution of the extra hydrogen on the amide nitrogen is crucial to achieve higher yield. This enhancement was returned to the formation of the reaction favoured conformation.

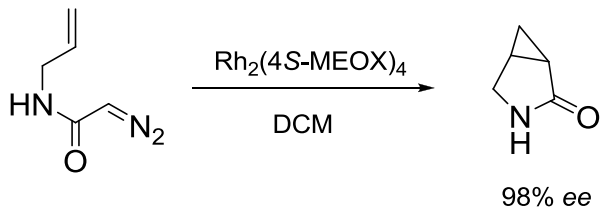

Scheme 1.25. Decomposition of *N*-allyl diazoacetamide in the presence of catalytic amount of $Rh_2(4S\text{-MEOX})_4$.[164]

Further, the original sequence of two successive intramolecular cyclopropanations involving bis-diazoacetate and employing $Rh_2(4S, 2S\text{-BSPIM})_4$ as a catalyst was also reported (Scheme 1.26).[177]

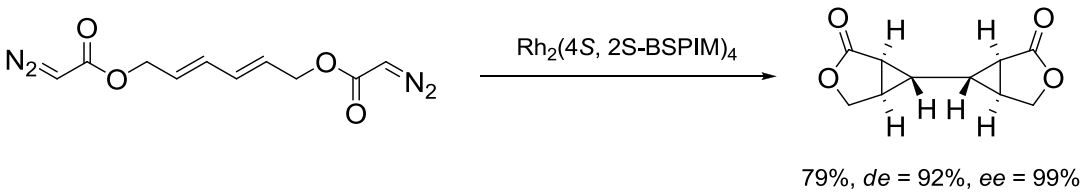

Scheme 1.26. $Rh_2(4S, 2S\text{-BSPIM})_4$-catalyzed double intramolecular cyclopropanation.[177]

Very recently, A mild and highly stereoselective $Rh_2(4S\text{-IBAZ})_4$ (**71**)-catalyzed cyclopropanation of alkenes and alkynes, with *diacceptor* diazo compounds was reported by Charette.[178] The *iso*steric character of carboxylic acid derivatives allowed the alternative use of both α-cyano diazocarboxylate esters in the process, leading to α-cyano cycloprop(en)ylcarboxylates in high yields and stereoselectivities (Scheme 1.27). Charette extended the scope of compatible substrates to include

substituted allenes, leading to the development of the first catalytic enantioselective method for accessing *diacceptor* alkylidenecyclopropanes.

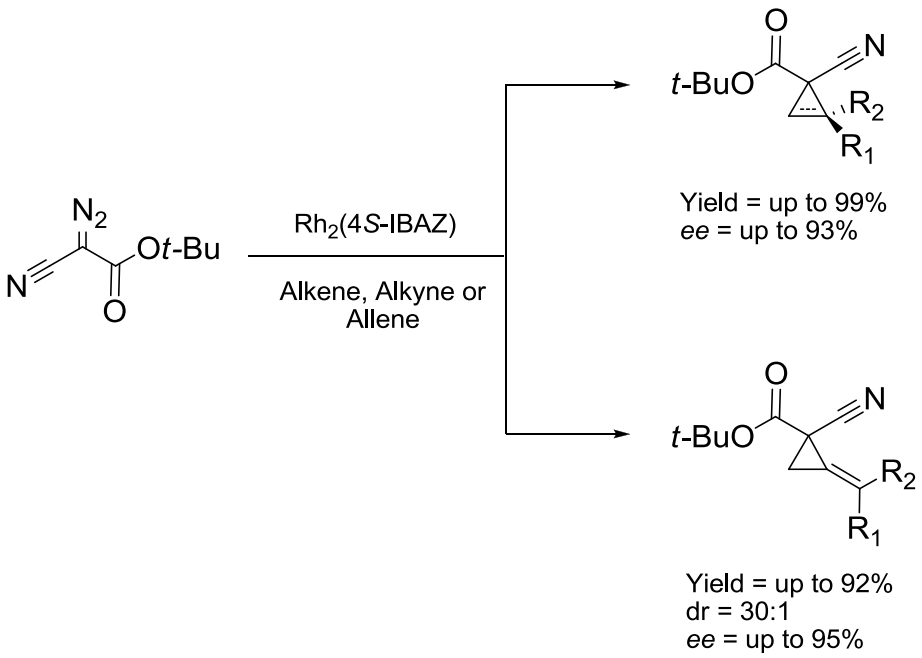

Scheme 1.27. Rh_2(*S*-IBAZ)$_4$-catalyzed cyclopropan(en)ation.[178]

As I illustrated earlier in this review, the cyclopropanation of *donor-acceptor* substituted diazo compounds have been reported to proceed with high stereoselectivities using dirhodium(II) carboxylate catalysts. However, common dirhodium(II) carboxamidate catalysts such as Rh_2(5*S*-MEPY)$_4$ (**57**), Rh_2(4*S*-MEOX)$_4$ (**62**) and Rh_2(4*S*-MBOIM)$_4$ (**80**) provided poor enantioselectivities with this class of substrates.[163] An increase in enantiomeric excess of **95** was observed upon the use of Rh_2(4*S*-TBOIM)$_4$ (**78**) yielding the cyclopropane product in 77% *ee* in DCM as reaction solvent (Table 1.17).[163] The use of pentanes as the reaction solvent did not affect the enantioselectivity to an appreciable degree.

Table 1.17. Dirhodium(II) carboxamidates-catalyzed cyclopropanation of styrene with methyl phenyldiazoacetate.[163]

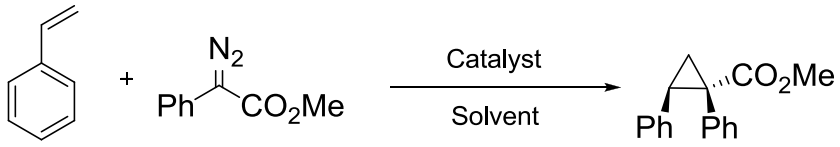

95

Entry	**Catalyst**	**Solvent**	**Yield (%), (*cis*/*trans*)**	***ee* (%)**
1	Rh_2(5*S*-MEPY)$_4$ (**57**)	CH_2Cl_2	27 (97:3)	49
2	Rh_2(4*S*-MEOX)$_4$ (**62**)	CH_2Cl_2	57 (96:4)	41
3	Rh_2(4*S*-MBOIM)$_4$ (**80**)	CH_2Cl_2	73 (96:4)	48
4	Rh_2(4*S*-TBOIM)$_4$ (**78**)	CH_2Cl_2	63 (95:5)	77
5	Rh_2(4*S*-TBOIM)$_4$ (**78**)	Pentanes	69 (94:6)	75

Poulter *et al.*[179] utilized Rh_2(5*S*-MEPY)$_4$ (**57**) during the synthesis of optically pure Presqualene diphosphate at which the key step in this synthesis was the stereoselective intramolecular cyclopropanation of farnesyl diazoacetate. Martin *et al.*[180] used Rh_2(5*S*-MEPY)$_4$ and its enantiomer Rh_2(5*R*-MEPY)$_4$ to prepare conformationally restricted peptide isosteres and extended this work to the preparation of cyclopropane peptidomimics as novel Enkephalin analogues.

The Hashimoto group did put forward the preparation of a dirhodium(II) carboxamidate complex, Rh_2(*S*-PTPI)$_4$ (Figure 1.28) with 3-(*S*)-phthalimido-2-piperidinonate as chiral bridging ligands.[181,182] Later, the same group introduced its analogue, Rh_2(*S*-BPTPI)$_4$, as a highly efficient Lewis acid catalyst for enantioselective hetero-Diels-Alder reactions.[183,43,42]

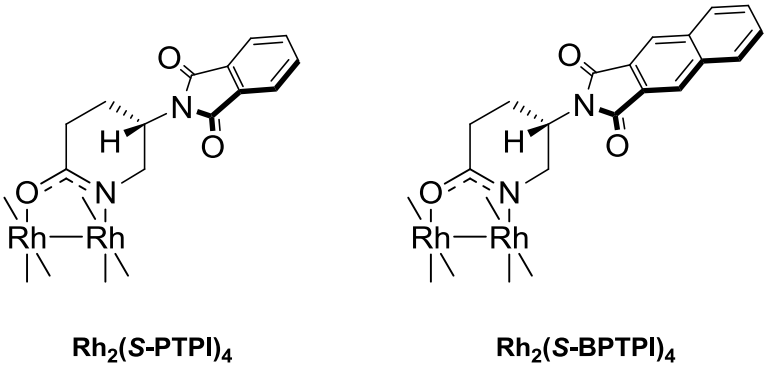

Figure 1.28. Structure of Hashimoto's Rh_2(*S*-PTPI)$_4$ and Rh_2(*S*-BPTPI)$_4$ catalysts.[181-183,43,42]

The use of Rh_2(*S*-PTPI)$_4$ delivered a high order of enantioselectivity in the cyclopropanation reactions that involved styrenes, *E*-1-phenylbutadiene and 1,1-disubstituted alkenes. The combinational use of 2,4-dimethyl-3-pentyl diazoacetate as carbene source and ether as a reaction solvent was crucial for the success of this catalyst (Scheme 1.28).[182]

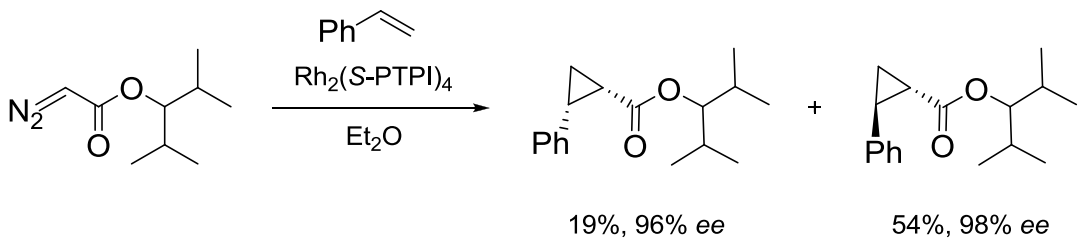

Scheme 1.28. Example for Rh_2(*S*-PTPI)$_4$-catalyzed enantioselective cyclopropanation of styrene with 2,4-dimethyl-3-pentyl diazoacetate.[182]

1.6.2. Heteroleptic complexes

Corey *et al.*[184] communicated a new dirhodium(II) carboxamidate having (*R*, *R*)-4,5-diphenyl-*N*-triflylimidazolidinone (DTPI) as bridging ligands (Figure 1.29). The new catalyst was tested in enantioselective cyclopropenation of ethyl diazoacetate with terminal acetylenes. The authors described the catalyst to be outstanding in terms enantioselectivity, yield, scope and efficiency of catalyst recovery. Later, the same group reported the new C_2-symmetric complex, $Rh_2(DTBTI)_2(OAc)_2$, having only

two *anti*-DTBTI ((*R*, *R*)-4,5-di-*tert*-butyl-*N*-triflylimidazolidinone) bridges (Figure 1.29).[185] This catalyst was highly effective in cyclopropenation reactions of a wide range of alkynes. It was notable due to its robustness, as well as the easy synthesis of the associated chiral ligand.

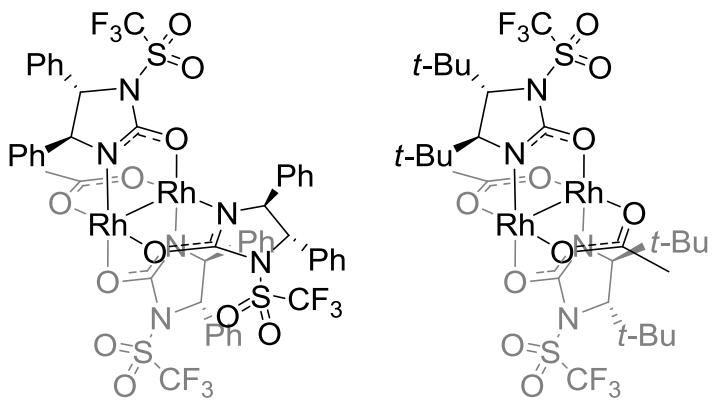

Figure 1.29. Structure of $Rh_2(DPTI)_3(OAc)$ and $Rh_2(DTBTI)_2(OAc)_2$.[184,185]

Doyle *et al.*[186] reported $Rh_2(1,6\text{-BPGlyc})_2(OAc)_2$ as a new member to dirhodium(II) carboxamidate family. The bridging ligands were 1,6-bis-(*N*-benzyl)-diphenylglycoluril (1,6-BPGlyc) and acetate ligands (Figure 1.30).

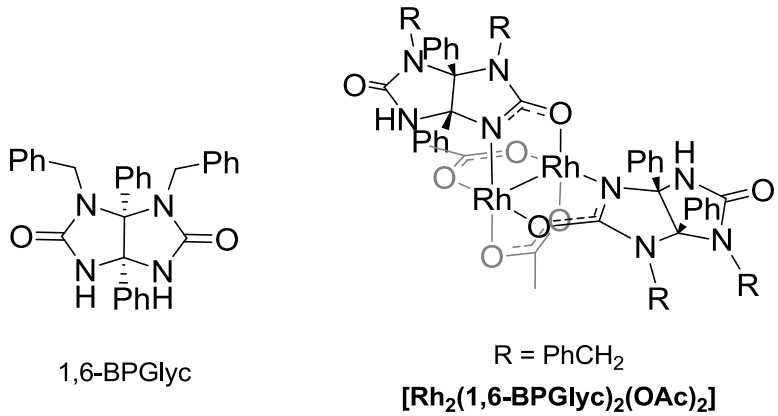

Figure 1.30. Structure of 1,6-BPGlyc and $Rh_2(1,6\text{-BPGlyc})_2(OAc)_2$.[186]

Despite the unusual steric profile of the ligand and the mixed substitution pattern of the new catalyst, there were only minor differences relative to previously reported dirhodium(II) carboxamidates.[186] As it contains only two carboxamide ligands, Rh_2(1,6-BPGlyc)$_2$(OAc)$_2$ could have been formed in four possible isomers: (2,2)-*cis*, (2,2)-*trans*, (1,3)-*cis* and (1,3)-*trans* (Figure 1.31). X-ray structure of the complex, not only confirmed the C_2-symmetery of Rh_2(1,6-BPGlyc)$_2$(OAc)$_2$, but also revealed the preference for the (1,3)-*cis* isomer. The authors attributed this preference to the *trans*-effect directing ligand substitution.

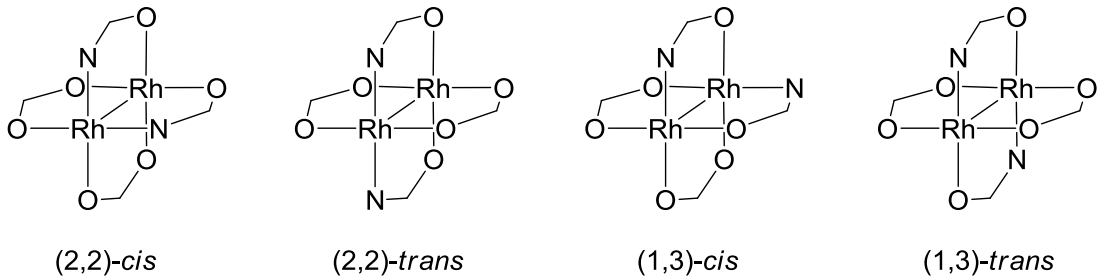

Figure 1.31. Possible geometrical isomers for Rh_2(1,6-BPGlyc)$_2$(OAc)$_2$.[186]

In addition to the selective ligand arrangement, formation of Rh_2(1,6-BPGlyc)$_2$(OAc)$_2$ is stereoselective. Glycoluril ligand is a *meso*-compound with two enantiotopic metal binding sites that would provide enantiomeric pairs upon substitution (A, *ent*-A) (Figure 1.32). Moreover, the (1,3)-*cis* complexes are helically chiral (*M*, *P*) about the Rh-Rh bond axis due to the fused nature of the μ-NCO bridging ligands. The Rh_2(1,6-BPGlyc)$_2$(OAc)$_2$ complex was found to be formed stereoselectively as a racemic mixture of the (A, A)-*P* and (*ent*-A, *ent*-A)-*P* diastereomers.[186]

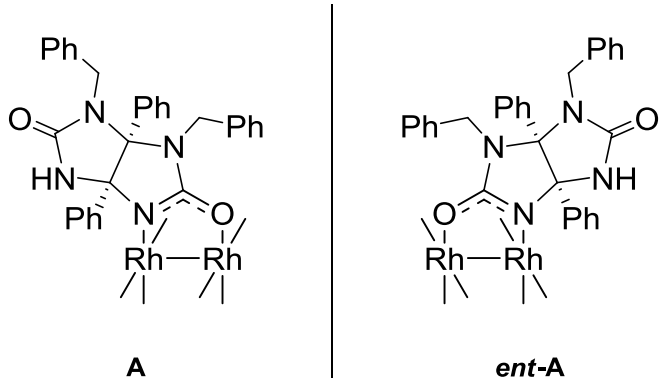

Figure 1.32. Enantiotopic binding of 1,6-BPGlyc on Rh_2(1,6-BPGlyc)$_2$(OAc)$_2$.[186]

The *cis*/*trans* selectivity of Rh_2(1,6-BPGlyc)$_2$(OAc)$_2$ in the formation of **96** was closer to Rh_2(5*S*-MEPY)$_4$ (**57**) than to the electronically related Rh_2(4*S*-MPPIM)$_4$ (**82**) (Table 1.18). The *cis*/*trans* selectivity of the formation of **97** was basically unchanged by Rh_2(1,6-BPGlyc)$_2$(OAc)$_2$ in comparison to the results of both dirhodium(II) carboxylates and carboxamidates except that Rh_2(1,6-BPGlyc)$_2$(OAc)$_2$ was more reactive than Rh_2(5*S*-MEPY)$_4$. The overall conclusion by the authors was that the distinct features of glycoluril as a ligand only offered a platform for expanded diversity within the dirhodium(II) carboxamidate family.

Table 1.18. *cis*/*trans*-Selectivity of $Rh_2(1,6\text{-BPGlyc})_2(OAc)_2$ in the formation of **96** and **97**.[186]

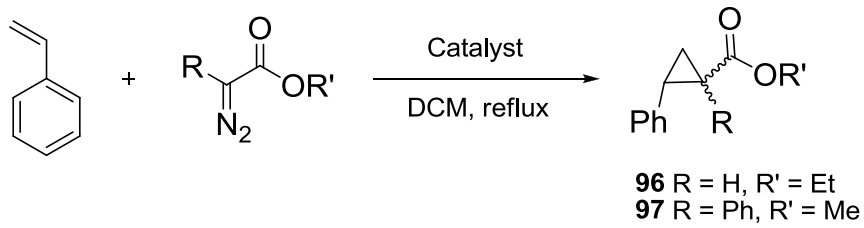

Entry	Catalyst	Yield (%), (*cis*/*trans*)	
		96	**97**
1	$Rh_2(4S\text{-MPPIM})_4$ (**82**)	64 (74:26)	66 (97:3)
2	$Rh_2(5S\text{-MEPY})_4$ (**57**)	59 (46:54)	27 (97:3)
3	$Rh_2(1,6\text{-BPGlyc})_2(OAc)_2$	43 (47:53)	55 (99:1)
4	$Rh_2(OAc)_4$	93 (38:62)	69 (98:2)

1.7. EFFECT OF AXIAL LIGANDS ON ENANTIOSELECTIVITY

The dirhodium core consists of a strong Rh–Rh single bond and this core provides the dirhodium(II) complex with an ability to form adducts at its two axial coordination sites. The two axial ligands are labile and therefore, they are considered to be the sites that give the dirhodium(II) complexes its catalytic activity during carbenoid transformations. As discussed earlier, the proposed mechanism considers that only one of the two coordination sites working as a carbene bonding site at a time throughout the catalytic cycle.[7,76]

The two axial positions of the dirhodium(II) are often occupied by solvent molecules that have the ability to establish weaker bonds with the dirhodium centre. As a consequence, the reaction solvent is able to critically affect the reaction outcome. Solvents with poor coordinative capabilities (e.g. DCM or non-polar solvents) are most efficient for carbenoid transformations. However, solvents that coordinate into dirhodium(II) complexes (e.g. ACN or THF) can partially or totally inhibit the generation of the carbenoid.[15,16,7,76,187-190]

Kinetic studies revealed that axial ligands, such as ACN, inhibit this kind of transformations through mixed kinetic inhibition mechanism. In this mechanism, the ligand can bind to both the free complex, as well as the catalyst-substrate complex.[7,76] In 2000, the Jessop group studied the effect of solvent on enantioselectivity of Rh_2(*S*-TBSP)$_4$-catalyzed asymmetric cyclopropanation of styrene with methyl *α*-phenyldiazoacetate (Scheme 1.29). They observed that the enantioselectivity is not only dependent on both the coordinating ability of the solvent, but also on its dielectric constant (the more polar solvent, the lower *ee* value obtained).[189]

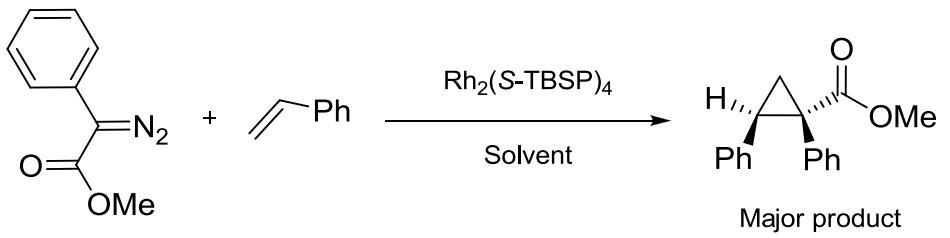

Major product

n-Hexane	90% *ee*
DCM	67% *ee*
THF	81% *ee*
ACN	73% *ee*
DMF	69% *ee*
scCO_2	84% *ee*

Scheme 1.29. Solvent effect on the enantioselectivity of Rh_2(*S*-TBSP)$_4$-catalyzed cyclopropanation of styrene.[189]

A few reports have emerged where the addition of Lewis base to the cyclopropanation reactions proved to be a useful and efficient method for tuning the properties of dirhodium(II) complexes.[15,21,129,140,141] Davies *et al.*[21] explored the addition of methyl benzoate to the Rh_2(*S*-biTISP)$_2$-catalyzed cyclopropanation reaction mixture. It did, not only improve the enantioselectivity of the cyclopropanation, but also allowed the utilization of very small amount of the catalyst (S/C = 100 000) with high efficiency (Scheme 1.30). At this stage, the authors were uncertain about the actual role of the additive, however they believed that this might be because of the coordination of the methyl benzoate additive to the carbenoid or to the other rhodium centre. Recently in 2013, computational studies on

dirhodium(II)-catalyzed cyclopropanations of electron-deficient alkenes carried out by the same research group gave a reasonable hypothesis. The authors concluded that the interaction between the carbenoid and the methyl benzoate's carbonyl is able to protect the rhodium carbene intermediates from self-destruction.[126]

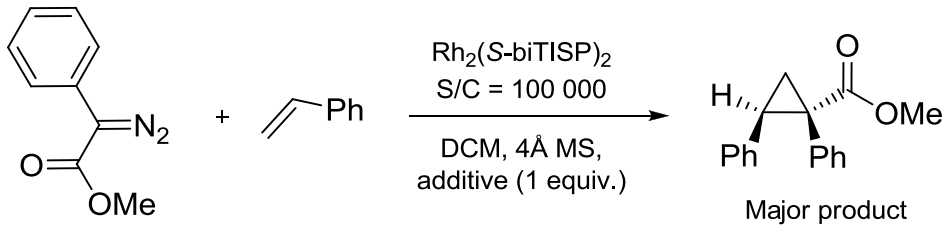

None	42 h, 82%, 65% *ee*
$PhCO_2Me$	28 h, 85%, 83% *ee*
TMU	>36 h, 48%, 74% *ee*
DIPEA	>36 h, 5%
$OP(Oct)_3$	>36 h, 36%, 78% *ee*

Scheme 1.30. Additive effect on the activity of Rh_2(*S*-biTISP)$_2$ in cyclopropanation reaction of Styrene with methyl α-phenyldiazoacetate.[21]

Charette *et al.*[129,140,141] also found that $TfNH_2$ and DMAP can be used as additive to moderately improve the chiral induction in cyclopropanation reactions involving *diacceptor* diazo compounds. The additive degree of success was highly dependent on the diazo substrate and reaction temperature. $TfNH_2$ and DMAP shown to be optimal with Rh_2(*S*-NTTL)$_4$ and Rh_2(*S*-TCPTTL)$_4$, respectively. The authors believed that the system is quite complex as the coordination onto one of the reactive sites could, not only modify the catalyst electronic properties, but also can alter the spatial arrangement of the chiral bridging ligands.[129]

On the other hand, chiral dirhodium(II) carboxamidates have a rigid structure if compared to chiral dirhodium(II) carboxylates. To the best of my knowledge, it is not reported that any of the known dirhodium(II) carboxamidates exhibits solvent effects on stereocontrol.[16,166]

1.8. CONCLUSION AND AIM OF WORK

As illustrated in this chapter, chiral dirhodium(II) complexes have been used as effective catalysts for highly stereoselective inter- and intramolecular cyclopropanation reactions. This superior level of diastereo- and enantioselectivity have reached the stage where they can serve as a powerful tool in the arsenal of synthetic chemists' in building up molecules with complex structures.

However, despite the number of available highly efficient dirhodium(II) catalysts, it is evident that none can be considered as a "universal catalyst" that is able to afford high enantiomeric induction with different classes of substrates and under different reaction conditions. For example, the high stereoselectivity of Rh_2(*S*-DOSP)$_4$ is strongly related to the use of methyl carboxylate ester as an *acceptor* group, along with non-polar reaction solvents.[80] Also, its enantioselectivity is sensitive to substitution on the carbenoid's aryl *donor* group.[98] Nevertheless, the careful choice of a suitable catalyst for the desired reaction can afford the cyclopropane product with high levels of chemo-, diastereo- and enantioselectivity.

Also, some of the currently reported catalysts suffer from technical problems. For example, although the emergence of Rh_2(*S*-PTAD)$_4$ circumvented to a great extent the selectivity limitations associated with Rh_2(*S*-DOSP)$_4$, the synthesis of the *S*-PTAD ligand is based on (*S*)-*α*-adamentylglycine which is not commercially available and its asymmetric synthesis is very tedious and tiresome. These ligand preparation related problems discourage the use of this catalyst.[149]

Therefore, the development of both synthetically accessible and highly enantioselective dirhodium(II) catalysts for asymmetric cyclopropanation reactions is required.

Developments in the field of chiral dirhodium(II) catalysts have essentially relied on the steric properties and conformations of the bridging ligands. The importance of catalyst sterics on chemo-, regio- and enantioselectivity of the catalyst has been confirmed through multiple reports.[112,131,124,19] Furthermore, the careful analysis of catalyst steric profile and conformation now allows prediction and explanation of the observed selectivity. The most coherent example would remain that the major differences between Hashimoto's *N*-phthalimide based catalytic series is the steric bulk at the ligand's *α*-position. The analysis of this series in some C-H insertion

reactions reported by Hashimoto and co-workers reveals a trend between the steric bulk at the *α*-position and the enantioselectivity of the catalyst.[111-113,116] The enantioselectivity increases with increasing steric bulk at the *α*-position and the highest enantioselectivity was observed by Rh_2(*S*-PTTL)$_4$ which is carrying the bulkiest *tert*-butyl group (Figure 1.33a). Later, the Davies group extended this idea and assumed that a catalyst carrying the more bulky adamantyl moiety at the *α*-carbon would surpass the ones carrying the standard PTTL ligands (Figure 1.33a).[124] Rh_2(*S*-PTAD)$_4$ demonstrated enhanced levels of enantioselectivity and acted as a complementary catalyst when Rh_2(*S*-DOSP)$_4$ failed to give high asymmetric induction with some of *donor-acceptor* systems.[98] In addition, Rh_2(*S*-PTAD)$_4$ was the optimal catalyst when the *acceptor* group of the *donor-acceptor* substrate is phosphonate ester,[124] nitrile,[145] trifluoromethyl[125] and keto groups[146] giving better enantioselectivities than Rh_2(*S*-PTTL)$_4$.

This trend, however, was not always valid for some other dirhodium(II)-catalyzed asymmetric transformations.[117,119,122,112] This gives the impression that the enantioselectivity of these catalysts is, not only dependant on the size of its *α*-carbon group, but also there must be a good match between the size of this group and the structures of reaction substrates and products themselves.

On the basis of these fundamental insights and previous findings of our research group, the core of the current project is the discovery of new chiral binuclear rhodium complexes as catalysts for highly enantioselective cyclopropanations. As a ligand backbone, commercially available L-amino acids will be mainly employed. The main focus lays on the exploration of the effect of lowering the symmetry of the amine protecting group on stereoselection (Figure 1.33b). This steric modification approach aimed to function as a development approach for the existing catalysts to achieve enhanced selectivity patterns while keeping the catalysts synthetically accessible. With the aid of X-ray crystallography, explanation of the observed selectivity will be proposed.

The project also aims towards the miniaturization of dirhodium(II)-catalyzed cyclopropanation reactions. The industry is suffering from a crisis in productivity and desperately needs new tools to guide the development of new drugs. As a consequence, research on synthesis in varied microreactors is having an increasing impact on chemical, biological and medical science. The microreactor technology is

able to solve several constraints related to conventional synthesis, e.g. high sample/reagent consumption, poor precision in catalytic reactions control and lack of integrated platforms for accurate product characterization and analysis.

The fabrication of microreactors using porous polymer monolith for the immobilization of dirhodium(II) complexes is to be investigated. The performance of the developed device is to be determined by performing cyclopropanation reaction in continuous flow with the determination of the reaction yield, stereoselectivity and catalyst leaching rate.

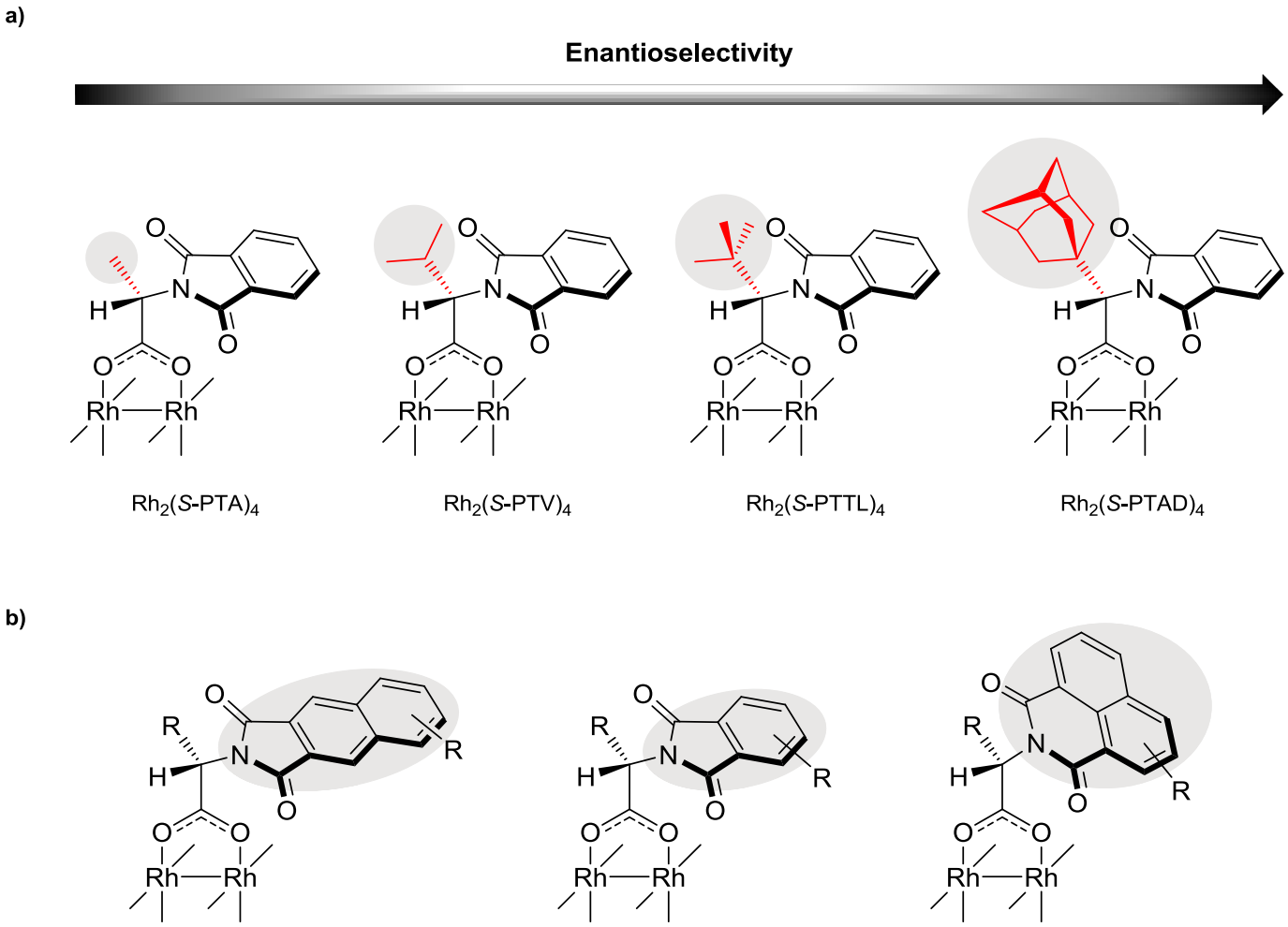

Figure 1.33. a) Trend of stereoselectivity in dirhodium(II) carboxylate-catalyzed cyclopropanations. b) The main focus of the current research.

1.9. REFERENCES

1. Corey, E. J.; Chen, C. P.; Reichard, G. A. *Tetrahedron Lett.* **1989**, *30*, 5547.
2. Waldrop, M. M. *Science* **1989**, *245*, 354.
3. Sasai, H.; Arai, T.; Satow, Y.; Houk, K. N.; Shibasaki, M. *J. Am. Chem. Soc.* **1995**, *117*, 6194.
4. Yao, S.; Johannsen, M.; Audrain, H.; Hazell, R. G.; Jørgensen, K. A. *J. Am. Chem. Soc.* **1998**, *120*, 8599.
5. Bjerre, J.; Rousseau, C.; Marinescu, L.; Bols, M. *Appl. Microbiol. Biotechnol.* **2008**, *81*, 1.
6. Ooi, T.; Kondo, Y.; Maruoka, K. *Angew. Chem., Int. Ed.* **1997**, *36*, 1183.
7. Pirrung, M. C.; Liu, H.; Morehead, A. T. *J. Am. Chem. Soc.* **2002**, *124*, 1014.
8. El-Deftar, M.; Adly, F. G.; Gardiner, M. G.; Ghanem, A. *Curr. Org. Chem.* **2012**, *16*, 1808.
9. Hansen, J.; Davies, H. M. L. *Coord. Chem. Rev.* **2008**, *252*, 545.
10. Davies, H. M. L.; Manning, J. R. *Nature* **2008**, *451*, 417.
11. Davies, H. M. L.; Morton, D. *Chem. Soc. Rev.* **2011**, *40*, 1857.
12. Colacot, T. J. *Proc. Indian Acad. Sci. (J. Chem. Sci.)* **2000**, *11*, 197.
13. Davies, H. M. L.; Bois, J. D.; Yu, J.-Q. *Chem. Soc. Rev.* **2011**, *40*, 1855.
14. Davies, H. M. L. *Eur. J. Org. Chem.* **1999**, 2459.
15. Trindade, A. F.; Coelho, J. A. S.; Afonso, C. A. M.; Veiros, L. F.; Gois, P. M. P. *ACS Catalysis* **2012**, *2*, 370.
16. Doyle, M. P.; Duffy, R.; Ratnikov, M.; Zhou, L. *Chem. Rev.* **2010**, *110*, 704.

17. Davies, H. M. L. *Curr. Org. Chem.* **1998**, *2*, 463.

18. Davies, H. M. L.; Hedley, S. J. *Chem. Soc. Rev.* **2007**, *36*, 1109.

19. Merlic, C. A.; Zechman, A. L. *Synthesis* **2003**, 1137.

20. Pelphrey, P.; Hansen, J.; Davies, H. M. L. *Chem. Sci.* **2010**, *1*, 254.

21. Davies, H. M. L.; Venkataramani, C. *Org. Lett.* **2003**, *5*, 1403.

22. Chernyaev, I. I.; Shenderetskaya, E. V.; Koryagina., A. A. *Russ. J. Inorg. Chem.* **1960**, *5*, 559.

23. Chernyaev, I. I.; Shenderetskaya, E. V.; Maiorova, A. G.; Koryagina, A. A. *Russ. J. Inorg. Chem.* **1965**, *10*, 537.

24. Nazarova, L. A.; Chernyaev, I. I.; Morozova, A. S. *Russ. J. Inorg. Chem.* **1965**, *10*, 539.

25. Nazarova, L. A.; Chernyaev, I. I.; Morozova, A. S. *Russ. J. Inorg. Chem.* **1966**, *11*, 2583.

26. Hubert, A. J.; Noels, A. F.; Anciaux, A. J.; Teyssie, P. *Synthesis* **1976**, *9*, 600.

27. Paulisse, R.; Reimlinger, H.; Hayez, E.; Hubert, A. J.; Teyssie, P. *Tetrahedron Lett.* **1973**, *14*, 2233.

28. Anciaux, A. J.; Demonceau, A.; Hubert, A. J.; Noels, A. F.; Petiniot, N.; Teyssie, P. *J. Chem. Soc., Chem. Commun.* **1980**, 765.

29. Doyle, M. P.; van Leusen, D.; Tamblyn, W. H. *Synthesis* **1981**, *10*, 787.

30. Zhang, X.-J.; Yan, M.; Huang, D. *Org. Biomol. Chem.* **2009**, *7*, 187.

31. Yamawaki, M.; Tanaka, M.; Abe, T.; Anada, M.; Hashimoto, S. *Heterocycles* **2007**, *72*, 709.

32. Catino, A. J.; Nichols, J. M.; Forslund, R. E.; Doyle, M. P. *Org. Lett.* **2005**, *7*, 2787.

33. Davies, H. M. L.; Denton, J. R. *Chem. Soc. Rev.* **2009**, *38*, 3061.

34. Doyle, M. P. *J. Org. Chem.* **2006**, *71*, 9253.

35. Doyle, M. P.; McKervey, M. A.; Ye, T. *Modern Catalytic Methods for Organic Synthesis with Diazo Compounds: From Cyclopropanes to Ylides*; Wiley: New York, 1998.

36. Hodgson, D. M.; Stupple, P. A.; Pierard, F. Y. T. M.; Labande, A. H.; Johnstone, C. *Chem.-Eur. J.* **2001**, *7*, 4465.

37. Doyle, M. P.; Forbes, D. C.; Vasbinder, M. M.; Peterson, C. S. *J. Am. Chem. Soc.* **1998**, *120*, 7653.

38. Doyle, M. P.; Hu, W. *Synlett* **2001**, 1364.

39. Doyle, M. P.; Phillips, I. M.; Hu, W. *J. Am. Chem. Soc.* **2001**, *123*, 5366.

40. Doyle, M. P.; Valenzuela, M.; Huang, P. *Proc. Natl. Acad. Sci. U. S. A.* **2004**, *101*, 5391.

41. Wang, Y.; Wolf, J.; Zavalij, P.; Doyle, M. P. *Angew. Chem., Int. Ed.* **2008**, *47*, 1439.

42. Watanabe, N.; Shimada, N.; Anada, M.; Hashimoto, S. *Tetrahedron: Asymmetry* **2014**, *25*, 63.

43. Anada, M.; Washio, T.; Shimada, N.; Kitagaki, S.; Nakajima, M.; Shiro, M.; Hashimoto, S. *Angew. Chem., Int. Ed.* **2004**, *43*, 2665.

44. Hansen, J. H.; Parr, B. T.; Pelphrey, P.; Jin, Q.; Autschbach, J.; Davies, H. M. L. *Angew. Chem., Int. Ed.* **2011**, *50*, 2544.

45. Doyle, M. P.; Protopopova, M. N. *Tetrahedron* **1998**, *54*, 7919.

46. Davies, H. M. L.; Antoulinakis, E. G. *Org. React.* **2001**, *57*, 1.

47. Lebel, H.; Marcoux, J.-F.; Molinaro, C.; Charette, A. B. *Chem. Rev.* **2003**, *103*, 977.

48. Tsuji, J. *Modern Rhodium-Catalyzed Organic Reactions*; Wiley-VCH: Weinheim, 2005.

49. Wong, H. N. C.; Hon, M.-Y.; Tse, C.-W.; Yip, Y.-C.; Tanko, J.; Hudlicky, T. *Chem. Rev.* **1989**, *89*, 165.

50. Reissig, H.-U.; Zimmer, R. *Chem. Rev.* **2003**, *103*, 1151.

51. Goldberg, A. F. G.; O'Connor, N. R.; Craig, R. A.; Stoltz, B. M. *Org. Lett.* **2002**, *14*, 5314.

52. Hudlicky, T.; Reed, J. W. In *Comprehensive Organic Synthesis;* Trost, B. M.; Fleming, I. Eds.; Pergamon: New York, 1991; p. 899.

53. Rubin, M.; Rubina, M.; Gevorgyan, V. *Chem. Rev.* **2007**, *107*, 3117.

54. Donaldson, W. A. *Tetrahedron* **2001**, *57*, 8589.

55. Chen, D. Y.-K.; Pouwer, R. H.; Richard, J.-A. *Chem. Soc. Rev.* **2012**, *41*, 4631.

56. Liu, H. W.; Walsh, C. T. In *The Chemistry of the Cyclopropyl Group*; Patai, S.; Rappoport, Z. Eds.; Wiley: Chichester, 1987; p. 959.

57. Salaun, J. *Top. Curr. Chem.* **2000**, *207*, 1.

58. Gnad, F.; Reiser, O. *Chem. Rev.* **2003**, *103*, 1603.

59. Reichelt, A.; Martin, S. F. *Acc. Chem. Res.* **2006**, *39*, 433.

60. Staudinger, H.; Ruzicka, L. *Helv. Chim. Acta* **1924**, *7*, 177.

61. Arlt, D.; Jautelat, M.; Lantzsch, R. *Angew. Chem., Int. Ed.* **1981**, *20*, 703.

62. Zhang, X.; Hodgetts, K.; Rachwal, S.; Zhao, H.; Wasley, J. W. F.; Craven, K.; Brodbeck, R.; Kieltyka, A.; Hoffman, D.; Bacolod, M. D.; Girard, B.; Tran, J.; Thurkauf, A. *J. Med. Chem.* **2000**, *43*, 3923.

63. Kumar, J. S. R.; Roy, S.; Datta, A. *Bioorg. Med. Chem. Lett.* **1999**, *9*, 513.

64. Baldessarini, R. J. In *Goodman & Gilman's the Pharmacological Basis of Therapeutics*; Brunton, L. L.; Lazo, J. S.; Parker, K. L. Eds.; McGraw-Hill: New York, 2005.

65. Wipf, P.; Reeves, J. T.; Day, B. W. *Curr. Pharm. Des.* **2004**, *10*, 1417.

66. Yamada, K.; Ojika, M.; Kigoshi, H. *Nat. Prod. Rep.* **2007**, *24*, 798.

67. de Meijere, A.; Kozhushkov, S. I.; Fokin, A. A.; Emme, I.; Redlich, S.; Schreiner, P. R. *Pure Appl. Chem.* **2003**, *75*, 549.

68. Yates, P. *J. Am. Chem. Soc.* **1952**, *74*, 5376.

69. Nakamura, E.; Yoshikai, N.; Yamanaka, M. *J. Am. Chem. Soc.* **2002**, *124*, 7181.

70. Doyle, M. P. *Acc. Chem. Res.* **1986**, *19*, 348.

71. Hansen, J.; Autschbach, J.; Davies, H. M. L. *J. Org. Chem.* **2009**, *74*, 6555.

72. Nowlan, D. T.; Gregg, T. M.; Davies, H. M. L.; Singleton, D. A. *J. Am. Chem. Soc.* **2003**, *125*, 15902.

73. Sheehan, S. M.; Padwa, A.; Snyder, J. P. *Tetrahedron Lett.* **1998**, *39*, 949.

74. Wong, F. M.; Wang, J.; Hengge, A. C.; Wu, W. *Org. Lett.* **2007**, *9*, 1663.

75. Berry, J. F. *Dalton Trans.* **2012**, *41*, 700.

76. Pirrung, M. C.; Morehead, A. T. *J. Am. Chem. Soc.* **1996**, *118*, 8162.

77. Kornecki, K. P.; Briones, J. F.; Boyarskikh, V.; Fullilove, F.; Autschbach, J.; Schrote, K. E.; Lancaster, K. M.; Davies, H. M. L.; Berry, J. F. *Science* **2013**, *342*, 351.

78. Davies, H. M. L.; Beckwith, E. J. *Chem. Rev.* **2003**, *103*, 2861.

79. Fraile, J. M.; García, J. I.; Gissibl, A.; Mayoral, J. A.; Pires, E.; Reiser, O.; Roldán, M.; Villalba, I. *Chem.-Eur. J.* **2007**, *13*, 8830.

80. Davies, H. M. L.; Bruzinski, P. R.; Lake, D. H.; Kong, N.; Fall, M. J. *J. Am. Chem. Soc.* **1996**, *118*, 6897.

81. Cotton, F. A.; Walton, R. A. *Multiple Bonds between Metal Atoms*; Clarendon Press: Oxford, 1993.

82. Bonge, H. T.; Hansen, T. *J. Org. Chem.* **2010**, *75*, 2309.

83. Padwa, A.; Austin, D. J.; Hornbuckle, S. F.; Semones, M. A.; Doyle, M. P.; Protopopova, M. N. *J. Am. Chem. Soc.* **1992**, *114*, 1874.

84. Catino, A. J.; Nichols, J. M.; Choi, H.; Gottipamula, S.; Doyle, M. P. *Org. Lett.* **2005**, *7*, 5167.

85. Hansen, J.; Dikarev, E.; Autschbach, J.; Davies, H. M. L. *J. Org. Chem.* **2009**, *74*, 6564.

86. Durivage, J. C.; Gruhn, N. E.; Li, B.; Dikarev, E. V.; Lichtenberger, D. L. *J. Cluster Sci.* **2008**, *19*, 275.

87. Dikarev, E. V.; Gray, T. G.; Li, B. *Angew. Chem., Int. Ed.* **2005**, *44*, 1721.

88. Dikarev, E. V.; Li, B.; Zhang, H. *J. Am. Chem. Soc.* **2006**, *128*, 2814.

89. Trindade, A. F.; Gois, P. M. P.; Veiros, L. F.; Andre, V.; Duarte, M. T.; Afonso, C. A. M.; Caddick, S.; Cloke, F. G. N. *J. Org. Chem.* **2008**, *73*, 4076.

90. Gois, P. M. P.; Trindade, A. F.; Veiros, L. F.; Andre, V.; Duarte, M. T.; Afonso, C. A. M.; Caddick, S.; Cloke, F. G. N. *Angew. Chem., Int. Ed.* **2007**, *46*, 5750.

91. Hashimoto, S.; Watanabe, N.; Ikegami, S. *J. Chem. Soc., Chem. Commun.* **1992**, 1508.

92. Kennedy, M.; McKervey, M. A.; Maguire, A. R.; Roos, G. H. P. *J. Chem. Soc., Chem. Commun.* **1990**, 361.

93. Ye, T.; Garcia, F. C.; McKervey, M. A. *J. Chem. Soc., Perkin Trans. 1* **1995**, 1373.

94. Ye, T.; McKervey, M. A.; Brandes, B. D.; Doyle, M. P. *Tetrahedron Lett.* **1994**, *35*, 7269.

95. Davies, H. M. L.; Bruzinski, P. R.; Fall, M. J. *Tetrahedron Lett.* **1996**, *37*, 4133.

96. Davies, H. M. L.; Rusiniak, L. *Tetrahedron Lett.* **1998**, *39*, 8811.

97. Davies, H. M. L.; Townsend, R. J. *J. Org. Chem.* **2001**, *66*, 6595.

98. Chepiga, K. M.; Qin, C.; Alford, J. S.; Chennamadhavuni, S.; Gregg, T. M.; Olson, J. P.; Davies, H. M. L. *Tetrahedron* **2013**, *69*, 5765.

99. Davies, H. M. L.; Nagashima, T.; Klino, J. L. *Org. Lett.* **2000**, *2*, 823.

100. Corey, E. J.; Gant, T. J. *Tetrahedron Lett.* **1994**, *35*, 5373.

101. Nagashima, T.; Davies, H. M. L. *J. Am. Chem. Soc.* **2001**, *123*, 2695.

102. Davies, H. M. L.; Boebel, T. A. *Tetrahedron Lett.* **2000**, *41*, 8189.

103. Ni, A.; France, J. E.; Davies, H. M. L. *J. Org. Chem.* **2006**, *71*, 5594.

104. Hadley, S. J.; Ventura, D. L.; Dominiak, P. M.; Nygren, C. L.; Davies, H. M. L. *J. Org. Chem.* **2006**, *71*, 5349.

105. Davies, H. M. L.; Dai, X.; Long, M. S. *J. Am. Chem. Soc.* **2006**, *128*, 2485.

106. Gregg, T. M.; Farrugia, M. K.; Frost, J. R. *Org. Lett.* **2009**, *11*, 4434.

107. Gregg, T. M.; Algera, R. F.; Frost, J. R.; Hassan, F.; Stewart, R. J. *Tetrahedron Lett.* **2010**, *51*, 6429.

108. Davies, H. M. L.; Kong, N. *Tetrahedron Lett.* **1997**, *38*, 4203.

109. Davies, H. M. L.; Panaro, S. A. *Tetrahedron Lett.* **1999**, *40*, 5287.

110. Davies, H. M. L.; Doan, B. D. *J. Org. Chem.* **1999**, *64*, 8501.

111. Takahashi, T.; Tsutsui, H.; Tamura, M.; Kitagaki, S.; Nakajima, M.; Hashimoto, S. *Chem. Commun.* **2001**, 1604.

112. Kitagaki, S.; Anada, M.; Kataoka, O.; Matsuno, K.; Umeda, C.; Watanabe, N.; Hashimoto, S. *J. Am. Chem. Soc.* **1999**, *121*, 1417.

113. Tsutsui, H.; Matsuura, M.; Makino, K.; Nakamura, S.; Nakajima, M.; Kitagaki, S.; Hashimoto, S. *Isr. J. Chem.* **2001**, *41*, 283.

114. Yamawaki, M.; Tsutsui, H.; Kitagaki, S.; Anada, M.; Hashimoto, S. *Tetrahedron Lett.* **2002**, *43*, 9561.

115. Tsutsui, H.; Yamaguchi, Y.; Kitagaki, S.; Nakamura, S.; Anada, M.; Hashimoto, S. *Tetrahedron: Asymmetry* **2003**, *14*, 817.

116. Minami, K.; Saito, H.; Tsutsui, H.; Nambu, H.; Anada, M.; Hashimoto, S. *Adv. Synth. Catal.* **2005**, *347*, 1483.

117. Hashimoto, S.; Watanabe, N.; Ikegami, S. *Tetrahedron Lett.* **1990**, *31*, 5173.

118. Tsutsui, H.; Abe, T.; Nakamura, S.; Anada, M.; Hashimoto, S. *Chem. Pharm. Bull.* **2005**, *53*, 1366.

119. Hashimoto, S.; Watanabe, N.; Sato, T.; Shiro, M.; Ikegami, S. *Tetrahedron Lett.* **1993**, *34*, 5109.

120. Goto, T.; Takada, K.; Shimada, N.; Nambu, H.; Anada, M.; Shiro, M.; Ando, K.; Hashimoto, S. *Angew. Chem., Int. Ed.* **2011**, *50*, 6803.

121. Lindsay, V. N. G.; Lin, W.; Charette, A. B. *J. Am. Chem. Soc.* **2009**, *131*, 16383.

122. Collet, F.; Lescot, C.; Liang, C.; Dauban, P. *Dalton Trans.* **2010**, *39*, 10401.

123. Ghanem, A.; Gardiner, M. G.; Williamson, R. M.; Müller, P. *Chem.-Eur. J.* **2010**, *16*, 3291.

124. Reddy, R. P.; Lee, G. H.; Davies, H. M. L. *Org. Lett.* **2006**, *8*, 3437.

125. Denton, J. R.; Sukumaran, D.; Davies, H. M. L. *Org. Lett.* **2007**, *9*, 2625.

126. Wang, H.; Guptill, D. M.; Varela-Alvarez, A.; Musaev, D. G.; Davies, H. M. L. *Chem. Sci.* **2013**, *4*, 2844.

127. DeAngelis, A.; Dmitrenko, O.; Yap, G. P. A.; Fox, J. M. *J. Am. Chem. Soc.* **2009**, *131*, 7230.

128. Awata, A.; Arai, T. *Synlett* **2013**, *24*, 29.

129. Lindsay, V. N. G.; Nicolas, C.; Charette, A. B. *J. Am. Chem. Soc.* **2011**, *133*, 8972.

130. Goto, T.; Takada, K.; Anada, M.; Ando, K.; Hashimoto, S. *Tetrahedron Lett.* **2011**, *52*, 4200.

131. Müller, P.; Allenbach, Y.; Robert, E. *Tetrahedron: Asymmetry* **2003**, *14*, 779.

132. Müller, P.; Ghanem, A. *Synlett* **2003**, 1830.

133. Müller, P.; Lacrampe, F. *Helv. Chim. Acta* **2004**, *87*, 2848.

134. Müller, P.; Bernardinelli, G.; Allenbach, Y. F.; Ferri, M.; Flack, H. D. *Org. Lett.* **2004**, *6*, 1725.

135. Müller, P.; Bernardinelli, G.; Allenbach, Y.; Ferri, M.; Grass, S. *Synlett* **2005**, 1397.

136. Müller, P.; Allenbach, Y.; Chappellet, S.; Ghanem, A. *Synthesis* **2006**, 1689.

137. Müller, P.; Lacrampe, F. *Helv. Chim. Acta* **2004**, *87*, 2848.

138. Marcoux, D.; Goudreau, S. R.; Charette, A. B. *J. Org. Chem.* **2009**, *74*, 8939.

139. Marcoux, D.; Charette, A. B. *Angew. Chem.* **2008**, *47*, 10155.

140. Marcoux, D.; Lindsay, V. N. G.; Charette, A. B. *Chem. Commun.* **2010**, *46*, 910.

141. Marcoux, D.; Azzi, S.; Charette, A. B. *J. Am. Chem. Soc.* **2009**, *131*, 6970.

142. Müller, P.; Allenbach, Y.; Grass, S. *Tetrahedron: Asymmetry* **2005**, *16*, 2007.

143. Chuprakov, S.; Kwok, S. W.; Zhang, L.; Lercher, L.; Fokin, V. V. *J. Am. Chem. Soc.* **2009**, *131*, 18034.

144. Müller, P.; Ghanem, A. *Org. Lett.* **2004**, *6*, 4347.

145. Denton, J. R.; Cheng, K.; Davies, H. M. L. *Chem. Commun.* **2008**, 1238.

146. Denton, J. R.; Davies, H. M. L. *Org. Lett.* **2009**, *11*, 787.

147. Boruta, D. T.; Dmitrenko, O.; Yap, G. P. A.; Fox, J. M. *Chem. Sci.* **2012**, *3*, 1589.

148. Lindsay, V. N. G.; Charette, A. B. *ACS Catalysis* **2012**, *2*, 1221.

149. Qin, C.; Boyarskikh, V.; Hansen, J. H.; Hardcastle, K. I.; Musaev, D. G.; Davies, H. M. L. *J. Am. Chem. Soc.* **2011**, *133*, 19198.

150. Davies, H. M. L.; Hansen, J.; Changming, Q. In PCT/US2012/040608, 2012

151. Qin, C.; Davies, H. M. L. *J. Am. Chem. Soc.* **2013**, *135*, 14516.

152. Qin, C.; Davies, H. M. L. *Org. Lett.* **2013**, *15*, 310.

153. Dennis, A. M.; Korp, J. D.; Bernal, I.; Howard, R. A.; Bear, J. L. *Inorg. Chem.* **1983**, *22*, 1522.

154. Doyle, M. P.; Brandes, B. D.; Kazala, A. P.; Pieters, R. J.; Jarstfer, M. B.; Watkins, L. M.; Eagle, C. T. *Tetrahedron Lett.* **1990**, *31*, 6613.

155. Doyle, M. P.; Winchester, W. R.; Hoorn, J. A. A.; Lynch, V.; Simonsen, S. H.; Ghosh, R. *J. Am. Chem. Soc.* **1993**, *115*, 9968.

156. Doyle, M. P.; Winchester, W. R.; Protopopova, M. N.; Müller, P.; Bernardinelli, G.; Ene, D. G.; Motallebi, S. *Helv. Chim. Acta* **1993**, *76*, 2227.

157. Doyle, M. P.; Davies, S. B.; Hu, W. H. *Chem. Commun.* **2000**, 867.

158. Doyle, M. P.; Dyatkin, A. B.; Protopopova, M. N.; Yang, C. I.; Miertschin, C. S.; Winchester, W. R.; Simonsen, S. H.; Lynch, V.; Ghosh, R. *Recl. Trav. Chim. Pays-Bas* **1995**, *114*, 163.

159. Doyle, M. P.; Zhou, Q.-L.; Raab, C. E.; Roos, G. H. P.; Simonsen, S. H.; Lynch, V. *Inorg. Chem.* **1996**, *35*, 6064.

160. Doyle, M. P.; Davies, S. B.; Hu, W. *Org. Lett.* **2000**, *2*, 1145.

161. Doyle, M. P.; Hu, W.; Phillips, I. M.; Moody, C. J.; Pepper, A. G.; Slawin, A. G. *Adv. Synth. Catal.* **2001**, *343*, 112.

162. Lin, W.; Charette, A. B. *Adv. Synth. Catal.* **2005**, *347*, 1547.

163. Doyle, M. P.; Zhou, Q. L.; Charnsangavej, C.; Longoria, M. A.; McKervey, M. A.; Garcia, C. F. *Tetrahedron Lett.* **1996**, *37*, 4129.

164. Doyle, M. P.; Austin, R. E.; Bailey, A. S.; Dwyer, M. P.; Dyatkin, A. B.; Kalinin, A. V.; Kwan, M. M. Y.; Liras, S.; Oalmann, C. J.; Pieters, R. J.; Protopopova, M. N.; Raab, C. E.; Roos, G. H. P.; Zhou, Q. L.; Stephen, F. M. *J. Am. Chem. Soc.* **1995**, *117*, 5763.

165. Welch, C. J.; Tu, Q.; Wang, T.; Raab, C.; Wang, P.; Jia, X.; Bu, X.; Bykowski, D.; Hohenstaufen, B.; Doyle, M. P. *Adv. Synth. Catal.* **2006**, *348*, 821.

166. Doyle, M. P. In *Modern Rhodium-Catalyzed Organic Reactions*; Evans, P. A. Ed.; Wiley: Hoboken, 2005; pp. 341.

167. Doyle, M. P.; Morgan, J. P.; Colyer, J. T. *J. Organomet. Chem.* **2005**, *690*, 5525.

168. Doyle, M. P.; Morgan, J. P.; Fettinger, J. C.; Zavalij, P. Y.; Colyer, J. T.; Timmons, D. J.; Carducci, M. D. *J. Org. Chem.* **2005**, *70*, 5291.

169. Doyle, M. P.; Protopopova, M.; Müller, P.; Ene, D.; Shapiro, E. A. *J. Am. Chem. Soc.* **1994**, *116*, 8492.

170. Doyle, M. P.; Zhou, Q. L.; Simonsen, S. H.; Lynch, V. *Synlett* **1996**, 697.

171. Hu, W.; Timmons, D. J.; Doyle, M. P. *Org. Lett.* **2002**, *4*, 901.

172. Doyle, M. P.; Hu, W. *Adv. Synth. Catal.* **2001**, *343*, 299.

173. Bykowski, D.; Wu, K.-H.; Doyle, M. P. *J. Am. Chem. Soc.* **2006**, *128*, 16038.

174. Lin, W.; Charette, A. B. *Adv. Synth. Catal.* **2005**, *347*, 1547.

175. Doyle, M. P.; Zhou, Q. L.; Dyatkin, A. B.; Ruppar, D. A. *Tetrahedron Lett.* **1995**, *36*, 7579.

176. Doyle, M. P.; Peterson, C. S.; Zhou, Q. L.; Nishiyama, H. *J. Chem. Soc., Chem. Commun.* **1997**, 211.

177. Doyle, M. P.; Wang, Y.; Ghorbani, P.; Bappert, E. *Org. Lett.* **2005**, *7*, 5035.

178. Lindsay, V. N. G.; Fiset, D.; Gritsch, P. J.; Azzi, S.; Charette, A. B. *J. Am. Chem. Soc.* **2013**, *135*, 1463.

179. Rogers, D. H.; Yi, E. C.; Poulter, C. D. *J. Org. Chem.* **1995**, *60*, 941.

180. Martin, S. F.; Dwyer, M. P.; Hartmann, B.; Knight, K. S. *J. Org. Chem.* **2000**, *65*, 1305.

181. Watanabe, N.; Matsuda, H.; Kuribayashi, H.; Hashimoto, S. *Heterocycles* **1996**, *42*, 537.

182. Kitagaki, S.; Matsuda, H.; Watanabe, N.; Hashimoto, S. *Synlett* **1997**, 1171.

183. Washio, T.; Nambu, H.; Anada, M.; Hashimoto, S. *Tetrahedron: Asymmetry* **2007**, *18*, 2606.

184. Lou, Y.; Horikawa, M.; Kloster, R. A.; Hawryluk, N. A.; Corey, E. J. *J. Am. Chem. Soc.* **2004**, *126*, 8916.

185. Lou, Y.; Remarchuk, T. P.; Corey, E. J. *J. Am. Chem. Soc.* **2005**, *127*, 14223.

186. Nichols, J. M.; Liu, Y.; Zavalij, P.; Isaacs, L.; Doyle, M. P. *Inorg. Chim. Acta* **2008**, *361*, 3309.

187. Doyle, M. P.; Forbes, D. C. *Chem. Rev.* **1998**, *98*, 911.

188. Candeias, N. R.; Gois, P. M. P.; Afonso, C. A. M. *J. Org. Chem.* **2006**, *71*, 5489.

189. Wynne, D. C.; Olmstead, M. M.; Jessop, P. G. *J. Am. Chem. Soc.* **2000**, *122*, 7638.

190. Antos, J. M.; McFarland, J. M.; Iavarone, A. T.; Francis, M. B. *J. Am. Chem. Soc.* **2009**, *131*, 6301.

CHAPTER 2: DESIGN AND SYNTHESIS OF NOVEL CHIRAL DIRHODIUM(II) CARBOXYLATES FOR APPLICATION IN ASYMMETRIC INTERMOLECULAR CYCLOPROPANATION REACTIONS

2.1. INTRODUCTION

Within the context of catalyst sterics, symmetry is believed to be an important concept that plays an extensive role in chiral catalysis. The use of the highest symmetry catalyst is assumed to minimize the number of possible substrate trajectories in the catalytic steps of the reaction in question. This in turn, will afford a predictable more precise three dimensional transition state structure. Accordingly in the stage of chiral catalyst design, the use of ligands with the highest possible symmetry is mostly preferred. The utilization of such ligands can significantly simplify the prediction of stereoselection mechanisms. Moreover, the synthesis of such ligands, in most cases, is much simpler.[1]

However, Garcia *et al.*[1,2] studied a new family of bis(oxazoline) ligands that lacked the classical C_2-symmetry recommended for this type of ligands (Figure 2.1). Experimental results together with theoretical calculations for enantioselective Cu-catalyzed cyclopropanations using the new “lower symmetry” ligands were carried out. Surprisingly, high enantioinduction was observed with some of these ligands and they were able to induce enantioselectivity levels that are close to the best ones obtained by applying the classical C_2-ligands. The authors concluded that the symmetry of ligands is not a mandatory prerequisite for obtaining high levels of enantioselectivity. This is because enantioselection mechanisms mainly originate from the different preferred reaction channels as a function of the different steric interactions taking place between the substrate and the ligands.

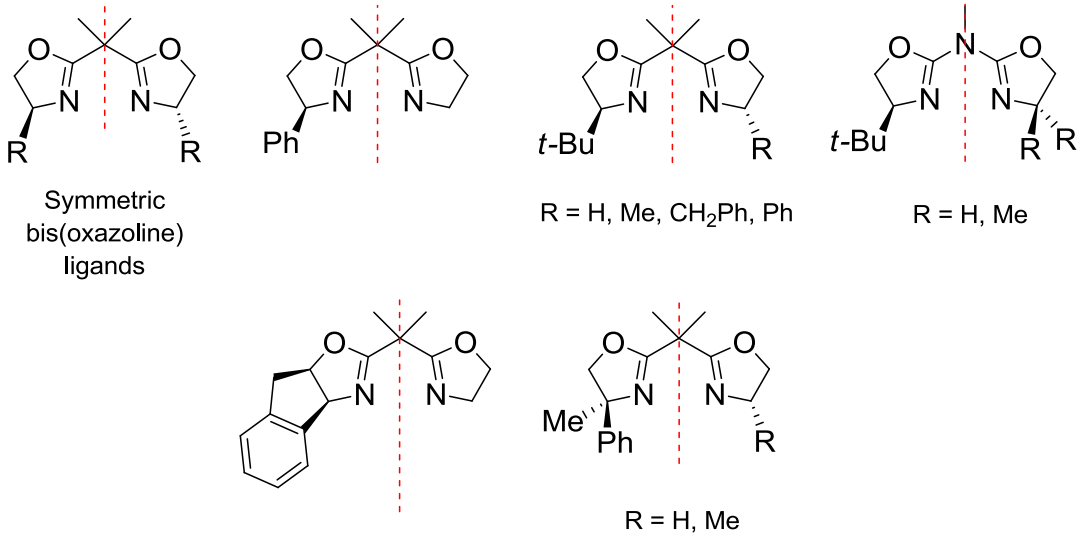

Figure 2.1. Structures of lower symmetry bis(oxazoline) ligands studied by Garcia *et al.*[1]

For dirhodium(II) complexes, their paddlewheel framework provides a distinguishable scaffolding for achieving higher symmetry chiral complexes through what is called a "Modular Approach".[3] In this approach, several identical C_1-symmetric ligands surround the inherently high symmetry core to afford a far superior symmetrical homochiral molecule compared to the individual ligand itself. It was believed that because of this interesting attribute, chiral dirhodium(II) complexes exhibit their exceptionally high stereoselectivities.[3] However as it was demonstrated in Chapter 1, Section 1.5.3.2, Fox[4] and Charette,[5] independently, explored the interruption of this high symmetry framework. They replaced one of the ligands with achiral ligand which led to the generation of lower symmetry heteroleptic complexes. Screening results revealed that lowering the overall symmetry of the catalysts had a beneficial effect on their asymmetric induction. Also as it was illustrated the same chapter, Section 1.6.2, Corey[6] and Doyle,[7] independently, reported a similar observation for chiral dirhodium(II) carboxamidates.

For dirhodium(II) catalysts derived from *N*-protected amino acid ligands, a long held opinion (based on enantioselectivities achieved with these systems) has been related to the influence of the *N*-aryl tethers that can act as steric blockers. The role of these tethers is considered pivotal in controlling the trajectory of the incoming substrates

during catalysis. Following the classical fashion of catalyst design described above, all reported dirhodium(II) complexes belonging to this family are designed to have a symmetric *N*-heterocyclic tether for the construction of the chiral ligands (Figure 2.2).

In 2004, however, Müller, Ghanem and co-workers[8,9] reported several Rh_2(*S*-NTTL)$_4$ analogues at which only one hydrogen on the hetereocyclic tether is substituted generating ligands carrying lower symmetry *N*-protecting groups (Figure 2.2). The results revealed that, Rh_2(*S*-4-Br-NTTL)$_4$-catalyzed cyclopropanation of styrene with dimethyl malonate proceeded with far improved levels of enantioselectivity (82% *ee*) compared to its parent, Rh_2(*S*-NTTL)$_4$ (37% *ee*) (Table 2.1).[8,10] The same catalyst was also effective for olefin cyclopropanation with Meldrum's acid giving 92% *ee* with styrene and 87% *ee* with 1-pentene.

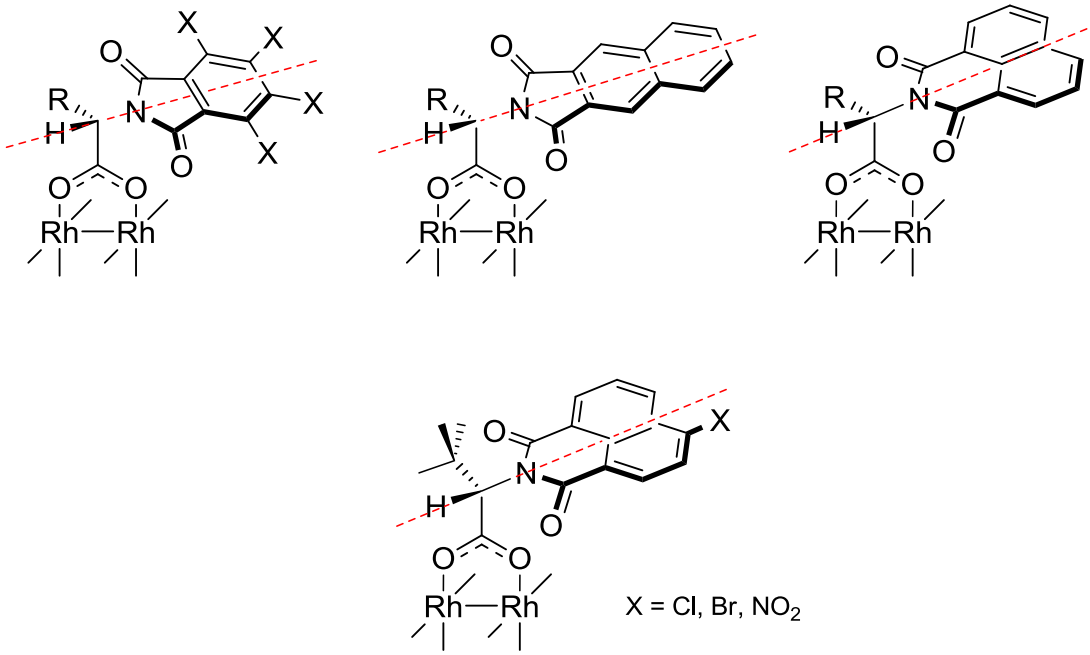

Figure 2.2. Ligands backbone structure comparison.

Table 2.1. Enantioselective cyclopropanation of styrene with dimethyl malonate *via* the *in situ* generated phenyliodonium ylide method.[8]

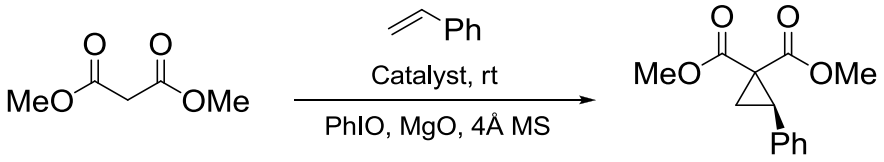

Entry	**Catalyst**	**Yield (%)**	***ee* (%)**
1	Rh_2(*S*-NTTL)$_4$	72	37
2	Rh_2(*S*-4-Cl-NTTL)$_4$	77	66
3	Rh_2(*S*-4-Br-NTTL)$_4$	75	82
4	Rh_2(*S*-4-NO_2-NTTL)$_4$	60	66

The X-ray crystal structure of Rh_2(*S*-NTTL)$_4$ revealed that *N*-1,8-naphthaloyl incorporation maintained the chiral nature of the crown cavity surrounding the rhodium axial site through a clockwise twist of these groups (Figure 2.3).[9] This X-ray served as a model to account for the higher enantioselectivity observed when using Rh_2(*S*-4-Br-NTTL)$_4$. The authors communicated that, if Rh_2(*S*-4-Br-NTTL)$_4$ is retaining a similar structure as Rh_2(*S*-NTTL)$_4$, the bromo substituents would lie at the cavity rim and is likely to exert a strong influence on the enantiofacial discrimination of the incoming alkene (Cavity Rim Steric Impedance).[9] The improved performance of the 4-Br-substituted catalyst over the 4-Cl analogue was also justified as the larger halide would exert more influence at the cavity rim.

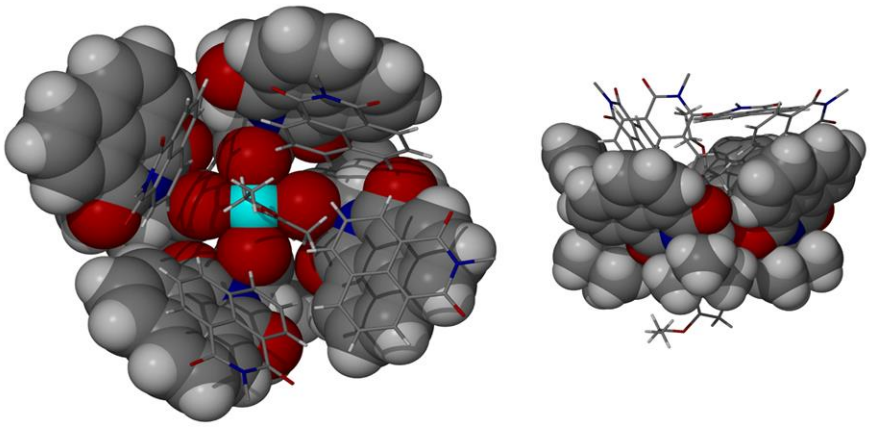

Figure 2.3. X-ray structure of Rh_2(*S*-NTTL)$_4$[9] (Reprinted from Ghanem, A.; Gardiner, M. G.; Williamson, R. M.; Müller, P. *Chem.-Eur. J.* **2010**, *16*, 3291, Copyright 2010, with permission from John Wiley and Sons).

Guided by the previous findings related to the nature of the chiral crown cavity complexes,[9,11] modifications of the *N*-heterocyclic tether protecting the amine functionality in ligands derived from amino acids are continued to be pursued. The trigger of the project reported herein was to profoundly explore the variation of ligand sterics through lowering the symmetry of the *N*-protecting group as an essential part in this type of ligands and its effect on stereoselection mechanisms in asymmetric cyclopropanations.

2.2. RESULTS AND DISCUSSION

2.2.1. Preparation of chiral dirhodium(II) carboxylate complexes

2.2.1.1. Synthesis of chiral carboxylate ligands

Unlike the previously reported tendency applied for the development of chiral dirhodium(II) paddlewheel catalysts where modifications focused on the use of symmetric *N*-protecting groups, a new catalytic series derived from chiral *N*-1,2-naphthaloyl-(*S*)-amino acid bridging ligands **1a-f** was constructed (Figure 2.4). *N*-1,2-Naphthaloyl-(*S*)-amino acids were chosen as they have a larger horizontal aromatic surface area that retains the *N*-phthaloyl rings of Hashimoto's series along with the horizontal naphthalene rings of Müller's series (Figure 2.4). In the new hybrid ligands, the mirror perpendicular to the plane of the heterocyclic tether is lost

as the multiple rings point to one side, which is dissimilar from Müller's and Ghanem's chemistry with one substituent around the rings.[8,9]

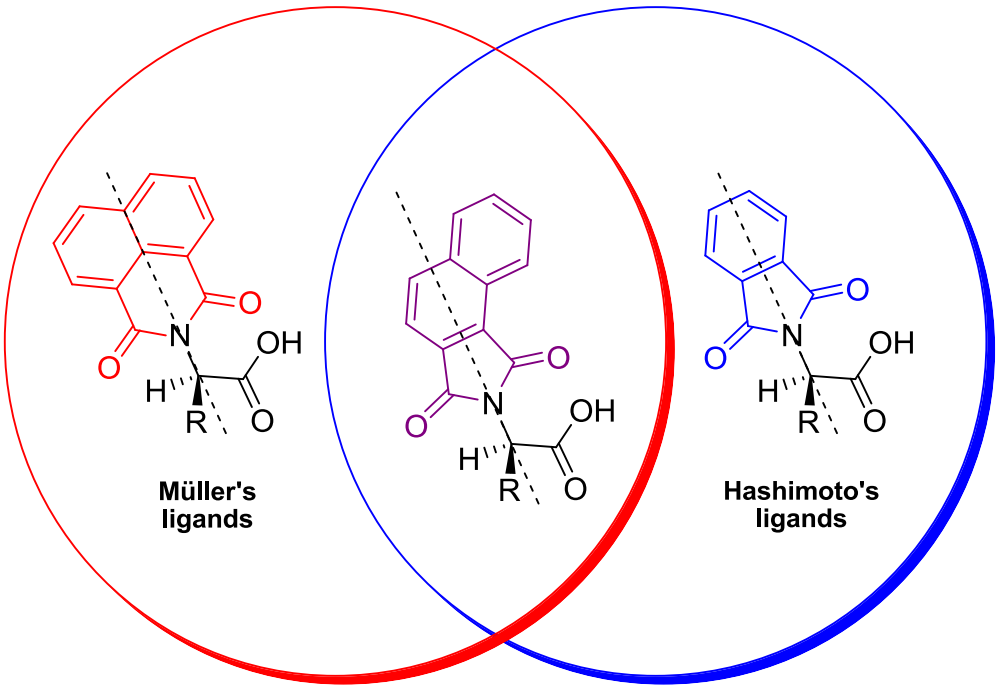

Figure 2.4. Structure of the new hybrid ligands derived from *N*-1,2-napthaloyl-(*S*)-amino acids.

As I indicated in Chapter 1, Section 1.5.3.1, the optimum group at the ligand's *α*-carbon can vary depending on the reaction.[3] As a consequence, it was decided to prepare different ligands by changing the L-amino acid and determine, for a later stage, which is the optimum *α*-substituent for my screening reactions. Also, it was a good opportunity to explore L-amino acids carrying substituents with heteroatoms at the *α*-carbon as this sort of amino acids was not reported before (see Chapter 1, Figure 1.14). The set of L-amino acids used was L-*tert*-leucine, L-leucine, L-alanine, L-tryptophan, L-tyrosine and L-histidine. The new ligands were prepared *via* the condensation of 1,2-naphthalic anhydride with different L-amino acids at refluxing conditions.

Confirmation of correct NH_2-protection conditions

The use of ligands with the highest optical purity is important for the facile access to extremely reliable catalysts. In 2005, Hashimoto explored the racemization free *N*-

phthaloylation of *tert*-leucine and reported that it can be achieved in refluxing toluene/TEA mixture with minimal racemization.[12] However, Charette reported the same reaction using different L-amino acids in refluxing DMF to achieve enantiomerically pure *N*-protected-L-amino acid ligands.[5] Likewise, racemization free *N*-1,8-[10,5] and *N*-2,3-naphthaloylation[13] of L-amino acids were claimed to take place in refluxing DMF. A different report indicated that racemization free *N*-protection of amino acids was possible in refluxing acetic acid.[14] These latter reports did not provide any information about the degree of racemization that accompanied the *N*-protection of L-amino acids under these different reaction conditions and no racemization was proposed to take place. As a consequence, the correct NH_2-protection conditions that are accompanied by the minimum degree of racemization must be confirmed before proceeding further in this research.

The NH_2-protections were carried out in three different reaction solvents including acetic acid, DMF and toluene/TEA (Scheme 2.1). The structures of the obtained products were confirmed on the basis of their 1D, 2D NMR, IR and MS data. The HMBC spectra for **1a**, **1b**, **1c**, **1d** and **1f** revealed a long range correlation between the asymmetric hydrogen and both carbonyl carbons of the cyclic imide (Scheme 2.1). This long range ^{1}H-^{13}C correlation verified the formation of the cyclic imides **1a-f** and not the open chain amides **2a** or **2b** under all the examined reaction conditions.

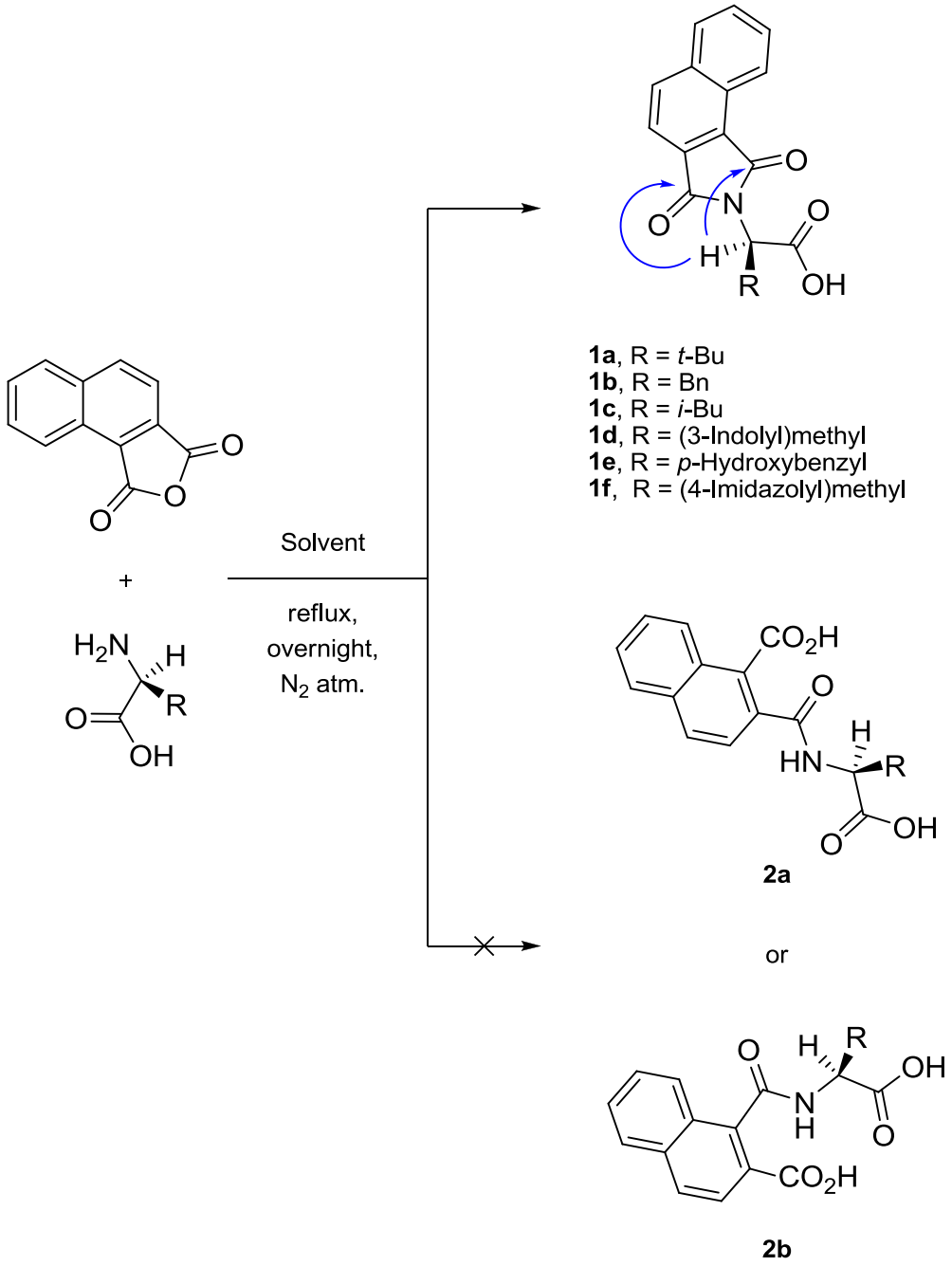

Scheme 2.1. Preparation of chiral ligands; HMBC correlations are represented in blue arrows.

Chiral HPLC trace of enantiomeric purities

At this stage, a quick, direct and sensitive method for tracing the degree of racemization of the prepared ligands under the different *N*-1,2-naphthaloylation conditions was highly desirable. After some experimentation, it was found that racemization tracing can be readily achieved through chiral HPLC analysis and by

employing the covalently immobilized type CSP, Chiralpak® ID, which is based on amylose(3-chlorophenylcarbamate). The solvent versatility of this immobilized phase is not only useful for tracking the degree of racemization of *N*-1,2-naphthaloyl-protection of amino acids, but is also able to provide a direct reaction monitoring without going through the time consuming work-up or other purification procedures.

Enantioselective analysis results of *N*-1,2-naphthaloyl-amino acid enantiomers on Chiralpak® ID are illustrated in Table 2.2. The efficiency of the enantioselective separation on Chiralpak® ID was assessed on the basis of separation (α) and resolution (R*s*) factors for the two resolved peaks.[15] The separation factor (α) indicates the potential of the chromatographic system for separating the two enantiomers and all α values were calculated according to the equation:

$$\alpha = \frac{t_{\mathrm{R2}} - t_0}{t_{\mathrm{R1}} - t_0}$$

Where t_{R1} is the retention time of the first peak, t_{R2} is the retention time of the second peak and t_0 is the retention time of an unretained compound.

The resolution factor (R*s*) is defined as the ratio between the distance between the two peaks maxima (the distance between the two retention times; t_{R2} - t_{R1}) and the arithmetic mean of the two peaks width. All R*s* values were calculated according to the equation:

$$Rs = 2\,\frac{t_{\mathrm{R2}} - t_{\mathrm{R1}}}{W_1 + W_2}$$

Where t_{R1} and t_{R2} are the peaks retention times, W_1 and W_2 are the peaks' base widths.

In general, Chiralpak® ID afforded fairly good separation for the enantiomers of *N*-1,2-naphthaloyl-protected amino acids. All investigated *N*-naphthaloyl amino acids were baseline separated (α = 1.54-2.48, R*s* = 1.64-2.61) except for *N*-1,2-

naphthaloyl-(*S*)-*tert*-leucine (**1a**) which was partially separated with R*s* of 1.04 (Table 2.2, entry 1).

Table 2.2. Enantiomer separation of *N*-1,2-naphthaloyl-(*S*)-amino acids on Chiralpak® ID.

Entry	**Ligand**	**Code**	**Flow rate (mL/min)**	***α***	**R*s***	**Retained enantiomer**
1	*S*-1,2-NTTL	**1a**	0.25	1.39	1.04	*S*
2	*S*-1,2-NTPA	**1b**	0.5	1.54	1.70	*R*
3	*S*-1,2-NTLU	**1c**	0.25	2.50	2.61	*R*
4	*S*-1,2-NTTR	**1d**	0.5	2.38	2.59	*R*
5	*S*-1,2-NTTY	**1e**	0.5	2.48	1.64	*R*

All enantiomer separations were achieved through chiral HPLC using Chiralpak® ID column, 10% 2-propanol in *n*-hexane (*v/v*%) with 0.1% TFA, 254 nm. See experimental section for more details.

Better separation of *N*-1,2-naphthaloyl-(*S*)-*tert*-leucine ligand **1a** was achieved by using Chiralpak® IB column which is also a covalently immobilized type CSP based on cellulose(3,5-dimethylphenylcarbamate) chiral selector. Chiralpak® IB afforded a better separation of *N*-1,2-naphthaloyl-(*S*)-*tert*-leucine (α = 1.68, R*s* = 1.43) with a shorter analysis time compared to Chiralpak® ID under the same mobile phase combination and flow rate (Figure 2.5).

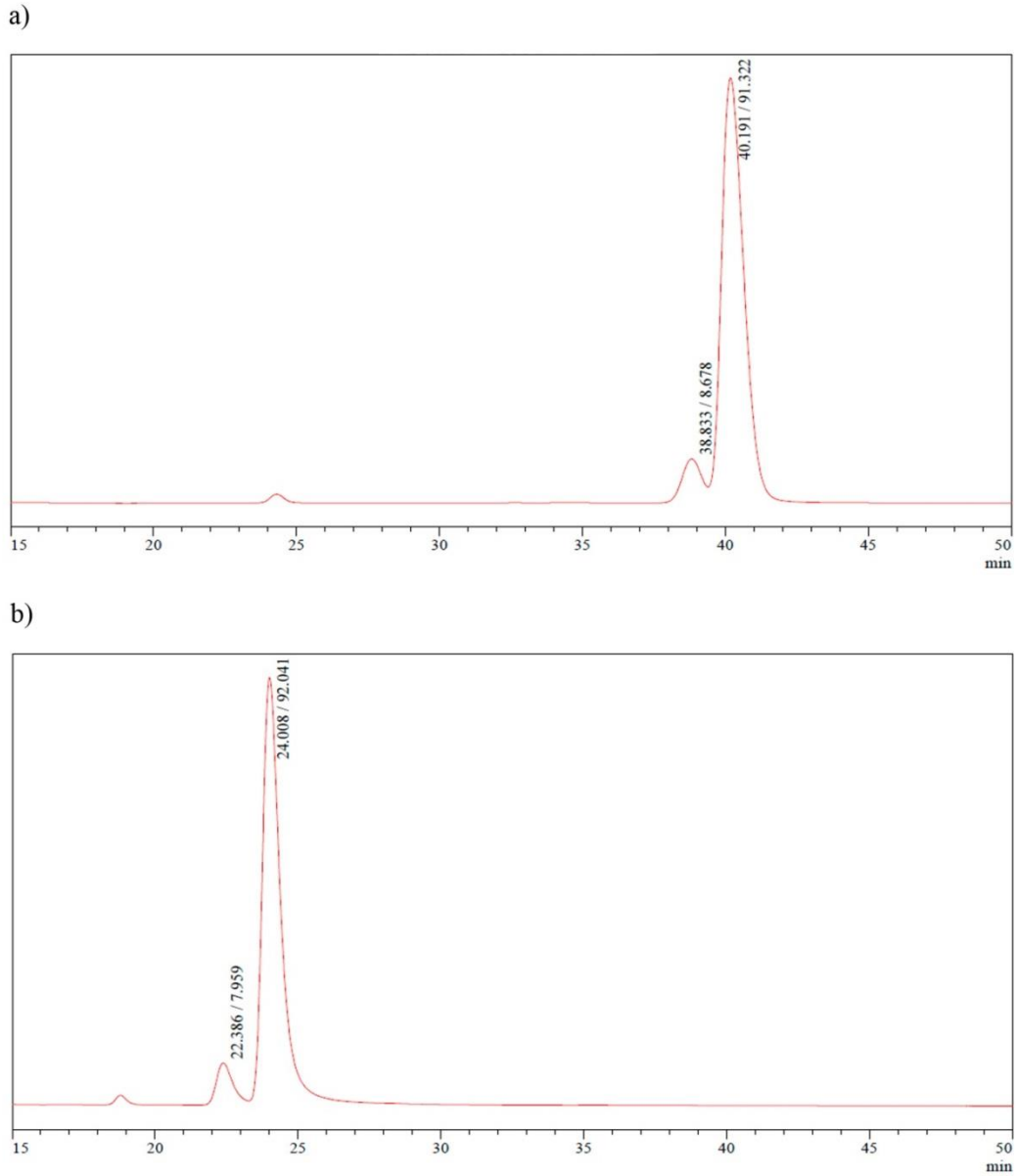

Figure 2.5. Enantiomer separation of *N*-(1,2-naphthaloyl)-(*S*)-*tert*-leucine (**1a**). Conditions for chiral HPLC trace: a) Chiralpak® ID column, 10% 2-propanol in *n*-hexane (*v/v*%) with 0.1% TFA, 0.25 mL/min, 254 nm. b) Chiralpak® IB column, 10% 2-propanol in *n*-hexane (*v/v*%) with 0.1% TFA, 0.25 mL/min, 254 nm.

Table 2.3 and Figure 2.6 illustrates the effect of changing the reaction solvent on the extent of racemization and it can be concluded from these analytical results that different degrees of racemization were observed with the alteration of the reaction solvent. It is also clear from the analytical results that the goal of getting ligands with minimal racemization can be readily achieved by employing toluene/TEA mixture as

reaction solvent. By the utilization of this reaction conditions, the degree of racemization for the prepared *N*-protected amino acids is limited and kept to a minimum. However, an exception to this was found in the case of *N*-1,2-naphthaloyl phenylalanine (**1b**), where, ~15% racemization took place (Table 2.3, entry 2). Recrystallization of products from hot MeOH provided optically pure ligands ready for ligand exchange except for **1a** which was obtained as oil and used as it is.

Table 2.3. Effect of changing the reaction solvent on yield and enantiomeric purity of the prepared ligands.

Entry	Ligand	Code	Acetic Acid		DMF		Toluene/TEA	
			Yield (%)	*ee* (%)	Yield (%)	*ee* (%)	Yield (%)	*ee* (%)
1	*S*-1,2-NTTL[a]	**1a**	33	84	71	74	89	>99
2	*S*-1,2-NTPA[b]	**1b**	74	2	82	70	89	84
3	*S*-1,2-NTLU[b]	**1c**	84	60	87	36	90	97
4	*S*-1,2-NTTR[b]	**1d**	65	60	96	92	85	>99
5	*S*-1,2-NTTY[b]	**1e**	56	14	90	95	17	98

Enantiomeric excess percentages (*ee*%) were determined by chiral HPLC using [a]Chiralpak® IB column, [b]Chiralpak® ID column, 10% 2-propanol in *n*-hexane (*v/v*%) with 0.1% TFA, 254 nm, See experimental section for more details.

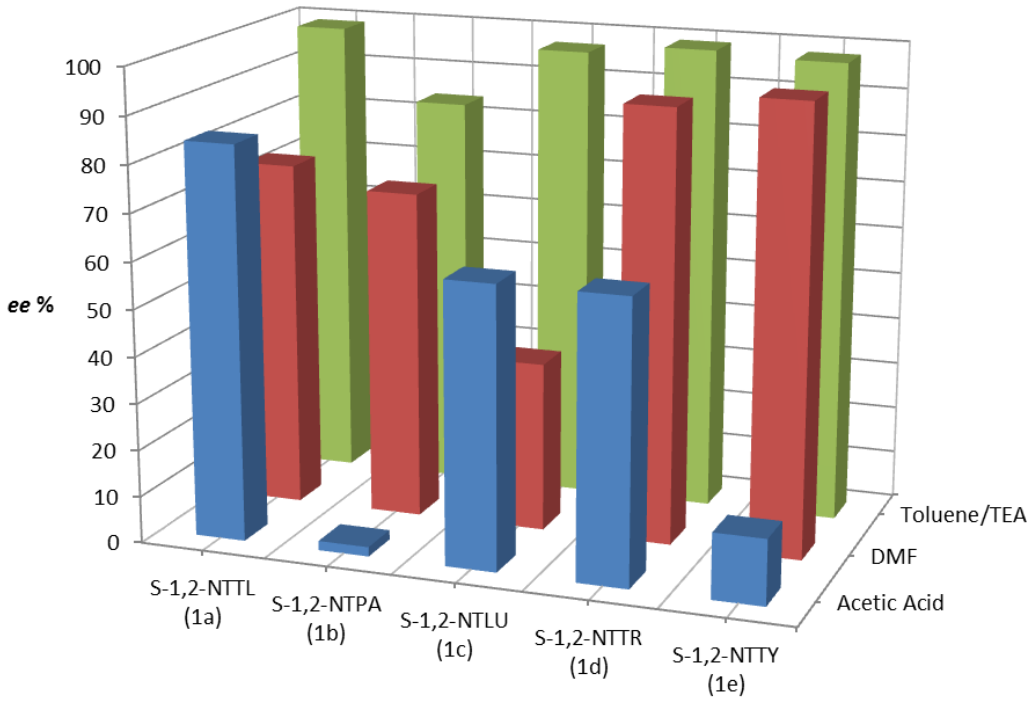

Figure 2.6. Effect of changing the reaction solvent on enantiomeric purity of the obtained ligands.

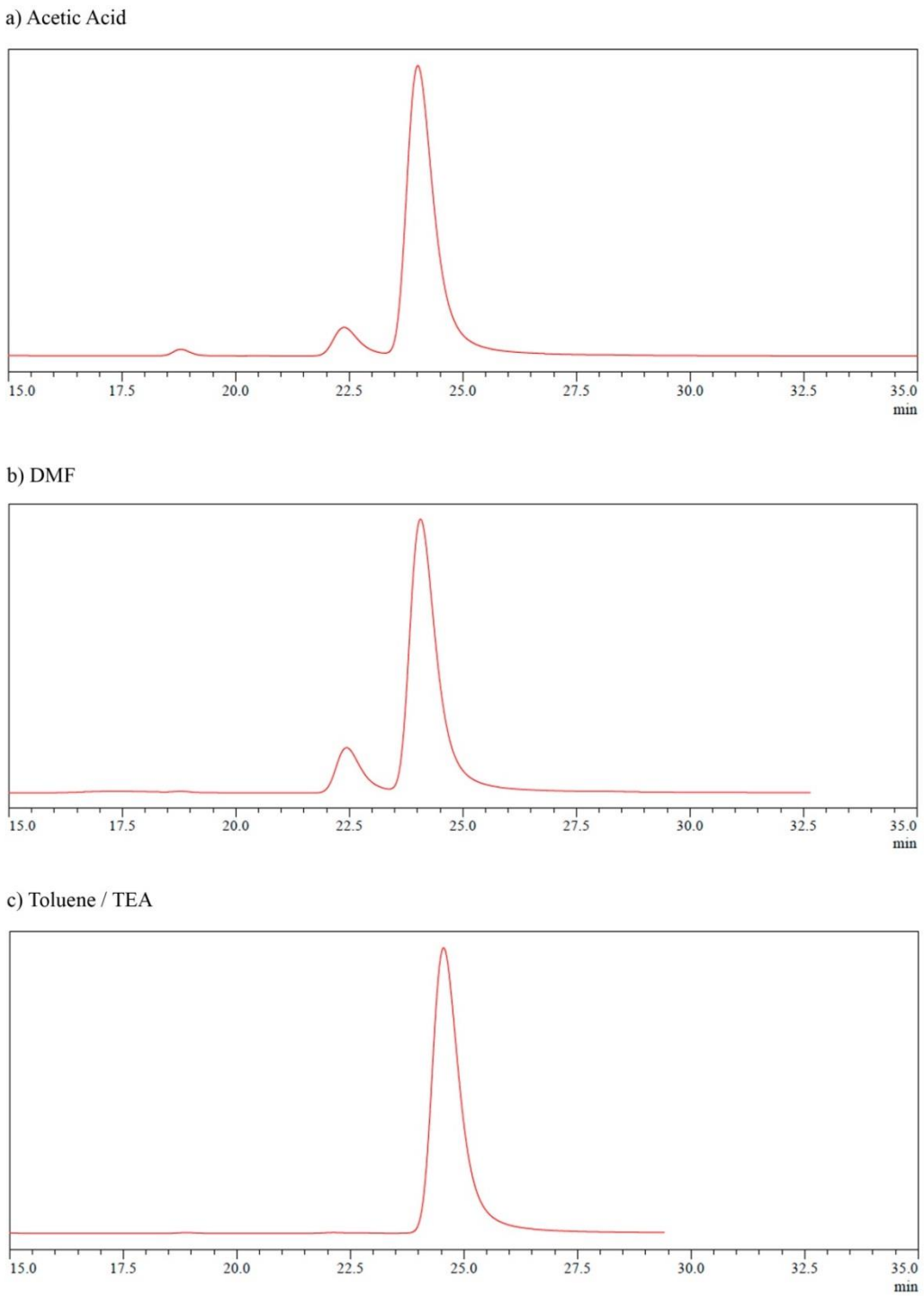

Figure 2.7. Enantiomer separation of *N*-(1,2-naphthaloyl)-(*S*)-*tert*-leucine (**1a**) prepared using a) acetic acid, b) DMF or c) toluene/TEA as reaction solvents. Conditions for chiral HPLC trace: Chiralpak® IB column, 10% 2-propanol in *n*-hexane (*v/v*%) with 0.1% TFA, 0.25 mL/min, 254 nm.

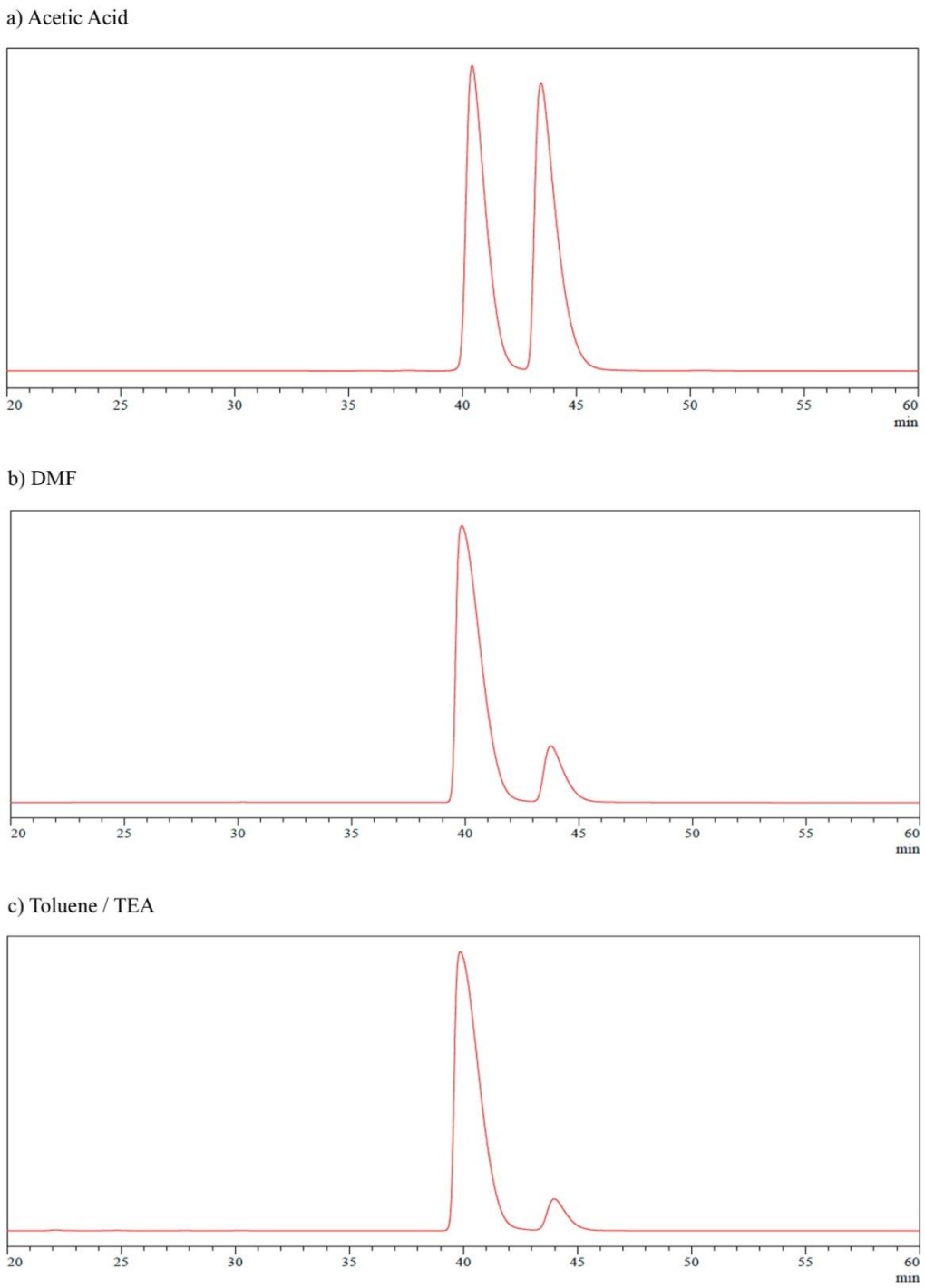

Figure 2.8. Enantiomer separation of *N*-(1,2-naphthaloyl)-(*S*)-phenylalanine (**1b**) prepared using a) acetic acid, b) DMF or c) toluene/TEA as reaction solvents. Conditions for chiral HPLC trace: Chiralpak® ID column, 10% 2-propanol in *n*-hexane (*v/v*%) with 0.1% TFA, 0.5 mL/min, 254 nm.

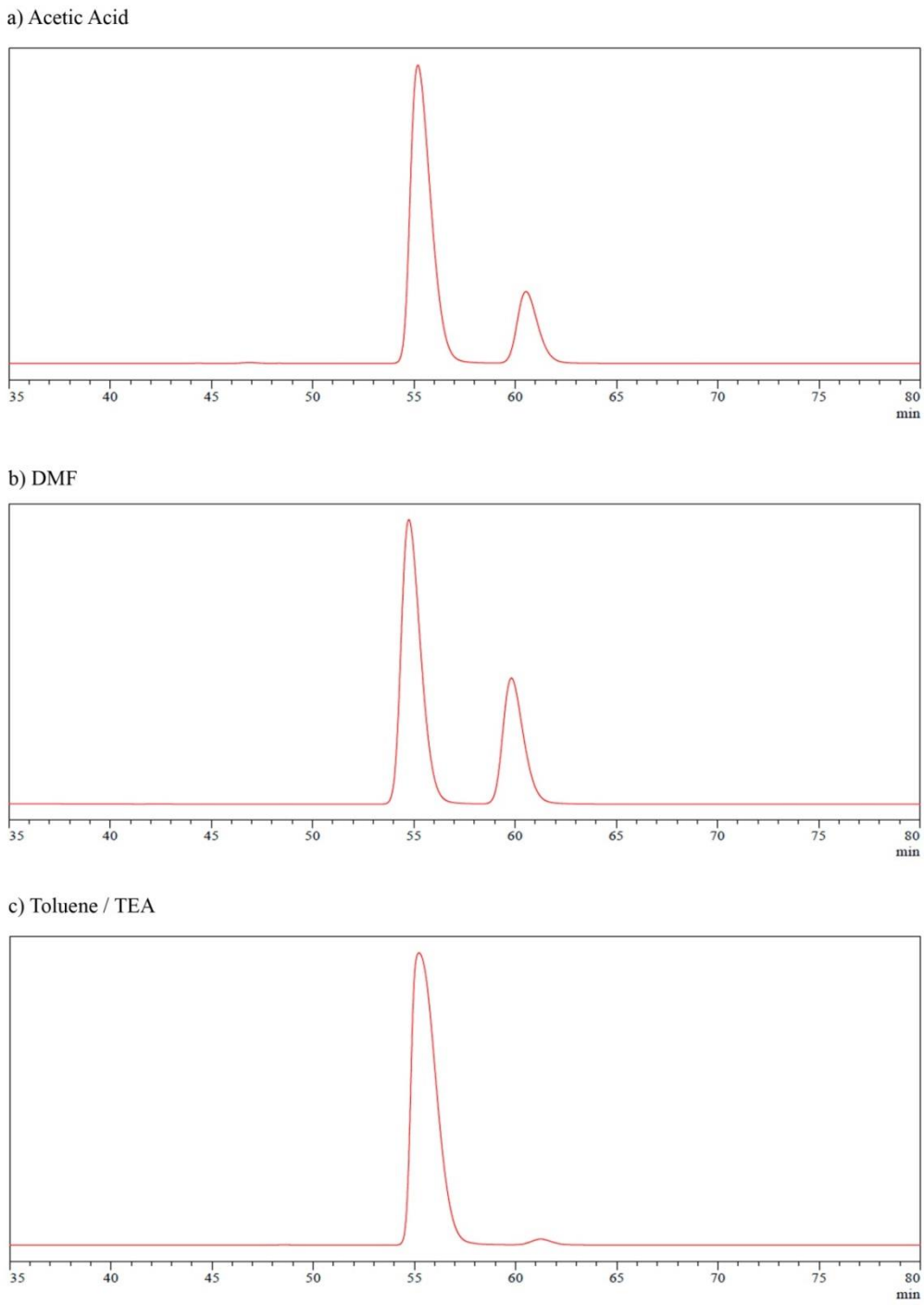

Figure 2.9. Enantiomer separation of *N*-(1,2-naphthaloyl)-(*S*)-leucine (**1c**) prepared using a) acetic acid, b) DMF or c) toluene/TEA as reaction solvents. Conditions for chiral HPLC trace: Chiralpak® ID column, 10% 2-propanol in *n*-hexane (*v/v*%) with 0.1% TFA; 0.25 mL/min, 254 nm.

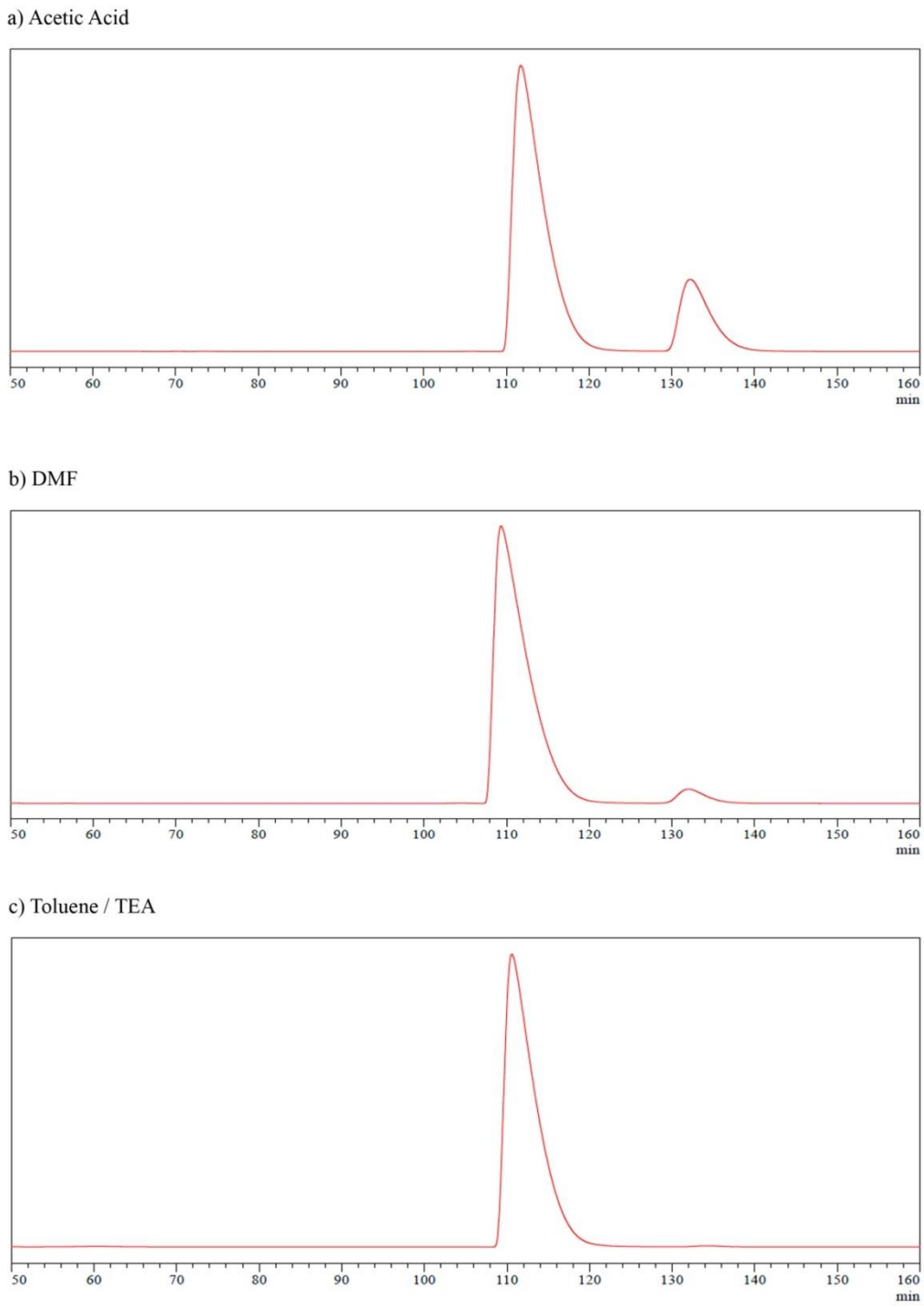

Figure 2.10. Enantiomer separation of *N*-(1,2-naphthaloyl)-(*S*)-tryptophan (**1d**) prepared using a) acetic acid, b) DMF or c) toluene/TEA as reaction solvents. Conditions for chiral HPLC trace: Chiralpak® ID column; 10% 2-propanol in *n*-hexane (*v/v*%) with 0.1% TFA, 0.5 mL/min, 254 nm.

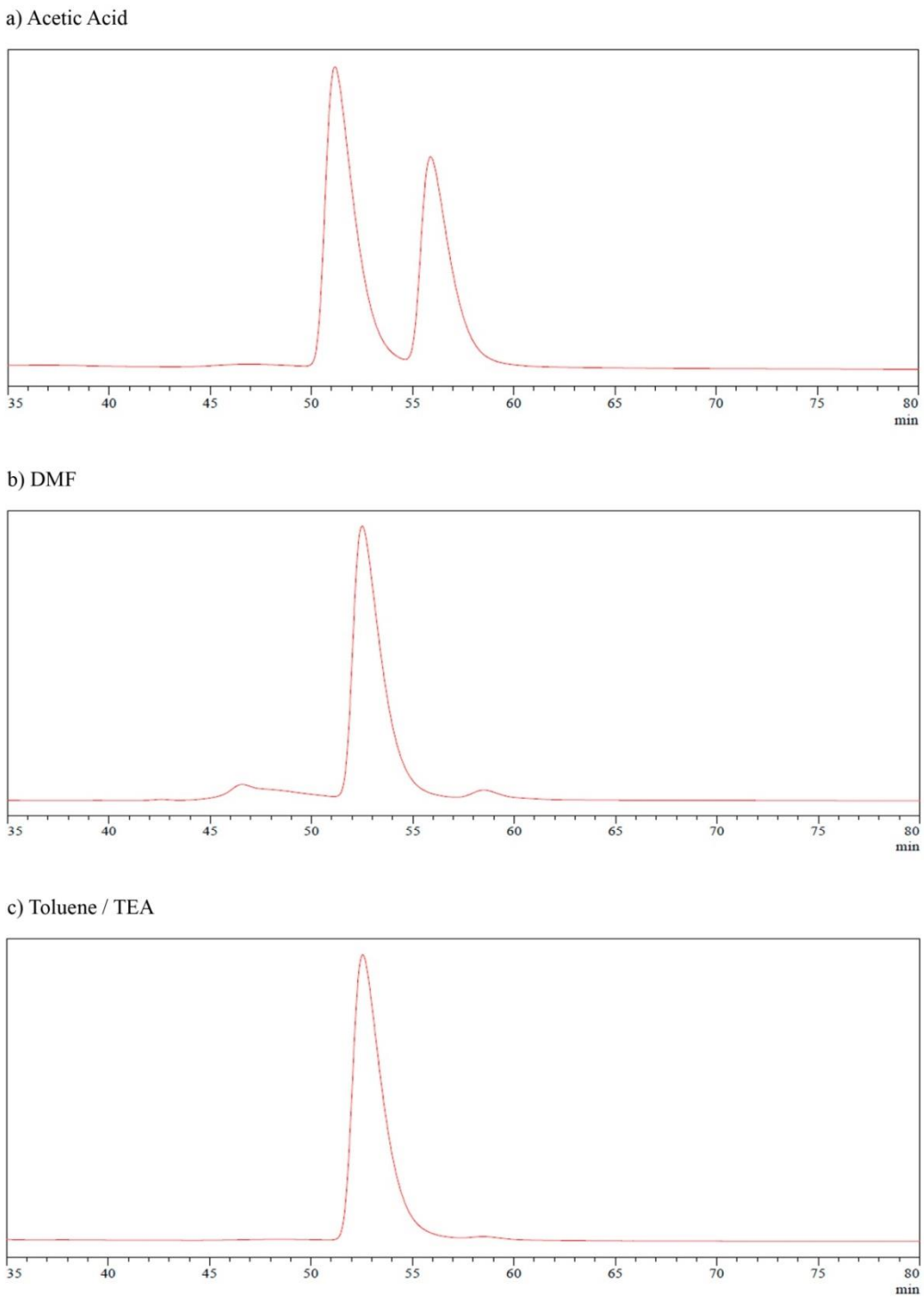

Figure 2.11. Enantiomer separation of *N*-(1,2-naphthaloyl)-(*S*)-tyrosine (**1e**) prepared using a) acetic acid, b) DMF or c) toluene/TEA as reaction solvents. Conditions for chiral HPLC trace: Chiralpak® ID column, 10% 2-propanol in *n*-hexane (*v/v*%) with 0.1% TFA, 0.5 mL/min, 254 nm.

2.2.1.2. Synthesis of dirhodium(II) carboxylate complexes

At this point, high temperature ligand exchange was carried out using the prepared chiral carboxylic acid ligands (**1a-e**) and rhodium acetate ($Rh_2(OAc)_4$).[16] Ligand exchange proceeded successfully affording the corresponding dirhodium(II) tetrakis[*N*-(1,2-naphthaloyl)-(*S*)-amino acid] complexes, **3a-e** (Scheme 2.2). The structures of the prepared complexes were confirmed on the basis of their NMR, IR and MS data.

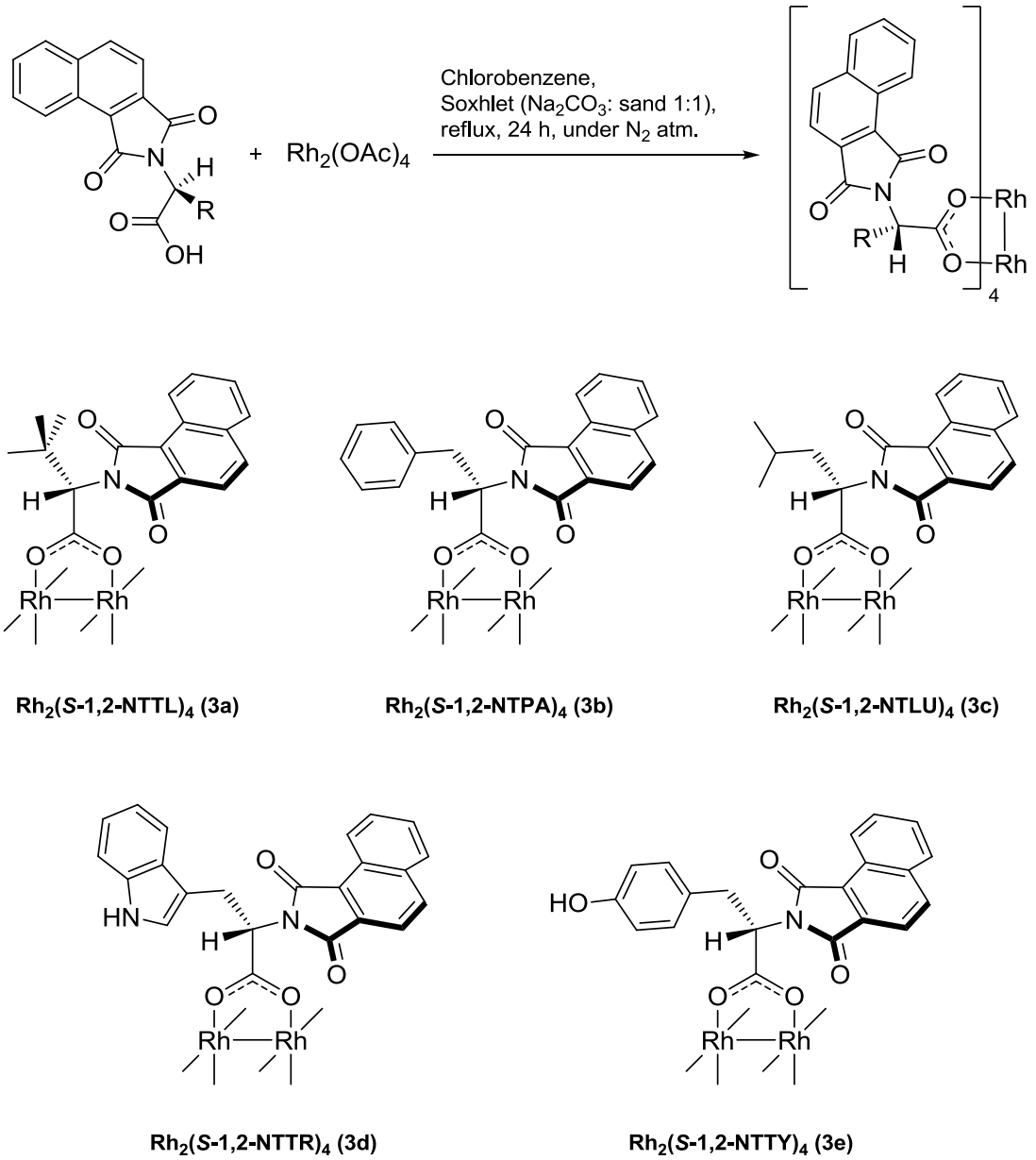

Scheme 2.2. Preparation and structure of the new catalytic series.

The preparation of Rh_2(*S*-1,2-NTHS)$_4$ complex (**3f**, Figure 2.12) was also attempted using the procedure described above for catalyst preparation. However, ^{1}H and ^{13}C NMR spectra of the isolated solid were identical to the obtained NMR data for the ligand. MS spectroscopic analysis also returned a major peak at 336.1 which corresponds to the ligand's M+1 ion. This is beside the generation of none of cyclopropane products when the isolated solid was subjected to screening in various cyclopropanation reactions.

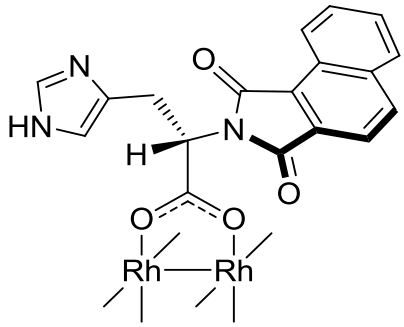

Figure 2.12. Structure of Rh_2(*S*-1,2-NTHS)$_4$ complex (**3f**).

2.2.2. Screening for asymmetric cyclopropanation with *donor-acceptor* substrates

2.2.2.1. Enantioselective synthesis of chiral cyclopropylphosphonate derivatives

Cyclopropylphosphonate and cyclopropylphosphonic acid derivatives have been extensively studied during the last decade as they display several interesting biological activities (Figure 2.13). For example, they have been used as structural moieties of nucleotides,[17,18] as insecticides,[19] herbicides and plant growth regulators.[20] They were also used as analogues of the antidepressant Milnacipran,[21] the antibiotic Fosmidomycin,[22] the unusual amino acids (-)-Allonorcoronamic acid[23] and (*Z*)-2,3-Methanohomoserine,[24] the $GABA_B$ receptor antagonist Phaclophen,[25] and L-Glu.[26] Further, cyclopropylphoshonate derivatives can act as *N*-methyl-D-aspartate (NMDA) receptor antagonists,[27] as important P1 moieties for potent HCV NS3 protease inhibitors[28] and as mimics of 1-Aminocyclopropane carboxylic acid (ACC) with a high inhibitory activity for ACC-deaminase and alanine racemase.[29,30] Moreover, they also possess anti-proliferation properties,[31] are virostatics,[32] antidiabetic agents,[33] antitumor agents,[34] selective anti-HBV agents,[35] cytostatic agents[36] and displays antiviral activity.[37] Cyclopropylphosphonates are also very convenient for the synthesis of alkylidenecyclopropane derivatives through the Wadsworth-Emmons reaction.[38,39]

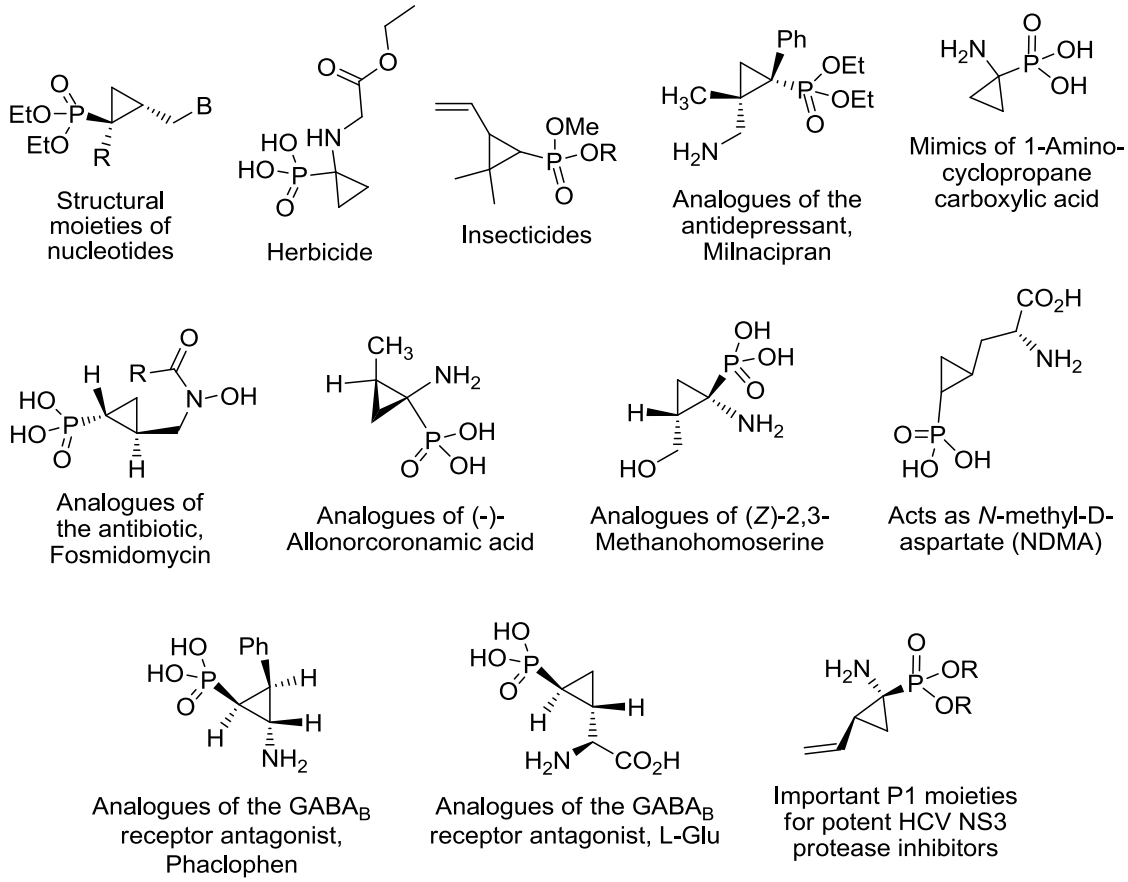

Figure 2.13. Model applications of cyclopropylphosphonate and cyclopropylphosphonic acid derivatives.

Cyclopropylphosphonates have been synthesized using variety of methods,[40] for example, through Arbuzov reaction by the phosphonylation of halogenated cyclopropanes,[41] the cyclopropanation of vinyl phosphonates with diazoalkanes,[42] Simmons-Smith reaction,[43] electrochemical synthesis,[44,45] intermolecular cyclization,[46] the addition of phosphonates to iminium salts,[47] reaction of α-chlorophosphonates with alkyl acrylates in the presence of sodium hydride,[48] photo-induced fragmentation of epoxyphosphonates,[49] bis-alkylation of α-functional phosphonate carbanions with 1,2-dibromoethane,[50,20] the addition of α,β-unsaturated esters to phosphonylated sulfonium ylides[51] and $SnCl_4$ promoted [2+1] cycloaddition of 1-seleno-2-silylethane with 2-phosphonoacrylates.[24]

Metal-catalyzed decomposition of diazophosphonates in the presence of an alkene emerged recently as one of the powerful and most successive methods for the enantioselective synthesis of cyclopropylphosphonate derivatives. In 2004,

Simonneaux *et al*. reported the asymmetric cyclopropanation of styrene derivatives with *monoacceptor* di*iso*propyl diazomethylphosphonate using chiral ruthenium-porphyrin as a catalyst (Scheme 2.3).[52] The reaction proceeded under mild conditions and gave *trans*-cyclopropylphosphonates in good yields and high *ee* values (up to 92%). Later in 2004, the same group reported the use of chiral 2,6-bis(thiazolinyl)pyridines as ligands in ruthenium-catalyzed asymmetric cyclopropanations of olefins with phosphonate diazoesters. Enantioselectivities of up to 90% *ee* for the *trans*-cyclopropylphosphonate were observed.[53]

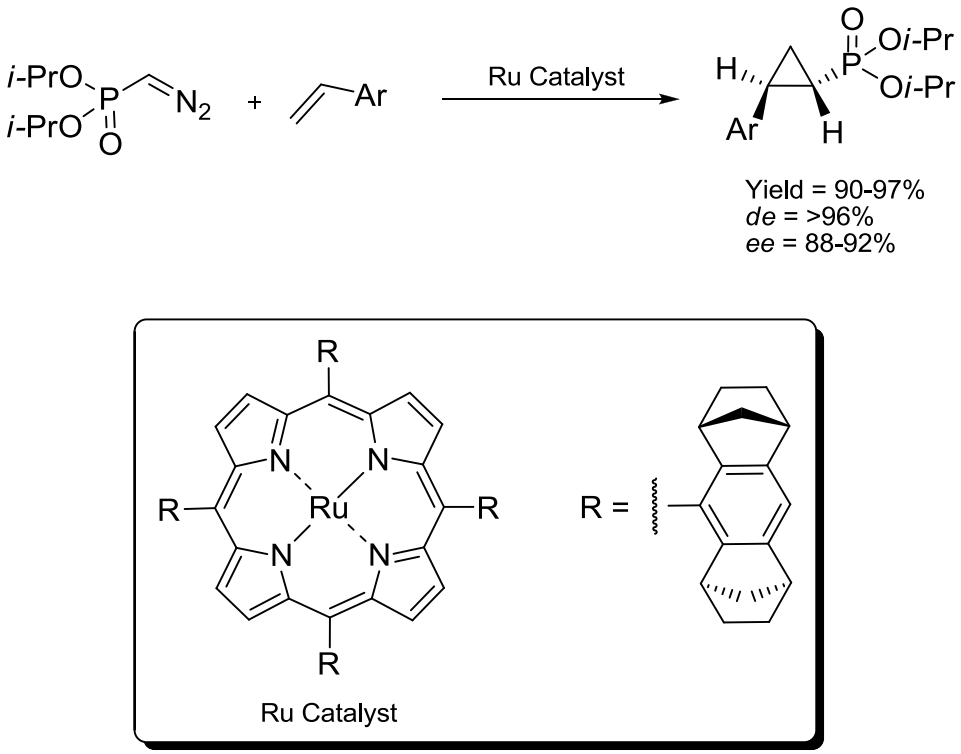

Scheme 2.3. Ruthenium-porphyrin-catalyzed cyclopropanation of styrene derivatives with di*iso*propyl diazomethylphosphonate.[52]

Very recently in 2014, Iwasa *et al.*[54] developed a highly stereoselective cyclopropanation of various classes of alkenes with *monoacceptor* diethyl diazomethylphosphonate using Ru(II)-Pheox complex as a catalyst (Scheme 2.4). The results also revealed that cyclopropanations of electron-deficient alkenes such as *α*,*β*-unsaturated ester, ketone and amides can be achieved smoothly under mild

reaction conditions to afford the corresponding cyclopropylphosphonate product in high yield, diastereoselectivity and enantioselectivity.

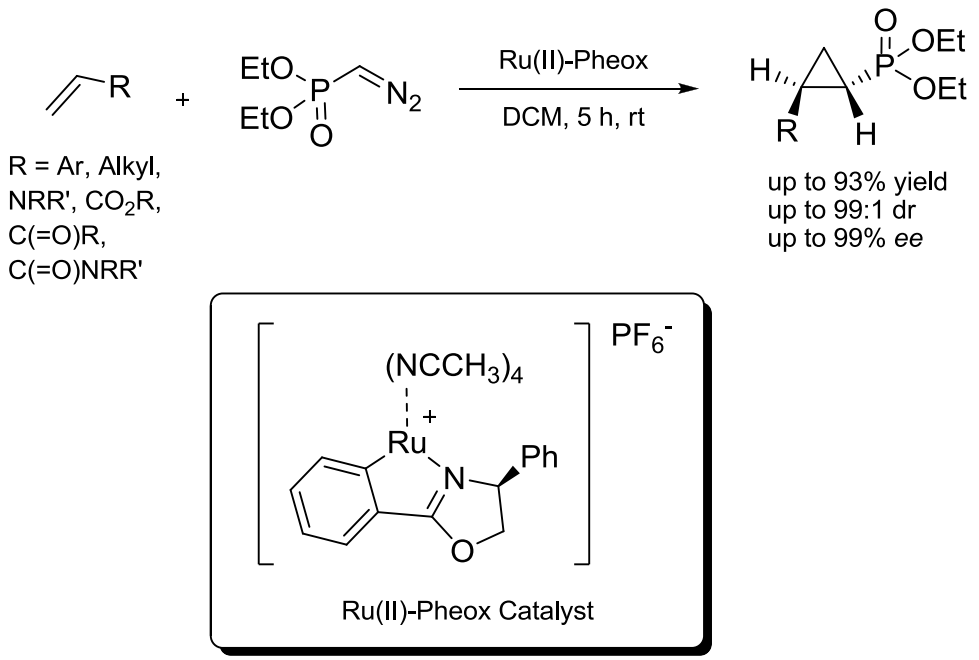

Scheme 2.4. Ru(II)-Pheox-catalyzed asymmetric cyclopropanation of various classes of alkenes with diethyl diazomethylphosphonate.[54]

Charette and co-workers[55] also reported the *trans*-$RuCl_2$((*S*, *S*)-*i*-Pr-pybox)(ethylene)-catalyzed cyclopropanation of *p*-methoxystyrene with di*iso*propyl diazomethylphosphonate to give the di*iso*propyl (1*R*, 2*S*)-2-(4-methoxyphenyl)cyclopropylphosphonate product. The achiral version of the reaction proceeds well with copper, rhodium and ruthenium catalysts, however, the best catalysts for the enantioselective version are either Evans' Cu-bis(oxazoline) or Nishiyama's Ru-pybox.

The same research group reported a highly stereoselective Rh(II)-catalyzed cyclopropanation with *diacceptor* diazo substrates and utilizing the phosphonate moiety as a powerful *trans*-directing group (Scheme 2.5).[56] The first asymmetric synthesis towards *diacceptor* cycloprop(en)ylphosphonate derivatives was achieved starting from *α*-cyanodiazophosphonate in the presence of chiral Rh_2(*S*-IBAZ)$_4$ as a catalyst. The optimization of the nature of the catalyst and the substrate revealed that, in terms of selectivity, Rh_2(*S*-PTTL)$_4$, Rh_2(*S*-NTTL)$_4$ and Rh_2(*S*-TCPTTL)$_4$ were

totally incompatible with *diacceptor* diazophosphonate substrates and the maximum selectivity was achieved by having the bulky *iso*propyl as phosphonate ester group.

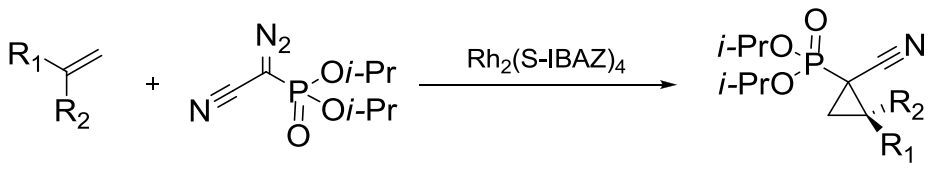

Scheme 2.5. Rh_2(*S*-IBAZ)$_4$-catalyzed cyclopropanations of alkenes with di*iso*propyl *α*-cyano-*α*-diazophosphonates.[56]

As it was illustrated in Chapter 1, although Rh_2(*S*-DOSP)$_4$-catalyzed cyclopropanations of alkenes with several *donor-acceptor* diazo substrates proceed in a highly stereoselective manner, it was reported that Rh_2(*S*-DOSP)$_4$-catalyzed cyclopropanation of styrene with *donor-acceptor* dimethyl *α*-diazobenzylphosphonate resulted in the formation of the cyclopropane product in a very poor enantioselectivity (34% *ee*).[57] In 2004, Davies and co-workers reported the Rh_2(*S*-biTISP)$_2$-catalyzed asymmetric cyclopropanations of a variety of alkenes with aryldiazomethylphosphonate derivatives. The cyclopropanation generated the corresponding cyclopropane products in high yields (85-96%), diastereoselectivities (98% *de*) and enantioselectivities (76-92% *ee*).[57] Later in 2006, the same group demonstrated that Rh_2(*S*-PTTL)$_4$ and Rh_2(*S*-PTAD)$_4$ are far superior catalysts for the enantioselective synthesis of dimethyl 1,2-diphenylcyclopropylphosphonate, with Rh_2(*S*-PTAD)$_4$ giving the highest enantioselectivity (99% *ee*).[58]

So, with the new catalytic series in hand and inspired by the importance of cyclopropylphosphonate derivatives, the evaluation of these catalysts was carried out in the standard cyclopropanation reaction of styrene (as olefin substrate) and dimethyl *α*-diazobenzylphosphonate **4** (as carbene precursor) in 2,2-DMB to generate dimethyl 1,1-diphenylcyclopropylphosphonate **5**. The reaction conditions were reported to be optimal for similar catalytic systems[58,57] and also proved to be the best for my new complexes. The previously reported Rh_2(*S*-PTAD)$_4$, Rh_2(*S*-PTTL)$_4$, Rh_2(*S*-NTTL)$_4$ and Rh_2(*S*-4-Br-NTTL)$_4$ catalysts were included in the screening as well established catalysts for enantioselective cyclopropanation reactions and the results are summarized in Table 2.4.

Table 2.4. Asymmetric cyclopropanation of styrene with dimethyl *α*-diazobenzylphosphonate.

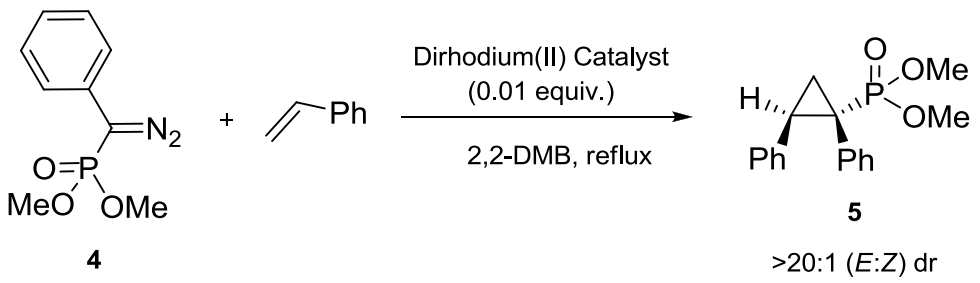

Entry	Catalyst	Catalyst code	Reaction Time (h)	Yield (%)	*ee* (%)
1	Rh_2(*S*-PTAD)$_4$	-	10	88	94[a]
2	Rh_2(*S*-PTTL)$_4$	-	10	83	92
3	Rh_2(*S*-NTTL)$_4$	-	5	91	90
4	Rh_2(*S*-4-Br-NTTL)$_4$	-	10	83	72
5	Rh_2(*S*-1,2-NTTL)$_4$	**3a**	5	93	92
6	Rh_2(*S*-1,2-NTPA)$_4$	**3b**	5	91	34
7	Rh_2(*S*-1,2-NTLU)$_4$	**3c**	5	94	64
8	Rh_2(*S*-1,2-NTTR)$_4$	**3d**	20	76	22
9	Rh_2(*S*-1,2-NTTY)$_4$	**3e**	20	80	26

[a]Orginally reported to be 99% *ee*,[58] however, when the reaction was repeated under the reported conditions the maximum of 94% *ee* was obtained. Diastereomeric ratios (dr) were determined by ^{1}H NMR of the crude mixture. Enantiomeric excess percentages (*ee*%) were determined by chiral HPLC using Chiralcel® OJ column, 2% 2-propanol in *n*-hexane (*v*/*v*%), 1 mL/min, 220 nm, τ_1 = 18 min, τ_2 = 21 min. See experimental section for more details

The yields of cyclopropane product **5** were generally high for all catalysts ranging from 76% to 93%. The observed yield of the product resulting from the reaction catalyzed by Rh_2(*S*-1,2-NTTL)$_4$ (**3a**) was slightly higher than those resulting from reactions catalyzed by Rh_2(*S*-PTTL)$_4$ and Rh_2(*S*-NTTL)$_4$ (Table 2.4). This can be

rationalized by the ligand's larger aromatic moiety which offers a relatively higher solubility of Rh_2(*S*-1,2-NTTL)$_4$ (**3a**) in non-polar solvents. Its better solubility also offered a quicker conversion into products resulting in a shorter reaction time if compared to Rh_2(*S*-PTTL)$_4$.

In all cases, the diastereoselectivity of these reactions was excellent favouring the *E*-isomer **5** over the *Z*-isomer by a diastereomeric ratio (dr) of more than 20:1. A reasonable explanation for this extremely high diastereoselectivity would be due the favoured aryl rings π-stacking attractions during cyclopropanation. This is in addition to the blockage of the substrate approaching over the bulky phosphonate acceptor group (Figure 2.14).[57]

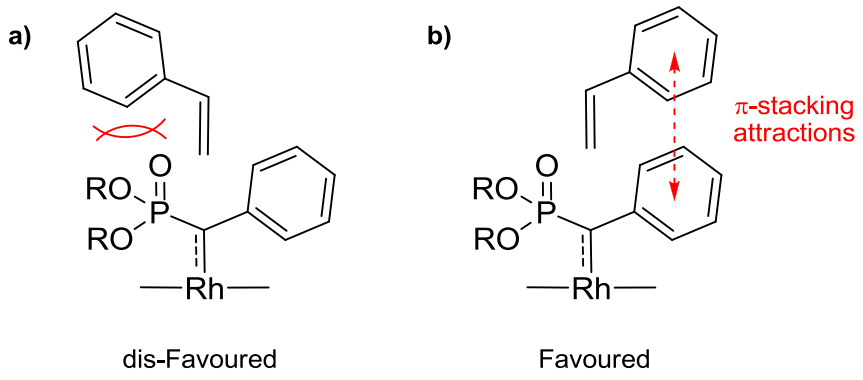

Figure 2.14. Illustration to justify the observed high levels of diastereoselectivities a) dis-Favoured, blockage of the approach of the substrate over the phosphonate group, b) Favoured, attractive π-stacking attractions between the aryl rings.

In terms of enantioselectivity, the results in Table 2.4 indicated that the catalyst bearing the bulky *tert*-butyl group (**3a**) was the best catalyst among the series. This was followed by those bearing the *iso*butyl (**3c**) and benzyl (**3b**) groups and finally those carrying the (3-indolyl)methyl (**3d**) and the 4-hydroxybenzyl (**3e**) groups.

The cyclopropanation reaction catalyzed by Rh_2(*S*-1,2-NTTL)$_4$ (**3a**) generated the cyclopropane product in 92% *ee* (Figure 2.15 and Table 2.4, entry 5), which is similar to the same reaction catalyzed by Rh_2(*S*-PTTL)$_4$ (Table 2.4, entry 2) and slightly better than the one catalyzed by Rh_2(*S*-NTTL)$_4$ (90% *ee*, Table 2.4, entry 3).

However, these results are still lower than that for Rh_2(*S*-PTAD)$_4$ (reported 99% *ee*,[58] obtained 94% *ee*, Table 2.4, entry 1).

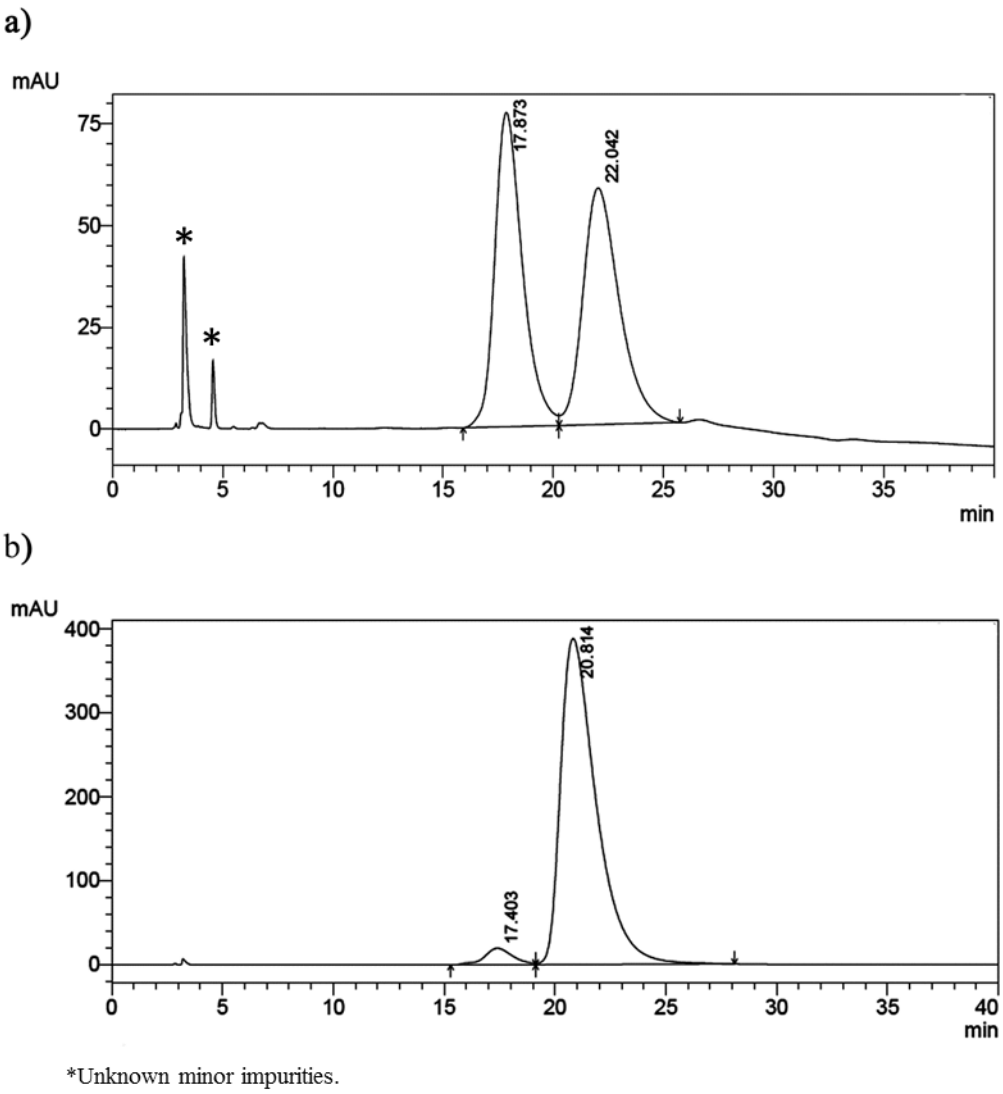

Figure 2.15. Chiral HPLC trace of (1*S*, 2*R*)-dimethyl 1,2-diphenylcyclopropylphosphonate (**5**) a) prepared using $Rh_2(OAc)_4$ (Racemic sample), b) prepared using Rh_2(*S*-1,2-NTTL)$_4$. Chromatographic conditions: Chiralcel® OJ column, 2% 2-propanol in *n*-hexane (*v/v*%), 1 mL/min, 220 nm.

2.2.2.2. Hypothetical model for the observed asymmetric induction

For this particular family of catalysts, there are still ambiguities that surround the arrangement of ligands during catalysis in solution. These uncertainties led to doubts related to their mechanism of asymmetric discrimination during carbenoid

transformations. As a consequence, a number of models have emerged trying to justify the stereoselection mechanisms during dirhodium(II)-catalyzed reactions.

The first model was proposed by Hashimoto[59-61] and it was proposed after the X-ray crystal structure of Rh_2(*S*-PTPA)$_4$ was determined. Rh_2(*S*-PTPA)$_4$ was found to have two adjacent *N*-phthalimido rings oriented on the upper face of the complex, while the other two are oriented towards its lower face in solid state. In Hashimoto's model, it was proposed that dirhodium(II) carboxylates derived from *N*-phthalimido protected amino acid ligands adapts preferentially the *α*,*α*,*β*,*β*-conformation during catalysis (Figure 2.16). This model was also applied successfully to predict the stereochemical outcome for asymmetric C-H insertions catalyzed by Rh_2(*S*-PTAD)$_4$.[62]

Fox subsequently proposed that these complexes adapt an "all-up" conformation during catalysis. Fox proposal was based on the X-ray crystal structure of Rh_2(*S*-PTTL)$_4$ with the four *N*-phthalimido groups oriented towards one face of the complex creating a "chiral crown cavity" (Figure 2.16).[63,64] Other research groups have also reported X-ray structures of other catalysts belonging to the same family and all of these catalysts were having the same "all-up" conformation in solid state.[65-67,9,11] According to Fox's model, two opposite *N*-phthalimido groups are acting as blocking walls, while the other two are slightly tilted leading to a narrow (~11 Å) and wide (~15 Å) chiral cavity. The carbene is predicted to align with the wide dimension of the chiral cavity and this leaves the *si* face of the carbene accessible for reaction with the alkene *via* end on approach. While, according to Fox, the *tert*-butyl groups are necessary to limit reactivity to only one of the catalyst faces.

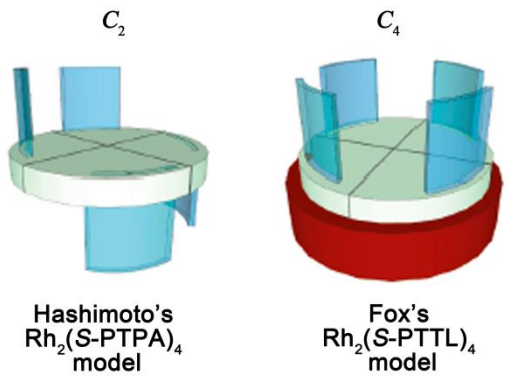

Figure 2.16. 3D models for the distinct ligand orientations used to rationalize the observed enantioselectivity of dirhodium(II) carboxylates derived from *N*-protected amino acid ligands.[68] (Reprinted with permission from Qin, C.; Boyarskikh, V.; Hansen, J. H.; Hardcastle, K. I.; Musaev, D. G.; Davies, H. M. L. *J. Am. Chem. Soc.* **2011**, *133*, 19198. Copyright 2011).

Later, 2D Heteronuclear NOESY studies by Charette[66] and Duddeck,[11] independently, confirmed that Rh_2(*S*-PTTL)$_4$ and similar catalysts have a mobile conformation in solution which allows the existence of other conformers with at least one *N*-phthaloyl group flipped down (Figure 2.17). More investigations are necessary for the determination of the defined ligand's orientations in Hashimoto's and related complexes in solution to be able to account for all sorts of asymmetric transformations achieved using this important class of catalysts.

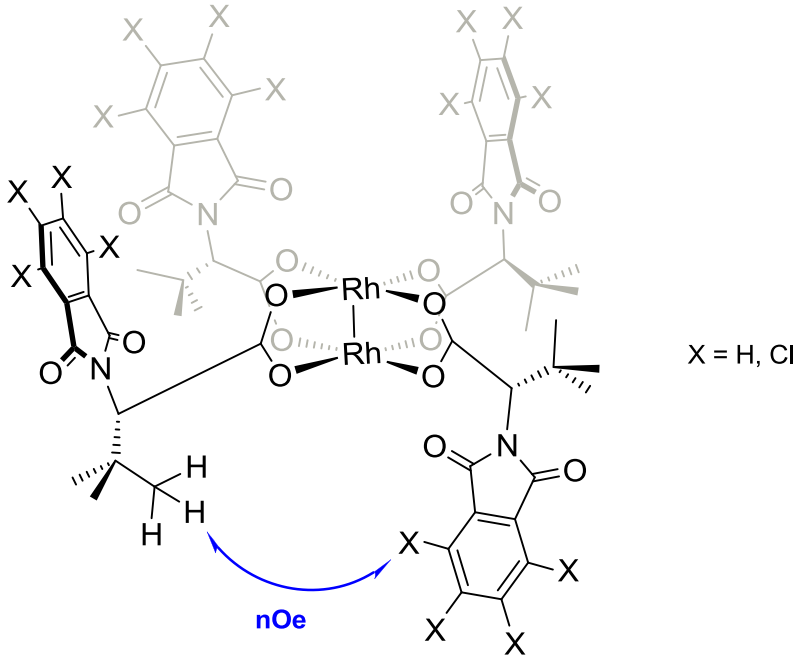

Figure 2.17. 2D-Heteronuclear NOESY experiments on Rh_2(*S*-PTTL)$_4$ and related complexes.[66,11]

Unfortunately, all endeavours for growing crystals of **3a-e** that are suitable for X-ray crystallographic analysis were unsuccessful, except for Rh_2(*S*-1,2-NTPA)$_4$ (**3b**). The crystal quality was adequate only for partial connectivity establishment. With the current refinement, all what can be said is that the complex forms a bis(ACN) adduct when crystallised from acetonitrile and adopting the so-called *α*,*α*,*β*,*β*-conformation in solid state (Figure 2.18).

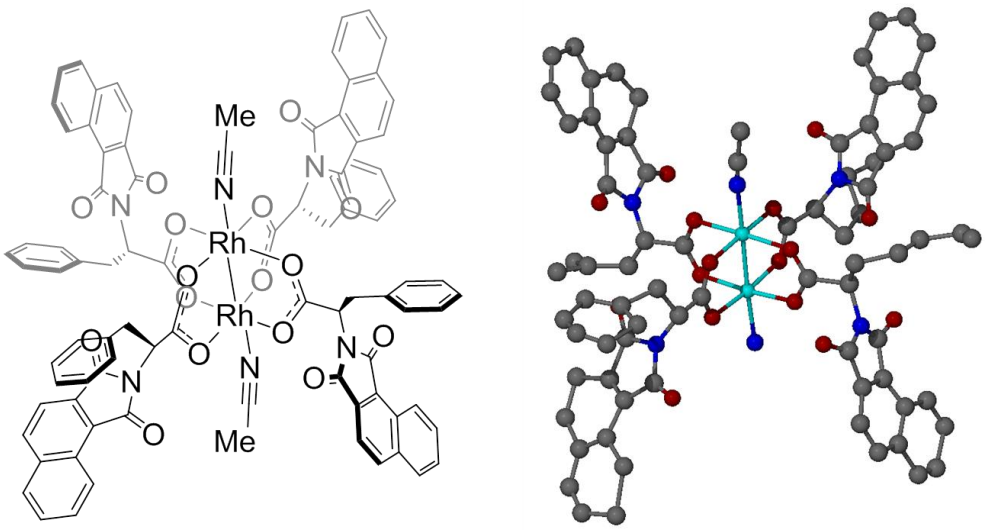

Figure 2.18. X-ray structure of bis(ACN) adduct of Rh_2(*S*-1,2-NTPA)$_4$ (**3b**) (side view). As shown, not all ligand atoms could be located in the structure refinement.

Based on the available information offered by the X-ray crystal structure of Rh_2(*S*-1,2-NTPA)$_4$ and on the illustrated background, Hashimoto's C_2-asymmetric model was adopted to Rh_2(*S*-1,2-NTTL)$_4$ (**3a**) in solution at which, the *N*-1,2-naphthaloyl groups are oriented in an "up, up, down, down" arrangement across the rhodium core.

The asymmetric nature of the *N*-1,2-naphtahloyl protecting group will generate two possible orientations in space at 180° from each other. This will in turn lead to an enormous number of possible catalyst conformations. For simplification, conformers **I** and **II** displayed in Figure 2.19 will be only considered as they are expected of being the lowest free-energy conformations. In these two conformers, the aromatic groups on each catalyst face will remain in a similar environment, either clockwise or anti-clockwise (Figure 2.19).

The much bulkier dimethyl phosphonate ester group (having tetrahedral geometry) orients itself away to avoid the steric interaction with the *N*-1,2-napthaloyl walls (Figure 2.19). The alkene is predicted to approach from the front and lead to the observed product. This may justify the high enantiomeric excess of the cyclopropyl derivatives when using carbenoid with bulky phosphonate group (Table 2.4).

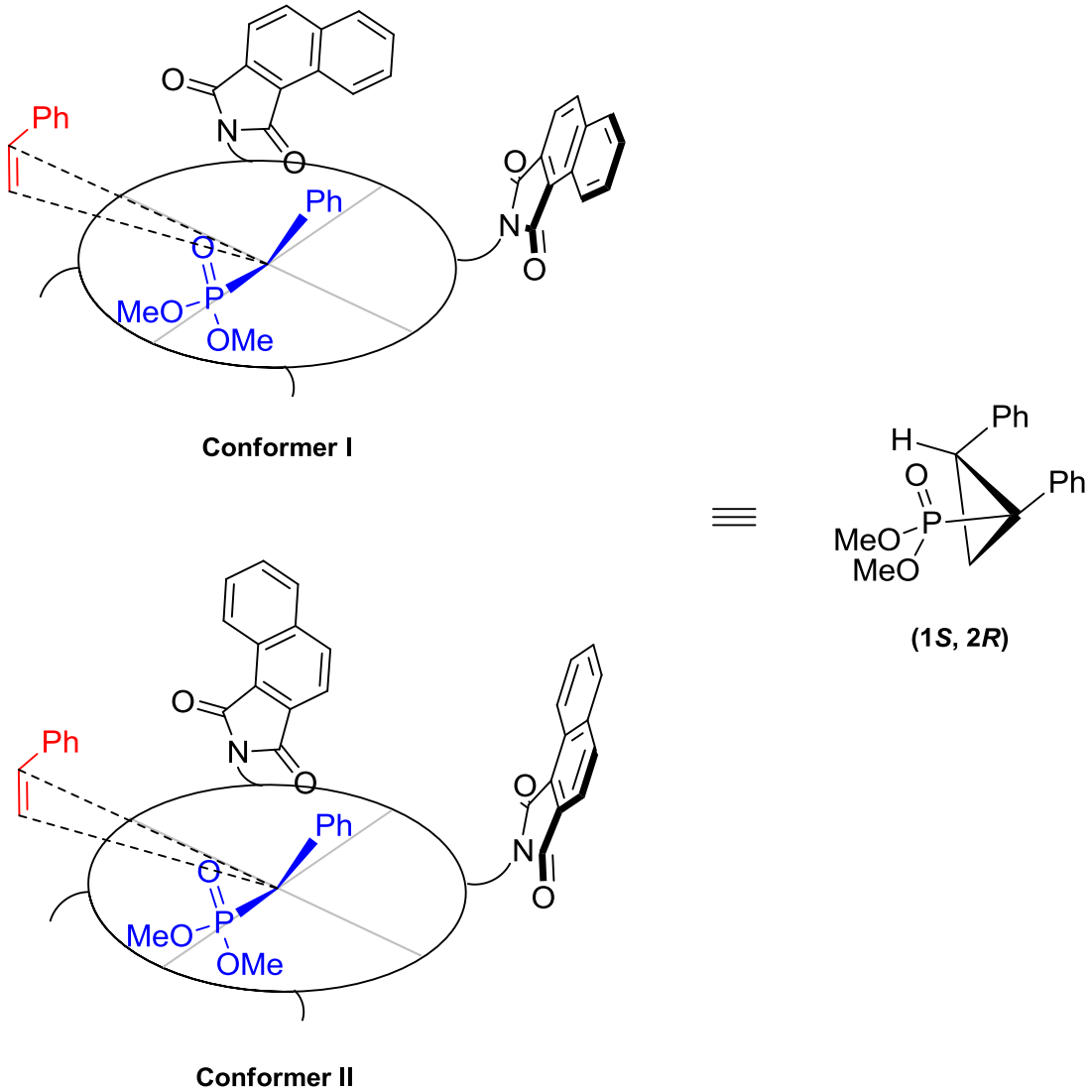

Figure 2.19. Predictive model for the observed asymmetric Rh_2(*S*-1,2-NTTL)$_4$-catalyzed cyclopropanation.

The Fox model was also applied and, as shown in Figure 2.20, the bulky phosphonate group should be located in the less hindered quadrant of the catalyst cavity. The alkene should approach from the front, over one of the *N*-1,2-naphthalimido groups. However, the current version of this model predicted the wrong absolute stereochemistry to what was actually observed for the reaction.

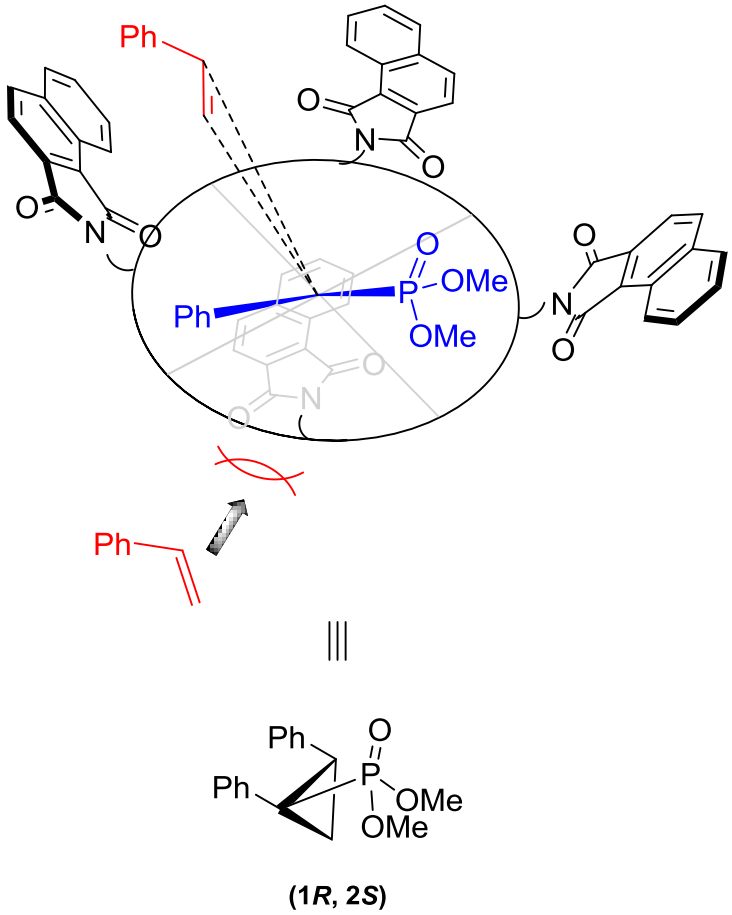

Figure 2.20. Application of Fox's predictive model for the asymmetric cyclopropanation catalyzed by Rh_2(*S*-1,2-NTTL)$_4$ (**3a**).

2.2.3. Screening for asymmetric cyclopropanation with *diacceptor* substrates

Studies were also targeted probing the enantioselectivity of the prepared catalysts in asymmetric cyclopropanations involving variety of alkenes with *diacceptor* Meldrum's acid (Table 2.5). I thought about including this particular substrate in the screening as, recently, there has been an expanding passion in 1,1-cyclopropane diesters derivatives as useful synthesis intermediates. This class of substrates was utilized in a variety of cycloaddition reactions involving imines,[69-71] nitrones,[72-77] aldehydes[78-84] and others[85-90] providing a wide range of useful synthesis building blocks (Figure 2.21). Moreover, the reactivity of this class of substrates played a crucial part in the synthesis of molecules with complex structures. For example, cyclopropane derivative **6** is a useful starting material for accessing a variety of biologically relevant molecules as illustrated in Figure 2.21.[91] This kept 1,1-

cyclopropane diesters as valuable chiral intermediates and an attractive target for synthetic chemists. However, the preparation of this class of compounds in an enantiomerically pure form continues to be a big challenge for chemists. Dirhodium(II)-catalyzed cyclopropanations can be considered as the most straight forward route for accessing 1,1-cyclopropane diesters and several synthetic examples have already been highlighted earlier in Chapter 1.

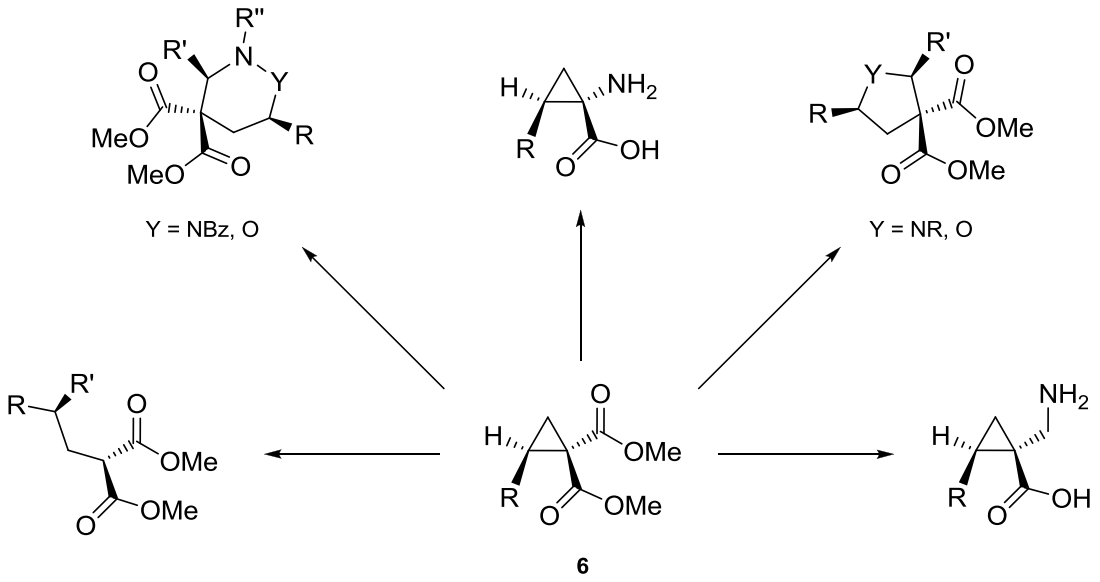

Figure 2.21. Examples for reactivity and application of 1,1-cyclopropane diesters.[91]

To facilitate the screening, a previously developed user-friendly one-pot cyclopropanation procedure was used, wherein the phenylidonium ylides are generated and decomposed *in situ*.[16,92,8,10]. All the reactions were carried out at room temperature in methylene chloride as reaction solvent and data are summarised in Table 2.5.

Table 2.5. Asymmetric cyclopropanation with Meldrum's acid (*diacceptor* substrate).

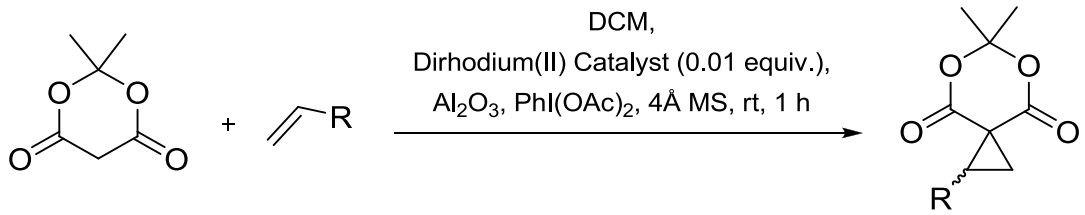

R	Rh_2(*S*-PTTL)$_4$		Rh_2(*S*-NTTL)$_4$		Rh_2(*S*-1,2-NTTL)$_4$ (3a)		Rh_2(*S*-1,2-NTPA)$_4$ (3b)		Rh_2(*S*-1,2-NTLU)$_4$ (3c)		Rh_2(*S*-1,2-NTTR)$_4$ (3d)		Rh_2(*S*-1,2-NTTY)$_4$ (3e)	
	Yield (%)	*ee* (%)[a]	Yield (%)	*ee* (%)[a]	Yield (%)	*ee* (%)[a]	Yield (%)	*ee* (%)[a]	Yield (%)	*ee* (%)[a]	Yield (%)	*ee* (%)[a]	Yield (%)	*ee* (%)[a]
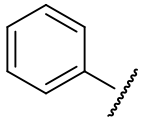	45	37	38	32	60	30	47	12[b]	54	16[b]	18	18	14	13
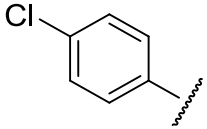	52	36	40	31[b]	57	28[b]	51	9[b]	59	15[b]	20	18	16	14[b]
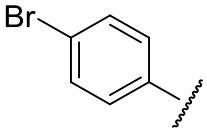	42	35	63	20	46	27	41	11	55	12	11	17	14	9

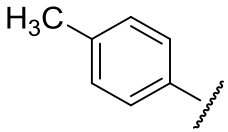	33	29	36	23	32	22	30	8	47	8	13	17	13	12
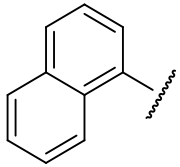	53	27	28	17[b]	44	20	38	8[b]	46	9[b]	12	13	15	7

[a]The (*R*)-enantiomer is the major product. [b]Analyzed as crude mixture. Enantiomeric excess percentages (*ee*%) were determined by chiral HPLC analysis. See experimental section for chromatographic conditions and details.

All catalysts revealed moderate isolated yields, except for Rh_2(*S*-1,2-NTTR)$_4$ (**3d**) and Rh_2(*S*-1,2-NTTY)$_4$ (**3e**). The asymmetric induction exhibited by the prepared catalysts ranged from moderate to low (30-7% *ee*) for all substrates. In terms of enantiomeric excess of the resulting cyclopropane derivatives, Rh_2(*S*-1,2-NTTL)$_4$ (**3a**) was the best among the series (30-20% *ee*) and it revealed similar enantiomeric induction to Rh_2(*S*-NTTL)$_4$ (32-17% *ee*) but both were lower than Rh_2(*S*-PTTL)$_4$ (37-27% *ee*).

2.3. RE-EVALUATION OF CONCEPT AND PREPARATION OF MORE DIRHODIUM(II) CATALYSTS WITH LOWER SYMMETRY *N*-PROTECTING GROUPS

At this point, I re-considered what might be necessary for a ligand to be efficient. Four more ligands (**7**, **8**, **9** and **10**) were synthesized as illustrated in scheme 2.6 using the *N*-protection conditions confirmed earlier in this chapter. The *tert*-butyl group at the *α*-carbon was fixed as obviously it is the most optimum match for the explored chemistry. Standard ligand exchange conditions between the prepared ligands and $Rh_2(OAc)_4$ generated Rh_2(*S*-1-Ph-BPTTL)$_4$ (**11**), Rh_2(*S*-^{tert}PTTL)$_4$ (**12**), Rh_2(*S*-BHTL)$_4$ (**13**) and Rh_2(*S*-BOTL)$_4$ (**14**) as green solids in 67%, 71%, 83% and 92% yields, respectively (Figure 2.22).

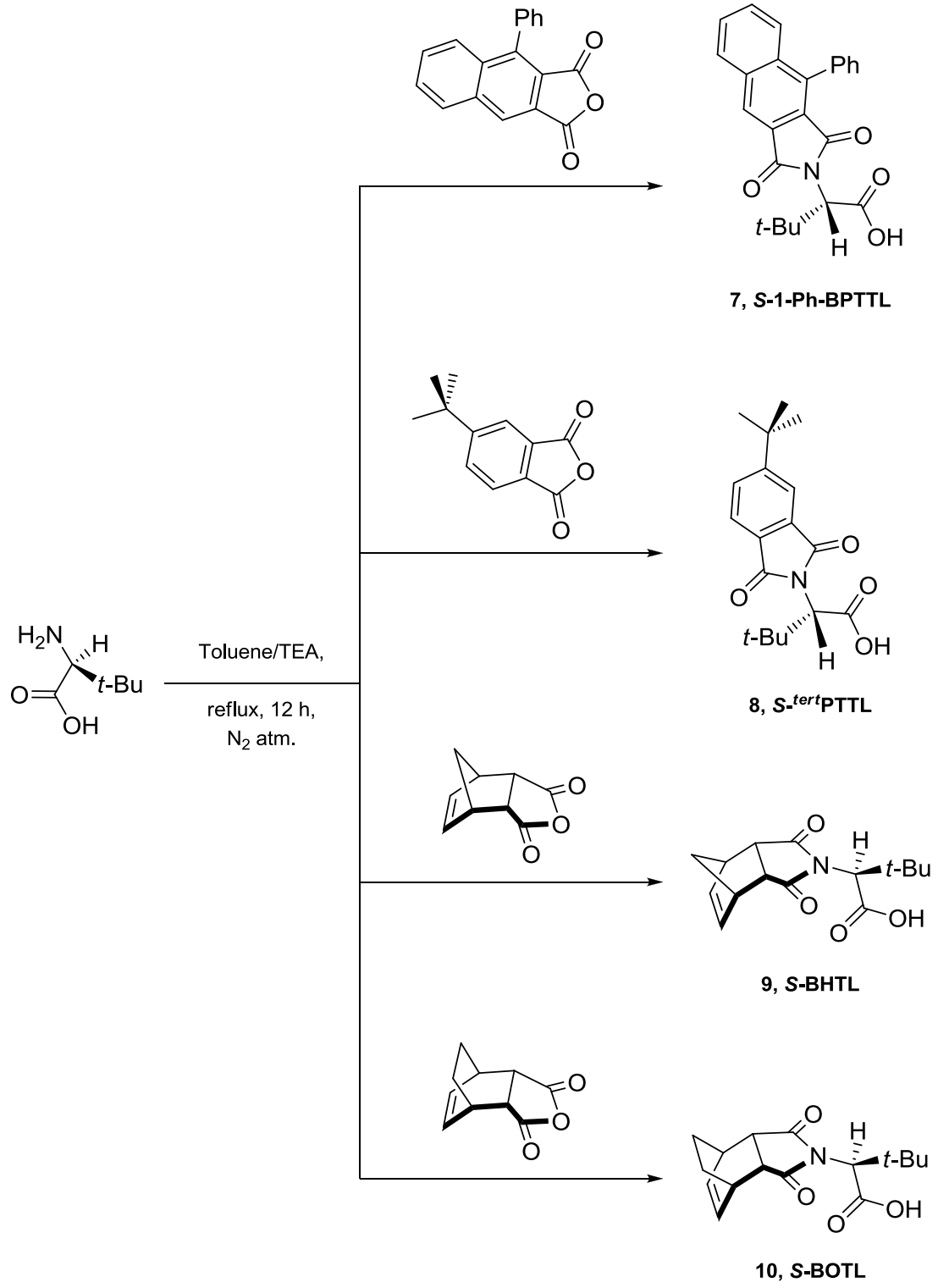

Scheme 2.6. Preparation of chiral ligands **7**, **8**, **9** and **10**.

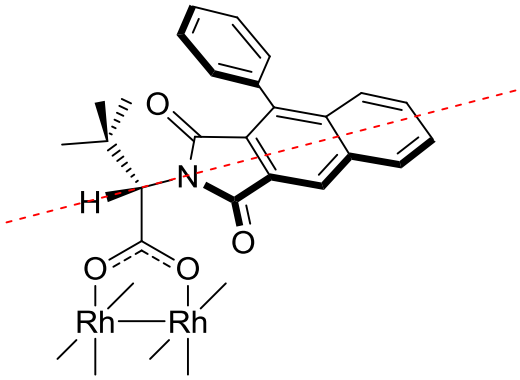

Rh_2(*S*-1-Ph-BPTTL)$_4$ (11)

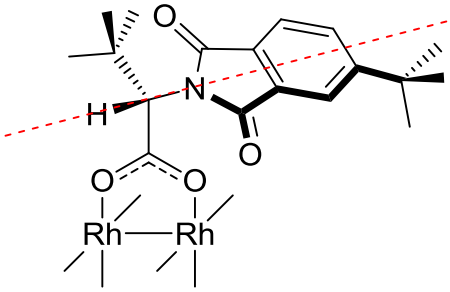

Rh_2(*S*-^{tert}PTTL)$_4$ (12)

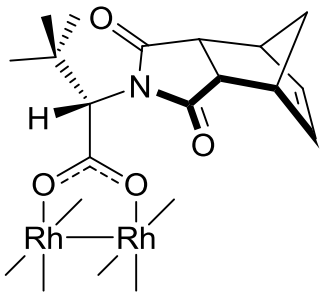

Rh_2(*S*-BHTL)$_4$ (13)

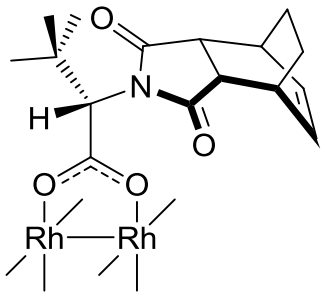

Rh_2(*S*-BOTL)$_4$ (14)

Figure 2.22. Structures of prepared catalysts.

These four catalysts emerged as a result of applying alternative strategies for lowering the symmetry of the *N*-protecting group. Instead of reducing its symmetry by fusing a ring on only one of its sides (e.g. as in the case of *N*-1,2-NTTL ligand (**1a**)), partial substitution of the ring can also reduce the symmetry as in the case of Rh_2(*S*-1-Ph-BPTTL)$_4$ (**11**) and Rh_2(*S*-^{tert}PTTL)$_4$ (**12**). For the two complexes, the planarity of the *N*-phthaloyl section is maintained, but the local symmetry of the *N*-protecting group is reduced from C_{2v} to C_s by virtue of the substituents.

As illustrated in Figure 2.23a, introducing a substituent at either position 3 or 4 for the PTTL derived catalyst **12** will reduce the symmetry of the phthalimido protecting group. But in order to get the advantage of the "Cavity Rim Steric Impedance effect"[9] discussed earlier, introduction of the substituent at position 4 was favoured over position 3. While for the BPTTL derived catalyst **11** (Figure 2.23b), positions 5 and 6 are far away from the rhodium reactive centre and the introduction of the

substituent at any of these two spots is expected to exert minimal influence on the stereoselectivity of the catalyst. As a consequence, introduction of the substituent at position 4 was favoured.

I was fortunate to find the commercially available 4-*tert*-butylphthalic anhydride and 1-phenyl-2,3-naphthalenedicarboxylic anhydride which were chosen for protection of *tert*-leucine amino group. As using a commercially available anhydride definitely simplifies the preparation process making the final catalyst more synthetically accessible. *tert*-Butyl and phenyl substituents were suitable as being bulky substituents following the common strategy in chiral catalysts design to limit the number of possible orientations of substrates while interacting with the catalyst.[93]

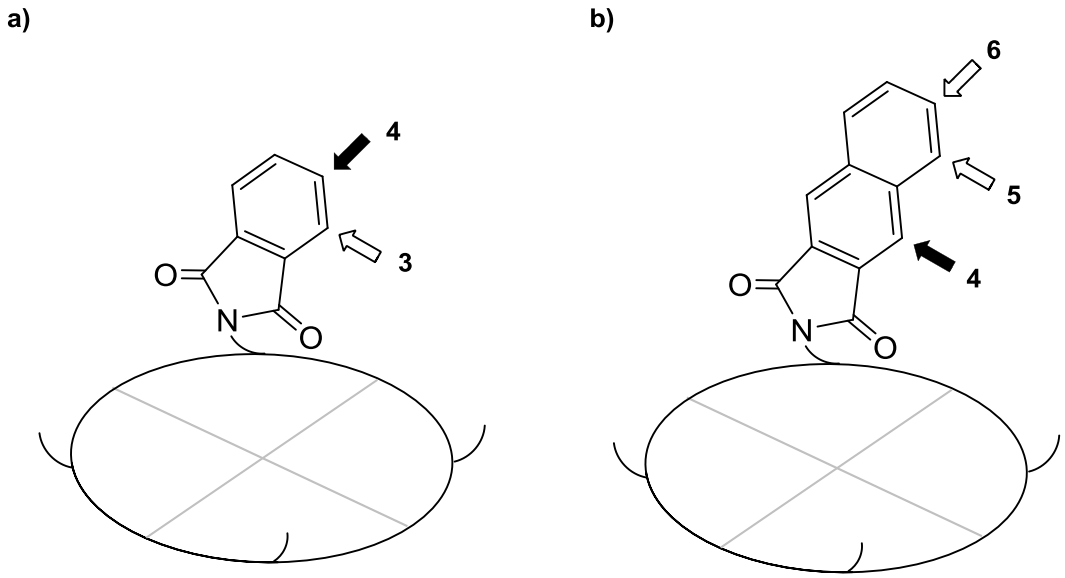

Figure 2.23. Suitable positions for substituent introduction; favoured substitution positions are represented in black arrows.

On the other hand, the reduction of symmetry in Rh_2(*S*-BHTL)$_4$ (**13**) and Rh_2(*S*-BOTL)$_4$ (**14**) complexes is quite interesting. The *N*-protecting group has C_s symmetry, which means that all four *N*-protecting groups will be equivalently positioned around the extremity of the chiral crown cavity and not reducing the C_4-symmetry of the final complex.

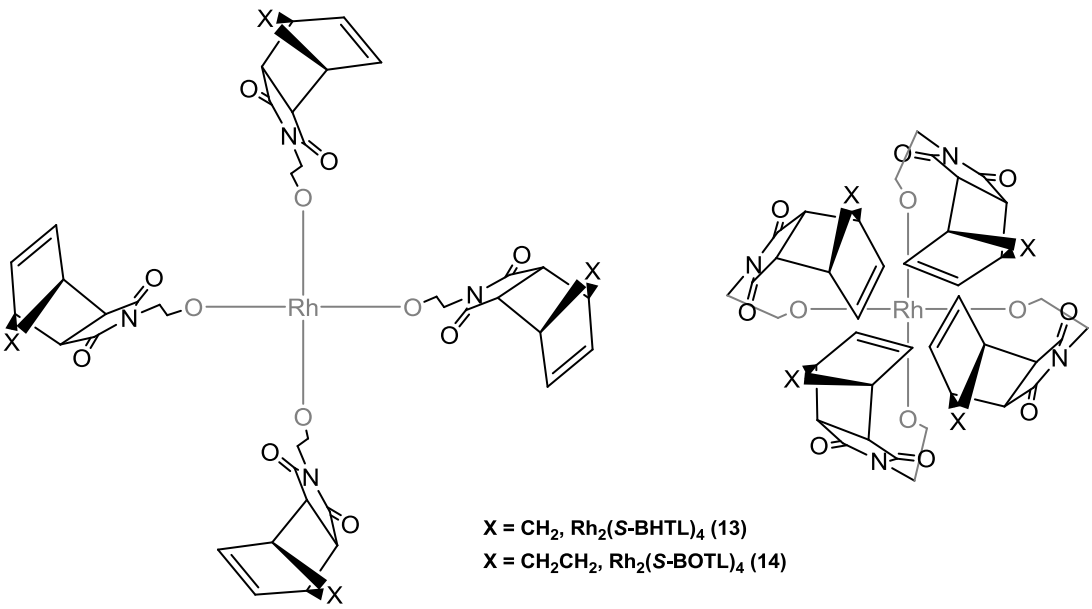

Figure 2.24. The two possible orientations of the *N*-protecting group in Rh_2(*S*-BHTL)$_4$ (**13**) and Rh_2(*S*-BOTL)$_4$ (**14**).

To the best of my knowledge, there are still no published catalyst structure where flipping the ligands' rings over makes a difference (Figure 2.24). The only similar example to Rh_2(*S*-BHTL)$_4$ (**13**) and Rh_2(*S*-BOTL)$_4$ (**14**) was a dirhodium(II) complex reported by Bertilsson and Andersson[94] where it was carrying (1*S*, 3*R*, 4*R*)-2-(*p-tert*-butylphenylsulphonyl)-2-aza-bicyclo[2.2.1]heptane-3-carboxylate ligands (Figure 2.25). However, the authors claimed that this complex is adopting a locked D_2-symmetry.

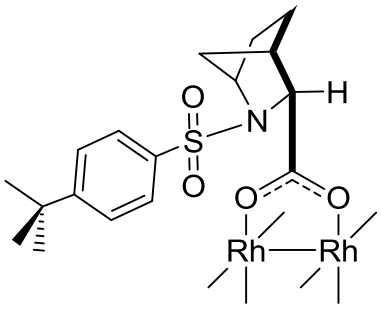

Figure 2.25. Structure of dirhodium(II,II) tetrakis[(1*S*, 3*R*, 4*R*)-2-(*p-tert*-butylphenylsulphonyl)-2-aza-bicyclo[2.2.1]heptane-3-carboxylate].

The attempt to use *exo*-3,6-epoxy-1,2,3,6-tetrahydrophthalic anhydride **15** as a protecting group generated a single major product as indicated by TLC. However, spectral data inspection of the generated product indicated that it is not the desired *N*-protected *tert*-leucine **16**. Instead, a Retro-Diels-Alder reaction took place to afford (*E*)-4-(1-carboxy-2,2-dimethylpropylamino)-4-oxobut-2-enoic acid product (**17**) (Scheme 2.7).

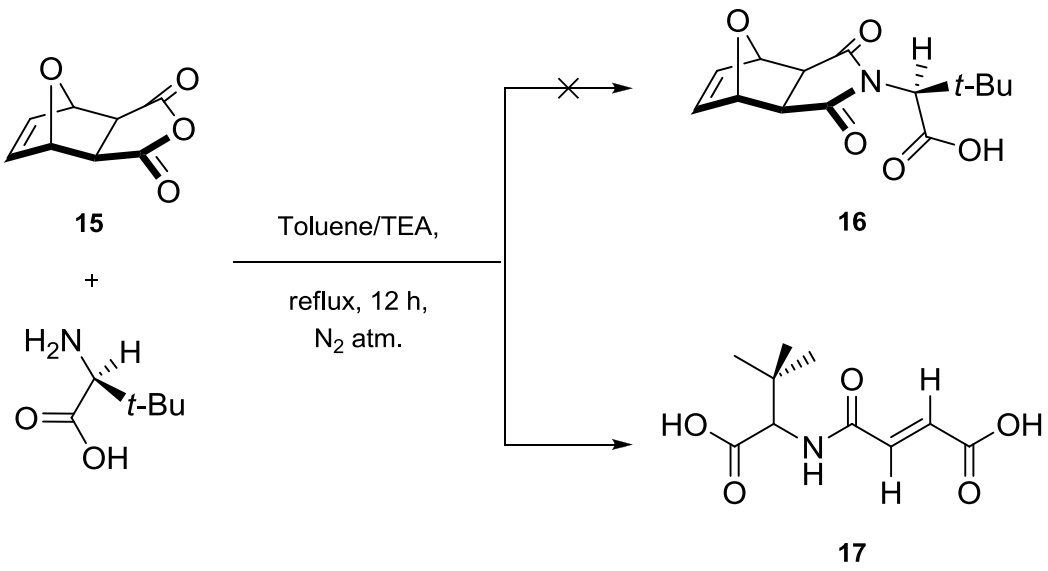

Scheme 2.7. The attempt to use *exo*-3,6-epoxy-1,2,3,6-tetrahydrophthalic anhydride **15** as a protecting group for L-*tert*-leucine amino acid.

Moreover, using *N*-phthaloyl-L-glutamic anhydride as *N*-protecting group for L-*tert*-leucine proceeded unsuccessfully. After refluxing for 12 h, TLC analysis of the reaction

mixture indicated the complete decomposition of starting materials with no generation of a major product (Scheme 2.8). Repeating the reaction in DMF instead of toluene/TEA as a reaction solvent did not lead to a different observation.

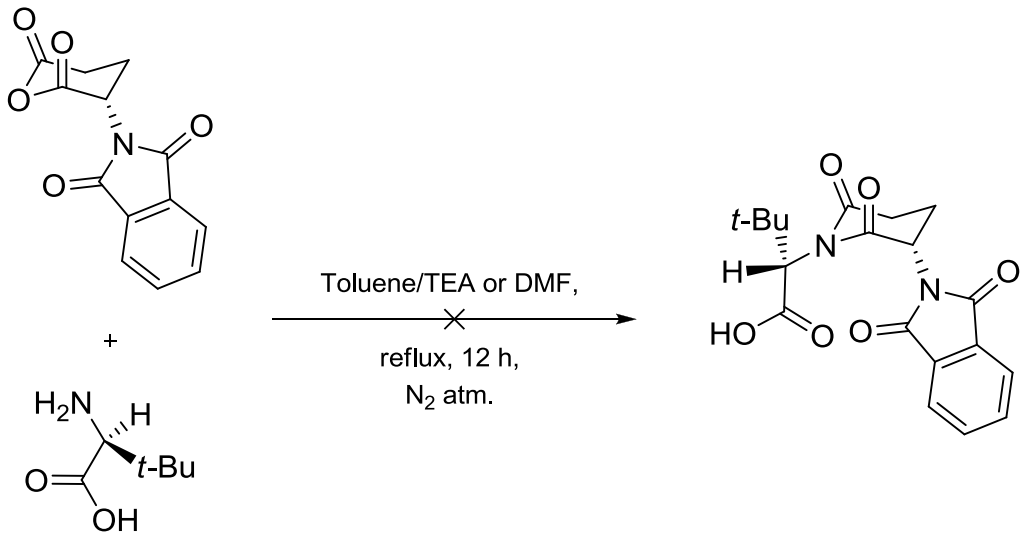

Scheme 2.8. The attempt to use *N*-phthaloyl-L-glutamic anhydride as a protecting group for L-*tert*-leucine amino acid.

The synthesis of a 4-*tert*-butyl-substituted *S*-NTTL ligand was also attempted. The proposed synthetic strategy was the introduction of a *tert*-butyl group to acenaphthene, followed by sodium dichromate oxidation[95] to the corresponding anhydride. The introduction of the *tert*-butyl group through $FeCl_3$-catalyzed Friedel-Crafts alkylation generated the desired product but in a very low yield (12%). This was due to the high volatility of *tert*-butyl chloride that quickly evaporates leaving the reaction mixture with the evolving HCl gas (Scheme 2.9). Slow introduction of *tert*-butyl chloride to the reaction mixture did not solve the problem.

Moreover, sodium dichromate oxidation of the generated 3-*tert*-butylacenaphthene was also undertaken. While IR analysis indicated the generation of the anhydride functionality, ^{1}H and ^{13}C NMR spectroscopy indicated the absence of the *tert*-butyl group from the reaction major product. Connectivity investigations through 2-dimensional COSY, HSQC and HMBC experiments revealed that 4,4'-binaphthyl-1,1',8,8'-tetracarboxylic dianhydride dimer (**18**) was generated as the reaction major product instead of the desired 4-*tert*-butyl-1,8-naphthalic anhydride (Scheme 2.9).

The HMBC spectrum of **18** revealed that the aromatic proton H_3 at δ_H 7.96 ppm correlates to C_1 at δ_c 119.8 ppm, C_{4a} at δ_c 130.3 ppm and C_4' at δ_c 142.9 ppm which established the dimerization to **18**. Mass spectrometric analysis also confirmed the structure of **18** as reaction product which was formed after the *tert*-butyl substituent was knocked off during the sodium dichromate oxidation.

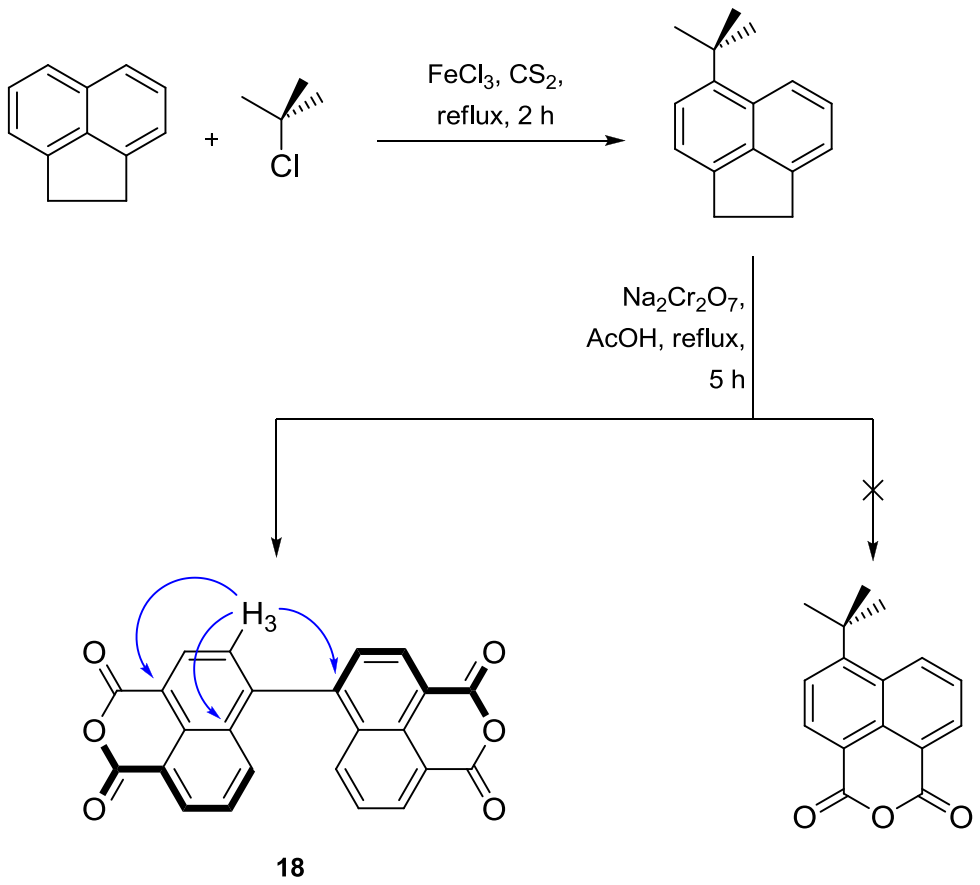

Scheme 2.9. Attempt for the preparation of 4-*tert*-butyl-1,8-naphthalic anhydride; HMBC correlations are represented in blue arrows.

2.3.1. Screening in enantioselective synthesis of phosphonate-substituted cyclopropanes

With the four catalysts in hand, again their efficiencies were examined in the same standard reaction between styrene and dimethyl *α*-diazobenzylphosphonate in 2,2-DMB as reaction solvent. In all cases, the cyclopropylphosphonate product **5** was generated in good to excellent yield (84-92%) and with levels of diastereoselectivity of >20:1 *E*:*Z* dr.

In terms of enantioselectivity, the results indicated that the introduction of a substituent on the heterocyclic tether resulted in a significant improvement in enantioselectivity. For example, Rh_2(*S*-BPTTL)$_4$ generated the cyclopropane product in 86% *ee*, while, the introduction of an extra phenyl substituent on one of the protecting group sides in Rh_2(*S*-1-Ph-BPTTL)$_4$ (**11**) resulted in the generation of the product in 90% *ee* under the same reaction conditions (Table 2.6, entries 5 *vs.* 6).

Moreover, the influence of introducing a *tert*-butyl group at the 4-position of the phthalimido group in Rh_2(*S*-^{tert}PTTL)$_4$ (**12**) was dramatic. Rh_2(*S*-^{tert}PTTL)$_4$ was fully soluble in 2,2-DMB at room temperature and, indeed, it provided improved levels of enantioinduction over Rh_2(*S*-PTTL)$_4$ and Rh_2(*S*-NTTL)$_4$ (Table 2.6, entries 7 *vs*. 3 and 4). In the presence of Rh_2(*S*-PTTL)$_4$ and Rh_2(*S*-NTTL)$_4$, the cyclopropane **5** was generated with 92% and 91% *ee*, respectively. While, after stirring for 5 h at room temperature, the Rh_2(*S*-^{tert}PTTL)$_4$-catalyzed reaction proceeded smoothly generating the cyclopropane product **5** in 98% *ee*.

The obtained result was comparable to the result reported when Rh_2(*S*-PTAD)$_4$ was used as a catalyst in the same reaction carried out under refluxing conditions for 10 h.[58] A Rh_2(*S*-PTAD)$_4$-catalyzed cyclopropanation reaction stirred at room temperature overnight was also carried out at which the cyclopropane product was isolated in 49% yield with enantioselectivity of 66% *ee* (Table 2.6, entry 2). At this point and based on the obtained results, it was realized that a much more synthetically accessible alternative to Rh_2(*S*-PTAD)$_4$ might has been discovered.

Unfortunately, the bicyclo- complexes **13** and **14** did not return the expected success. The cyclopropanation reactions proceeded successfully giving the cyclopropane product with moderate enantioselectivities of 66% and 74% *ee* exhibited by Rh_2(*S*-BOTL)$_4$ (**14**) and Rh_2(*S*-BHTL)$_4$ (**13**), respectively (Table 2.6, entries 8 and 9).

Table 2.6. Asymmetric cyclopropanation of styrene with dimethyl α-diazobenzylphosphonate.

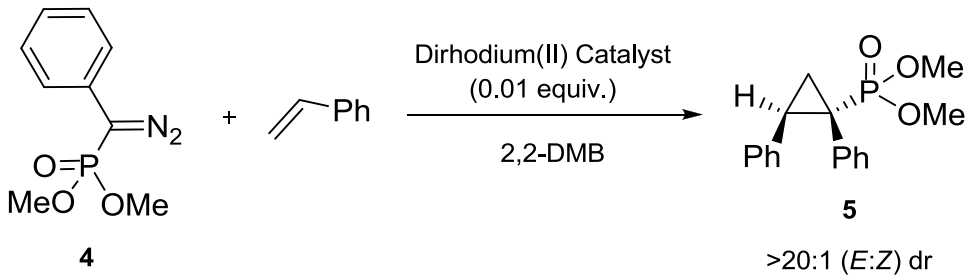

Entry	Catalyst	Catalyst code	Reaction temp (^{o}C)	Yield (%)	*ee* (%)
1	Rh_2(*S*-PTAD)$_4$	-	59	88	94
2	Rh_2(*S*-PTAD)$_4$	-	23[a]	49	66
3	Rh_2(*S*-PTTL)$_4$	-	59	85	92
4	Rh_2(*S*-NTTL)$_4$	-	59	87	91
5	Rh_2(*S*-BPTTL)$_4$	-	59	83	86
6	Rh_2(*S*-1-Ph-BPTTL)$_4$	**11**	59	87	90
7	Rh_2(*S*-^{tert}PTTL)$_4$	**12**	23[b]	92	98

8	Rh_2(*S*-BOTL)$_4$	**14**	59	89	66
9	Rh_2(*S*-BHTL)$_4$	**13**	59	84	74

[a]Stirring overnight, [b]Stirring for 5 h. Diastereomeric ratios (dr) were determined by ^{1}H NMR of the crude mixture. Enantiomeric excess percentages (*ee*%) were determined by chiral HPLC using Chiralcel® OJ column, 2% 2-propanol in *n*-hexane (*v*/*v*%), 1 mL/min, 220 nm, τ_1 = 18 min, τ_2 = 21 min. See experimental section for more details.

2.3.1.1. Scope of catalysts with respect to the olefin

The carbenoid cyclopropanation reaction of **4** was applied to a range of olefins using Rh_2(*S*-1,2-NTTL)$_4$ (**3a**), Rh_2(*S*-1-Ph-BPTTL)$_4$ (**11**) and Rh_2(*S*-^{tert}PTTL)$_4$ (**12**) as catalysts and results are illustrated in Table 2.7. All reactions involving Rh_2(*S*-^{tert}PTTL)$_4$ (**12**) were carried out at room temperature, while the reactions involving the other two complexes **3a** and **11** were carried out at 59 ^{o}C. In all cases, the reactions proceeded smoothly resulting in the formation of corresponding cyclopropylphosphonate products in very high yields (86-93%) and diastereoselectivities (>20:1 *E*:*Z* dr). In terms of enantioselectivity, Rh_2(*S*-^{tert}PTTL)$_4$ (**12**) was the best catalyst among the three screened catalysts giving the corresponding cyclopropane products with very high levels of enantioselectivity (>98-99% *ee*).

Table 2.7. Scope of the catalysts investigations with respect to the alkene.

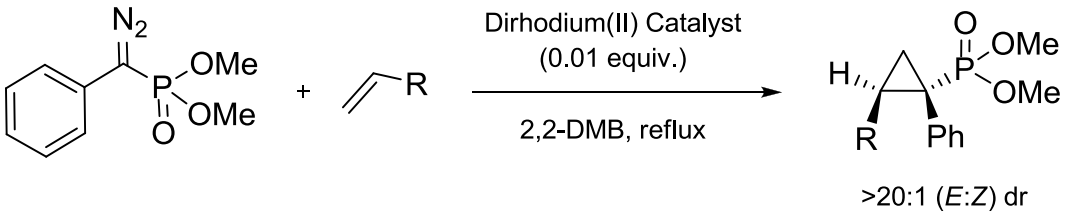

Entry	R	Product	Rh_2(*S*-1,2-NTTL)$_4$ (3a)		Rh_2(*S*-1-Ph-BPTTL)$_4$ (11)		Rh_2(*S*-^{tert}PTTL)$_4$[a] (12)	
			Yield (%)	*ee* (%)	Yield (%)	*ee* (%)	Yield (%)	*ee* (%)
1	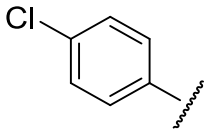	**19**	92	94	89	84	94	>98
2	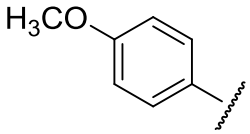	**20**	93	>99	86	93	90	99
3	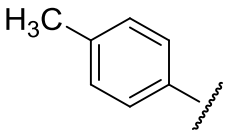	**21**	90	95	88	90	93	>99

4	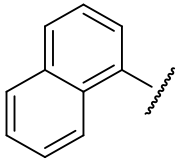	**22**	86	>98	82	90	85	>98

[a]Stirring at room temperature, Diastereomeric ratios (dr) were determined by ^{1}H NMR of the crude mixture. Enantiomeric excess percentages (*ee*%) were determined by chiral HPLC. See experimental section for chromatographic conditions and details.

The relative and absolute configuration of dimethyl 1-pheny-2-(*p*-methylphenyl)-cyclopropylphosphonate (**21**) was readily determined by X-ray crystallographic analysis. It was assigned to be (1*S*, 2*R*) (Figure 2.26), which is in agreement with the predicted assignment. While the structures of all the other cyclopropylphosphonate derivatives were tentatively assigned the same relative and absolute configuration by analogy to **21** and based on the assumption that all reactions occur through a similar transition state.

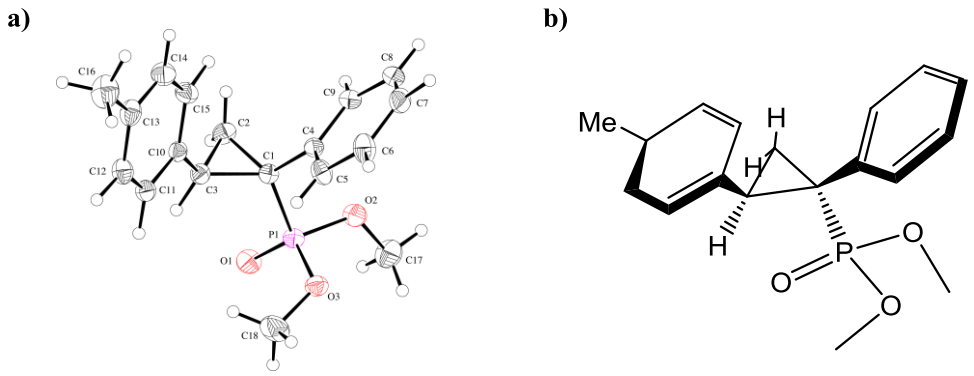

Figure 2.26. ORTEP for (1*S*, 2*R*)-dimethyl 1-pheny-2-(*p*-methylphenyl)-cyclopropylphosphonate (**21**) product.

2.3.1.2. Effect of phosphonate ester group size on the enantioselectivity of catalysts

The effect of diazophosphonate ester group size on the enantioselectivity of the catalysts was next examined using a series of diazophosphonate esters and results are summarized in Table 2.8. The results revealed that, the diastereoselectivity is independent on the size of the phosphonate group and not greatly influenced by the ester group size. However, in all cases, increasing the ester group size caused a drastic decrease in both yield and enantioselectivity where the highest levels of enantioselectivity were observed with dimethyl α-diazobenzylphosphonate **4** (Table 2.8, entry 1).

Table 2.8. Effect of the α-diazophosphonate ester group size on the enantioselectivity of the catalysts.

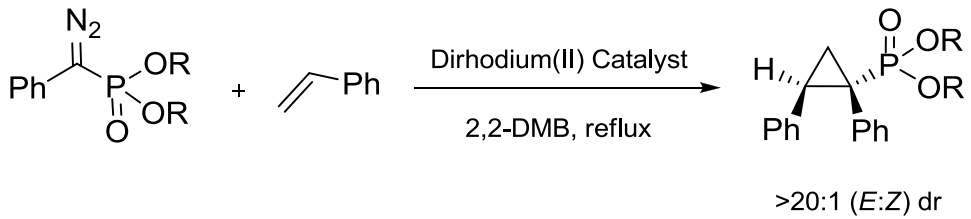

Entry	R	Product	Rh_2(*S*-1,2-NTTL)$_4$ (3a)		Rh_2(*S*-1-Ph-BPTTL)$_4$ (11)		Rh_2(*S*-^{tert}PTTL)$_4$[a] (12)	
			Yield (%)	***ee* (%)**	**Yield (%)**	***ee* (%)**	**Yield (%)**	***ee* (%)**
1	Me	**4**	93	92	87	92	92	99
2	Et	**23**	69	60	66	54	74	92
3	*i*-Pr	**24**	43	68[b]	38	48[b]	40	64[b]

[a]Stirring at room temperature, [b]Reflux for 3 days. Diastereomeric ratios (dr) were determined by ^{1}H NMR of the crude mixture. Enantiomeric excess percentages (*ee*%) were determined by chiral HPLC. See experimental section for chromatographic conditions and details.

2.3.2. Single crystal X-ray diffraction analysis

Crystallographic studies on Rh_2(*S*-^{tert}PTTL)$_4$ (**12**), Rh_2(*S*-1-Ph-BPTTL)$_4$ (**11**), Rh_2(*S*-BHTL)$_4$ (**13**) and Rh_2(*S*-BOTL)$_4$ (**14**) in comparison with solid state geometries of Rh_2(*S*-PTTL)$_4$[63,64] and Rh_2(*S*-PTAD)$_4$ were carried out to clarify the nature of the observed enhancement effect exhibited by lowering the symmetry of the *N*-protecting group on enantioinduction.

In the published structure of the mono(EtOAc) adduct of Rh_2(*S*-PTTL)$_4$,[63,64] the ligand based chirality can be seen to give rise to a "chiral binding pocket" or "chiral crown cavity". The nature of the chirality of this binding pocket is based on two important features (Figure 2.27a); (i) the C_α-CO_2 single bond torsion (carboxylate carbon to α-carbon bond) which lies so as to direct the C_α-N bond in a clockwise twist towards the carbene binding pocket (when viewed along the Rh-Rh axis into the chiral cavity) and (ii) N-C_α bond torsion so as to allow docking of the adjacent *N*-phthaloyl units featuring O$^{\cdots}$CH closest contacts of an alternating σ/π nature. Figure 2.27 (b and c) schematically depicts the daisy chain manner in which the rectangular binding pocket is built up. Visually, the overall effect is to cause an alternation of the positions of the eight oxygen atoms of the *N*-phthaloyl units, which thus reside at high and low positions around the rim of the crown cavity as a result (Gardiner *et al.* unpublished results).

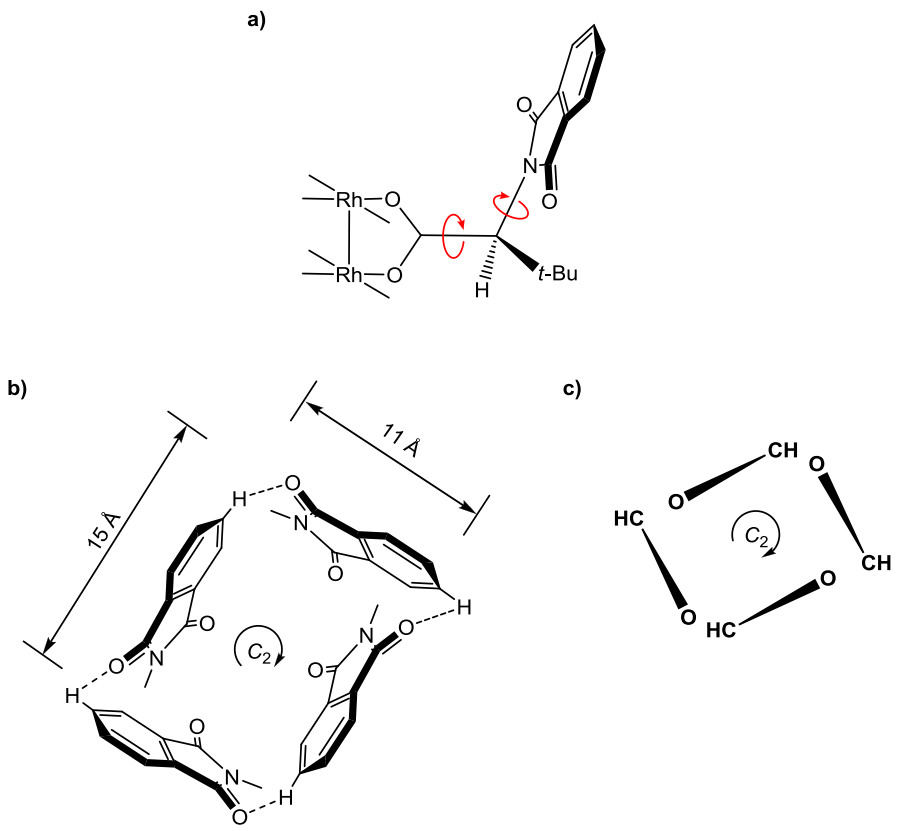

Figure 2.27. a) Features that gives the nature of chirality to the binding pocket of Rh_2(*S*-PTTL)$_4$ and analogues, b) and c) Schematic illustration of the daisy chain manner in which the rectangular binding pocket of Rh_2(*S*-PTTL)$_4$ is built up (Gardiner *et al.* unpublished results).

X-ray crystal structure were obtained from samples of both bis(ACN) and bis(THF) adducts of Rh_2(*S*-^{tert}PTTL)$_4$ (**12**) recrystallized from acetonitrile and THF, respectively. Both adducts revealed full *α,α,α,α* conformation, featuring all for *N*-protecting groups are equivalently positioned around the extremity of the chiral crown cavity while not reducing the C_4-symmetry of the catalyst (Figure 2.28). The *tert*-butyl substituent is similarly disposed towards the "corner" of the square-shaped cavity. The chiral cavity is rigorously C_4-symmetrical in solid state (in both bis(ACN) and bis(THF) adducts), while the four *N*-4-*tert*-butyl-phthaloyl group incorporation maintains the chiral nature of the crown cavity surrounding the axial Rh coordination site through the clockwise twist of these groups.

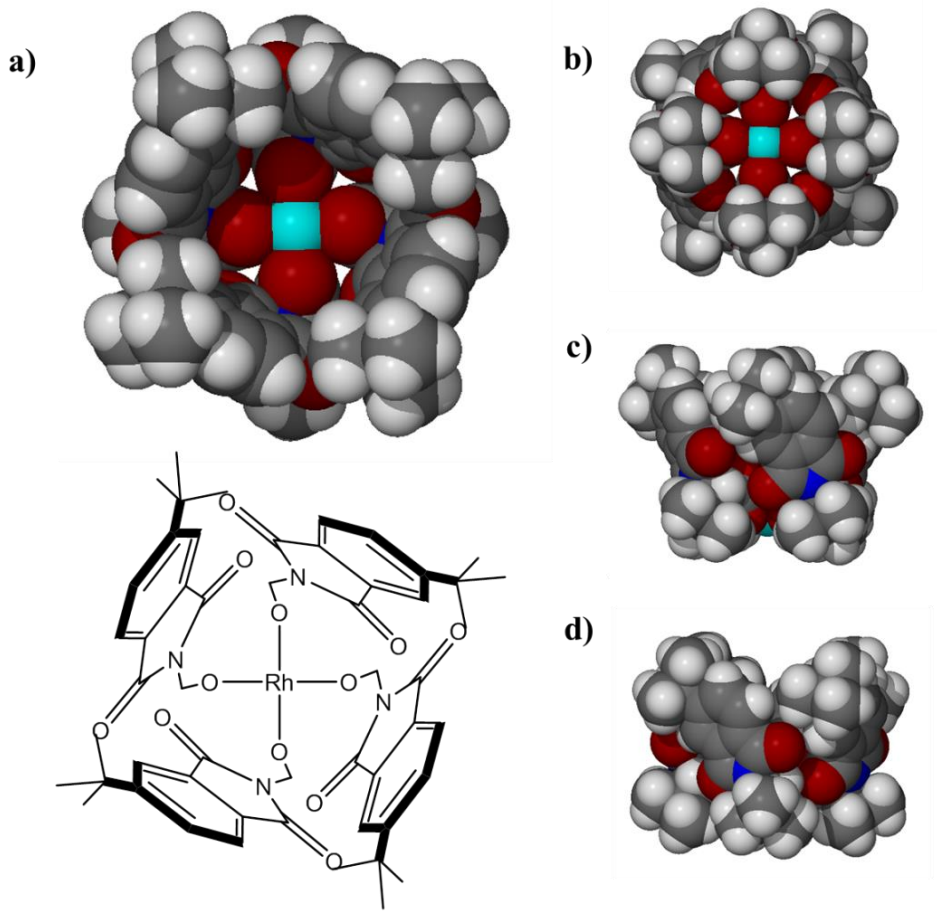

Figure 2.28. Molecular structure of bis(THF) adduct of $Rh_2(S\text{-}^{tert}PTTL)_4$ (**12**). Space filling representation; a) top view, b) bottom view, c) and d) side views (A second similar molecule, as well as axial ligands were omitted for clarity).

The cavity of $Rh_2(S\text{-}^{tert}PTTL)_4$ is fairly square if compared to the *α,α,α,α* conformer originally reported for the mono(EtOAc) adduct of $Rh_2(S\text{-}PTTL)_4$ (Figure 2.29).[63] The added substitution on the *N*-phthaloyl group in $Rh_2(S\text{-}^{tert}PTTL)_4$ can be seen to nicely extend the width of each of cavity walls to the point that adjacent ligands are nearly at Van der Waals contact. Furthermore, from the space filling representation comparisons of $Rh_2(S\text{-}^{tert}PTTL)_4$ and $Rh_2(S\text{-}PTTL)_4$, it is clear that the extra *tert*-butyl substituents in $Rh_2(S\text{-}^{tert}PTTL)_4$ are introducing greater ligand conformational rigidity through $C_\alpha\text{-}CO_2$, as well as $N\text{-}C_\alpha$ bond torsions of the ligands. On the other hand, this is not the case for the unsubstituted $Rh_2(S\text{-}PTTL)_4$ and various contorted chiral cavities that have been crystalographically observed. The gaps at the corners of these cavities allow substantial variation around $C_\alpha\text{-}CO_2$ and $N\text{-}C_\alpha$ bond torsions. Therefore, the added *tert*-butyl substitution in $Rh_2(S\text{-}^{tert}PTTL)_4$ relieves the overall

chiral twist of the cavity, while, at the same time, not placing added steric hindrance to the binding at the axial positions. Therefore, if this geometry is also relevant to the solution structures adopted during catalysis, it is likely justifying the observed enhanced enantioinduction relative to its parent, Rh_2(*S*-PTTL)$_4$ catalyst.

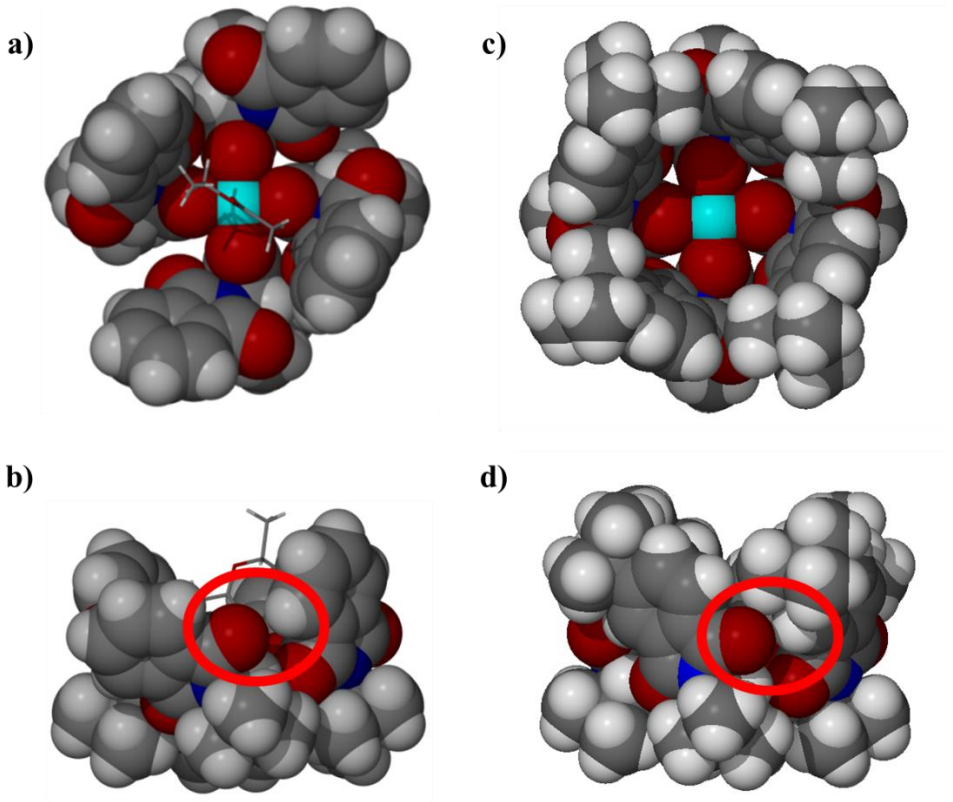

Figure 2.29. Space filling structure comparison between mono(EtOAc) adduct of Rh_2(*S*-PTTL)$_4$ and bis(THF) adduct of Rh_2(*S*-^{tert}PTTL)$_4$ (**12**); a) and c) top views of Rh_2(*S*-PTTL)$_4$ and Rh_2(*S*-^{tert}PTTL)$_4$, respectively, b) and d) side views of Rh_2(*S*-PTTL)$_4$ and Rh_2(*S*-^{tert}PTTL)$_4$, respectively.

The described X-ray structure for Rh_2(*S*-^{tert}PTTL)$_4$ resembles the X-ray crystal structure of Rh_2(*S*-PTAD)$_4$ catalyst displayed in Figure 2.30 to a large extent. Rh_2(*S*-PTAD)$_4$ was observed to form a bis(EtOAc) adduct when crystallized from ethyl acetate/*n*-hexane solvent mixture with a full *α,α,α,α* conformation in solid state. All the four *N*-phthaloyl protecting groups were evenly sitting around the edge of a fairly square cavity affording a C_4-symmetric catalyst molecule (Figure 2.30). The width across the cavity faces was found to be between 14.1-16.0 Å. From the space filling

representation of Rh_2(*S*-PTAD)$_4$, it can be anticipated that the much bulkier adamantyl groups introduced a greater conformational rigidity through only C_α-CO_2 bonds torsion of ligands, while N-C_α bonds torsion are still flexible to move. Therefore, Rh_2(*S*-PTAD)$_4$ has a more rigid chiral cavity if compared to its parent, Rh_2(*S*-PTTL)$_4$, but less rigid if compared to Rh_2(*S*-^{tert}PTTL)$_4$ (**12**). In addition, Rh_2(*S*-PTAD)$_4$ is still retaining the gaps at the corners of the chiral cavity found in Rh_2(*S*-PTTL)$_4$.

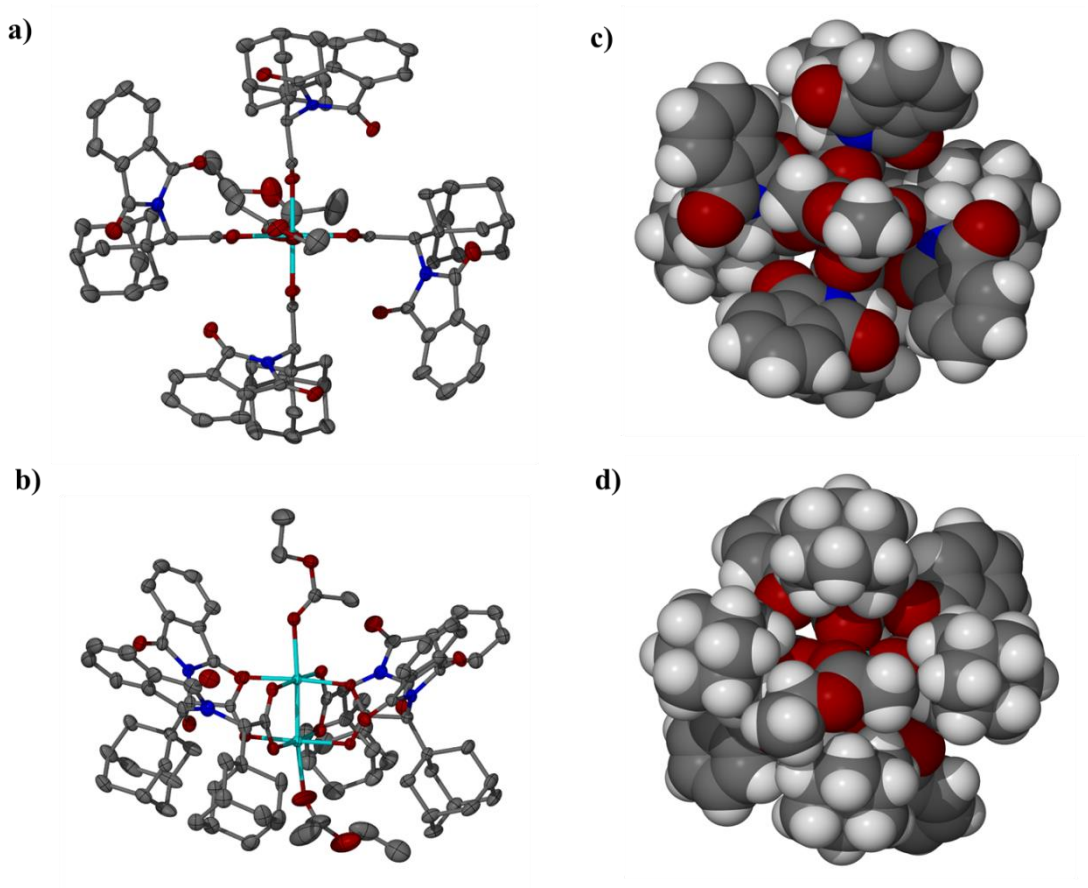

Figure 2.30. Molecular structure of bis(EtOAc) adduct of Rh_2(*S*-PTAD)$_4$; a) viewed into the chiral crown cavity, b) general view (All hydrogen atoms, a second similar molecule and lattice solvent were omitted for clarity). Space filling representation viewed along the Rh-Rh axis c) into the chiral crown cavity, d) onto the axial Rh coordination site shrouded by the adamantyl groups.

Another important thing to note is that, Rh_2(*S*-PTAD)$_4$ crystal structure has an ethyl acetate molecule coordinated to each rhodium centre. This confirms that there is still

enough room for a Lewis basic ligand to coordinate to the "achiral" axial rhodium coordination site (the site shrouded by the adamantyl substituents). This observation provides direct evidence that both Rh atoms can be still accessible by the diazo substrates even after the introduction of the more bulky adamantyl groups. This observation is in complete contradiction with the hypothesis first introduced by Fox[63] and was the foundation for the development of the Rh_2(*S*-PTAD)$_4$ catalyst.[58]

The X-ray crystal structure determination of bis(EtOAc) adduct of Rh_2(*S*-1-Ph-BPTTL)$_4$ was also achieved (**11**, Figure 2.32). The refinement of this structure was relatively problematic due to extensive disorder of the axial EtOAc ligands. The Rh-Rh vector lies on a C_4-symmetry axis and the geometry of the bound EtOAc molecules was breaking this symmetry. The EtOAc from adjacent molecules were also partly overlapping in the same space which was adding to the problem (Figure 2.31).

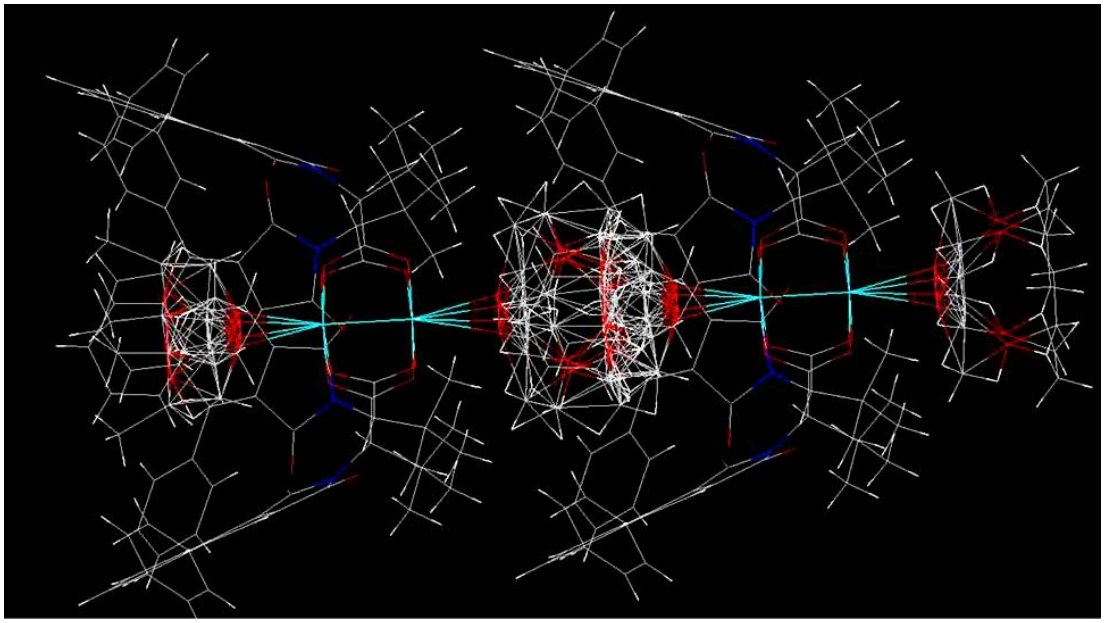

Figure 2.31. Molecular structure of bis(EtOAc) adduct of Rh_2(*S*-1-Ph-BPTTL)$_4$ (**11**) collected on MX1 beamline at the Australian Synchrotron, Victoria. The structure suffers from a severe disorder of the axial EtOAc ligands.

The X-ray crystal structure of Rh_2(*S*-1-Ph-BPTTL)$_4$ (**11**) shows the complex to adopt the *α,α,α,α*-conformation in the solid state with all the four protected *N*-amino acid

ligands being directed towards the same axial coordination of the C_4-symmetric chiral paddlewheel complex (Figure 2.32). The molecule exhibits a perfectly regular cavity with each of the four aryl units comprising the cavity walls having a clockwise twisted arrangement with cavity width across opposite faces of 11.9 Å. While retaining the same clockwise twist, the phenyl substituents are pointing towards the opposite side of the protecting group rings compared to the *tert*-butyl substituents in $Rh_2(S\text{-}^{tert}PTTL)_4$ (**12**). The substituents are ordered with respect to the catalyst's C_4 axis. This again broadens the walls of the cavity relative to its parent $Rh_2(S\text{-}BPTTL)_4$[11] structure creating significantly less gaps at the corners of the cavity and significantly less variation in C_α-CO_2 and N-C_α bond rotations.

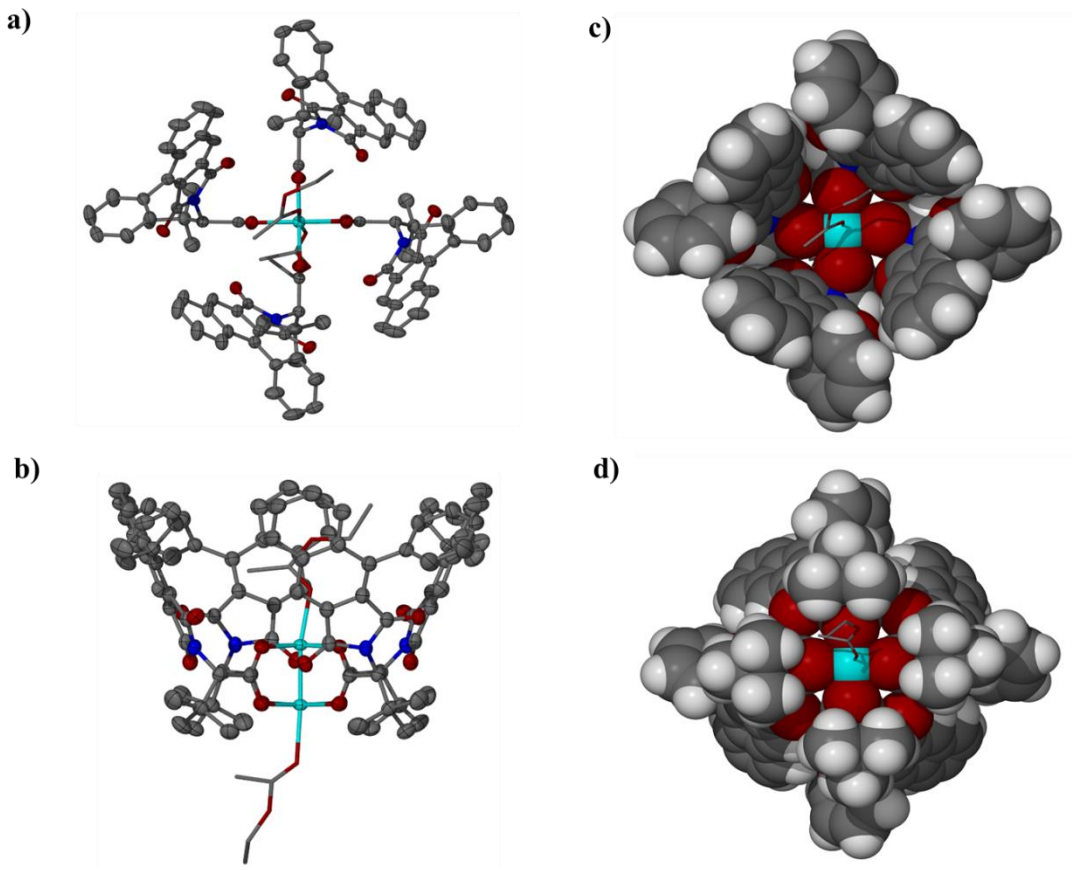

Figure 2.32. Molecular structure of bis(EtOAc) adduct of Rh_2(*S*-1-Ph-BPTTL)$_4$ (**11**); a) viewed into the chiral crown cavity, b) general view (All hydrogen atoms, a second similar molecule and lattice solvent were omitted for clarity). Space filling representation viewed along the Rh-Rh axis c) into the chiral crown cavity, d) onto the axial Rh coordination site shrouded by the *tert*-butyl groups.

The X-ray crystal structures of Rh_2(*S*-BOTL)$_4$ (**14**) and Rh_2(*S*-BHTL)$_4$ (**13**) were obtained. Both structures were revealing crown conformations as described above for Rh_2(*S*-PTTL)$_4$, Rh_2(*S*-PTAD)$_4$, Rh_2(*S*-^{tert}PTTL)$_4$ and Rh_2(*S*-1-Ph-BPTTL)$_4$. The asymmetrical *N*-protecting groups in Rh_2(*S*-BHTL)$_4$ (**13**) are all directed the same with the bulk of the rings pointing into the cavity and the axially bonded prolate shaped ACN ligand is entirely shrouded by the cavity walls (Figure 2.33). This of course did not reduce the overall higher order chirality of the complex as each ligand is similarly disposed and the ligand extremities contribute to the overall C_4-symmetry of the chiral cavity. The top of the cavity is actually looking typically "square" and it is very congested for binding of substrates during catalysis, which is apparent in the space filling picture of the complex (Figure 2.33a and b). In order for this complex to

be a functional catalyst, it is anticipated that some of the *N*-protecting groups need to rotate to give enough room for binding of larger substrates (Figure 2.24). Otherwise, the crown cavity will remain too crowded for the substrate to bind and give the chance to the other "achiral" Rh centre to play a greater role. If the latter is the case, this can justify the observed relatively low enantioselectivity of **13**.

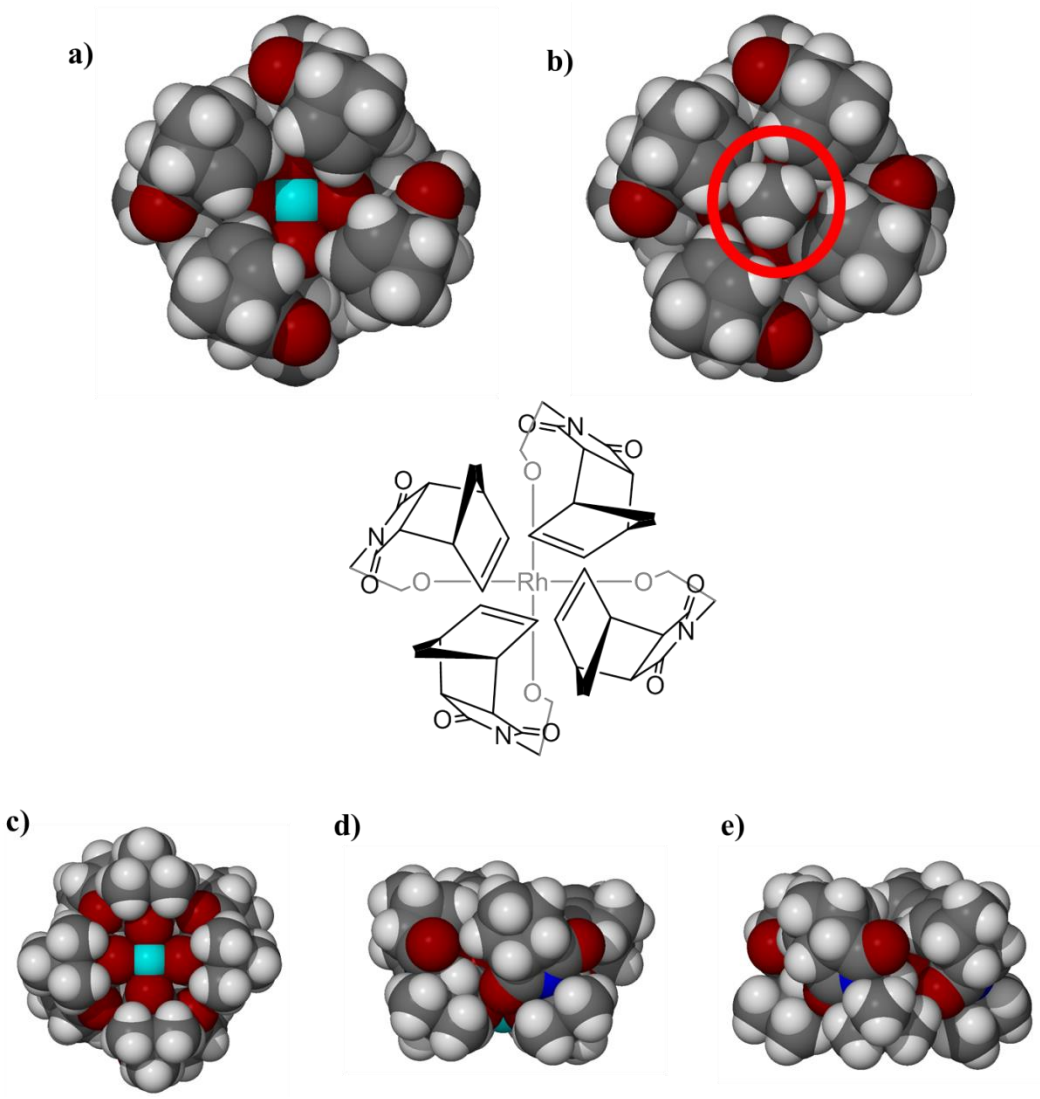

Figure 2.33. Molecular structure of bis(ACN) adduct of Rh_2(*S*-BHTL)$_4$ (**13**). Space filling representation; a) top view, b) prolate shaped ACN axial ligand entirely shrouded by cavity walls, c) bottom view, d) and e) side views.

The pale green needles from a Rh_2(*S*-BOTL)$_4$ (**14**) sample revealed an *α*,*α*,*α*,*α* crown conformer with one ligand that is orientated differently to normally seen in other

α,α,α,α analogues while all four amino acid derived ligands still maintains their (*S*)-stereogenic carbon centres (Figure 2.34). The examination of several crystals indicated the same morphology with the same cell. This is in contrast to the clockwise twist observed for Rh_2(*S*-BHTL)$_4$ (**13**) discussed above. For Rh_2(*S*-BOTL)$_4$ (**14**) crystallised from MeOH, the positioning of the non-Rh bound MeOH lattice molecule which hydrogen bonds to the MeOH bounded to the Rh in the chiral cavity is influential. The catalyst was forced to unusually shift one of the *S*-BOTL ligands to create room for the H-bonded MeOH molecule (Figure 2.34a, b). Another important thing to highlight is that the extremities of the *N*-protecting group don't face towards the top of the cavity but outwards which is opposite to the related complex **13** described above.

The observations related to complexes **13** and **14** are very important as it gives strong indication that these two complexes lack the conformational rigidity through both C_α-CO_2 and N-C_α bond torsions of the ligands. It can be speculated that the flexibility of ligands in both Rh_2(*S*-BHTL)$_4$ (**13**) and Rh_2(*S*-BOTL)$_4$ (**14**) might have led to irregular cavities similar to the one observed for **14** when the substrates binds on. This, in turn, could have resulted in different selectivities and led to the relatively low enantioselectivities observed with these complexes.

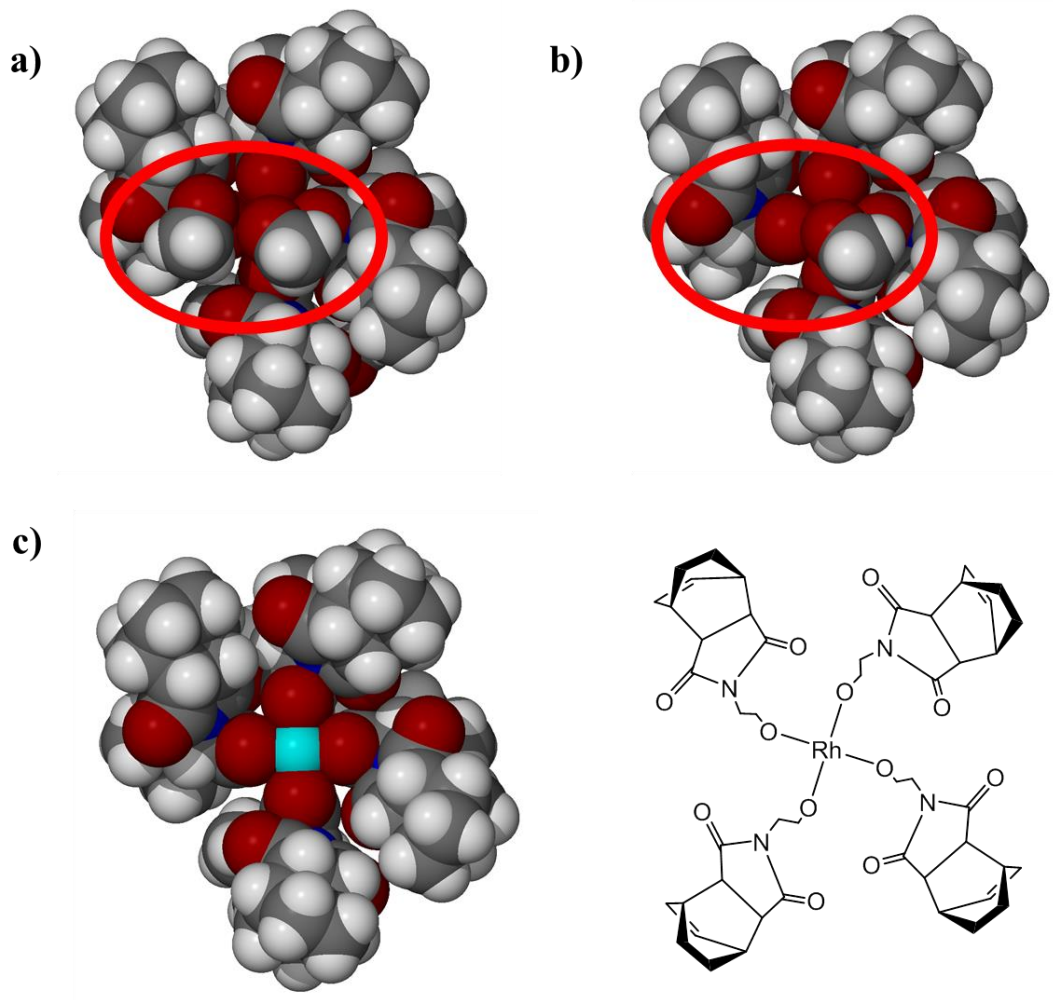

Figure 2.34. Molecular Structure of bis(MeOH) adduct of Rh_2(*S*-BOTL)$_4$ (**14**). Space filling structure representation; a), b) and c) three pictures of the complex in various states of "undressing" the MeOH ligands around the cavity.

2.3.3. Screening in enantioselective synthesis of trifluoromethyl-substituted cyclopropanes

The scope of the new catalysts was further investigated by looking into cyclopropanations involving *donor-acceptor* carbenoid intermediates containing -CF_3 as an electron withdrawing group using the reported optimized reaction conditions.[96] Fluoro functionality has the means to significantly impact on the chemical, physical and biological properties of organic compounds.[97-100] It is generally used to adjust the pharmacokinetic, electronic,[101,102] steric,[103] and lipophilic[104] attributes of different pharmaceutical agents.

Generally in all the cases, the screening results for the cyclopropanation of styrene with 1-phenyl-2,2,2-trifluromethyldiazoethane **25** generated the product **26** in high yield and high levels of diastereoselectivity (>20:1 *E*:*Z* dr).

In regard to enantioselectivity, the results manifested a similar enhancement in enantioselectivity. With Rh_2(*S*-^{tert}PTTL)$_4$ (**12**) as a catalyst, the product was generated in 88% *ee* (Table 2.9, entry 5), while, changing the reaction solvent to 2,2-DMB did not impact on its enantioselectivity (Table 2.9, entries 5 and 6). The observed Rh_2(*S*-^{tert}PTTL)$_4$ enantioselectivity was analogous to the observed selectivity when Rh_2(*S*-PTAD)$_4$ was applied in the same reaction under the same reaction conditions (Table 2.9, entries 5 *vs.* 1). Whereas, with the Rh_2(*S*-PTTL)$_4$-, Rh_2(*S*-NTTL)$_4$ and Rh_2(*S*-1,2-NTTL)$_4$ (**3a**)-catalyzed reactions the cyclopropane product **26** was generated in lower enantioselectivity of 82%, 79% and 82% *ee*, respectively (Table 2.9, entries 2, 3 and 7). Rh_2(*S*-1-Ph-BPTTL)$_4$ (**11**) was unsuited with this reaction generating the cyclopropane in 42% *ee* (Table 2.9, entry 8). The relative and absolute stereochemistry of the product was again unambiguously assigned through X-ray crystallography to be (1*S*, 2*R*) (Figure 2.35).

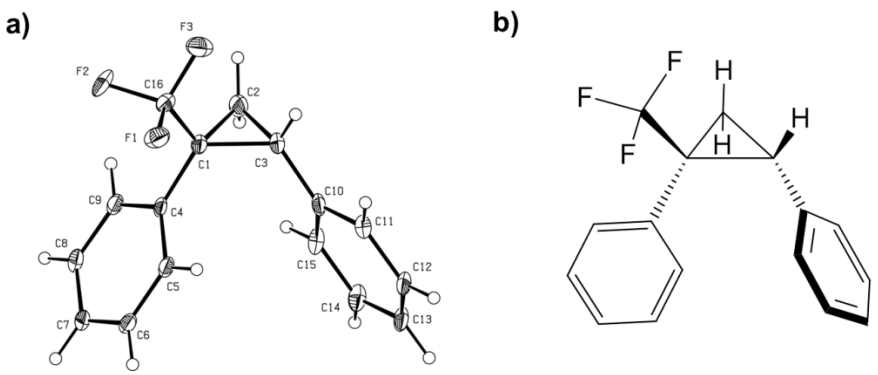

Figure 2.35. ORTEP for (1*S*, 2*R*)-1-trifluoromethyl-1,2-diphenylcyclopropane product.

Table 2.9. Asymmetric cyclopropanation of styrene with 1-phenyl-2,2,2-trifluromethyldiazoethane (*donor-acceptor* substrate).

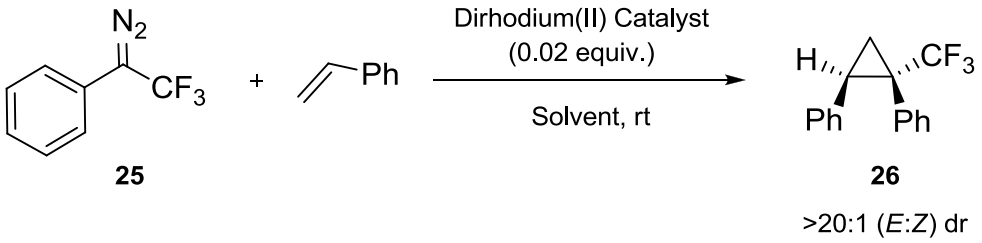

Entry	Catalyst	Catalyst code	Solvent	Yield (%)	*ee* (%)
1	Rh_2(*S*-PTAD)$_4$	-	TFT	95	88
2	Rh_2(*S*-PTTL)$_4$	-	TFT	96	82
3	Rh_2(*S*-NTTL)$_4$	-	TFT	95	79
4	Rh_2(*S*-4-Br-NTTL)$_4$	-	TFT	83	78
5	Rh_2(*S*-^{tert}PTTL)$_4$	**12**	TFT	99	88
6	Rh_2(*S*-^{tert}PTTL)$_4$	**12**	2,2-DMB	97	88
7	Rh_2(*S*-1,2-NTTL)$_4$	**3a**	TFT	85	82
8	Rh_2(*S*-1-Ph-BPTTL)$_4$	**11**	TFT	69	42

Diastereomeric ratios (dr) were determined by ^{1}H NMR of the crude mixture. Enantiomeric excess percentages (*ee*%) were determined by chiral HPLC using Chiralcel® OJ column, 1% 2-propanol in *n*-hexane (*v/v*%), 0.8 mL/min, 220 nm, τ_1 = 5.5 min, τ_2 = 6.8 min. See experimental section for more details.

2.3.4. Screening in enantioselective synthesis of carboxylate-substituted cyclopropanes

2.3.4.1. Using methyl *α*-diazo-*p*-methoxyphenyldiazoacetate and styrene

The next series of experiments were carried out on diazoacetates as another example of *donor-acceptor* diazo substrates. Initially, the evaluation of the new catalysts was carried out in the cyclopropanation reaction of styrene with methyl *p*-methoxyphenyldiazoacetate **27** for the generation of methyl 1,2-

diphenylcyclopropanecarboxylate **28** and results are summarized in Table 2.10. All catalysts afforded the cyclopropane product **28** in excellent diastereoselectivity (>18:1 *E*:*Z* dr).

Considering enantioselectivity, generally, the results revealed that, Rh_2(*S*-^{tert}PTTL)$_4$ (**12**) is behaving better than Rh_2(*S*-PTAD)$_4$ in the same reaction at catalyst loading of 0.01 equivalents, while behaving in the same manner of Rh_2(*S*-PTTL)$_4$ (Table 2.10, entries 7 *vs.* 1 and 2). On the contrary, Rh_2(*S*-1-Ph-BPTTL)$_4$ (**11**) and Rh_2(*S*-NTTL)$_4$ were totally incompatible with this class of substrate at which their enantioselectivities were quite poor (10% and 42% *ee*, respectively). Increasing the Rh_2(*S*-^{tert}PTTL)$_4$ catalyst loading from 0.01 to 0.05 equivalents has minimal effect on both yield and enantioselectivity (Table 2.10, entries 7 *vs.* 8). Furthermore, changing the reaction solvent to 2,2-DMB slightly enhanced the enantioselectivity of Rh_2(*S*-^{tert}PTTL)$_4$ to 78% *ee* (Table 2.10, entries 7 *vs.* 9).

Table 2.10. Asymmetric cyclopropanation of styrene with *p*-methoxyphenyldiazoacetate (*donor-acceptor* substrate).

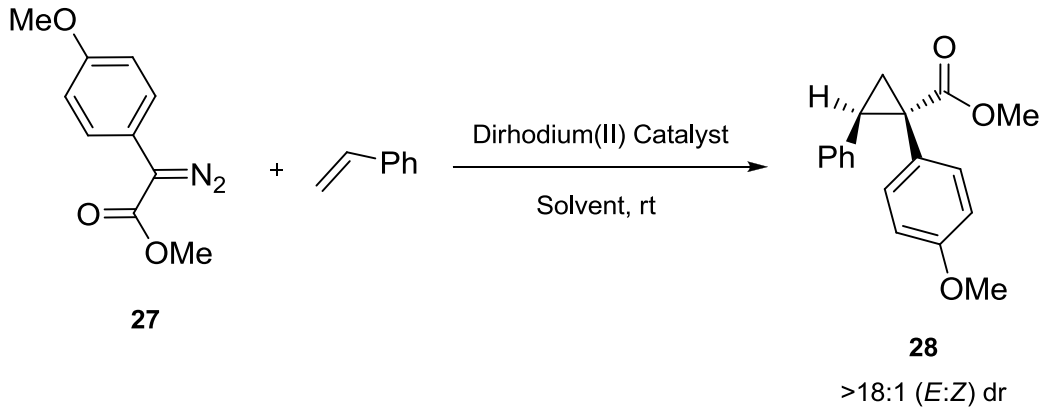

Entry	Catalyst	Catalyst Code	Solvent	Catalyst loading (equiv.)	Yield (%)	*ee* (%)
1	Rh_2(*S*-PTAD)$_4$	-	Pentane	0.01	96	73
2	Rh_2(*S*-PTTL)$_4$	-	Pentane	0.01	84	78
3	Rh_2(*S*-NTTL)$_4$	-	Pentane	0.01	83	42
4	Rh_2(*S*-1,2-NTTL)$_4$	**3a**	Pentane	0.01	84	70
5	Rh_2(*S*-1-Ph-BPTTL)$_4$	**11**	Pentane	0.01	80	8

6	Rh_2(*S*-1-Ph-BPTTL)$_4$	**11**	2,2-DMB	0.01	83	10
7	Rh_2(*S*-^{tert}PTTL)$_4$	**12**	Pentane	0.01	80	76
8	Rh_2(*S*-^{tert}PTTL)$_4$	**12**	Pentane	0.05	83	76
9	Rh_2(*S*-^{tert}PTTL)$_4$	**12**	2,2-DMB	0.01	85	78

Diastereomeric ratios (dr) were determined by ^{1}H NMR of the crude mixture. Enantiomeric excess percentages (*ee*%) were determined by chiral HPLC using Chiralcel® OD-H column, 0.7% 2-propanol in *n*-hexane (*v/v*%), 1 mL/min, 220 nm, τ_1 = 13 min, τ_2 = 23 min. See experimental section for more details.

2.3.4.2. Using methyl *α*-diazo-2-phenylacetate and styrene

The screening was further extended to the removal of the *p*-methoxy group from the *donor* aryl group of the diazoacetate. The cyclopropanation reaction of styrene with methyl *α*-diazo-2-phenylacetate (**29**) was employed with catalyst loading of 0.01 equivalents. As illustrated in Table 2.11, all catalysts afforded the cyclopropane product **30** in excellent to good yields (89-65%) and high diastereoselectivity (>18:1 *E*:*Z* dr). However, the asymmetric induction deteriorated dramatically with the removal of the *p*-methoxy group. The enantiomeric induction of the catalysts did not exceed 46% *ee* which was exhibited by Rh_2(*S*-^{tert}PTTL)$_4$ (**12**) (Table 2.11, entry 5). Also, varying the group at the *α*-carbon of the ligands did not result in any selectivity enhancement.

A very important observation to annotate is, although Rh_2(*S*-1-Ph-BPTTL)$_4$ (**11**) is derived from protected L-*tert*-leucine, like the rest of complexes screened, it resulted in the formation of the corresponding cyclopropane product **30** in 30% *ee* but with an opposite absolute configuration (Table 2.11, entry 4). This is likely due to the opposite alignment of the phenyl substituents on the *N*-protecting group rings.

Table 2.11. Asymmetric cyclopropanation with phenyldiazoacetate (*donor-acceptor* substrate).

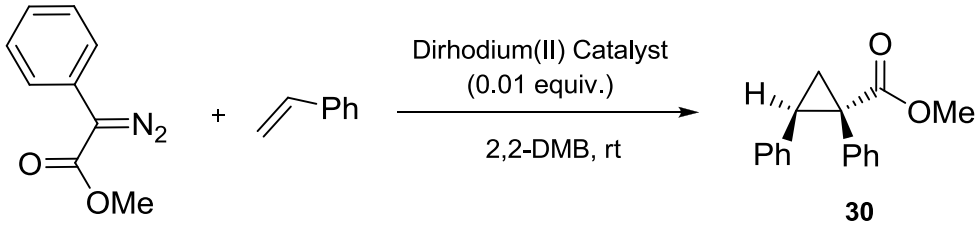

29 **30**

>18:1 (*E*:*Z*) dr

Entry	Catalyst	Catalyst code	Yield (%)	*ee* (%)
1	Rh_2(*S*-PTAD)$_4$[105]	-	87	21[a]
2	Rh_2(*S*-PTTL)$_4$	-	87	20
3	Rh_2(*S*-NTTL)$_4$	-	88	8
4	Rh_2(*S*-1-Ph-BPTTL)$_4$	**11**	90	30[b]
5	Rh_2(*S*-^{tert}PTTL)$_4$	**12**	87	46
6	Rh_2(*S*-1,2-NTTL)$_4$	**3a**	89	30
7	Rh_2(*S*-1,2-NTPA)$_4$	**3b**	86	18
8	Rh_2(*S*-1,2-NTLU)$_4$	**3c**	86	14
9	Rh_2(*S*-1,2-NTTR)$_4$	**3d**	63	20
10	Rh_2(*S*-1,2-NTTY)$_4$	**3e**	65	16
11	Rh_2(*S*-BOTL)$_4$	**14**	66	38
12	Rh_2(*S*-BHTL)$_4$	**13**	58	17

[a]In toluene as reaction solvent, [b]The opposite enantiomer is observed. Diastereomeric ratios (dr) were determined by ^{1}H NMR of the crude mixture. Enantiomeric excess percentages (*ee*%) were determined by chiral HPLC using Chiralcel® OJ column, 0.5% 2-propanol in *n*-hexane (*v*/*v*%), 1 mL/min, 220 nm, τ_1 = 14 min, τ_2 = 20 min. See experimental section for more details.

The effect of changing the reaction solvent and temperature was investigated using Rh_2(*S*-1,2-NTTL)$_4$ catalyst (**3a**) as a strive to enhance the levels of enantioselectivity (Table 2.12). The variation of temperature had a little influence on the enantioselectivity of Rh_2(*S*-1,2-NTTL)$_4$ (**3a**) over a reaction temperature range from 23 to -20 ^{o}C (Table 2.12, entries 1 and 2). While, a slight decrease in enantioselectivity was observed when using DCM as a reaction solvent (Table 2.12, entry 4), a dramatic decrease was observed when using toluene or pentane instead of 2,2-DMB (Table 2.12, entries 3 and 5).

Table 2.12. Effect of solvent and temperature on the stereoselectivity of Rh_2(*S*-1,2-NTTL)$_4$ (**3a**) with phenyldiazoacetate substrate.

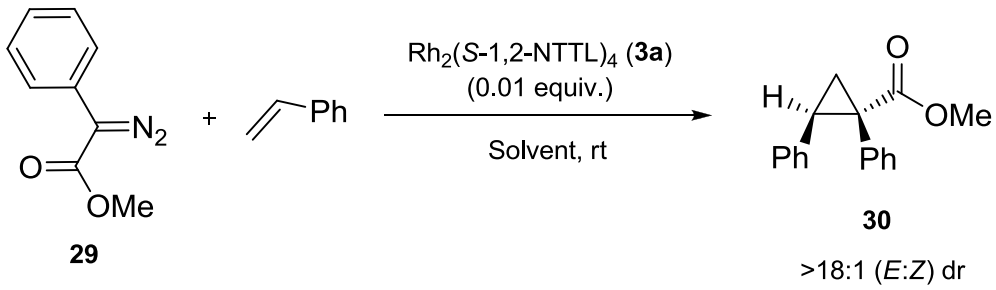

Entry	Solvent	Temperature (^{o}C)	Yield (%)	*ee* (%)
1	2,2-DMB	23	89	30
2	2,2-DMB	-20	82	28
3	Toluene	23	88	2[a]
4	CH_2Cl_2	23	90	26
5	Pentane	23	87	18

[a]The opposite enantiomer was observed. Diastereomeric ratios (dr) were determined by ^{1}H NMR of the crude mixture. Enantiomeric excess percentages (*ee*%) were determined by chiral HPLC using Chiralcel® OJ column, 0.5% 2-propanol in *n*-hexane (*v*/*v*%), 1 mL/min, 220 nm, τ_1 = 14 min, τ_2 = 20 min. See experimental section for more details.

2.3.4.3. Using (*E*)-methyl *α*-diazo-4-phenylbut-3-enoate and styrene

The final series of experiments were carried out with (*E*)-methyl *α*-diazo-4-phenylbut-3-enoate **31** (Table 2.13). In all cases, excellent levels of diastereoselectivity were observed for the obtained product **32**. But, the enantiomeric induction did not exceed 44% *ee* when using $Rh_2(S\text{-}^{tert}PTTL)_4$ (**12**) as a catalyst (Table 2.13, entry 4). Again, varying the group at the *α*-carbon of the ligands did not result in any selectivity enhancement.

A similar behaviour to the one discussed previously was witnessed one more time. $Rh_2(S\text{-1-Ph-BPTTL})_4$ (**11**) resulted in the formation of the cyclopropane product **32** in 19% *ee*, but with the opposite absolute configuration (Table 2.13, entry 3).

Table 2.13. Asymmetric cyclopropanation with styryldiazoacetate (*donor-acceptor* substrate).

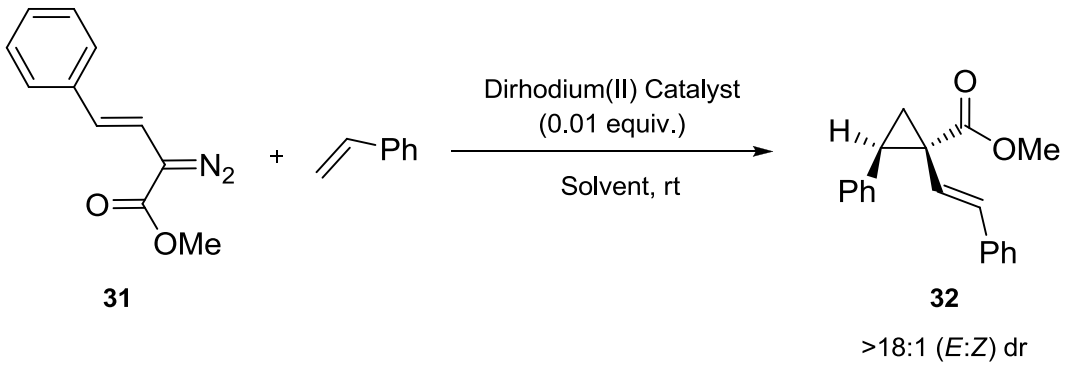

Entry	Catalyst	Catalyst code	Solvent	Yield (%)	*ee* (%)
1	Rh_2(*S*-PTTL)$_4$	-	CH_2Cl_2	83	40
2	Rh_2(*S*-NTTL)$_4$	-	CH_2Cl_2	82	16
3	Rh_2(*S*-1-Ph-BPTTL)$_4$	**11**	2,2-DMB	86	19[a]
4	Rh_2(*S*-^{tert}PTTL)$_4$	**12**	2,2-DMB	86	44
5	Rh_2(*S*-1,2-NTTL)$_4$	**3a**	CH_2Cl_2	88	10
6	Rh_2(*S*-1,2-NTTL)$_4$	**3a**	Pentane	87	10

7	Rh_2(*S*-1,2-NTPA)$_4$	**3b**	CH_2Cl_2	82	18
8	Rh_2(*S*-1,2-NTLU)$_4$	**3c**	CH_2Cl_2	89	23
9	Rh_2(*S*-1,2-NTTR)$_4$	**3d**	CH_2Cl_2	65	20
10	Rh_2(*S*-1,2-NTTY)$_4$	**3e**	CH_2Cl_2	67	20
11	Rh_2(*S*-BOTL)$_4$	**14**	Pentane	69	4
12	Rh_2(*S*-BHTL)$_4$	**13**	2,2-DMB	77	2

[a]The opposite enantiomer was observed. Diastereomeric ratios (dr) were determined by ^{1}H NMR of the crude mixture. Enantiomeric excess percentages (*ee*%) were determined by chiral HPLC using Chiralcel® OJ column, 1.5% 2-propanol in *n*-hexane (*v/v*%), 1 mL/min, 254 nm, τ_1 = 15 min, τ_2 = 21 min. See experimental section for more details.

2.3.5. Screening in enantioselective synthesis of nitrile-substituted cyclopropanes

The scope of the new catalysts was furthermore investigated by examining cyclopropanation reactions involving *donor-acceptor* carbenoid intermediates containing -CN as an electron withdrawing group using the reported optimized reaction conditions.[106] The screening results are illustrated in Table 2.14.

For all the reactions, the cyclopropane product **34** was generated in high yields. In terms of diastereoselectivity, while Rh_2(*S*-PTTL)$_4$ and Rh_2(*S*-^{tert}PTTL)$_4$ (**12**) offered an acceptable diastereoselectivity of >20:1 (*E*:*Z*) dr (Table 2.14, entries 3 and 8), Rh_2(*S*-PTAD)$_4$ was the best among the screened complexes giving a diastereomeric ratio of 64:1 (*E*:*Z*) (Table 2.14, entry 2). The diastereoselectivity of the cyclopropane product generated by Rh_2(*S*-1,2-NTTL)$_4$ (**3a**) did not exceed 11:1 (*E*:*Z*) dr. The variable diastereoselectivity observed with this system was previously returned to the small size of the nitrile acceptor group.[106]

With regard to enantioselectivity, Rh_2(*S*-^{tert}PTTL)$_4$ (**12**), Rh_2(*S*-1,2-NTTL)$_4$ (**3a**), Rh_2(*S*-PTTL)$_4$ and Rh_2(*S*-PTAD)$_4$ revealed comparable enantioselectivity for the major diastereomer (80-86% *ee*). Erosion of both diastereo- and enantioselectivity was not observed when Rh_2(*S*-^{tert}PTTL)$_4$ loading was decreased from 0.02 to 0.01 equivalents (Table 2.14, entries 7 *vs.* 8). Also, changing the reaction solvent to 2,2-DMB did not affect the enantioselectivity for the major diastereomer, however, the diastereoselectivity was diminished to 16:1 (*E*:*Z*) dr (Table 2.14, entries 7 *vs.* 9).

Regardless of its relatively low diastereoselectivity, Rh_2(*S*-NTTL)$_4$ was the best catalyst in terms of enantioselectivity for this catalytic system. The catalyst offered cyclopropane products in 91% and 92% *ee* for the major and the minor diastereomers, respectively (Table 2.14, entry 4). On the other hand, Rh_2(*S*-1-Ph-BPTTL)$_4$ (**11**) was completely incompatible with this catalytic system at which the cyclopropane product **34** was generated in 7:1 (*E*:*Z*) dr and with 30% enantioselectivity for the major diastereomer (Table 2.14, entry 6).

Table 2.14. Asymmetric cyclopropanation of styrene with α-diazo-2-phenylacetonitrile.

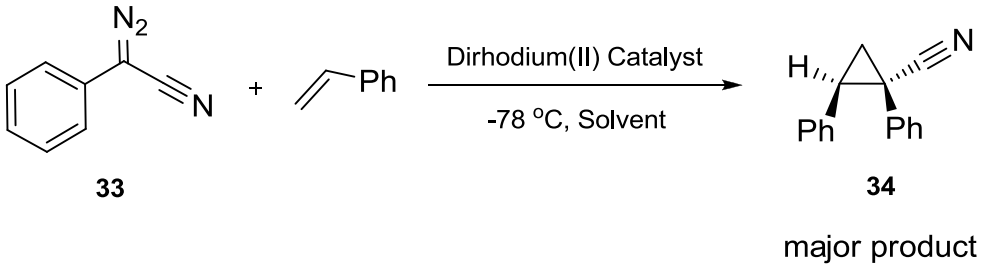

Entry	Catalyst	Catalyst code	Catalyst loading (equiv.)	Solvent	Yield (%)[a]	dr (*E*:*Z*)	*ee* (%)	
							Major diastereomer	Minor diastereomer
1	$Rh_2(OAc)_4$	-	0.02	Toluene	82	4:1[b]	-	-
2	Rh_2(*S*-PTAD)$_4$	-	0.02	Toluene	85	64:1	80	74
3	Rh_2(*S*-PTTL)$_4$	-	0.02	Toluene	84	27:1	86	78
4	Rh_2(*S*-NTTL)$_4$	-	0.02	Toluene	84	13:1	91	92
5	Rh_2(*S*-1,2-NTTL)$_4$	**3a**	0.02	Toluene	80	11:1	83	76

6	Rh_2(*S*-1-Ph-BPTTL)$_4$	**11**	0.02	Toluene	84	7:1	30	78
7	Rh_2(*S*-^{tert}PTTL)$_4$	**12**	0.02	Toluene	83	25:1	82	84
8	Rh_2(*S*-^{tert}PTTL)$_4$	**12**	0.01	Toluene	81	26:1	82	86
9	Rh_2(*S*-^{tert}PTTL)$_4$	**12**	0.02	2,2-DMB	83	16:1	82	82

[a]Yield for both diastereomers, [b]Carried out at room temperature. Diastereomeric ratios (dr) were determined by ^{1}H NMR of the crude mixture. Enantiomeric excess percentages (*ee*%) were determined by chiral HPLC using Chiralcel® OD column, 0.8% 2-propanol in *n*-hexane (*v/v*%), 1 mL/min, 220 nm, τ_1 = 19 min, τ_2 = 29 min. See experimental section for more details.

2.3.6. Screening in enantioselective synthesis of sulfonate-substituted cyclopropanes

As an extension to the illustrated screening, investigation on the suitability of the new catalysts in the asymmetric synthesis of sulfonate-substituted cyclopropanes was very attractive. In addition to the importance of the sulfonyl-derived functional groups which features in a myriad of applications,[107-115] high levels of enantioselectivity were expected for this class of substrates comparable to the ones obtained for cyclopropylphosphonate derivatives examined earlier in this thesis. This expectation was based on the fact that the sulfonate *acceptor* group has a big size (having a tetrahedral geometry).

Although my primary interest, the preparation of **37** as a suitable starting point for the proposed investigation was unsuccessful. Attempts for the direct preparation of the desired methyl α-diazobenzylsulfonate **37** from methyl benzylsulfonate **35** were carried out by treating **35** with *p*-ABSA and DBU. However, all the attempts returned the decomposition of the starting material with no formation of the desired product (Scheme 2.10).

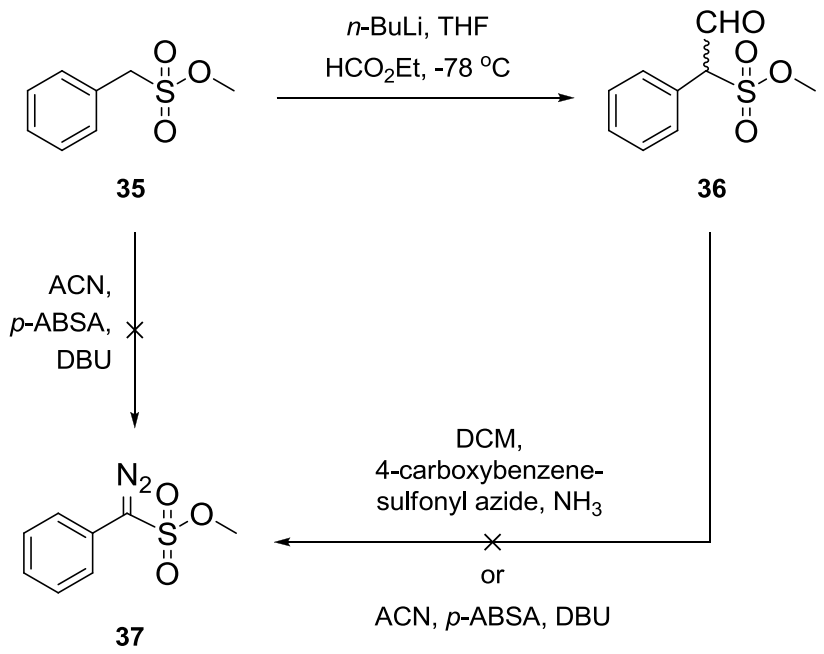

Scheme 2.10. Attempts for the preparation of methyl α-diazobenzylsulfonate.

The procedure reported by Berkessel and Voges[116] for the preparation of similar derivatives was also applied at which methyl α-diazobenzylsulfonate (**35**) was first converted into methyl 1-formylbenzylsulfonate **36** through the deprotonation of **35** with *n*-butyllithium at -78 ^{o}C and subsequent reaction with ethyl formate. Again, attempts to apply the diazo transfer reaction, in which the formylated sulfonate **36** was treated with either *p*-ABSA or *p*-carboxybenzenesulfonyl azide in the presence of a base, failed to generate the desired methyl α-diazobenzylsulfonate product.

2.4. PRELIMINARY RESULTS FOR A SECOND GENERATION CATALYST WITH LIGANDS CARRYING LOWER SYMMETRY *N*-PROTECTING GROUPS WITH BULKIER SUBSTITUENTS

2.4.1. Endeavours for the preparation of *N*-(4-adamantylphthaloyl)-(*S*)-*tert*-leucine

As it was previously emphasized on the correlation between increasing the steric bulk of the substituents and the enhancement in enantioselectivity for a particular reaction, it was concluded that a reasonable way for further development of Rh_2(*S*-^{tert}PTTL)$_4$ catalyst (**12**) is through having a bulkier substituent on the *N*-protecting group. With the fact that an adamantyl moiety would impart a greater steric bulk than the original *tert*-butyl group, 4-(1-adamantyl)phthalic anhydride was assumed to be the *N*-protecting group of choice for the forthcoming research (Figure 2.36).

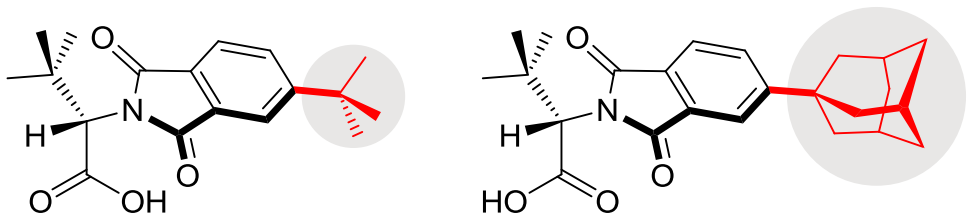

Figure 2.36. Structures of ligands containing *tert*-butyl and adamantyl substituents.

Direct introduction of the adamantyl moiety to phthalic anhydride through Friedel-Crafts alkylation using $AlCl_3$ in refluxing CS_2 overnight returned the starting materials with no conversion into product. Subsequently, a different strategy was proposed which involves the connection of the adamantyl moiety to *o*-xylene

followed by the transformation of the two methyl groups of the resulting *o*-xylene derivative into two carboxylic acid groups.

4-(1-Adamantyl)-*o*-xylene (**38**) was prepared in multigram scale through Friedel-Crafts alkylation of *o*-xylene with 1-bromo-adamantane in the presence of $ZnCl_2$ as a Lewis acid (Scheme 2.11). The second step which involves the oxidation of 4-(1-adamantyl)-*o*-xylene (**38**) was attained through the reported procedure of Betnev *et al.*[117] using molecular oxygen, $Co(OAc)_2$ and acetaldehyde as a promoter. Although, the authors reported 86% conversion into diacid **39**, However, NMR and MS analysis indicated that only one methyl group was oxidized under the reaction conditions giving 4-(1-adamantyl)-2-methylbenzoic acid **40** in 17% yield instead of the desired 4-(1-adamantyl)phthalic acid **39** (Scheme 2.11).

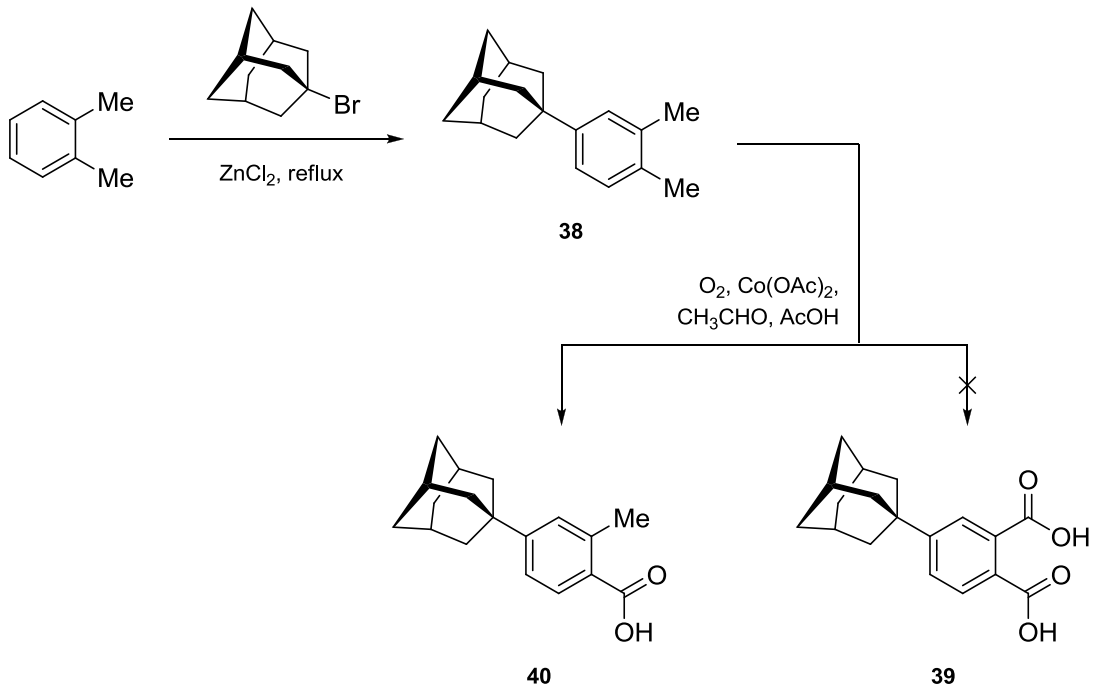

Scheme 2.11. Endeavours for the synthesis of 4-(1-adamantyl)phthalic acid **39**.

This was further confirmed after the treatment of obtained product with acetic anhydride followed by direct reaction with L-*tert*-leucine in refluxing toluene/TEA (Scheme 2.12). In addition to adamantyl, phenyl and methyl protons signals, ^{1}H NMR of the reaction product revealed two doublets at 7.92 and 4.06 ppm having the same coupling constant (*J*) of 8.9 Hz and integrating one proton each. This ^{1}H NMR

signal pattern indicated the formation of **41** as the reaction major product (Scheme 2.12).

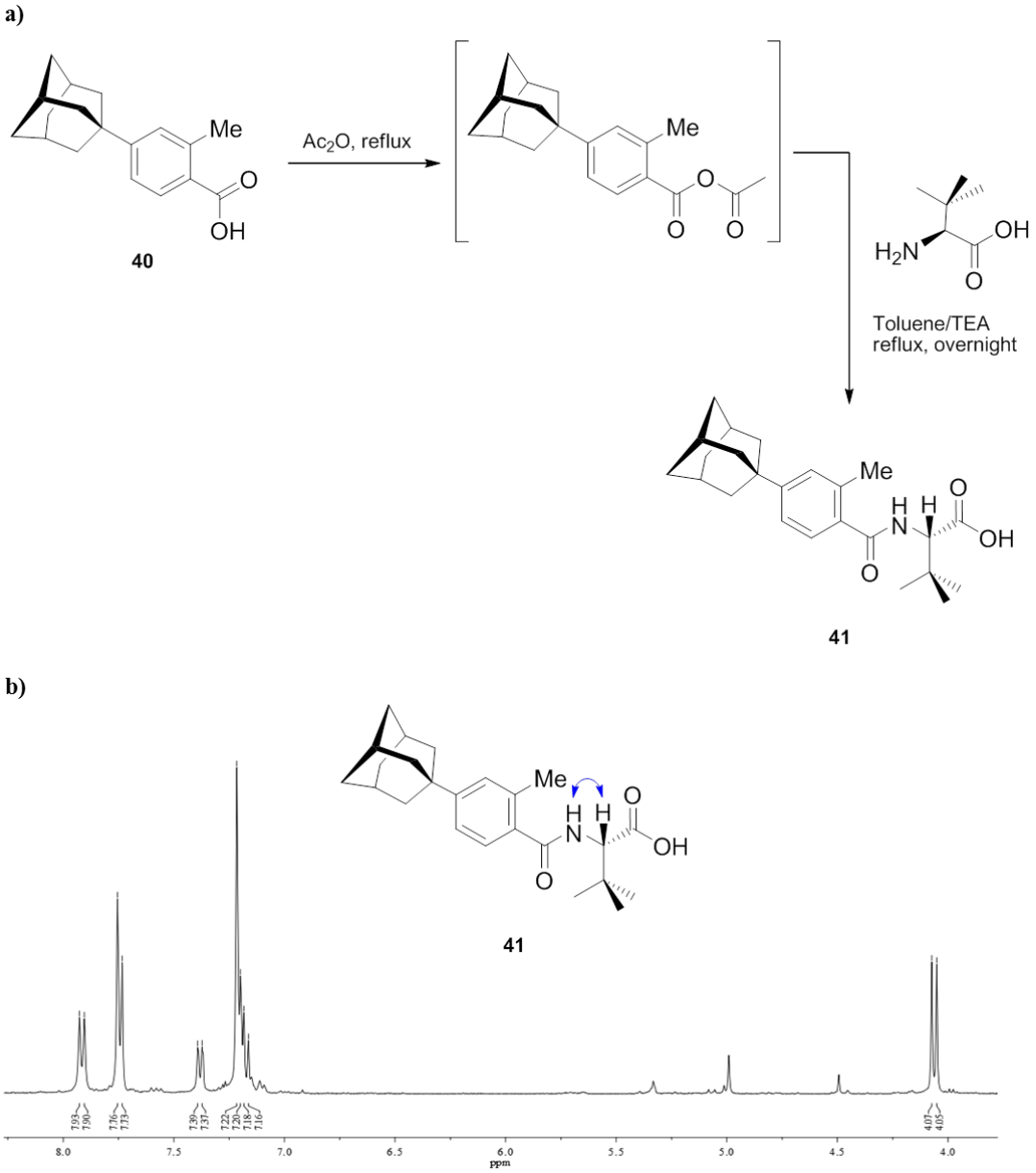

Scheme 2.12. a) Reaction of **40** with L-*tert*-leucine and b) ^{1}H NMR of reaction product **41**.

Applying a modified method of Balakin *et al.*[118] in which **38** was exposed to liquid-phase oxidation with molecular oxygen in the presence of transition metal ions and NaBr as a promoting additive. However, the reaction proceeded smoothly to give **40** in 76% yield with no formation of the desired product **39**. Standard alkaline $KMnO_4$

oxidations were also explored and yet, complete failure was achieved as decomposition of the starting material was observed with no formation of the desired product. I was not able to proceed further to the full synthesis of the desired ligand and unfortunately, the work towards the preparation of this catalyst has been ceased at this stage.

2.5. OTHER INVESTIGATED DIRHODIUM(II) COMPLEXES WITH LOWER SYMMETRY LIGANDS

2.5.1. Complexes derived from D-glucuronic acid ligands

In the past few years, impressive data has been obtained using carbohydrates derived ligands in a broad range of asymmetric transformations. Carbohydrates has the ability to offer many advantages; they are cheap and readily available, are highly functionalized, their chemistry is well developed and are naturally enantiomerically pure compounds with multiple stereogenic centres. These enabled a series of chiral ligands derived from carbohydrate entities to be synthesized and screened for higher stereoselectivities.[119-126] The first chiral ligands derived from carbohydrates were reported in the late 70's by Descotes and Sinou.[127] They prepared phosphines **42**, **43** and **44** (Figure 2.37) starting from D-xylose and D-glucose. These ligands were tested in rhodium-catalyzed asymmetric hydrogenation reactions. The results revealed that, by using rhodium/**44** catalytic system, the authors succeeded to obtain 85% *ee* in hydrogenation of α-acetamidocinnamic and α-acetamidoacrylic acids.

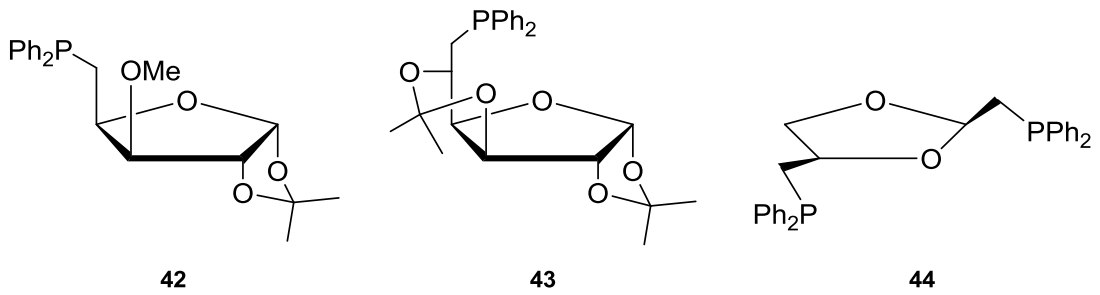

Figure 2.37. First chiral ligands prepared from carbohydrates.[127]

Inspired by the advantages and the success of carbohydrates as ligands for metal-catalyzed asymmetric catalysis, I thought about the usage of a carbohydrate derived ligand in my dirhodium(II) cyclopropanation chemistry. To the best of my knowledge, there are no reports related to the usage of such kind of ligands along with dirhodium(II) complexes so far.

The studies were initiated by the acetylation of commercially available D-glucuronic acid according to the previously described literature procedure[128,129] using acetic anhydride and catalytic amount of iodine as an acetyl transfer reagent to give the 1,2,3,4-tetra-*O*-acetyl protected mixed anhydride **45** (Scheme 2.13). Next, compound **45** was subjected to react with water to afford the corresponding 1,2,3,4-tetra-*O*-acetyl-*β*-D-glucuronic acid **46** in 99% yield (Scheme 2.13).

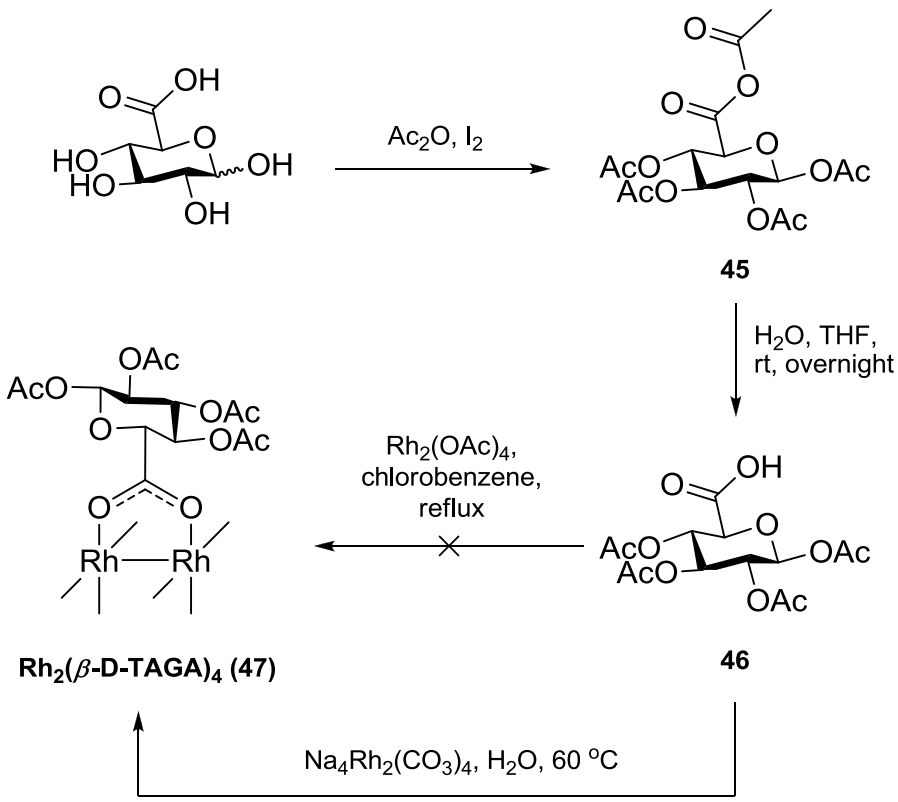

Scheme 2.13. Preparation of Rh_2(*β*-D-TAGA)$_4$ complex (**47**).

Per-*O*-acetylated D-glucuronic acid **46** is particularly useful as a ligand for this part of investigation. It is a C_1-symmetric molecule with five stereogenic centres in enantiomerically pure form, having a COOH group which is required as an anchoring

group for ligand exchange and having five acetyl groups that are expected to prevent side insertion reactions from occurring during metal-carbene transformations, as well as increasing the bulkiness of the ligand.

The common method of ligand exchange using $Rh_2(OAc)_4$ in refluxing chlorobenzene was carried out, however, the reaction suffered from series of complications. The carbohydrate ligand did not sustain at the refluxing temperature of chlorobenzene and it decomposed as the reaction was going on (Scheme 2.13). Changing the reaction solvent to toluene with lower boiling point did not solve the problem. Alternatively, Rh_2(*β*-D-TAGA)$_4$ (**47**) was prepared using a modified procedure of Roos[130] at which 1,2,3,4-tetra-*O*-acetyl-*β*-D-glucuronic acid ligand **46** was allowed to react with $Na_4Rh_2(CO_3)_4$ in H_2O at 60 ^oC for 6 h (Scheme 2.13) and the product structure was confirmed on the basis of its MS, IR and NMR spectroscopic data.

Screening Rh_2(*β*-D-TAGA)$_4$ (**47**) in the cyclopropanation of styrene with methyl *α*-diazo-2-phenylacetate and dimethyl *α*-diazobenzylphoshonate was carried out (Table 2.15, entries 1 and 2). Both reactions did not reach completion and afforded the product in 36% and 30% yields, respectively. Although, the products were formed with high levels of diastereoselectivity, the enantioselectivity of Rh_2(*β*-D-TAGA)$_4$ towards these two substrates was not as expected and did not exceed 12% *ee*. TLC analysis for the Rh_2(*β*-D-TAGA)$_4$-catalyzed cyclopropanation of styrene with 1-phenyl-2,2,2-triflurodiazoethane reaction indicated the complete consumption of starting diazo material after running for 5 hours. However, the product yield was extremely low for either diastereomeric ratio (dr) or enantiomeric excess (*ee*) determination (Table 2.15, entry 3).

Table 2.15. $Rh_2(\beta\text{-D-TAGA})_4$-catalyzed asymmetric cyclopropanation of styrene.

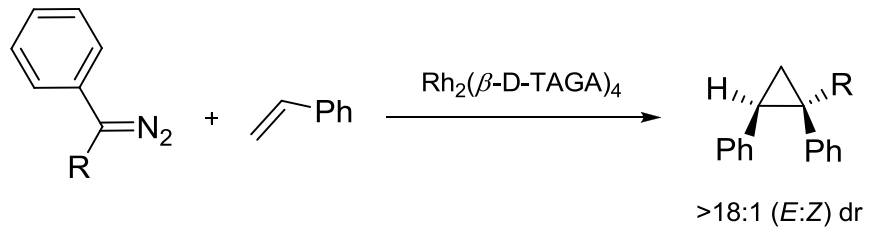

Entry	R	Reaction time (h)	Yield (%)	*ee* (%)
1	CO_2Me	24[a,b]	36	6[e]
2	$PO(OMe)_2$	48[a,b,c]	30	12
3	CF_3	5[d]	<5[f]	ND

[a]Did not reach completion, [b]Carried out in 2,2-DMB, [c]Reflux at 59 °C, [d]Carried out in TFT, [e]The opposite enantiomer was observed, [f]Yield was too low for either dr or *ee* to be determined. Diastereomeric ratios (dr) were determined by ^{1}H NMR of the reaction crude mixture. Enantiomeric excess percentages (*ee*%) were determined by chiral HPLC. See experimental section for more details.

The same situation applies to $Rh_2(\beta\text{-D-TAGA})_4$-catalyzed cyclopropanation of styrene with Meldrum's acid at which the reaction product yield was extremely low for purification and *ee* determination (Scheme 2.14).

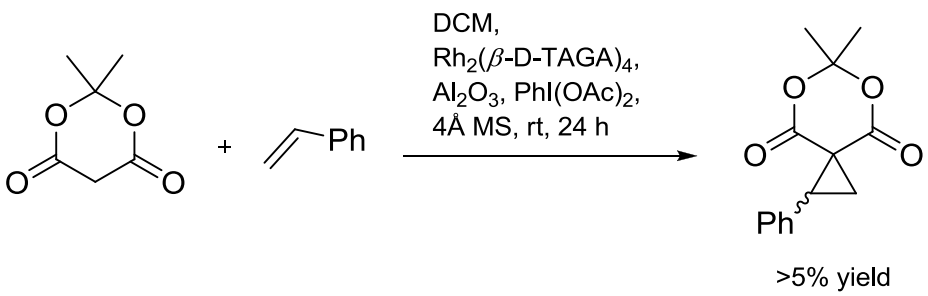

Scheme 2.14. $Rh_2(\beta\text{-D-TAGA})_4$-catalyzed cyclopropanation of styrene with Meldrum's acid.

I have also proceeded towards the preparation of the carbohydrate derivative **49** to be used as a ligand after ester hydrolysis. Again, **49** has six enantiomerically pure

stereogenic centres, it has a CO_2Et group which can act as an anchoring group for ligand exchange after hydrolysis and it has three benzyl ether groups for increasing the bulkiness of the ligand. In addition to that, the structure of **49** contains a cyclopropane ring that connects the anchoring COOH group to the rest of the ligand. Having a cyclopropane ring as part of the ligand's structure can restrict its conformational mobility as in Rh_2(*R*-BTPCP)$_4$ and analogues[68] discussed earlier in Chapter 1, Section 1.5.4.

Per-*O*-benzylated-D-glucal **48** was prepared starting from D-glucal following the procedure of Mikula *et al.*[131] $Rh_2(OAc)_4$-catalyzed cyclopropanation of **48** and ethyl diazoacetate following the procedure of van Boom *et al.*[132] was carried out. However, repeating the reaction several times indicated no formation of the reported compound (Scheme 2.15). Employing Rh_2(*S*-^{tert}PTTL)$_4$ as a catalyst in the same reaction also did not return the desired product.

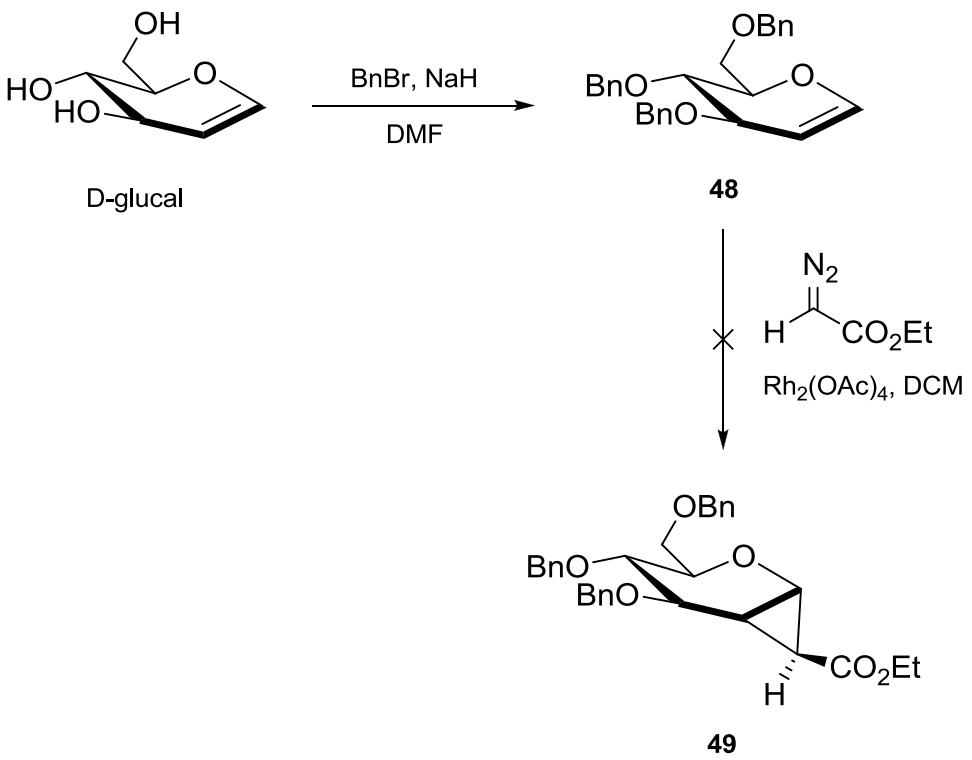

Scheme 2.15. Endeavours for the preparation of **49**.

2.6. CONCLUSION

In conclusion, dirhodium(II) tetrakis[*N*-(1,2-naphthaloyl)-(*S*)-*tert*-leucine] (Rh_2(*S*-1,2-NTTL)$_4$, **3a**) was initially introduced as a new member of the chiral dirhodium(II) catalysts family derived from *N*-protected L-amino acid ligands. The efficiency and selectivity of this catalyst has been demonstrated in a variety of diastereo- and enantioselective reactions of *donor-acceptor* and *diacceptor* carbenoids. However, the results did not provide a clear advantage for the "lower symmetry" approach.

The reduction of the symmetry of the *N*-protecting group in another two ways was further investigated; either side of the planar core of the functionality as in the Rh_2(*S*-BOTL)$_4$ (**14**) and Rh_2(*S*-BHTL)$_4$ (**13**) and by partial substitution of the ring as in Rh_2(*S*-^{tert}PTTL)$_4$ (**12**) and Rh_2(*S*-1-Ph-BPTTL)$_4$ (**11**). Among the prepared complexes, Rh_2(*S*-^{tert}PTTL)$_4$ (**12**) proved to be an exceptional catalyst with extraordinary enantioselectivity (up to 99% *ee*). Screening of a number of different *donor-acceptor* diazo substrates revealed that, generally, Rh_2(*S*-^{tert}PTTL)$_4$ (**12**) is a much more enantioselective than Rh_2(*S*-PTTL)$_4$, while being a more synthetically accessible alternative for the well-known Rh_2(*S*-PTAD)$_4$ catalyst with comparable selectivity. In preparation of cyclopropylphosphonate derivatives, Rh_2(*S*-^{tert}PTTL)$_4$ (**12**) proved to offer an extra advantage than Rh_2(*S*-PTAD)$_4$. For **12**, after stirring at room temperature for 5 h, the corresponding cyclopropane products were generated in high yields, diastereoselectivity and enantioselectivity, while results reported for similar reactions catalyzed by Rh_2(*S*-PTAD)$_4$ were under refluxing conditions for 13 h. On the other side, Rh_2(*S*-^{tert}PTTL)$_4$ (**12**) was incompatible with *donor-acceptor* diazoacetate substrates at which their enantioselectivities were sensitive to the substitution on the aromatic *donor* group of the diazo substrate.

X-ray structures for Rh_2(*S*-^{tert}PTTL)$_4$ (**12**), Rh_2(*S*-1-Ph-BPTTL)$_4$ (**11**), Rh_2(*S*-BOTL)$_4$ (**14**) and Rh_2(*S*-BHTL)$_4$ (**13**) were obtained which provided fruitful insights into the chemistry of these complexes. From the solid state structure comparisons, it was obvious that the extra *tert*-butyl group introduced in Rh_2(*S*-^{tert}PTTL)$_4$ (**12**) generated similar structural effects that was generated by increasing the size of the *α*-substituents from *tert*-butyl to adamantyl groups in Rh_2(*S*-PTAD)$_4$. This was further confirmed by the comparable enantioselectivity observed for both Rh_2(*S*-^{tert}PTTL)$_4$ (**12**) and Rh_2(*S*-PTAD)$_4$.

Finally, A liquid chromatographic method for the separation of enantiomers of *N*-(1,2-naphthaloyl)-(*S*)-amino acids on covalently immobilized type polysaccharide-derived CSP was demonstrated. The solvent versatility of Chiralpak® ID and Chiralpak® IB gave access to a direct analysis technique. The analysis method confirmed that employing toluene/TEA reaction solvent is the most suitable conditions for *N*-protection of L-amino acids with minimal racemization among the reported methods. Using such a solvent mixture is capable to provide a reliable access to high quality dirhodium(II) complexes**.**

2.7. EXPERIMENTAL SECTION

Chemicals

All starting materials and reagents were purchased from Sigma-Aldrich, Acros Organics and Tokyo Chemical Industry Co. (TCI) and used without any further purification. All solvents were of HPLC grade and solvents used in dirhodium(II) carbenoid reactions were dried, distilled and degassed immediately prior to use: DCM over calcium hydride, *n*-pentane and toluene over sodium wire and chlorobenzene over potassium hydroxide. Anhydrous 2,2-DMB, TFT and THF were purchased from Sigma-Aldrich and degassed prior to use. All reactions were performed using oven dried glassware and flame dried under vacuum prior to use. TLC was performed using Sigma-Aldrich pre-coated silica gel 60 F254 aluminium support (20 x 20 cm, 0.2 mm layer thickness) and spots were visualized by UV light (254 nm) or by using either 10% $KMNO_4$ solution or phosphomolybdic acid (PMA) stains as visualizing agents. Preparative TLC purifications were performed using Sigma-Aldrich pre-coated silica gel 60 F254 glass support (20 x 20 cm, 0.25 mm layer thickness). Column chromatography was carried out on silica gel 60 (130-270 mesh ASTM, Sigma-Aldrich) using the specified eluent compositions. Rh_2(*S*-PTTL)$_4$,[12] Rh_2(*S*-NTTL)$_4$,[10] Rh_2(*S*-BPTTL)$_4$[13] and Rh_2(*S*-4-Br-NTTL)$_4$[10] catalysts were prepared according the reported procedures. $Rh_2(OAc)_4$ and Rh_2(*S*-PTAD)$_4$ were purchased from Strem Chemicals, while $Na_4Rh_2(CO_3)_4.2.5H_2O$ was prepared according to the procedure reported by Roos.[130]

Instruments

Melting points were measured on Stuart-SMP10 melting point apparatus and are uncorrected. Optical rotations were measured using Perkin-Elmer 341 polarimeter at the sodium D line (589 nm) and reported as $[\alpha]_D^{25}$ in g/100 mL concentration (*c*) in the solvents indicated. IR spectroscopic measurements were carried out on PerkinElmer TravelIR FT-IR spectrometer and reported in units of cm^{-1}. 1D and 2D NMR spectra were recorded on Varian 400-MR and Varian Inova-500 spectrometers at room temperature in the solvents given. Chemical shifts were expressed in parts per million (ppm) and reported either relative to an internal tetramethylsilane standard (TMS δ = 0.0) or relative to solvent peaks ($CDCl_3$ δ = 7.2, DMSO-d_6 δ = 2.5, HOD δ = 3.3 for ^1H and $CDCl_3$ δ = 77.0, DMSO-d_6 δ = 39.5 for ^{13}C). Signals related atoms are represented in *italic*. Multiplicities are denoted as follows: s = singlet, d = doublet, t = triplet, q = quartet, dd = doublet of doublets, ddd = doublet of doublet of doublets, td = triplet of doublets, qd = quartet of doublets, m = multiplet, br = broad and apt = apparently. Coupling constants (*J*) were reported in Hertz (Hz). Mass spectrometric analyses were recorded on Finnigen mat LCQ MS/MS ESI, AB Sciex TripleTOF 5600 and AB MDS Sciex 4800 MALDI-TOF-TOF mass spectrometers.

HPLC analysis

All HPLC analysis were carried out at 25 ^oC using Prominence Shimadzu system that consists of LC-20AD solvent delivery unit, SPD-M20A photodiode array detector, SIL-$20A_{HT}$ auto sampler and CTO-20A column oven. For instrument control and data processing, LabSolutions data managing software, version 5.54 SP2 was utilized. Chiralpak® AD (0.46mm x 250mm), Chiralcel® OJ (0.46mm x 250mm), Chiralpak® IB (0.46mm x 250mm) and Chiralpak® ID (0.46mm x 250mm) were obtained from Daicel Chiral Technologies. HPLC grade *n*-hexane, ethyl acetate and 2-propanol were obtained from Scharlau Chemie S.A. Chiral HPLC separation conditions were determined by obtaining a separation of a standard racemic sample and by applying previously reported parameters if any.

X-Ray crystallography for dirhodium(II) complexes

X-ray quality crystals of the dirhodium(II) complexes were obtained as described below. Data were collected at -173 °C on crystals mounted on a Hampton Scientific cryoloop at the MX1 or MX2 beamlines, Australian Synchrotron, Victoria.[133,134] The structures were solved by direct methods with SHELXS-97, refined using full-matrix least-squares routines against F^2 with SHELXL-97,[135] and visualised using X-SEED.[136] All non-hydrogen atoms were anisotropically refined, while, all hydrogen atoms were positioned in calculated locations and refined using a riding model with fixed C-H distances of 0.95 Å (sp^2CH), 0.99 Å (CH_2), 0.98 Å (CH_3). The thermal parameters of all hydrogen atoms were estimated as U_{iso}(H) = 1.2U_{eq}(C) except for CH_3 where U_{iso}(H) = 1.5U_{eq}(C).

Preparation of racemic cyclopropane derivatives

All racemic cyclopropane standards for chiral HPLC analysis were synthesized following the same synthetic procedures designated below at which $Rh_2(OAc)_4$ was employed as a catalyst. Analytical samples were obtained through purification by means of preparative TLC.

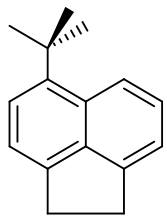

3-*tert*-Butylacenaphthene

To a vigorously stirred solution of anhydrous $FeCl_3$ (0.5 g, 3.1 mmol) and acenaphthene (2.5 g, 16.2 mmol) in CS_2 at 40 ^oC, *tert*-butyl chloride (2 mL, 18.4 mmol) was added drop-wise using a syringe pump over a period of 1 h. The reaction was allowed to reflux for another hour and, after that time, the reaction mixture was filtered through Celite® and concentrated *in vacuo*. The reddish brown residue was subjected to column chromatography using *n*-hexane as mobile phase to afford the title compound as a yellow oil (0.4 g, 12%); R_f = 0.23 (*n*-hexane); ^{1}H NMR (400 MHz, $CDCl_3$): δ 7.48 (d, 1H, Ar-*H*), 7.38 (d, 1H, Ar-*H*), 7.28 (s, 3H, Ar-*H*), 3.48 (s, 4H, CH_2-CH_2), 0.07 (s, 9H, C(CH_3)$_3$); ^{13}C NMR (100 MHz, $CDCl_3$): δ 146.0, 145.5,

139.4, 133.5, 131.0, 129.5, 127.7, 121.5, 119.2, 119.0 (10 x Ar-*C*), 30.8 ($C(CH_3)_3$), 30.6 (CH_2), 30.1 (CH_2), 1.0 ($C(CH_3)_3$); IR (KBr) *ν* 2954, 2924, 2866, 2372, 2341 cm^{-1}; MS (ESI) *m/z*: 420.3 (2 x $C_{16}H_{18}$; calc. 420.3). In addition to the recovery of 2.1 g of unreacted acenaphthene starting material.

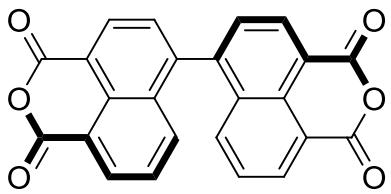

4,4'-Binaphthyl-1,1',8,8'-tetracarboxylic dianhydride (18)[137]

Sodium dichromate (0.525 g, 1.76 mmol) was added to a solution of 3-*tert*-butylacenaphthene (175 mg, 0.83 mmol) in boiling acetic acid (5 mL) and the mixture was refluxed for 5 h. After this time has elapsed, ice cold water was added to the reaction mixture and the resulting solid was collected by filtration, washed with deionized water and dried to afford the title compound as a yellow solid (111 mg, 34%). An analytical sample was purified by means of column chromatography (ethyl acetate: *n*-hexane); mp 227-230 ^{o}C (dec.); R_f = 0.39 (1:2 ethyl acetate: *n*-hexane); ^{1}H NMR (400 MHz, DMSO-d_6): δ 8.68 (d, 1H, *J* = 7.5 Hz, Ar-*H*), 8.56 (d, 1H, *J* = 7.0 Hz, Ar-*H*), 7.96 (d, 1H, *J* = 7.4 Hz, Ar-*H*), 7.77 (t, 1H, *J* = 8.0 Hz, Ar-*H*), 7.70 (d, 1H, *J* = 8.4 Hz, Ar-*H*); ^{13}C NMR (125 MHz, DMSO-d_6): δ 160.6, 160.5 (CO_2CO), 142.9, 132.7, 132.8, 131.9, 130.3, 130.1, 129.3, 128.3, 119.8, 119.7 (20 x Ar-*C*); IR (film) *ν* 2923, 2853, 1770, 1728, 1588, 1013, 783, 750, 729 cm^{-1}; MS (ESI) *m/z*: 393.34 ($C_{24}H_{10}O_6$ - H^+; calc. 393.04), 171.03 ($C_{12}H_5O_3$ - CO_2 + H_2O; calc. 171.04). ^{1}H, ^{13}C NMR and IR spectroscopic data are all in excellent agreement with the reported data for the same structure.[137] Further, 2-dimentional COSY, HSQC and HMBC experiments were in complete agreement with the proposed product structure.

Synthesis of new dirhodium(II) carboxylate complexes

General procedure for ligands preparation

To a mixture of the diacid anhydride (1.1 equiv.) and the L-amino acid (1 equiv.) in anhydrous toluene, triethylamine (0.1 equiv.) was added and the mixture was heated to reflux for 12 h under nitrogen atmosphere. After that time, the reaction mixture

was diluted with ethyl acetate, washed twice with 0.1M hydrochloric acid solution, dried over anhydrous Na_2SO_4, filtered and concentrated *in vacuo*. The residue was then purified by means of silica gel column chromatography using ethyl acetate: *n*-hexane as mobile phase to afford the corresponding desired product. The amounts of the diacid anhydride and L-amino acid are presented below in that order.

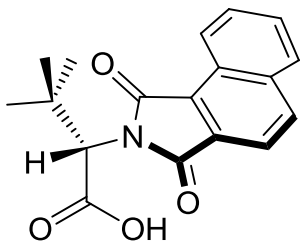

***N*-(1,2-Naphthaloyl)-(*S*)-*tert*-Leucine (*S*-1,2-NTTL, 1a)**

1,2-Naphthalic anhydride (0.650 g, 3.28 mmol), L-*tert*-Leucine (0.391 g, 2.98 mmol); yellow oil (0.825 g, 89%); $[\alpha]_D^{25}$ = -0.89 (*c* 1, $CHCl_3$); R_f = 0.38 (1:3 ethyl acetate: *n*-hexane); ^{1}H NMR (400 MHz, $CDCl_3$): δ 9.47 (br s, 1H, COO*H*), 8.79 (d, 1H, *J* = 8.1 Hz, Ar-*H*), 8.03 (d, 1H, *J* = 8.3 Hz, Ar-*H*), 7.81 (d, 1H, *J* = 8.1 Hz, Ar-*H*), 7.74 (d, 1H, *J* = 8.2 Hz, Ar-*H*), 7.58-7.52 (m, 2H, Ar-*H*), 4.68 (s, 1H, NC*H*), 1.12 (s, 9H, $C(CH_3)_3$); ^{13}C NMR (100 MHz, $CDCl_3$): δ 172.8 (*C*OOH), 168.0, 167.5 (2 x *C*ON), 135.6, 134.2, 129.8, 128.5, 127.8, 127.6, 126.9, 125.9, 123.9, 117.5 (10 x Ar-*C*), 58.7 (N*C*H), 34.6 ($C(CH_3)_3$), 26.9 ($C(CH_3)_3$); IR (film) *v* 3231, 2922, 1751, 1698, 1374, 1104, 1014, 796, 766, 725, 662 cm^{-1}; MS (ESI) *m/z*: 309.9 ($C_{18}H_{16}NO_4^-$; calc. 310.1), 266.0 ($C_{18}H_{16}NO_4^-$ - CO_2; calc. 266.1), 209.2 ($C_{18}H_{16}NO_4^-$ - CO_2 - C_4H_9; calc. 209.1).

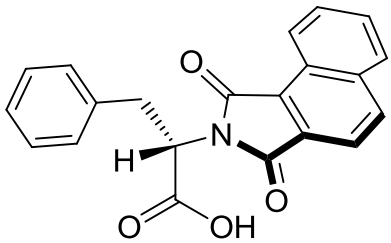

***N*-(1,2-Naphthaloyl)-(*S*)-Phenylalanine (*S*-1,2-NTPA, 1b)**

1,2-Naphthalic anhydride (0.5 g, 2.52 mmol), L-Phenylalanine (0.35 g, 2.10 mmol); pale yellow solid (0.65 g, 89%); mp 182 ^oC; $[\alpha]_D^{25}$ = -0.81 (*c* 1, $CHCl_3$); R_f = 0.20

(1:2 ethyl acetate: *n*-hexane); ^{1}H NMR (400 MHz, $CDCl_3$): δ 8.85 (d, 1H, *J* = 8.3 Hz, Ar-*H*), 8.12 (d, 1H, *J* = 8.2 Hz, Ar-*H*), 7.92 (d, 1H, *J* = 8.1 Hz, Ar-*H*), 7.78 (d, 1H, *J* = 8.3 Hz, Ar-*H*), 7.66 (dt, 2H, *J* = 14.9, 6.9 Hz, Ar-*H*), 7.38-7.00 (m, 5H, Ar-*H*), 5.27 (dd, 1H, *J* = 9.3, 6.9 Hz, NC*H*), 3.74-3.52 (m, 2H, CH_2); ^{13}C NMR (100 MHz, $CDCl_3$): δ 174.3 (*C*OOH), 168.6, 167.9 (2 x *C*ON), 136.6, 136.5, 135.1, 130.8, 129.5, 128.8, 128.7, 128.6, 127.9, 126.9, 124.9, 118.5 (16 x Ar-*C*), 52.9 (N*C*H), 34.5 (CH_2); IR (film) *v* 3327, 2943, 1701, 1375, 1287, 769, 700 cm^{-1}; MS (ESI) *m/z*: 343.9 ($C_{21}H_{14}NO_4^-$; calc. 344.0), 299.9 ($C_{21}H_{14}NO_4^-$ - CO_2; calc. 300.1), 209.1 ($C_{21}H_{14}NO_4^-$ - CO_2 - C_7H_7; calc. 209.0). Re-crystallized from hot MeOH.

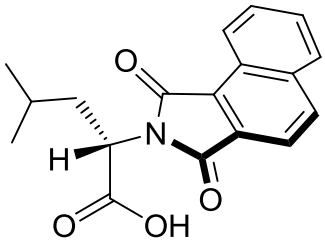

***N*-(1,2-Naphthaloyl)-(*S*)-Leucine (*S*-1,2-NTLU, 1c)**

1,2-Naphthalic anhydride (0.5 g, 2.52 mmol), L-Leucine (0.3 g, 2.29 mmol); pale yellow solid (0.64 g, 90%); mp 138-139 ^{o}C; R_f = 0.22 (1:3 ethyl acetate: *n*-hexane); ^{1}H NMR (400 MHz, $CDCl_3$): δ 10.94 (br s, 1H, COO*H*), 8.78 (d, 1H, *J* = 8.3 Hz, Ar-*H*), 8.03 (d, 1H, *J* = 8.2 Hz, Ar-*H*), 7.81 (d, 1H, *J* = 8.1 Hz, Ar-*H*), 7.73 (d, 1H, *J* = 8.2 Hz, Ar-*H*), 7.56 (dt, 2H, *J* = 24.8, 7.0 Hz, Ar-*H*), 4.94 (dd, 1H, *J* = 11.5, 4.3 Hz, NC*H*), 2.32 (ddd, 1H, *J* = 14.8, 11.0, 4.1 Hz, CH_2), 1.89 (ddd, 1H, *J* = 14.4, 10.2, 4.4 Hz, CH_2), 1.52-1.41 (m, 1H, C*H*$(CH_3)_2$), 0.86 (dd, 6H, *J* = 13.3, 6.6 Hz, CH(CH_3)$_2$); ^{13}C NMR (100 MHz, $CDCl_3$): δ 175.2 (*C*OOH), 167.8, 167.3 (2 x *C*ON), 135.6, 134.1, 129.9, 128.5, 127.8, 127.6, 126.9, 126.0, 123.9, 117.5 (10 x Ar-*C*), 49.3 (N*C*H), 36.1 (CH_2), 24.0 (*C*H$(CH_3)_2$), 22.0, 19.9 (2 x CH(*C*H_3)$_2$); IR (film) *v* 2968, 1705, 1373, 1276, 764, 655 cm^{-1}; MS (ESI) *m/z*: 309.9 ($C_{18}H_{16}NO_4^-$; calc. 310.1), 266.0 ($C_{18}H_{16}NO_4^-$ - CO_2; calc. 266.1), 209.2 ($C_{18}H_{16}NO_4^-$ - CO_2 - C_4H_9; calc. 209.1). Re-crystallized from hot MeOH.

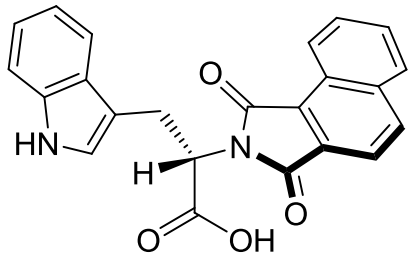

***N*-(1,2-Naphthaloyl)-(*S*)-Tryptophan (*S*-1,2-NTTR, 1d)**

1,2-Naphthalic anhydride (0.5 g, 2.52 mmol), L-Tryptophan (0.47 g, 2.29 mmol); yellow solid (0.83 g, 85%); mp 238-239 ^{o}C; R_f = 0.51 (1:1 ethyl acetate: *n*-hexane); ^{1}H NMR (400 MHz, DMSO-d_6): δ 13.30 (br s, 1H, COO*H*), 10.71 (s, 1H, N*H*), 8.68 (d, 1H, *J* = 8.3 Hz, Ar-*H*), 8.34 (d, 1H, *J* = 8.3 Hz, Ar-*H*), 8.11 (d, 1H, *J* = 8.2 Hz, Ar-*H*), 7.81-7.69 (m, 3H, Ar-*H*), 7.51 (d, 1H, *J* = 7.9 Hz, Ar-*H*), 7.22 (d, 1H, *J* = 8.1 Hz, Ar-*H*), 7.06 (d, 1H, *J* = 2.3 Hz, Ar-*H*), 6.96 (t, 1H, *J* = 7.5 Hz, Ar-*H*), 6.87 (t, 1H, *J* = 7.4 Hz, Ar-*H*), 5.14 (dd, 1H, *J* = 10.3, 5.6 Hz, NC*H*), 3.71-3.51 (m, 2H, CH_2); ^{13}C NMR (100 MHz, DMSO-d_6): δ 170.9 (*C*OOH), 168.9, 168.1 (2 x *C*ON), 136.6, 136.4, 136.2, 130.9, 130.5, 129.6, 129.4, 127.4, 127.3, 126.4, 124.1, 123.8, 121.3, 118.8, 118.3, 111.8, 110.3 (18 x Ar-*C*), 53.1 (N*C*H), 24.6 (CH_2); IR (film) ν 3458, 3317, 2917, 1700, 1380, 1282, 769, 740 cm^{-1}; MS (ESI) *m/z*: 382.9 ($C_{23}H_{15}N_2O_4^-$; calc. 383.1), 339.2 ($C_{23}H_{15}N_2O_4^-$ - CO_2; calc. 339.1), 210.2 ($C_{23}H_{15}N_2O_4^-$ - CO_2 - C_9H_7N; calc. 210.1). Re-crystallized from hot MeOH.

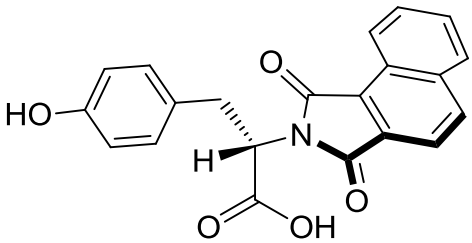

***N*-(1,2-Naphthaloyl)-(*S*)-Tyrosine (*S*-1,2-NTTY, 1e)**

1,2-Naphthalic anhydride (0.5 g, 2.52 mmol), L-Tyrosine (0.42 g, 2.29 mmol); yellow solid (0.74 g, 90%); mp 248-249 ^{o}C; $[\alpha]_D^{25}$ = -1.43 (*c* 1, $CHCl_3$); R_f = 0.25 (1:1 ethyl acetate: *n*-hexane); ^{1}H NMR (400 MHz, DMSO-d_6): δ 9.11 (br s, 1H, COO*H*), 8.70 (d, 1H, *J* = 8.4 Hz, Ar-*H*), 8.38 (d, 1H, *J* = 8.2 Hz, Ar-*H*), 8.14 (d, 1H, *J* = 8.2 Hz, Ar-*H*), 7.88-7.69 (m, 3H, Ar-*H*), 6.94 (apt d, 2H, *J* = 8.5 Hz, Ar-*H*), 6.51 (apt d, 2H, *J* = 8.5 Hz, Ar-*H*), 5.01 (dd, 1H, *J* = 11.6, 4.8 Hz, NC*H*), 3.40-3.25 (m,

3H, C*H*$_2$ and O*H* overlapping); ^{13}C NMR (100 MHz, DMSO-d_6): δ 170.3 (*C*OOH), 168.4, 167.5 (2 x *C*ON), 155.8, 136.4, 135.9, 130.3, 130.1, 129.6, 129.2, 129.1, 127.3, 127.0, 125.9, 123.7, 118.4, 115.1 (16 x Ar-*C*), 53.3 (N*C*H), 33.2 (*C*H$_2$); IR (film) ν 3437, 3243, 2943, 1734, 1686, 1387, 1225, 772, 675 cm^{-1}; MS (ESI) *m/z*: 359.9 ($C_{21}H_{14}NO_5^-$; calc. 360.1), 210.2 ($C_{21}H_{14}NO_5^-$ - CO_2 - C_7H_6O; calc. 210.1). Re-crystallized from hot MeOH.

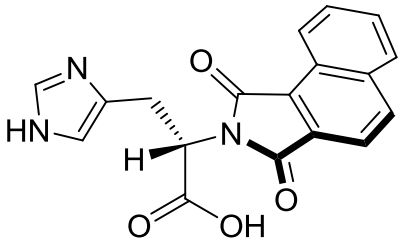

***N*-(1,2-Naphthaloyl)-(*S*)-Histidine (*S*-1,2-NTHS, 1f)**

1,2-Naphthalic anhydride (0.5 g, 2.52 mmol), L-Histidine (0.36 g, 2.32 mmol); bright yellow solid (0.73 g, 94%); R_f = 0.54 (100% MeOH); ^{1}H NMR (400 MHz, DMSO-d_6): δ 8.74 (d, 1H, *J* = 8.2 Hz, Ar-*H*), 8.41 (d, 1H, *J* = 8.0 Hz, Ar-*H*), 8.18 (d, 1H, *J* = 7.9 Hz, Ar-*H*), 7.97-7.64 (m, 3H, Ar-*H*), 7.53 (s, 1H, Ar-*H*), 6.80 (s, 1H, Ar-*H*), 4.99 (apt t, 1H, *J* = 6.1 Hz, C*H*N), 3.39 (apt d, 2H, *J* = 6.1 Hz, C*H*$_2$); ^{13}C NMR (100 MHz, DMSO-d_6): δ 170.7 (*C*OOH), 168.9, 168.1 (2 x *C*ON), 136.7, 136.1, 135.3, 131.1, 130.4, 129.6, 129.4, 127.5, 126.7, 124.2, 118.9 (13 x Ar-*C*), 52.8 (N*C*H), 26.6 (C*H*$_2$); IR (film) ν 3140, 1716, 1373, 842, 770, 655 cm^{-1}; MS (ESI) *m/z*: 333.9 ($C_{18}H_{12}N_3O_4^-$; calc. 334.0), 289.9 ($C_{18}H_{12}N_3O_4^-$ - CO_2 ; calc. 290.0). Re-crystallized from hot MeOH.

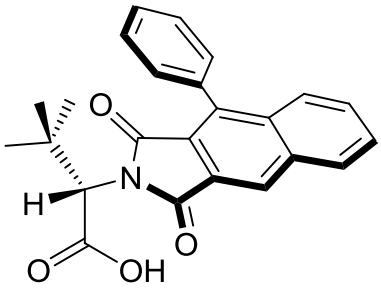

***N*-(1-Phenyl-2,3-naphthaloyl)-(*S*)-*tert*-Leucine (*S*-1-Ph-BPTTL, 7)**

1-Phenyl-2,3-naphthalenedicarboxylic anhydride (0.47 g, 1.7 mmol), L-*tert*-Leucine (0.2 g, 1.6 mmol); colourless oil (0.6 g, 99%); $[\alpha]_D^{25}$ = -0.35 (*c* 1, $CHCl_3$); R_f = 0.59 (1:1 ethyl acetate: *n*-hexane); ^{1}H NMR (400 MHz, $CDCl_3$): δ 8.30 (s, 1H, Ar-*H*), 7.98 (d, 1H,, *J* = 7.8 Hz, Ar-*H*), 7.70 (d, 1H, *J* = 8.2 Hz, Ar-*H*), 7.62-7.37 (m, 5H, Ar-*H*), 7.30 (m, 2H, Ar-*H*), 4.65 (s, 1H, C*H*N), 1.08 (s, 9H, C(C*H*$_3$)$_3$); ^{13}C NMR (100 MHz, $CDCl_3$): δ 172.9 (*C*OOH), 167.6, 166.9 (2 x *C*ON), 140.6, 135.5, 134.2, 130.3, 129.9, 129.2, 129.0, 128.6, 128.5, 128.2, 128.1, 127.2, 124.7, 123.1 (16 x Ar-*C*), 60.0 (N*C*H), 35.1 (*C*(CH$_3$)$_3$), 28.1 (C(*C*H$_3$)$_3$); IR (film) *ν* 2962, 1709, 1368, 1241, 1114, 767, 699 cm^{-1}; MS (ESI) *m/z*: 388.16 ($C_{24}H_{21}NO_4$ + H^+; calc. 388.15), 342.15 ($C_{24}H_{20}NO_4^-$ - CO_2; calc. 342.15).

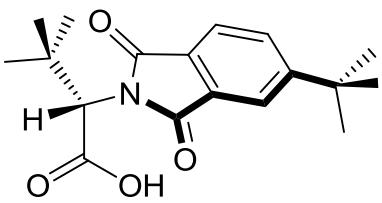

***N*-(4-*tert*-Butylphthaloyl)-(*S*)-*tert*-Leucine (*S*-^{tert}PTTL, 8)**

4-*tert*-Butylphthalic anhydride (0.514 g, 2.52 mmol), L-*tert*-Leucine (0.3 g, 2.29 mmol); colourless oil (0.7 g, 96%); $[\alpha]_D^{25}$ = -0.35 (*c* 1, $CHCl_3$); R_f = 0.7 (1:1 ethyl acetate: *n*-hexane); ^{1}H NMR (400 MHz, $CDCl_3$): δ 7.88-7.71 (m, 3H, Ar-*H*), 4.69 (s, 1H, NC*H*), 1.34 (s, 9H, C(C*H*$_3$)$_3$), 1.15 (s, 9H, C(C*H*$_3$)$_3$); ^{13}C NMR (100 MHz, $CDCl_3$): δ 173.3 (*C*OOH), 168.4, 168.0 (2 x *C*ON), 158.9, 131.8, 131.3, 128.9, 123.4, 120.8 (6 x Ar-*C*), 59.8 (N*C*H), 35.7, 35.6 (2 x *C*(CH$_3$)$_3$), 31.1, 27.9 (2 x C(*C*H$_3$)$_3$); IR (film) *ν* 2963, 1711, 1372, 1101, 908, 729 cm^{-1}; MS (ESI) *m/z*: 318.17 ($C_{18}H_{23}NO_4$ + H^+; calc. 318.17), 272.17 ($C_{18}H_{22}NO_4^-$ - CO_2; calc. 272.17).

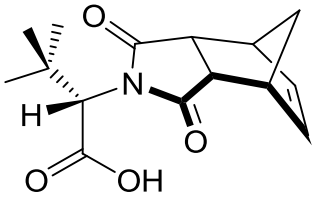

***N*-(*endo*-Bicyclo[2.2.1]hept-5-ene-2,3-oyl)-(*S*)-*tert*-Leucine (*S*-BHTL, 9)**

cis-5-Norbornene-*endo*-2,3-dicarboxylic anhydride (0.413 g, 2.52 mmol), L-*tert*-Leucine (0.3 g, 2.29 mmol); white solid (0.57 g, 90%); $[\alpha]_D^{25}$ = -0.55 (*c* 1, $CHCl_3$); R_f = 0.30 (1:1 ethyl acetate: *n*-hexane); ^{1}H NMR (400 MHz, $CDCl_3$): δ 6.13-6.09 (ddd, 2H, C*H*=C*H*), 4.34 (s, 1H, C*H*N), 3.40 (br s, 2H, 2 x C*H*), 3.35-3.30 (m, 2H, 2 x C*H*), 1.63 (dd, 2H, *J* = 74.8, 8.8 Hz, CH_2), 1.02 (s, 9H, C(CH_3)$_3$); ^{13}C NMR (100 MHz, $CDCl_3$): δ 177.4, 177.3 (2 x *C*ON), 172.4 (*C*OOH), 135.2 (=*C*H), 134.5 (=*C*H), 60.2 (N*C*H), 52.5 (CH_2), 46.0, 45.7 (2 x *C*H), 45.3, 44.9 (2 x *C*H), 35.4 (*C*(CH_3)$_3$), 27.8 (C(*C*H_3)$_3$); IR (film) *v* 3294, 2960, 2870, 1739, 1687, 1380, 1339, 1169, 1145, 713 cm^{-1}; MS (ESI) *m/z*: 278.13 ($C_{15}H_{19}NO_4$ + H^+; calc. 278.13). Re-crystallized from hot MeOH.

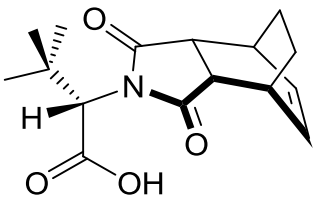

***N*-(*endo*-Bicyclo[2.2.2]oct-5-ene-2,3-oyl)-(*S*)-*tert*-Leucine (*S*-BOTL, 10)**

endo-Bicyclo[2.2.2]oct-5-ene-2,3-dicarboxylic anhydride (0.5 g, 2.8 mmol), L-*tert*-Leucine (0.3 g, 2.3 mmol); white solid (0.65 g, 98%); $[\alpha]_D^{25}$ = -0.45 (*c* 1, $CHCl_3$); R_f = 0.31 (1:1 ethyl acetate: *n*-hexane); ^{1}H NMR (400 MHz, $CDCl_3$): δ 6.19 (m, 2H, C*H*=C*H*), 4.43 (s, 1H, C*H*N), 3.17 (s, 2H, 2 x C*H*), 2.90 (qd, 2H, *J* = 8.4, 2.9 Hz, 2 x C*H*), 1.61 (d, 2H, *J* = 7.7 Hz, CH_2), 1.39 (d, 2H, *J* = 8.8 Hz, CH_2), 1.05 (s, 9H, C(CH_3)$_3$); ^{13}C NMR (100 MHz, $CDCl_3$): δ 178.8, 178.6 (2 x *C*ON), 172.3 (*C*OOH), 132.8 (=*C*H), 132.4 (=*C*H), 60.2 (N*C*H), 44.3, 43.9 (2 x *C*H), 35.6 (*C*(CH_3)$_3$), 31.8, 31.5 (2 x *C*H), 27.8 (C(*C*H_3)$_3$), 23.7, 23.6 (2 x *C*H_2); IR (film) *v* 3294, 2958, 2870, 1746, 1683, 1389, 1366, 1166, 1145, 701 cm^{-1}; MS (ESI) *m/z*: 292.15 ($C_{16}H_{21}NO_4$ + H^+; calc. 292.15), 246.15 ($C_{16}H_{20}NO_4^-$ - CO_2; calc. 246.15). Re-crystallized from hot MeOH.

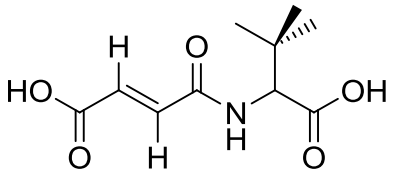

(*E*)-4-(1-Carboxy-2,2-dimethylpropylamino)-4-oxobut-2-enoic acid (17)

exo-3,6-Epoxy-1,2,3,6-tetrahydrophthalic anhydride (0.418 g, 2.52 mmol), L-*tert*-Leucine (0.3 g, 2.29 mmol); colourless oil (0.49 g, 94%); R_f = 0.38 (3:1 ethyl acetate: *n*-hexane); ^{1}H NMR (400 MHz, $CDCl_3$): δ 8.98 (d, 1H, J_{CH} = 8.8 Hz, N*H*), 6.41 (dd, 2H, *J* = 108.5, 12.5 Hz, C*H*=C*H*), 4.16 (d, 1H, J_{NH} = 8.8 Hz, C*H*), 0.96 (s, 9H, C(CH_3)$_3$); ^{13}C NMR (100 MHz, $CDCl_3$): δ 172.0 (*C*OOH), 166.7 (*C*ONH), 165.3 (*C*OOH), 133.22 (=*C*H), 130.7 (=*C*H), 61.3 (N*C*H), 34.0 (*C*(CH_3)$_3$), 27.0 (C(*C*H_3)$_3$); IR (film) *ν* 3305, 2970, 1716, 1624, 1566, 1404, 1249, 1219 cm^{-1}; MS (ESI) *m/z*: 457.18 (2 x $C_{10}H_{15}NO_5$ - H^+; calc. 457.18), 228.08 ($C_{10}H_{14}NO_5^-$; calc. 228.08).

General procedure for ligand exchange

A mixture of the carboxylic acid ligand (6 equiv.) and dirhodium(II) tetraacetate ($Rh_2(OAc)_4$, 1 equiv.) in dry chlorobenzene was refluxed for 24 h under nitrogen atmosphere using a Soxhlet extractor fitted with a thimble containing dry mixture of Na_2CO_3 and sand (1:1) for trapping the eliminated acetic acid molecules. After that time, the solvent was evaporated *in vacuo* and the residue was re-dissolved in DCM, washed with saturated $NaHCO_3$ solution, dried over anhydrous Na_2SO_4, filtered and concentrated *in vacuo*. The green residue was then purified by means of silica gel column chromatography using ethyl acetate: *n*-hexane as mobile phase. The pure products were dried overnight under vacuum at 50 ^{o}C before analysis. The amounts of carboxylic acid ligand and $Rh_2(OAc)_4$ are presented below in that order.

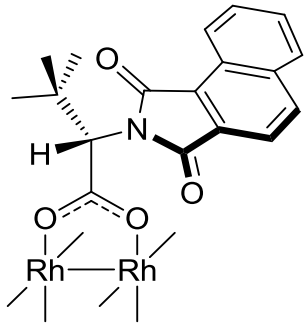

Dirhodium(II,II) tetrakis[*N*-(1,2-naphthaloyl)-(*S*)-*tert*-Leucinate] (Rh_2(*S*-1,2-NTTL)$_4$, 3a)

Ligand (0.69 g, 2.23 mmol), $Rh_2(OAc)_4$ (0.17 g, 0.38 mmol); green solid (0.36 g, 65%); R_f = 0.54 (1:2 ethyl acetate: *n*-hexane); ^{1}H NMR (400 MHz, $CDCl_3$): δ 8.84 (br s, 4H, Ar-*H*), 7.92 (br s, 4H, Ar-*H*), 7.74 (br s, 8H, Ar-*H*), 7.52 (br s, 8H, Ar-*H*), 4.92 (s, 4H, 4 x NC*H*), 1.16 (s, 36H, 4 x C(C*H*$_3$)$_3$); ^{13}C NMR (100 MHz, $CDCl_3$): δ 186.2 (*C*OO), 167.3 (*C*ON), 135.3, 133.5, 130.1, 128.2, 127.3, 126.9, 126.1, 124.3, 117.6 (Ar-*C*), 60.3 (N*C*H), 34.8 (*C*(CH$_3$)$_3$), 27.0 (C(*C*H$_3$)$_3$); IR (film) ν 2958, 1707, 1610, 1396, 1366, 1341, 1105, 783, 765 cm^{-1}; HRMS (MALDI-TOF) *m/z*: 1661.2025 ($C_{72}H_{61}N_4O_{16}Rh_2$ + K^+ + 2EtOAc; calc. 1661.4481), 1645.2306 ($C_{72}H_{61}N_4O_{16}Rh_2$ + Na^+ + 2EtOAc; calc. 1645.3395), 1485.1979 ($C_{72}H_{61}N_4O_{16}Rh_2$ + K^+; calc. 1485.3433), 1469.2275 ($C_{72}H_{61}N_4O_{16}Rh_2$ + Na^+; calc. 1469.2347).

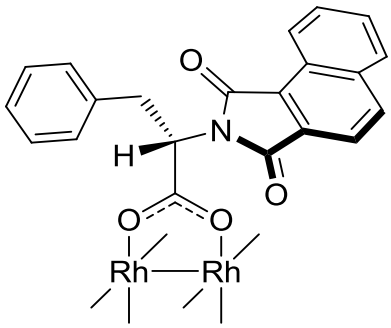

Dirhodium(II,II) tetrakis[*N*-(1,2-naphthaloyl)-(*S*)-Phenylalaninate] (Rh_2(*S*-1,2-NTPA)$_4$, 3b)

Ligand (0.5 g, 1.45 mmol), $Rh_2(OAc)_4$ (0.11 g, 0.24 mmol); green solid (0.25 g, 63%); R_f = 0.28 (1:1 ethyl acetate: *n*-hexane); ^{1}H NMR (400 MHz, $CDCl_3$): δ 8.72 (d, 4H, *J* = 8.1 Hz, Ar-*H*), 7.98 (d, 4H, *J* = 8.1 Hz, Ar-*H*), 7.82 (d, 4H, *J* = 7.4 Hz, Ar-*H*), 7.71 (d, 4H, *J* = 8.3 Hz, Ar-*H*), 7.57 (m, 8H, Ar-*H*), 7.35-6.99 (m, 20H, Ar-

H), 5.37 (dd, 4H, *J* = 11.4, 4.7 Hz, 4 x NC*H*), 3.73-3.50 (m, 8H, 4 x CH_2); ^{13}C NMR (100 MHz, $CDCl_3$): δ 188.5 (*C*OO), 168.4, 167.9 (*C*ON), 137.9, 136.5, 135.0, 131.1, 129.4, 128.6, 128.5, 128.0, 127.2, 126.6, 125.3, 118.8 (Ar-*C*), 54.6 (N*C*H), 35.7 (CH_2); IR (film) *v* 2944, 1734, 1716, 1373, 1229, 770, 697 cm^{-1}; HRMS (ESI-TOF) *m/z*: 1721.2692 ($C_{84}H_{60}N_4O_{16}Rh_2$ + 2Acetone + Na^+; calc. 1721.2536), 1663.2191 ($C_{84}H_{60}N_4O_{16}Rh_2$ + Acetone + Na^+; calc. 1663.2118), 1646.2117 ($C_{84}H_{60}N_4O_{16}Rh_2$ + H_2O + 2Na^+; calc. 1646.1702), 1606.1798 ($C_{84}H_{60}N_4O_{16}Rh_2$ + Na^+ + H^+; calc. 1606.1777).

Recrystallization of Rh_2(*S*-1,2-NTPA)$_4$ (3b)

Single crystal X-ray diffraction crystals of Rh_2(*S*-1,2-NTPA)$_4$ were obtained by dissolving the pure complex (~40 mg) in ACN (~1 mL). The resulting solution was subjected to sonication and Pasteur pipette filtration. Tiny crystals were obtained by the slow evaporation of the solvent and used directly for measurement. Single crystal X-ray diffraction was recorded on MX2 beamline at the Australian Synchrotron, Victoria. Data collection and refinement were carried out using the general X-ray crystallographic conditions described earlier.

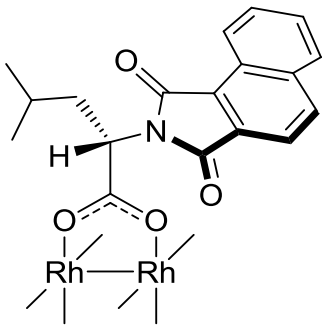

Dirhodium(II,II) tetrakis[*N*-(1,2-naphthaloyl)-(*S*)-Leucinate] (Rh_2(*S*-1,2-NTLU)$_4$, 3c)

Ligand (0.5 g, 1.60 mmol), $Rh_2(OAc)_4$ (0.12 g, 0.27 mmol); green solid (0.166 g, 61%); R_f = 0.69 (1:2 ethyl acetate: *n*-hexane); ^{1}H NMR (400 MHz, $CDCl_3$): δ 8.90 (d, 4H, *J* = 7.8 Hz, Ar-*H*), 8.22-7.95 (m, 4H, Ar-*H*), 7.95-7.73 (m, 8H, Ar-*H*), 7.73-7.43 (m, 8H, Ar-*H*), 5.02 (br s, 4H, 4 x NC*H*), 2.23 (br s, 4H, 2 x CH_2), 2.03 (br s, 4H, 2 x CH_2), 1.50 (br s, 4H, 4 x C*H*(CH_3)$_2$), 1.01 (br s, 12H, 2 x CH(CH_3)$_2$), 0.93

(br s, 12H, 2 x CH(C*H*$_3$)$_2$); ^{13}C NMR (100 MHz, $CDCl_3$): δ 188.9 (*C*OO), 168.5, 168.0 (*C*ON), 136.3, 134.5, 131.2, 129.1, 128.5, 128.4, 128.0, 127.9, 127.2, 125.2, 118.7, 118.6 (Ar-*C*), 51.8 (N*C*H), 38.2, 38.0 (*C*H$_2$), 25.1 (*C*H(CH$_3$)$_2$), 23.4, 21.4, 21.3 (CH(*C*H$_3$)$_2$); IR (film) ν 2954, 1734, 1716, 1374, 1229, 770, 675 cm^{-1}; HRMS (MALDI-TOF) *m/z*: 1661.2783 ($C_{72}H_{61}N_4O_{16}Rh_2$ + K^+ + 2EtOAc; calc. 1661.4481), 1645.3109 ($C_{72}H_{61}N_4O_{16}Rh_2$ + Na^+ + 2EtOAc; calc. 1645.3395), 1485.2178 ($C_{72}H_{61}N_4O_{16}Rh_2$ + K^+; calc. 1485.3433), 1469.2975 ($C_{72}H_{61}N_4O_{16}Rh_2$ + Na^+; calc. 1469.2347).

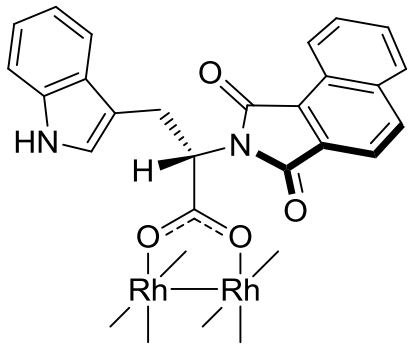

Dirhodium(II,II) tetrakis[*N*-(1,2-naphthaloyl)-(*S*)-Tryptophanate] (Rh_2(*S*-1,2-NTTR)$_4$, 3d)

Ligand (0.73 g, 1.90 mmol), $Rh_2(OAc)_4$ (0.14 g, 0.32 mmol); green solid (0.30 g, 55%); R_f = 0.20 (2:1 ethyl acetate: *n*-hexane); ^{1}H NMR (400 MHz, DMSO-d_6): δ 10.75 (s, 4H, 4 x N*H*), 8.50 (m, 4H, Ar-*H*), 8.31 (br s, 4H, Ar-*H*), 8.07 (br s, 4H, Ar-*H*), 7.80-7.41 (m, 12H, Ar-*H*), 7.25 (d, 4H, *J* = 7.8 Hz, Ar-*H*), 7.17-6.69 (m, 16H, Ar-*H*), 5.27 (br s, 4H, 4 x NC*H*), 3.57 (br s, 8H, 4 x C*H*$_2$); ^{13}C NMR (125 MHz, DMSO-d_6): δ 188.6 (*C*OO), 168.0, 167.2 (*C*ON), 136.0, 135.5, 130.3, 129.8, 128.9, 128.8, 127.1, 126.8, 125.9, 123.8, 123.5, 120.9, 118.3, 118.2, 118.1, 117.9, 111.4, 109.7 (Ar-*C*), 53.8 (N*C*H), 24.9 (*C*H$_2$); IR (film) ν 2970, 1734, 1699, 1374, 1228, 768, 740 cm^{-1}; MS (ESI) *m/z*: 1760.6 ($C_{92}H_{60}N_8O_{16}Rh_2$ + Na^+ - H^+; calc. 1760.2), 1376.7 ($C_{92}H_{60}N_8O_{16}Rh_2$ + Na^+ - $C_{23}H_{16}N_2O_4$; calc. 1377.1), 992.7 ($C_{92}H_{60}N_8O_{16}Rh_2$ + Na^+ - 2 x $C_{23}H_{16}N_2O_4$; calc. 992.9).

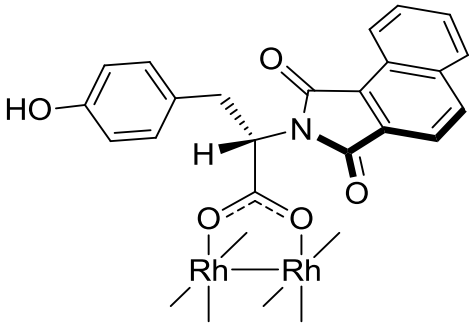

Dirhodium(II,II) tetrakis[*N*-(1,2-naphthaloyl)-(*S*)-Tyrosinate] (Rh_2(*S*-1,2-NTTY)$_4$, 3e)

Ligand (0.63 g, 1.76 mmol), $Rh_2(OAc)_4$ (0.13 g, 0.30 mmol); green solid (0.27 g, 56%); R_f = 0.23 (2:1 ethyl acetate: *n*-hexane); ^{1}H NMR (400 MHz, DMSO-d_6): δ 8.43-8.25 (m, 4H, Ar-*H*), 8.21-8.04 (m, 4H, Ar-*H*), 7.92-7.25 (m, 16H, Ar-*H*), 7.04-6.82 (m, 8H, Ar-*H*), 6.65-6.34 (m, 8H, Ar-*H*), 5.18-4.90 (m, 4H, 4 x N*C*H), 3.50-3.05 (m, 12H, 4 x CH_2 and 4 x O*H* overlapping); ^{13}C NMR (125 MHz, DMSO-d_6): δ 188.4 (*C*OO), 170.4, 168.5, 167.9, 167.7, 167.1 (*C*ON), 155.8, 155.7, 136.2, 136.1, 135.8, 130.3, 130.1, 129.9, 129.7, 129.6, 129.2, 129.1, 129.0, 128.9, 128.4, 127.2, 127.0, 126.9, 126.8, 125.9, 125.8, 123.7, 118.4, 115.2, 115.1 (Ar-*C*), 54.4, 53.4 (N*C*H), 33.9, 33.3 (CH_2); IR (film) *v* 3294, 2970, 1734, 1699, 1375, 1217, 770, 742, 685 cm^{-1}; MS (ESI) *m/z*: 1751.21 ($C_{84}H_{56}N_4O_{20}Rh_2$ + 2ACN + Na^+, calc. 1751.20), 1729.18 ($C_{84}H_{56}N_4O_{20}Rh_2$ + 2ACN + H^+, calc. 1729.20), 1710.17 ($C_{84}H_{56}N_4O_{20}Rh_2$ + ACN + Na^+, calc. 1710.17).

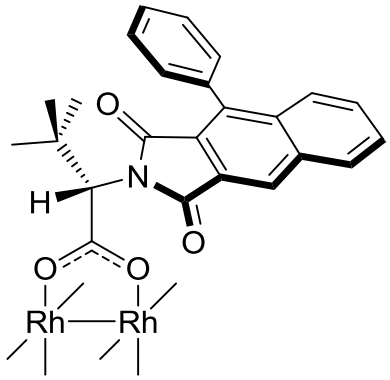

Dirhodium(II,II) tetrakis[*N*-(1-phenyl-2,3-naphthaloyl)-(*S*)-*tert*-Leucinate] (Rh_2(*S*-1-Ph-BPTTL)$_4$, 11)

Ligand (0.621 g, 1.60 mmol), $Rh_2(OAc)_4$ (0.12 g, 0.27 mmol); green solid (0.31 g, 67%); R_f = 0.77 (1:1 ethyl acetate: *n*-hexane); ^{1}H NMR (400 MHz, $CDCl_3$): δ 8.07 (s, 4H, Ar-*H*), 7.60 (d, 8H, *J* = 8.2 Hz, Ar-*H*), 7.51-7.30 (m, 24H, Ar-*H*), 7.12 (d, 4H, *J* = 6.9 Hz, Ar-*H*), 4.92 (s, 4H, 4 x C*H*N), 1.19-1.16 (m, 36H, 4 x C(CH_3)$_3$); ^{13}C NMR (100 MHz, $CDCl_3$): δ 186.2 (*C*OO), 166.3, 165.5 (*C*ON), 138.2, 134.5, 134.1, 133.8, 129.6, 129.2, 128.9, 127.4, 127.2, 127.0, 126.8, 126.6, 123.4, 122.9 (Ar-*C*), 60.4 (N*C*H), 34.7 (*C*(CH_3)$_3$), 27.0 (C(*C*H_3)$_3$); IR (film) ν 2962, 1709, 1617, 1397, 1365, 1340, 1260, 1109, 1030, 801, 761, 696 cm^{-1}; MS (ESI) *m/z*: 1758.1 ($C_{96}H_{80}N_4O_{16}Rh_2$ + 7H$^+$; calc. 1758.4), 1369.1 ($C_{96}H_{80}N_4O_{16}Rh_2$ + 5H$^+$ - $C_{24}H_{20}NO_4$; calc. 1369.2), 980.1 ($C_{96}H_{80}N_4O_{16}Rh_2$ + 2H$^+$ - 2 x $C_{24}H_{20}NO_4$; calc. 980.1), 608.9 ($C_{96}H_{80}N_4O_{16}Rh_2$ - 3 x $C_{24}H_{20}NO_4$ - H$^+$; calc. 608.9), 341.7 ($C_{24}H_{20}NO_4$ - CO_2; calc. 342.1).

Recrystallization of Rh_2(*S*-1-Ph-BPTTL)$_4$ (11)

Single crystal X-ray diffraction quality crystals of Rh_2(*S*-1-Ph-BPTTL)$_4$ were obtained by dissolving the pure complex (~40 mg) in ethyl acetate: *n*-hexane (1:1) mixture (~1 mL). The resulting solution was subjected to sonication and Pasteur pipette filtration. Bright green needles were obtained by the slow evaporation of the solvent and used directly for measurement. Single crystal X-ray diffraction was recorded on MX1 beamline at the Australian Synchrotron, Victoria.

In addition to the general X-ray crystallographic conditions described earlier for data collection and refinement, diffuse lattice solvent areas (ethyl acetate) were treated with SQUEEZE.[138] Rh-bound ethyl acetate solvent was apparent in difference maps, which was extensively disordered around the rotational axis. The isotropic

refinement model for these solvent molecules required a number of positional and thermal parameter restraints.

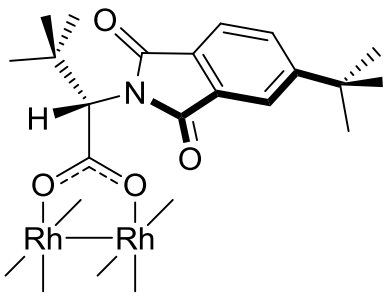

Dirhodium(II) tetrakis[*N*-(4-*tert*-butylphthaloyl)-(*S*)-*tert*-Leucine] (Rh_2(*S*-^{tert}PTTL)$_4$, 12)

Ligand (0.645 g, 2.032 mmol), $Rh_2(OAc)_4$ (0.150 g, 0.339 mmol); green solid (0.35 g, 71%); R_f = 0.50 (1:2 ethyl acetate: *n*-hexane); ^{1}H NMR (400 MHz, $CDCl_3$): δ 7.85 (br s, 4H, Ar-*H*), 7.67-7.62 (m, 8H, Ar-*H*), 4.88 (s, 4H, 4 x NC*H*), 1.35 (s, 36H, 4 x C(C*H*$_3$)$_3$), 1.11 (s, 36H, 4 x C(C*H*$_3$)$_3$); ^{13}C NMR (100 MHz, $CDCl_3$): δ 187.1 (*C*OO), 172.1, 168.2 (*C*ON), 158.0, 132.1, 130.5, 129.4, 122.9, 120.5 (Ar-*C*), 61.26 (N*C*H), 35.6, 35.5 (2 x *C*(CH$_3$)$_3$), 31.1, 27.9 (2 x C(*C*H$_3$)$_3$); IR (film) ν 2959, 1713, 1612, 1366, 1103, 752, 693 cm^{-1}; MS (ESI) *m/z*: 1476.8 ($C_{72}H_{88}N_4O_{16}Rh_2$ + 6H$^+$; calc. 1476.4), 1158.1 ($C_{72}H_{88}N_4O_{16}Rh_2$ + 4H$^+$ - $C_{18}H_{22}NO_4$; calc. 1158.3), 839.5 ($C_{72}H_{88}N_4O_{16}Rh_2$ + 2H$^+$ - 2 x $C_{18}H_{22}NO_4$; calc. 840.1).

Recrystallization of Rh_2(*S*-^{tert}PTTL)$_4$ (12)

Single crystal X-ray diffraction quality crystals of Rh_2(*S*-^{tert}PTTL)$_4$ were obtained by dissolving the pure complex (~40 mg) in THF (~1 mL). The resulting solution was subjected to sonication and Pasteur pipette filtration. Green needles crystals were obtained by the slow evaporation of the solvent and used directly for measurement. Single crystal X-ray diffraction was recorded on MX2 beamline at the Australian Synchrotron, Victoria. Data collection and refinement were carried out using the general X-ray crystallographic conditions described earlier.

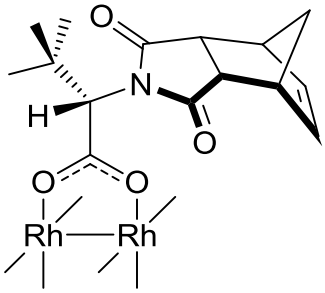

Dirhodium(II,II) tetrakis[*N*-(*endo*-bicyclo[2.2.1]hept-5-ene-2,3-oyl)-(*S*)-*tert*-Leucinate] (Rh_2(*S*-BHTL)$_4$, 13)

Ligand (0.49 g, 1.77 mmol), $Rh_2(OAc)_4$ (0.13 g, 0.29 mmol); green solid (0.32 g, 83%); R_f = 0.22 (1:1 ethyl acetate: *n*-hexane); ^{1}H NMR (400 MHz, $CDCl_3$): δ 6.32-5.86 (m, 8H, 4 x C*H*=C*H*), 4.70-3.96 (m, 4H, 4 x C*H*N), 3.38-3.10 (m, 16H, 16 x C*H*), 1.79-1.41 (m, 8H, 4 x CH_2), 0.87 (br s, 36H, 4 x C(CH_3)$_3$); ^{13}C NMR (100 MHz, $CDCl_3$): δ 186.0 (*C*OO), 176.4, 175.2 (*C*ON), 135.1, 132.0 (*C*H=*C*H), 60.9 (N*C*H), 50.7 (*C*H_2), 45.5, 44.4 (*C*H), 43.9 43.7 (*C*H), 34.2 (*C*(CH_3)$_3$), 26.8 (C(*C*H_3)$_3$); IR (film) ν 2961, 1703, 1610, 1398, 1372, 1345, 1172, 1039, 803, 778, 692 cm^{-1}; MS (ESI) *m/z*: 1315.9 ($C_{60}H_{80}N_4O_{16}Rh_2$ + 6H$^+$; calc. 1316.3), 1249.6 ($C_{60}H_{80}N_4O_{16}Rh_2$ + 5H$^+$ - C_5H_6; calc. 1249.3), 1183.2 ($C_{60}H_{80}N_4O_{16}Rh_2$ + 5H$^+$ - 2 x C_5H_6; calc. 1183.2), 1037.5 ($C_{60}H_{80}N_4O_{16}Rh_2$ + 4H$^+$ - $C_{15}H_{20}NO_4$; calc. 1038.2), 971.1 ($C_{60}H_{80}N_4O_{16}Rh_2$ + 3H$^+$ - $C_{15}H_{20}NO_4$ - C_5H_6; calc. 971.1), 759.1 ($C_{60}H_{80}N_4O_{16}Rh_2$ + H$^+$ - 2 x $C_{15}H_{20}NO_4$; calc. 759.0).

Recrystallization of Rh_2(*S*-BHTL)$_4$ (13)

Single crystal X-ray diffraction quality crystals of Rh_2(*S*-BHTL)$_4$ were obtained by dissolving the pure complex (~40 mg) in ACN (~1 mL). The resulting solution was subjected to sonication and Pasteur pipette filtration. Pale green needles were obtained by the slow evaporation of the solvent and used directly for measurement. Single crystal X-ray diffraction was recorded on MX1 beamline at the Australian Synchrotron, Victoria. Data collection and refinement were carried out using the general X-ray crystallographic conditions described earlier.

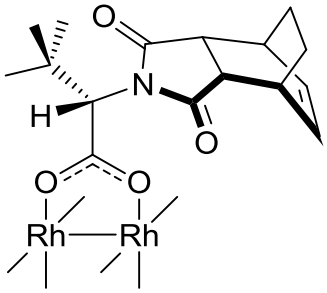

Dirhodium(II,II) tetrakis[*N*-(*endo*-bicyclo[2.2.2]oct-5-ene-2,3-oyl)-(*S*)-*tert*-Leucinate] (Rh_2(*S*-BOTL)$_4$, 14)

Ligand (0.53 g, 1.82 mmol), $Rh_2(OAc)_4$ (0.13 g, 0.30 mmol); green solid (0.38 g, 92%); R_f = 0.34 (1:1 ethyl acetate: *n*-hexane); ^{1}H NMR (400 MHz, $CDCl_3$): δ 6.15 (br s, 8H, C*H*=C*H*), 4.41 (br s, 4H, 4 x C*H*N), 3.11 (br s, 8H, 8 x C*H*), 2.73 (br s, 8H, 8 x C*H*), 1.56 (br s, 8H, 4 x CH_2), 1.36 (br s, 8H, 4 x CH_2), 1.05 (s, 36H, 4 x C(CH_3)$_3$); ^{13}C NMR (100 MHz, $CDCl_3$): δ 185.5, 185.3 (*C*OO), 177.8, 176.2 (*C*ON), 132.9, 132.0, 131.8, 129.6, 128.7, 127.6, 127.0, 125.3 (*C*H=*C*H), 60.7 (N*C*H), 43.77, 43.15, 42.9, 42.7, 42.5 (*C*H), 34.4 (*C*(CH_3)$_3$), 30.6 (*C*H), 26.8 (C(*C*H_3)$_3$), 22.8 (*C*H_2); IR (film) ν 2953, 2868, 1703, 1612, 1375, 1174, 781, 695 cm^{-1}; MS (ESI) *m/z*: 1372.3 ($C_{64}H_{86}N_4O_{16}Rh_2$ + 6H$^+$; calc. 1372.4), 1079.7 ($C_{64}H_{86}N_4O_{16}Rh_2$ + 4H$^+$ - $C_{16}H_{20}NO_4$; calc. 1080.2), 787.2 ($C_{64}H_{86}N_4O_{16}Rh_2$ + H$^+$ - 2 x $C_{16}H_{20}NO_4$; calc. 787.1).

Recrystallization of Rh_2(*S*-BOTL)$_4$ (14)

Single crystal X-ray diffraction quality crystals of Rh_2(*S*-BOTL)$_4$ were obtained by dissolving the pure complex (~40 mg) in MeOH (~1 mL). The resulting solution was subjected to sonication and Pasteur pipette filtration. Pale green needles were obtained by the slow evaporation of the solvent and used directly for measurement. Single crystal X-ray diffraction was recorded on MX1 beamline at the Australian Synchrotron, Victoria. Data collection and refinement were carried out using the general X-ray crystallographic conditions described earlier.

Recrystallization of Rh_2(*S*-PTAD)$_4$

For the purpose of crystal structure comparisons, single crystal X-ray diffraction quality crystals of Rh_2(*S*-PTAD)$_4$ were obtained using the "vapour diffusion

crystallization" method. The complex (~40 mg) was transferred to a small glass vial and dissolved in EtOAc (~1 mL). The small vial containing the complex was placed in a larger glass vial containing *n*-hexane and the large vial was then sealed. Green needles crystals were obtained by the slow diffusion of *n*-hexane into ethyl acetate and were used directly for data collection. Single crystal X-ray diffraction data were collected on MX1 beamline at the Australian Synchrotron, Victoria.

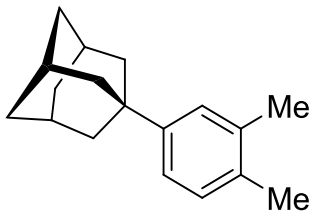

4-Adamantyl-*o*-xylene (38)[117]

To a stirred mixture of 1-bromo-adamantane (8.0 g, 37.2 mmol) in *o*-xylene (8.4 mL, 69.5 mmol), $ZnCl_2$ (1.68 g, 12.3 mmol) was added and the resulting mixture was refluxed overnight. After the mixture was allowed to cool down to room temperature, a solution of 8% HCl (88 mL) was added followed by the addition of ice-cold water. The aqueous layer was extracted with DCM three times and the combined organic layers were dried over anhydrous Na_2SO_4, filtered and evaporated *in vacuo*. The black residue was subjected to silica gel column chromatography using ethyl acetate: *n*-hexane as a mobile phase to afford the title compound as a white solid (6.5 g, 73%); mp 109-110 ^oC; R_f = 0.54 (*n*-hexane); ^1H NMR (400 MHz, $CDCl_3$): δ 7.37 (s, 1H, Ar-*H*), 7.32 (s, 2H, Ar-*H*), 2.50 (s, 3H, CH_3), 2.46 (s, 3H, CH_3), 2.32 (s, 3H, 3 x Ad-C*H*), 2.15 (s, 6H, 3 x Ad-CH_2), 2.00 (s, 6H, 3 x Ad-CH_2); ^{13}C NMR (100 MHz, $CDCl_3$): δ 149.2, 136.1, 133.7, 129.6, 126.4, 122.4 (6 x Ar-*C*), 43.5 (3 x Ad-*C*H_2), 37.1 (3 x Ad-*C*H_2) 35.9 (Ad-*C*), 29.3 (3 x Ad-*C*H), 20.3, 19.5 (2 x *C*H_3); IR (KBr) ν 2897, 2846, 1504, 1448, 1342, 802 cm^{-1}.

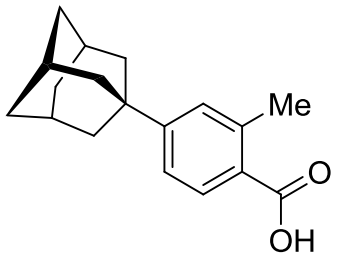

4-(1-Adamantyl)-2-methylbenzoic acid (40)

To a stirred solution of $Co(OAc)_2.4H_2O$ (93 mg, 0.374 mmol), $Mn(OAc)_2.4H_2O$ (10 mg, 0.042 mmol), NaBr (43 mg, 0.416 mmol) and 4-adamantyl-*o*-xylene (1 g, 4.16 mmol) in acetic acid (20 mL) and 1,4-dioxane (2 mL) maintained at 90 ^oC, oxygen gas was introduced by bubbling through the reaction mixture. After 2 h, the reaction solvent was evaporated and the residue was purified by means of column chromatography using ethyl acetate: *n*-hexane as a mobile phase to afford the title compound as a white solid (0.95 g, 76%); mp 280 ^oC; R_f = 0.42 (1:3 ethyl acetate: *n*-hexane); ^1H NMR (400 MHz, DMSO-d_6): δ 7.74 (d, 1H, J = 6.3 Hz, Ar-*H*), 7.23 (br s, 2H, Ar-*H*), 2.49 (s, 3H, CH_3), 2.02 (s, 3H, 3 x Ad-C*H*), 1.83 (s, 6H, 3 x Ad-CH_2), 1.70 (s, 6H, 3 x Ad-CH_2); ^{13}C NMR (100 MHz, DMSO-d_6): δ 168.9 (*C*OOH), 155.1, 139.4, 130.8, 128.5, 122.7 (6 x Ar-*C*), 42.7 (3 x Ad-CH_2), 36.5 (3 x Ad-CH_2), 36.2 (Ad-*C*), 28.6 (3 x Ad-*C*H), 21.7 (CH_3) ; IR (KBr) ν 2908, 2846, 1685, 1276 cm^{-1}; MS (ESI) *m/z*: 269.2 ($C_{18}H_{21}O_2^-$, calc. 269.15).

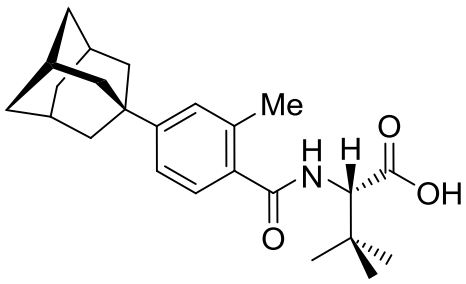

(*S*)-2-(4-Adamantyl-2-methylbenzamido)-3,3-dimethylbutanoic acid (41)

A solution of 4-(1-adamantyl)-2-methylbenzoic acid (**40**, 191 mg, 0.64 mmol) in acetic anhydride (2 mL) was allowed to reflux for 4 h. After that time, the acetic anhydride was evaporated *in vacuo* and the residue was re-dissolved in toluene. L-*tert*-Leucine (92 mg, 0.7 mmol) and triethylamine (8.87 µL, 0.064 mmol) were added and the resulting mixture was allowed to reflux for another 18 h. After this

time has elapsed, the reaction mixture was diluted with ethyl acetate, washed twice with 0.1M hydrochloric acid solution, dried over anhydrous Na_2SO_4, filtered and concentrated *in vacuo* to afford the product as a yellowish oil (227 mg, 86%); ^{1}H NMR (400 MHz, $CDCl_3$): δ 12.54 (br s, 1H, COO*H*), 7.92 (d, J_{CH} = 8.8 Hz, 1H, N*H*), 7.74 (d, *J* = 8.7 Hz, 2H, Ar-*H*), 7.38 (d, *J* = 7.8 Hz, 1H, Ar-*H*), 4.06 (d, J_{NH} = 8.9 Hz, 1H, C*H*), 2.48 (s, 3H, CH_3), 2.00 (s, 3H, 3 x Ad-C*H*), 1.80 (s, 6H, 3 x Ad-CH_2), 1.68 (s, 6H, 3 x Ad-CH_2), 0.90 (s, 9H, C(CH_3)$_3$).

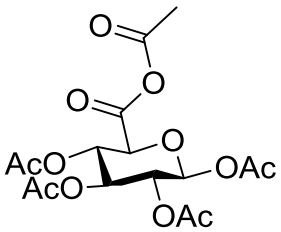

1,2,3,4-Tetra-*O*-acetyl-*β*-D-glucopyranuronic acetic anhydride (45)[128,129]

To a stirred suspension of D-glucuronic acid (2 g, 10.30 mmol) in acetic anhydride (30 mL) stirred at 0 ^{o}C, iodine (140 mg, 0.55 mmol) was added and the solution was left to stir for 30 min at 0 ^{o}C. After that time, the reaction was allowed to stir for another 2 h at room temperature at which time the reddish solution became completely clear. Acetic anhydride was mostly removed under reduced pressure and the formed solid was re-dissolved in DCM (50 mL). The organic layer was washed with 1M $Na_2S_2O_3$ solution (2 x 30 mL), dried over anhydrous Na_2SO_4, filtered and concentrated *in vacuo* to afford the title compound as a white solid (4.08 g, 98%). ^{1}H NMR (270 MHz, $CDCl_3$): δ 5.80 (d, 1H, $J_{1\text{-}2}$ = 6.9 Hz, H-1), 5.32 (m, 2H, H-3 and H-4 overlapping), 5.12 (apt t, 1H, H-2), 4.31 (d, 1H, $J_{5\text{-}4}$ = 8.7 Hz, H-5), 2.28 (s, 3H, COCOOCH_3), 2.13 (s, 3H, COCH_3), 2.05 (s, 6H, 2 x COCH_3), 2.04 (s, 3H, COCH_3). The spectroscopic data were consistent with previously reported data.[128,129]

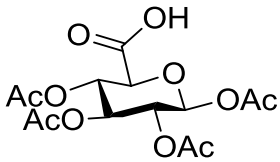

1,2,3.4-Tetra-*O*-acetyl-*β*-D-glucopyranuronic acid (46)[128,129]

1,2,3,4-Tetra-*O*-acetyl-*β*-D-glucuronic acetic anhydride (4.08 g, 10.09 mmol) was dissolved in a mixture of water and THF (90 mL, 1:2) and left to stir overnight. After that time, THF was mostly evaporated *in vacuo* and the product was extracted into DCM (3 x 30 mL) from the residual aqueous solution. The combined organic layers were dried over anhydrous Na_2SO_4, filtered and evaporated *in vacuo* to yield the title compound as a white foam (3.61 g, 99%). ^{1}H NMR (270 MHz, DMSO-d_6): δ 6.00 (d, 1H, $J_{1\text{-}2}$ = 8.1 Hz, H-1), 5.48 (apt t, 1H, H-3), 5.05 (apt t, 1H, H-4), 4.95 (apt t, 1H, H-2), 4.52 (d, 1H, $J_{5\text{-}4}$ = 8.2 Hz, H-5), 3.44 (br s, 1H, COO*H*), 2.08 (s, 3H, COCH_3), 2.01 (s, 3H, COCH_3), 1.97 (s, 6H, 2 x COCH_3). The spectroscopic data were consistent with previously reported data.[128,129]

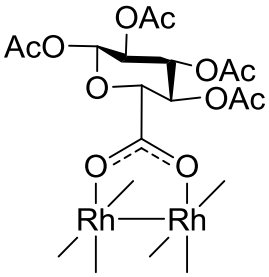

Dirhodium(II) tetrakis[1,2,3.4-tetra-*O*-acetyl-*β*-D-Glucopyranuronate] (Rh_2(*β*-D-TAGA)$_4$, 47)

To a stirred solution of $Na_4Rh_2(CO_3)_4.2.5H_2O$ (0.02 g, 0.035 mmol) in distilled H_2O (10 mL), 1,2,3.4-tetra-*O*-acetyl-*β*-D-glucopyranuronic acid (0.102 g, 0.283 mmol) was added and the reaction was kept at 60 ^oC for 6 h during which time, the deep blue color of the reaction mixture fades and turns into green. The reaction was then extracted with DCM, washed with saturated $NaHCO_3$ soution, dried over anhydrous Na_2SO_4, filtered and concentarted *in vacuo* to afford the title product as a green solid (31 mg, 53%); R_f = 0.44 (ethyl acetate); ^{1}H NMR (400 MHz, $CDCl_3$): δ 5.67 (d, 4H, $J_{1\text{-}2}$ = 6.5 Hz, H-1), 5.15 (apt t, 4H, H-3), 5.06 (apt t, 4H, H-4), 4.99 (m, 4H, H-2), 4.12 (d, 4H, $J_{5\text{-}4}$ = 9.2 Hz, H-5), 2.05 (s, 12H, 4 x COCH_3), 1.96 (s, 12H, 4 x

COC*H*$_3$), 1.94 (s, 24H, 8 x COC*H*$_3$); ^{13}C NMR (125 MHz, $CDCl_3$): δ 186.1 (*C*OO) 170.4, 169.6 (CH_3*C*O), 91.3 (*C*-1), 72.9 (*C*-5) 72.1, 70.7, 69.5, 69.3, 69.0, 68.7 (*C*-2–*C*-4), 21.8, 20.7 (*C*H_3CO); IR (film) ν 2935, 1759, 1620, 1427, 1373, 1219, 1076, 1041 cm^{-1}; MS (ESI) *m/z*: 1673.2 ($C_{56}H_{68}O_{44}Rh_2$ + Na^+; calc. 1673.1), 1371.2 ($C_{56}H_{68}O_{44}Rh_2$ + Na^+ - $C_{12}H_{14}O_9$; calc. 1371.1), 1069.1 ($C_{56}H_{68}O_{44}Rh_2$ + Na^+ - 2 x $C_{12}H_{14}O_9$; calc. 1069.1), 766.9 ($C_{56}H_{68}O_{44}Rh_2$ + Na^+ - 3 x $C_{12}H_{14}O_9$; calc. 767.0).

General procedure for the preparation of *donor-acceptor α*-diazophosphonate intermediates

Donor-acceptor α-diazophosphonate intermediates were prepared in three steps as follows:

a) Preparation of benzoylphosphonate derivatives[139]

These compounds were prepared *via* Arbuzov reaction where the corresponding acid chloride (1.1 equiv.) was added drop-wise to trimethyl, triethyl or tri*iso*propyl phosphite (1 equiv.) stirred at 0 ^{o}C. The reaction mixture was allowed to warm up to room temperature and was left to stir overnight. After that time, the unreacted phosphite was eliminated under high vacuum. Further product purification was carried out by means of silica gel column chromatography using ethyl acetate: *n*-hexane as a mobile phase to afford the corresponding pure benzoylphosphonate derivative.

b) Preparation of benzoylphosphonate tosylhydrazone derivatives[140]

To a stirred solution of tosylhydrazine (1 equiv.) in THF at 0 ^{o}C, concentrated HCl (0.5 equiv.) was added drop-wise. The resulting solution was stirred in an ice bath while the benzoylphoshonate derivative (1 equiv.) prepared in step (*a*) was added drop-wise over a period of 5 min. After allowing the reaction mixture to stir at room temperature overnight, the solvent was evaporated *in vacuo* and the residue was subjected to silica gel column chromatography using ethyl acetate: *n*-hexane as mobile phase to afford the corresponding benzoylphosphonate tosylhydrazone derivative.

c) Hydrolysis of benzoylphosphonate tosylhydrazone derivatives[140]

To a stirred suspension of benzoylphosphonate tosylhydrazone derivative (1 equiv.) prepared in step (*b*) in water, sodium carbonate (1.1 equiv.) was added. The reaction mixture was allowed to stir overnight during which time the hydrazone slowly dissolved and the solution became orange and opaque. The reaction mixture was extracted twice with diethyl ether and the combined organic layers were washed with deionized water, dried over anhydrous Na_2SO_4, filtered and concentrated *in vacuo* to afford the corresponding *α*-diazophosphonate derivative. The prepared *α*-diazophosphonate derivatives were stored at -20 ^{o}C and used in the next step without any further purification.

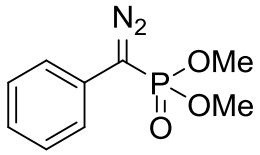

Dimethyl *α*-diazobenzylphosphonate (4)[140]

Orange oil; R_f = 0.13 (1:3 diethyl ether: *n*-hexane); ^{1}H NMR (400 MHz, $CDCl_3$): *δ* 8.23 (m, 1H, Ar-*H*), 8.08 (m, 1H, Ar-*H*), 7.66-7.42 (m, 3H, Ar-*H*), 3.85 (dd, 6H, J_{HP} = 54.3, *J* = 11.4 Hz, 2 x OCH_3). The spectroscopic data were consistent with previously reported data.[140]

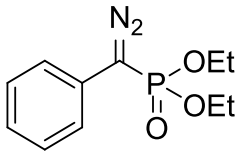

Diethyl *α*-diazobenzylphosphonate[141]

Orange oil; R_f = 0.20 (1:3 diethyl ether: *n*-hexane); ^{1}H NMR (400 MHz, $CDCl_3$): *δ* 7.31 (t, 2H, *J* = 7.9 Hz, Ar-*H*), 7.15-7.07 (m, 3H, Ar-*H*), 4.21-4.04 (m, 4H, 2 x OCH_2CH$_3$), 1.29 (td, 6H, *J* = 7.1, 0.7 Hz, 2 x OCH$_2$CH_3). The spectroscopic data were consistent with previously reported data.[141]

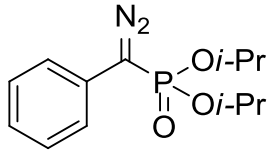

Di*iso*propyl *α*-diazobenzylphosphonate[142]

Orange oil; R_f = 0.30 (1:3 diethyl ether: *n*-hexane); ^{1}H NMR (400 MHz, $CDCl_3$): δ 7.30 (t, 2H, *J* = 7.8 Hz, Ar-*H*), 7.16-7.06 (m, 3H, Ar-*H*), 4.76-4.67 (m, 2H, 2 x C*H*(CH_3)$_2$), 1.36 (d, 6H, *J* = 6.2 Hz, CH(C*H*$_3$)$_2$), 1.21 (d, 6H, *J* = 6.3 Hz, CH(C*H*$_3$)$_2$). The spectroscopic data were consistent with previously reported data.[142]

General procedure for the preparation of cyclopropylphosphonate derivatives

To a stirred solution of the alkene (5 equiv.) and a dirhodium(II) catalyst (0.01 equiv.) in 2,2-DMB (3 mL) heated under reflux (59 ^{o}C) under nitrogen atmosphere, a solution of *α*-diazobenzylphosphonate (1 equiv.) in 2,2-DMB (10 mL) was added drop-wise *via* syringe pump over a period of 10 min. After the addition, the reaction was refluxed until the TLC indicated complete consumption of the diazo starting material. The diastereomeric ratio (dr) of the generated product was determined by ^{1}H NMR of the crude mixture. The product was purified by means of preparative TLC (ethyl acetate: *n*-hexane) and the enantiomeric excess (*ee* %) of the product was determined by chiral HPLC analysis.

General procedure for the preparation of cyclopropylphosphonate derivatives using Rh_2(*S*-^{tert}PTTL)$_4$ (12)

To a stirred solution of alkene (5 equiv.) and Rh_2(*S*-^{tert}PTTL)$_4$ (0.01 equiv.) in 2,2-DMB (3 mL) under nitrogen atmosphere, a solution of *α*-diazobenzylphosphonate (1 equiv.) in 2,2-DMB (10 mL) was added drop-wise *via* syringe pump over a period of 10 min. After the addition, the reaction was stirred at room temperature until the TLC indicated a complete consumption of the diazo starting material. The diastereomeric ratio (dr) of the generated product was determined by ^{1}H NMR of the crude mixture. The product was purified by means of preparative TLC (ethyl acetate: *n*-hexane) and the enantiomeric excess (*ee*%) of the product was determined by chiral HPLC analysis.

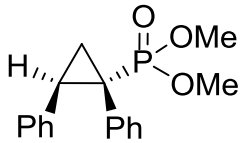

(*E*)-Dimethyl 1,2-diphenylcyclopropylphosphonate (5)[143,57]

Colourless oil; $[\alpha]_D^{25}$ = -0.25 (*c* 0.53, $CHCl_3$, 98% *ee*); R_f = 0.15 (1:1 ethyl acetate: *n*-hexane); ^{1}H NMR (400 MHz, $CDCl_3$): δ 7.00 (m, 3H, Ar-*H*), 6.99 (m, 5H, Ar-*H*), 6.68 (m, 2H, Ar-*H*), 3.67 (d, 3H, J_{HP} = 10.5 Hz, OCH_3), 3.62 (d, 3H, J_{HP} = 10.5 Hz, OCH_3), 2.95 (ddd, 1H, J_{HP} = 16.5, *J* = 8.8, 6.7 Hz, C*H*), 1.99 (ddd, 1H, J_{HP} = 17.3, *J* = 8.8, 5.1 Hz, CH_2), 1.66 (ddd, 1H, J_{HP} = 12.2, *J* = 6.7, 5.1 Hz, CH_2). The spectroscopic data were consistent with previously reported data.[143,57] The enantiomeric excess was determined by chiral HPLC (Chiralcel® OJ column, 25 x 0.46 cm, 2% 2-propanol in *n*-hexane (*v*/*v*%); 1 mL/min, 220 nm, τ_1 = 18 min, τ_2 = 21 min).

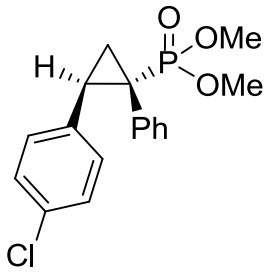

(*E*)-Dimethyl 1-pheny-2-(*p*-chlorophenyl)cyclopropylphosphonate (19)[57]

Colourless oil; $[\alpha]_D^{25}$ = -0.54 (*c* 0.87, $CHCl_3$, 98% *ee*); R_f = 0.11 (1:1 ethyl acetate: *n*-hexane); ^{1}H NMR (400 MHz, $CDCl_3$): δ 7.14-7.11 (m, 3H, Ar-*H*), 7.04 (m, 2H, Ar-*H*), 7.01 (d, 2H, *J* = 8.5 Hz, Ar-*H*), 6.64 (d, 2H, *J* = 8.4 Hz, Ar-*H*), 3.70 (d, 3H, J_{HP} = 10.6 Hz, OCH_3), 3.66 (d, 3H, J_{HP} = 10.6 Hz, OCH_3), 2.96 (ddd, 1H, J_{HP} = 16.5, *J* = 8.8, 6.7 Hz, C*H*), 2.06 (ddd, 1H, J_{HP} = 17.4, *J* = 9.0, 5.3 Hz, CH_2), 1.66 (ddd, 1H, J_{HP} = 12.4, *J* = 6.5, 5.3 Hz, CH_2). The spectroscopic data were consistent with previously reported data.[57] The enantiomeric excess was determined by chiral HPLC (Chiralcel® OJ column, 25 x 0.46 cm, 8% 2-propanol in *n*-hexane (*v*/*v*%); 1 mL/min, 220 nm, τ_1 = 10 min, τ_2 = 12 min).

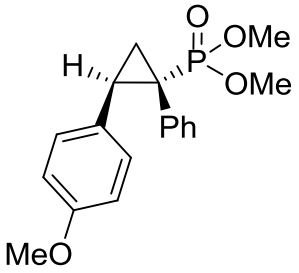

(*E*)-Dimethyl 1-pheny-2-(*p*-methoxyphenyl)cyclopropylphosphonate (20)[57]

Colourless oil; $[\alpha]_D^{25}$ = -0.57 (*c* 1, $CHCl_3$, 99% *ee*); R_f = 0.11 (1:1 ethyl acetate: *n*-hexane); ^{1}H NMR (400 MHz, $CDCl_3$): δ 7.12-7.10 (m, 3H, Ar-*H*), 7.05 (m, 2H, Ar-*H*), 6.62 (dd, 4H, *J* = 23.0, 8.9 Hz, Ar-*H*), 3.71 (d, 3H, J_{HP} = 10.6 Hz, OCH_3), 3.68 (s, 3H, OCH_3), 3.66 (d, 3H, J_{HP} = 10.6 Hz, OCH_3), 2.96 (ddd, 1H, J_{HP} = 16.1, *J* = 9.1, 6.6 Hz, C*H*), 2.03 (ddd, 1H, J_{HP} = 17.5, *J* = 9.1, 5.2 Hz, CH_2), 1.64 (ddd, 1H, J_{HP} = 12.4, *J* = 6.5, 5.3 Hz, CH_2). The spectroscopic data were consistent with previously reported data.[57] The enantiomeric excess was determined by chiral HPLC (Chiralcel® OJ column, 25 x 0.46 cm, 3% 2-propanol in *n*-hexane (*v*/*v*%); 1 mL/min, 220 nm, τ_1 = 37 min, τ_2 = 42 min).

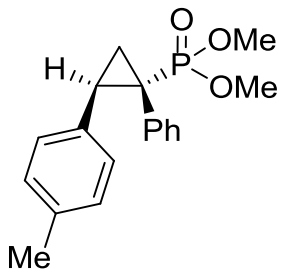

(*E*)-Dimethyl 1-pheny-2-(*p*-methylphenyl)cyclopropylphosphonate (21)

White solid; $[\alpha]_D^{25}$ = -0.57 (*c* 0.93, $CHCl_3$, 99% *ee*); R_f = 0.17 (1:1 ethyl acetate: *n*-hexane); ^{1}H NMR (400 MHz, $CDCl_3$): δ 7.13-7.10 (m, 3H, Ar-*H*), 7.07-7.04 (m, 2H, Ar-*H*), 6.85 (d, 2H, *J* = 7.8 Hz, Ar-*H*), 6.61 (d, 2H, *J* = 8.2 Hz, Ar-*H*), 3.72 (d, 3H, J_{HP} = 10.6 Hz, OCH_3), 3.66 (d, 3H, J_{HP} = 10.6 Hz, OCH_3), 2.97 (ddd, 1H, J_{HP} = 16.1, *J* = 9.1, 6.6 Hz, C*H*), 2.19 (s, 3H, CH_3), 2.03 (ddd, 1H, J_{HP} = 17.5, *J* = 9.0, 5.1 Hz, CH_2), 1.67 (ddd, 1H, J_{HP} = 12.5, *J* = 6.6, 5.1 Hz, CH_2). The enantiomeric excess was determined by chiral HPLC (Chiralcel® OJ column, 25 x 0.46 cm, 3% 2-propanol in *n*-hexane (*v*/*v*%); 1 mL/min, 220 nm, τ_1 = 12 min, τ_2 = 15 min).

Recrystallization of (1*S*, 2*R*)-dimethyl 1-pheny-2-(*p*-methylphenyl)cyclopropyl-phosphonate (21)

Single crystal X-ray quality crystals of **21** were obtained by dissolving ~0.1 g of the prepared compound from $Rh_2(S\text{-}^{tert}PTTL)_4$ (**12**) in ethyl acetate: *n*-hexane (1:3) mixture (~2 mL). The resulting solution was subjected to sonication and Pasteur pipette filtration. Colourless crystals were obtained by the slow evaporation of the solvent and it was used directly for measurement. Single crystal X-ray diffraction data were collected on Nonius KappaCCD diffractometer equipped with Graphite monochromated MoK_α radiation (λ = 0.71073 Å).

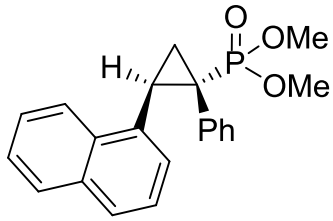

(*E*)-Dimethyl 1-pheny-2-(1-naphthyl)cyclopropylphosphonate (22)

Colourless oil; $[\alpha]_D^{25}$ = -0.24 (*c* 0.5, $CHCl_3$, 98% *ee*); R_f = 0.14 (1:1 ethyl acetate: *n*-hexane); ^{1}H NMR (400 MHz, $CDCl_3$): δ 7.72-7.53 (m, 2H, Ar-*H*), 7.50 (d, 1H, *J* = 7.50 Hz, Ar-*H*), 7.35 (m, 2H, Ar-*H*), 7.29 (s, 1H, Ar-*H*), 7.07 (m, 4H, Ar-*H*), 6.76 (dd, 1H, *J* = 8.5, 1.8 Hz, Ar-*H*), 3.75 (d, 3H, J_{HP} = 10.6 Hz, OCH_3), 3.70 (d, 3H, J_{HP} = 10.6 Hz, OCH_3), 3.16 (ddd, 1H, J_{HP} = 16.1, *J* = 9.1, 6.6 Hz, C*H*), 2.14 (ddd, 1H, J_{HP} = 17.5, *J* = 9.0, 5.3 Hz, CH_2), 1.85 (ddd, 1H, J_{HP} = 12.5, *J* = 6.6, 5.1 Hz, CH_2). The enantiomeric excess was determined by chiral HPLC (Chiralpak® AD column, 25 x 0.46 cm, 1% 2-propanol in *n*-hexane (*v*/*v*%); 2 mL/min, 220 nm, τ_1 = 36 min, τ_2 = 42 min).

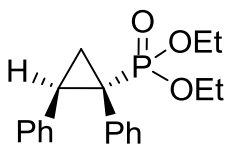

(*E*)-Diethyl 1,2-diphenylcyclopropylphosphonate (23)[57]

Colourless oil; $[\alpha]_D^{25}$ = -0.11 (*c* 0.4, $CHCl_3$, 92% *ee*); R_f = 0.26 (1:1 ethyl acetate: *n*-hexane); ^{1}H NMR (400 MHz, $CDCl_3$): δ 7.11-7.07 (m, 4H, Ar-*H*), 7.06-7.01 (m, 4H,

Ar-*H*), 6.72 (m, 2H, Ar-*H*), 4.11-3.95 (m, 4H, 2 x OC*H*$_2$CH$_3$), 2.98 (ddd, 1H, J_{HP} = 16.5, *J* = 8.8, 6.5 Hz, C*H*), 1.99 (ddd, 1H, J_{HP} = 17.5, *J* = 9.0, 5.1 Hz, C*H*$_2$), 1.68 (ddd, 1H, J_{HP} = 12.2, *J* = 6.7, 5.1 Hz, C*H*$_2$), 1.26 (td, 3H, *J* = 7.0, 0.4 Hz, OCH$_2$C*H*$_3$), 1.22 (td, 3H, *J* = 7.0, 0.5 Hz, OCH$_2$C*H*$_3$). The spectroscopic data were consistent with previously reported data.[57] The enantiomeric excess was determined by chiral HPLC (Chiralpak® AD column, 25 x 0.46 cm, 0.6% 2-propanol in *n*-hexane (*v/v*%); 0.8 mL/min, 220 nm, τ_1 = 69 min, τ_2 = 76 min).

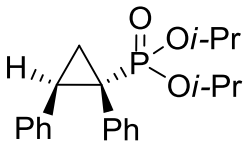

(*E*)-Di*iso*propyl 1,2-diphenylcyclopropylphosphonate (24)[57]

Colourless oil; R$_f$ = 0.40 (1:1 ethyl acetate: *n*-hexane); ^{1}H NMR (400 MHz, CDCl$_3$): δ 7.08 (m, 5H, Ar-*H*), 7.02 (m, 3H, Ar-*H*), 6.73 (m, 2H, Ar-*H*), 4.67-4.56 (m, 2H, 2 x C*H*(CH$_3$)$_2$), 2.95 (ddd, 1H, J_{HP} = 16.8 Hz, *J* = 8.9, 6.5 Hz, C*H*), 2.02 (ddd, 1H, J_{HP} = 17.5, *J* = 8.9, 5.1 Hz, C*H*$_2$), 1.67 (ddd, 1H, J_{HP} = 12.4 Hz, *J* = 6.5, 5.0 Hz, C*H*$_2$), 1.27 (d, 3H, *J* = 2.0 Hz, CH(C*H*$_3$)$_2$), 1.25 (d, 3H, *J* = 2.0 Hz, CH(C*H*$_3$)$_2$), 1.23 (d, 3H, *J* = 6.2 Hz, CH(C*H*$_3$)$_2$), 1.19 (d, 3H, *J* = 6.2 Hz, CH(C*H*$_3$)$_2$). The spectroscopic data were consistent with previously reported data.[57] The enantiomeric excess was determined by chiral HPLC (Chiralpak® AD column, 25 x 0.46 cm, 0.6% 2-propanol in *n*-hexane (*v/v*%); 0.8 mL/min, 220 nm, τ_1 = 49 min, τ_2 = 54 min).

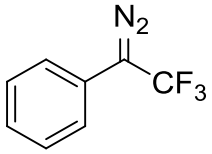

1-Phenyl-2,2,2-triflurodiazoethane (25)

1-Phenyl-2,2,2-triflurodiazoethane (**25**) was prepared in three steps using a modified literature procedure as follows:

a) Preparation of 4-methyl-N'-(2,2,2-trifluoro-1-phenylethylidene) benzene-sulfonohydrazide[96]

To a solution of 2,2,2-trifluoroacetophenone (0.36 mL, 2.6 mmol) in ethanol (5 mL) stirred at room temperature, *p*-toluenesulfonylhydrazide (0.410 g, 2.2 mmol) and 2 drops of acetic acid were added. The reaction mixture was stirred at room temperature until it became a clear solution. A condenser was then attached and the contents were heated to reflux for 8 h. After that time, the reaction mixture was diluted with ice cold water (10 mL) and left to stir at room temperature for another 10 min. During that time, white lumps of product are formed which was collected by filtration, washed with distilled water and dried under vacuum (0.374 g, 43%). The dry product was directly used in the next step without any further purification.

b) Hydrolysis of 4-methyl-N'-(2,2,2-trifluoro-1-phenylethylidene)benzene-sulfonohydrazide[96,144]

A solution of potassium hydroxide (0.325 g, 5.8 mmol) in MeOH (7.5 mL) was prepared by stirring at room temperature. To the prepared solution, 4-methyl-*N'*-(2,2,2-trifluoro-1-phenylethylidene)benzenesulfonohydrazide (1 g, 2.9 mmol) from step (*a*) was added in one portion and the reaction mixture was then refluxed for 4 h, during which time, the reaction mixture colour turned into orange. After this time has elapsed, the mixture was diluted with ice cold water (7.5 mL) and extracted with DCM twice. The combined organic layers were dried over anhydrous Na_2SO_4, filtered and concentrated *in vacuo* at room temperature to afford the desired 1-phenyl-2,2,2-triflurodiazoethane product (**25**) as an orange oil (0.327 g, 60%). The product was further purified on silica gel column chromatography using *n*-hexane as a mobile phase and stored at -20 ^{o}C. ^{1}H NMR (400 MHz, $CDCl_3$): δ 7.42-7.38 (m,

2H, Ar-*H*), 7.22-7.18 (m, 1H, Ar-*H*), 7.10 (d, *J* = 8.4 Hz, Ar-*H*). The spectroscopic data were consistent with previously reported data.[96,144]

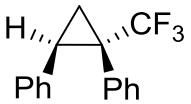

(*E*)-1-Trifluoromethyl-1,2-diphenylcyclopropane (26)[96]

To a solution of the styrene (5.0 equiv.) and a dirhodium(II) catalyst (0.02 equiv.) in dry and degassed TFT (3 mL) under nitrogen atmosphere, 1-phenyl-2,2,2-triflurodiazoethane (**25**, 1.0 equiv.) dissolved in dry and degassed TFT (2 mL) was added drop-wise over a period of 10 min using a syringe pump. The reaction was stirred for another hour, after which time, the reaction solvent was removed under reduced pressure. The diastereomeric ratio (dr) of the generated product was determined by ^{1}H NMR of the crude mixture. The product was purified by means of preparative TLC using *n*-hexane as an eluent. White solid; R_f = 0.29 (*n*-hexane); ^{1}H NMR (400 MHz, $CDCl_3$): δ 7.13-6.99 (m, 8H, Ar-*H*), 6.71-6.69 (m, 2H, Ar-*H*), 2.77 (dd, 1H, *J* = 9.6, 7.0 Hz, C*H*), 1.81 (dd, 1H, *J* = 9.6, 5.9 Hz, CH_2), 1.61 (m, 1H, CH_2). The spectroscopic data were consistent with previously reported data.[96] The enantiomeric excess was determined by chiral HPLC (Chiralcel® OJ column, 25 x 0.46 cm, 1% 2-propanol in *n*-hexane (*v/v*%); 0.8 mL/min, 220 nm, τ_1 = 6.5 min, τ_2 = 7.8 min).

Recrystallization of (1*S*, 2*R*)-1-trifluoromethyl-1,2-diphenylcyclopropane (26)

Single crystal X-ray quality crystals of **26** were obtained by dissolving ~0.05 g of the compound prepared from Rh_2(*S*-^{tert}PTTL)$_4$ (**12**) in IPA (~2 mL). Colourless crystals were obtained by the slow evaporation of the solvent which was used directly for measurement. Single crystal X-ray diffraction data were collected on Agilant SuperNova Dual diffractometer equipped with mirror monochromated CuK_α radiation (λ = 1.54180 Å).

Preparation of *α*-diazocarboxylate intermediates

These compounds were prepared *via* Regitz diazo transfer reaction as follows:

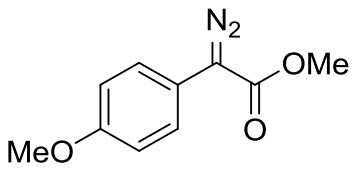

Methyl *α*-diazo-2-(*p*-methoxyphenyl)acetate (27)[145]

To a stirred solution of methyl *p*-methoxyphenylacetate (0.5 mL, 3.15 mmol) and *p*-ABSA (0.908 g, 3.78 mmol) in ACN at 0 ^{o}C, DBU (0.57 mL, 3.78 mmol) was added drop-wise. The reaction mixture was allowed to stir at room temperature overnight. The reaction solvent was then evaporated *in vacuo* and the residue was purified by means of silica gel column chromatography using *n*-hexane as eluent to give the title compound as orange oil (0.55 g, 85% yield) which was stored at -20 ^{o}C. R_f = 0.56 (1:3 diethyl ether: *n*-hexane); ^{1}H NMR (400 MHz, $CDCl_3$): δ 7.30 (d, 2H, J = 8.9 Hz, Ar-*H*), 6.86 (d, 2H, J = 8.9 Hz, Ar-*H*), 3.77 (s, 3H, CH_3), 3.73 (s, 3H, CH_3). The spectroscopic data were consistent with previously reported data.[145]

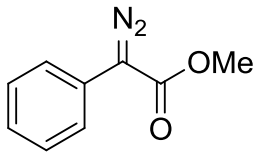

Methyl *α*-diazo-2-phenylacetate (29)[145,146]

To a stirred solution of methyl phenylacetate (1.4 mL, 10 mmol) and *p*-ABSA (2.88 g, 12 mmol) in ACN at 0 ^{o}C, DBU (1.83 mL, 12 mmol) was added drop-wise. The reaction mixture was allowed to stir at room temperature for 2 h. The reaction solvent was then evaporated *in vacuo* and the residue was purified by means of silica gel column chromatography using diethyl ether: *n*-hexane (1:10) as eluent to give the title compound as orange oil (1.3 g, 73% yield) which was stored at -20 ^{o}C. R_f = 0.60 (1:9 diethyl ether: *n*-hexane); ^{1}H NMR (400 MHz, $CDCl_3$): δ 7.42-7.39 (m, 3H, Ar-*H*), 7.33-7.29 (m, 2H, Ar-*H*), 3.79 (s, 3H, CH_3). The spectroscopic data were consistent with previously reported data.[145,146]

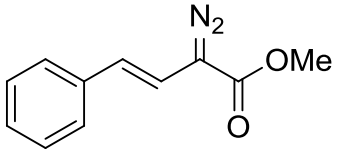

(*E*)-Methyl *α*-diazo-4-phenylbut-3-enoate (31)

(*E*)-Methyl *α*-diazo-4-phenylbut-3-enoate (**31**) was prepared in three steps as follows:

a) Preparation of (E)-4-phenylbut-3-enoic acid[147]

It was prepared using a modified procedure of Hoye and co-workers.[147] To a stirred solution of malonic acid (52.03 g, 0.5 mol) in pyridine (40.6 mL, 0.5 mol) under nitrogen atmosphere, phenyl acetaldehyde (29.5 mL, 0.25 mol) was added. After allowing the reaction mixture to stir at room temperature for 1 h, at which time, it was refluxed for extra 18 h. After that, the reaction mixture was diluted with ethyl acetate and the organic layer was washed with water and 10% HCl solution. The organic layer was then washed 2M NaOH solution twice and the separated aqueous layers were combined, acidified with concentrated H_2SO_4 to pH 1.5 and extracted with ethyl acetate three times. The combined organic layers were dried over anhydrous Na_2SO_4, filtered and concentrated *in vacuo* to give the title compound as a white solid (34 g, 84% yield). R_f = 0.51 (1:1 ethyl acetate: *n*-hexane); ^{1}H NMR (400 MHz, $CDCl_3$): δ 7.30-7.15 (m, 5H, Ar-*H*), 6.43 (d, 1H, *J* = 15.9 Hz, C*H*=CH-CH_2), 6.20 (dt, 1H, *J* = 15.9, 7.1 Hz, CH=C*H*-CH_2), 3.21 (dd, 2H, *J* = 7.1, 1.5 Hz, CH_2). The spectroscopic data were consistent with previously reported data.[147]

b) Preparation (E)-methyl 4-phenylbut-3-enoate[147]

To a stirring solution of 4-phenyl-3-butenoic acid (30 g, 184.8 mmol) from (*a*) in MeOH (375 mL) under nitrogen, acetyl chloride (15 mL) was added and the reaction mixture was allowed to stir for 12 h at room temperature. The reaction solvent was then evaporated *in vacuo* and the residue was re-dissolved in DCM, washed with saturated $NaHCO_3$ solution and brine, dried over anhydrous Na_2SO_4, filtered and concentrated *in vacuo* to give the desired compound as colourless oil (31 g, 96% yield). R_f = 0.7 (1:1 ether: petroleum ether); ^{1}H NMR (400 MHz, $CDCl_3$): δ 7.30-7.15 (m, 5H, Ar-*H*), 6.42 (d, 1H, *J* = 15.9 Hz, C*H*=CH-CH_2), 6.22 (dt, 1H, *J* = 15.9,

7.1 Hz, CH=C*H*-CH_2), 3.64 (s, 3H, CH_3), 3.18 (dd, 2H, *J* = 7.1, 1.3 Hz, CH_2). The spectroscopic data were consistent with previously reported data.[147]

c) Preparation of (E)-methyl α-diazo-4-phenylbut-3-enoate[148]

To a stirred solution of (*E*)-methyl 4-phenylbut-3-enoate (13.0 g, 73.8 mmol) from (*b*) and *p*-ABSA (21.3g, 88.5 mmol) in ACN at 0 ^{o}C, DBU (12.1 mL, 81.2 mmol) was added drop-wise. The reaction mixture was allowed to stir at room temperature for 2 h, at which time, it was quenched with saturated ammonium chloride solution. The aqueous layer was extracted with diethyl ether three times and the combined organic layers were washed with brine, dried over anhydrous Na_2SO_4, filtered and concentrated *in vacuo*. The residue was purified by means of silica gel column chromatography using diethyl ether: *n*-hexane (1:10) as eluent to give the title compound as red solid (12.0 g, 80% yield) which was stored at -20 ^{o}C. R_f = 0.64 (1:3 diethyl ether: *n*-hexane); ^{1}H NMR (400 MHz, $CDCl_3$): δ 7.38-7.18 (m, 5H, Ar-*H*), 6.41 (d, 1H, *J* = 16.3 Hz, C*H*=CH-C), 6.13 (d, 1H, *J* = 16.3 Hz, CH=C*H*-C), 3.78 (s, 3H, CH_3). The spectroscopic data were consistent with previously reported data.[148]

General procedure for the preparation of cyclopropylcarboxylates

To a solution of styrene (5.0 equiv.) and a dirhodium(II) catalyst (0.01 equiv.) in dry and degassed solvent under nitrogen atmosphere, the diazo compound (1.0 equiv.) dissolved in the same dry and degassed solvent was added drop-wise over a period of 10 min *via* syringe pump. After the addition, the mixture was stirred for at least one hour. When the diazo compound was fully consumed as indicated by TLC, the reaction solvent was removed *in vacuo*. The diastereomeric ratio (dr) of the generated product was determined by ^{1}H NMR of the crude mixture. The product was the purified by means of preparative TLC using ethyl acetate: *n*-hexane and the enantiomeric excess (*ee*%) of the product was determined by chiral HPLC analysis.

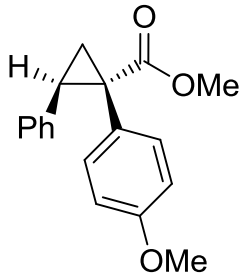

(*E*)-Methyl 1-*p*-methoxyphenyl-2-phenylcyclopropanecarboxylate (28)[105]

Colourless oil; R_f = 0.52 (1:4 ethyl acetate: *n*-hexane); ^{1}H NMR (400 MHz, $CDCl_3$): δ 7.10-7.07 (m, 3H, Ar-*H*), 6.95 (d, 2H, *J* = 8.8 Hz, Ar-*H*), 6.80-6.77 (m, 2H, Ar-*H*), 6.68 (d, 2H, *J* = 8.8 Hz, Ar-*H*), 3.74 (s, 3H, CH_3), 3.68 (s, 3H, CH_3), 3.09 (dd, 1H, *J* = 9.2, 7.6 Hz, C*H*), 2.14 (dd, 1H, *J* = 9.2, 4.8 Hz. CH_2), 1.84 (dd, 1H, *J* = 7.2, 4.8 Hz, CH_2). The spectroscopic data were consistent with previously reported data.[105] The enantiomeric excess was determined by chiral HPLC (Chiralcel® OD-H column, 25 x 0.46 cm, 0.7% 2-propanol in *n*-hexane (*v/v*%); 1 mL/min, 220 nm, τ_1 = 13 min, τ_2 = 23 min).

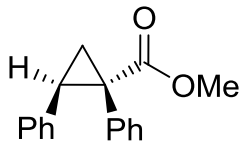

(*E*)-Methyl 1,2-diphenylcyclopropanecarboxylate (30)[149,105]

White solid; mp 60-62 ^{o}C; R_f = 0.30 (1:10 ethyl acetate: *n*-hexane); ^{1}H NMR (400 MHz, $CDCl_3$): δ 7.13-6.75 (m, 10H, Ar-*H*), 3.66 (s, 3H, CH_3), 3.11 (dd, 1H, *J* = 9.3, 7.3 Hz, C*H*), 2.13 (dd, 1H, *J* = 9.3, 4.9 Hz, CH_2), 1.88 (dd, 1H, 7.3, 4.9 Hz, CH_2). The spectroscopic data were consistent with previously reported data.[149,105] The enantiomeric excess was determined by chiral HPLC (Chiralcel® OJ column, 25 x 0.46 cm, 0.5% 2-propanol in *n*-hexane (*v/v*%); 1 mL/min, 220 nm, τ_1 = 14 min, τ_2 = 20 min).

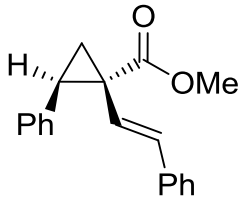

(*E*)-Methyl 2*β*-phenyl-1*β*-(2-(*Z*)-styryl)cyclopropane-1*α*-carboxylate (32)[150]

White solid; mp 58-61 ^{o}C; R_f = 0.63 (1:3 ethyl acetate: *n*-hexane); ^{1}H NMR (400 MHz, $CDCl_3$): δ 7.17-7.04 (m, 10H, Ar-*H*), 6.26 (d, 1H, *J* = Hz, C*H*=CH), 6.05 (d, 1H, *J* = Hz, CH=C*H*), 3.68 (s, 3H, CH_3), 2.93 (dd, 1H, *J* = 9.0, 7.5 Hz, C*H*), 1.94 (dd, 1H, *J* = 9.2, 5.0 Hz, CH_2), 1.75 (dd, 1H, 9.2, 5.0 Hz, CH_2). The spectroscopic data were consistent with previously reported data.[150] The enantiomeric excess was determined by chiral HPLC (Chiralcel® OJ column, 25 x 0.46 cm, 1.5% 2-propanol in *n*-hexane (*v*/*v*%); 1 mL/min, 254 nm, τ_1 = 15 min, τ_2 = 21 min).

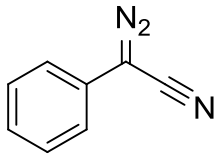

***α*-Diazo-2-phenylacetonitrile (33)**[151]

α-Diazo-2-phenylacetonitrile was prepared according to a modified literature procedure. To a stirred solution of 2-phenylglycinonitrile.HCl (1.5 g, 8.9 mmol) in water: diethyl ether (1:1 *v*/*v*, 10 mL) solvent mixture maintained at 0 ^{o}C, $NaNO_2$ solution (0.9 g, 13.0 mmol) was added drop-wise. After stirring for 5 min, the ether layer was removed and replaced by another 5 mL layer of fresh diethyl ether, which was also removed after another 5 min. The combined ether layers were washed with saturated Na_2CO_3 solution, dried over anhydrous Na_2SO_4, filtered and concentrated *in vacuo*. The red crude residue was purified on silica gel column chromatography using *n*-hexane as mobile phase to afford the title compound as red oil (120 mg, 10 %) which was stored at -20 ^{o}C. R_f = 0.49 (1:9 diethyl ether: *n*-hexane); ^{1}H NMR (400 MHz, $CDCl_3$): δ 7.35 (t, 2H, *J* = 7.6 Hz, Ar-*H*), 7.17-7.14 (m, 1H, Ar-*H*), 6.99 (d, 2H *J* = 7.6 Hz, Ar-*H*). The spectroscopic data were consistent with previously reported data.[151]

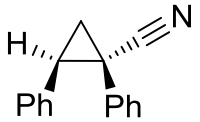

(*E*)-1,2-Diphenylcyclopropanecarbonitrile (34)[152,106]

To a stirred solution of styrene (5 equiv.) and a dirhodium(II) catalyst (0.02 equiv.) in dry and degassed toluene (3 mL) maintained at -78 ^{o}C and under nitrogen atmosphere, *α*-diazo-2-phenylacetonitrile (1 equiv.) dissolved in dry and degassed toluene (2 mL) was added drop-wise over a period of 10 min *via* syringe pump. The orange reaction mixture was allowed to slowly warm up to ~20 ^{o}C, during which time, the mixture colour returned back to green. The reaction solvent was then removed *in vacuo* and the diastereomeric ratio (dr) of the generated product was determined by ^{1}H NMR of the residue. The product was purified by means of preparative TLC using diethyl ether: *n*-hexane (1:10) as mobile phase. White solid; R_f = 0.32 (1:9 diethyl ether: *n*-hexane); ^{1}H NMR (400 MHz, $CDCl_3$): *δ* 7.17-7.01 (m, 8H, Ar-*H*), 6.82-6.80 (m, 2H, Ar-*H*), 3.09 (t, 1H, *J* = 8.6 Hz , C*H*), 2.14-2.00 (m, 2H, CH_2). The enantiomeric excess was determined by chiral HPLC (Chiralcel® OD column, 25 x 0.46 cm, 0.8% 2-propanol in *n*-hexane (*v/v*%); 1 mL/min, 220 nm, τ_1 = 19 min, τ_2 = 29 min).

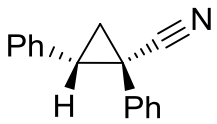

(*Z*)-1,2-Diphenylcyclopropanecarbonitrile

White solid; R_f = 0.32 (1:9 diethyl ether: *n*-hexane); ^{1}H NMR (400 MHz, $CDCl_3$): *δ* 7.34-7.23 (m, 10H, Ar-*H*), 2.72 (t, 1H, *J* = 8.4 Hz , C*H*), 2.06-1.91 (m, 2H, CH_2). The enantiomeric excess was determined by chiral HPLC (Chiralcel® OD column, 25 x 0.46 cm, 0.8% 2-propanol in *n*-hexane (*v/v*%); 1 mL/min, 220 nm, τ_1 = 22 min, τ_2 = 36 min).

General procedure for one-pot cyclopropanation of olefins with Meldrum's acid

To a stirred mixture of Meldrum's acid (1 equiv.), $PhI(OAc)_2$ (1.4 equiv.), a dirhodium(II) catalyst (0.01 equiv.), Al_2O_3 (2.3 equiv.) and 4Å MS in dry DCM

under nitrogen atmosphere, the olefin (10 equiv.) was added. After allowing the reaction mixture to stir at room temperature for 2 hours, the reaction was terminated by filtration through Celite® and concentrated under reduced pressure. The residue was then purified by means of preparative TLC chromatography using ethyl acetate: *n*-hexane (1:4) as an eluent to afford the corresponding cyclopropane product. The enantiomeric excess (*ee*%) of the generated product was determined by chiral HPLC analysis.

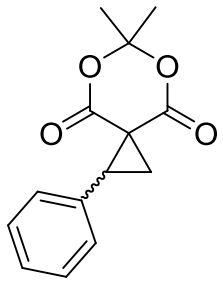

6,6-Dimethyl-1-phenyl-5,7-dioxaspiro[2.5]octane-4,8-dione[153]

White solid; mp 132 ^{o}C; R_f = 0.55 (1:3 ethyl acetate: *n*-hexane); ^{1}H NMR (400 MHz, $CDCl_3$): δ 7.35 (s, 5H, Ar-*H*), 3.46 (apt t, 1H , *J* = 9.5 Hz, C*H*), 2.70 (dd, 1H, *J* = 9.5 Hz, CH_2), 2.56 (dd, 1H, *J* = 9.6, 4.7 Hz, CH_2), 1.74 (s, 3H, CH_3), 1.73 (s, 3H, CH_3). The spectroscopic data were consistent with previously reported data.[153] The enantiomeric excess (*ee*%) was determined by chiral HPLC (Chiralpak® IB column, 25 x 0.46 cm, 10% ethyl acetate in *n*-hexane (*v*/*v*%); 1 mL/min, 254 nm, τ_1 = 10 min, τ_2 = 12.9 min).

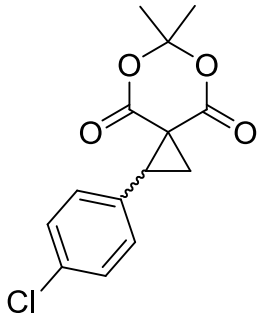

6,6-Dimethyl-1-(4-chlorophenyl)-5,7-dioxaspiro[2.5]octane-4,8-dione[153]

White solid; mp 157 ^{o}C; R_f = 0.71 (1:3 ethyl acetate: *n*-hexane); ^{1}H NMR (400 MHz, $CDCl_3$): δ 7.23 (dd, 4H, *J* = 15.4, 8.6 Hz, Ar-*H*), 3.34 (apt t, 1H, *J* = 9.5 Hz, C*H*),

2.56 (dd, 1H, J = 9.2, 4.8 Hz, CH_2), 2.48 (dd, 1H, J = 9.5, 4.9 Hz, CH_2), 1.67 (s, 3H, CH_3), 1.64 (s, 3H, CH_3). The spectroscopic data were consistent with previously reported data.[153] The enantiomeric excess (*ee*%) was determined by chiral HPLC (Chiralpak® IB column, 25 x 0.46 cm, 10% ethyl acetate in *n*-hexane (*v/v*%); 0.5 mL/min, 254 nm, τ_1 = 26 min, τ_2 = 32 min).

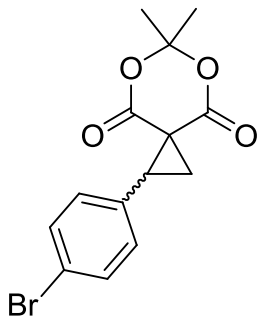

6,6-Dimethyl-1-(4-bromophenyl)-5,7-dioxaspiro[2.5]octane-4,8-dione

White solid; mp 144 ^{o}C; R_f = 0.40 (1:3 ethyl acetate: *n*-hexane); ^{1}H NMR (400 MHz, $CDCl_3$): δ 7.34 (dd, 4H, J = 8.5 Hz, Ar-H), 3.39 (apt t, 1H, J = 9.4 Hz, CH), 2.63 (dd, 1H, J = 9.3, 4.8 Hz, CH_2), 2.54 (dd, 1H, J = 9.5, 4.8 Hz, CH_2), 1.74 (s, 3H, CH_3), 1.71 (s, 3H, CH_3). The enantiomeric excess (*ee*%) was determined by chiral HPLC (Chiralpak® IB column, 25 x 0.46 cm, 10% ethyl acetate in *n*-hexane (*v/v*%); 0.5 mL/min, 254 nm, τ_1 = 31 min, τ_2 = 39 min).

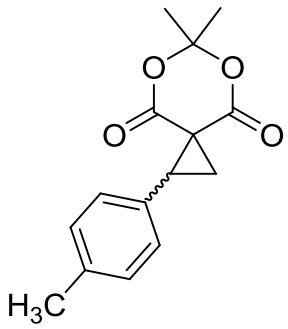

6,6-Dimethyl-1-(4-methylphenyl)-5,7-dioxaspiro[2.5]octane-4,8-dione[153]

White solid; mp 137 ^{o}C; R_f = 0.33 (1:3 ethyl acetate: *n*-hexane); ^{1}H NMR (400 MHz, $CDCl_3$): δ 7.18 (dd, 4H, J = 8.2 Hz, Ar-H), 3.42 (apt t, 1H, J = 9.5 Hz, CH), 2.67 (dd, 1H, J = 9.4, 4.8 Hz, CH_2), 2.53 (dd, 1H, J = 9.5, 4.8 Hz, CH_2), 2.33 (s, 3H, CH_3), 1.72 (s, 3H, CH_3), 1.71 (s, 3H, CH_3). The spectroscopic data were consistent with

previously reported data.[153] The enantiomeric excess (*ee*%) was determined by chiral HPLC (Chiralpak® IB column, 25 x 0.46 cm, 10% ethyl acetate in *n*-hexane (*v/v*%); 0.5 mL/min, 254 nm, $\tau_1 = 26$ min, $\tau_2 = 31$ min).

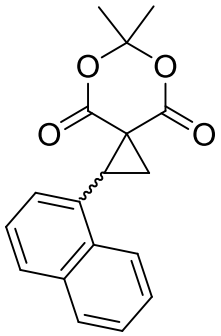

6,6-Dimethyl-1-naphthyl-5,7-dioxaspiro[2.5]octane-4,8-dione[153]

Yellowish solid; mp 120 ^{o}C; R_f = 0.68 (1:3 ethyl acetate: *n*-hexane); ^{1}H NMR (400 MHz, $CDCl_3$): δ 7.78-7.73 (m, 4H, Ar-*H*), 7.43-7.34 (m, 3H, Ar-*H*), 3.54 (apt t, 1H, *J* = 9.4 Hz, C*H*), 2.76 (dd, 1H, *J* = 9.3, 4.8 Hz, CH_2), 2.56 (dd, 1H, *J* = 9.5, 4.8 Hz, CH_2), 1.67 (s, 3H, CH_3), 1.65 (s, 3H, CH_3). The spectroscopic data were consistent with previously reported data.[153] The enantiomeric excess (*ee*%) was determined by chiral HPLC (Chiralpak® IB column, 25 x 0.46 cm, 10% ethyl acetate in *n*-hexane (*v/v*%); 0.5 mL/min, 254 nm, $\tau_1 = 46$ min, $\tau_2 = 56$ min).

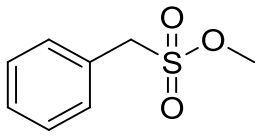

Methyl benzylsulfonate (35)

To a stirred solution of α-toluenesulfonyl chloride (2 g, 10.50 mmol) in anhydrous toluene at 0 ^{o}C, dry methanol (1 mL, 24.70 mmol) and TEA (2.5 mL, 17.80 mmol) were added. The reaction was allowed to stir at 0 ^{o}C for 30 min and at room temperature for another 30 min. The mixture was then diluted with saturated $NaHCO_3$ solution, extracted twice with DCM and the combined organic layers were dried over anhydrous Na_2SO_4, filtered and concentrated *in vacuo* to afford the title compound as a white solid (1.1 g, 56%); mp 56 ^{o}C; R_f = 0.36 (1:3 ethyl acetate: *n*-hexane); ^{1}H NMR (400 MHz, $CDCl_3$): δ 7.35 (s, 5H, Ar-*H*), 4.30 (s, 2H, CH_2), 3.70

(s, 3H, C*H*$_3$); ^{13}C NMR (100 MHz, $CDCl_3$): δ 130.7, 130.6, 129.1, 128.9 (6 x Ar-*C*), 56.8 (*C*H$_2$), 56.1 (*C*H$_3$); IR (film) ν 3032, 2970, 1346, 1159, 1139, 978, 814, 692 cm^{-1}; MS (ESI) *m/z*: 375.3 (2 x $C_8H_{10}O_3S$ + $3H^+$; calc. 375.5).

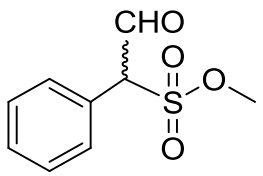

Methyl *α*-formylbenzylsulfonate (36)

To a stirred solution of methyl benzylsulfonate (**35**, 0.98 g, 5.26 mmol) in dry THF (10 mL) under nitrogen atmosphere maintained at -78 ^{o}C, 1.6 M solution of *n*-butyllithium in hexane (4 mL, 6.40 mmol) was added drop-wise. After stirring for 15 min at -78 ^{o}C, ethyl formate (0.85 mL, 10.44 mmol) was added drop-wise. When the addition was complete, the reaction was left to slowly warm up to ~-30 ^{o}C before the cooling bath was removed and it was allowed to stir at room temperature for another 30 min. The reaction was quenched by the slow addition of 1M HCl solution (10 mL) and resulting mixture was then extracted with DCM twice. The combined organic layers were dried over anhydrous Na_2SO_4, filtered and concentrated *in vacuo* to afford the crude product as a sticky residue. The residue was purified by means of silica gel column chromatography using ethyl acetate: *n*-hexane (1:10) as a mobile phase to yield the title compound as a colourless oil (0.959 g, 85%); R_f = 0.25 (1:2 ethyl acetate: *n*-hexane); ^{1}H NMR (400 MHz, $CDCl_3$): δ 9.78 (d, 1H, *J* = 2.2 Hz, C*H*O), 7.43 (s, 5H, Ar-*H*), 5.14 (d, 1H, *J* = 2.2 Hz, C*H*), 3.77 (s, 3H, C*H*$_3$); ^{13}C NMR (100 MHz, $CDCl_3$): δ 189.6 (*C*HO), 155.1, 130.4, 130.3, 130.2, 129.5, 128.9 (6 x Ar-*C*), 75.2 (*C*H), 58.0 (*C*H$_3$); IR (film) ν 3015, 2970, 2948, 1765, 1710, 1435, 1382, 1357, 1210, 979, 765, 696 cm^{-1}; MS (ESI) *m/z*: 213.0 ($C_9H_{10}O_4S$ - H^+; calc. 213.0).

2.8. REFERENCES

1. Fraile, J. M.; García, J. I.; Gissibl, A.; Mayoral, J. A.; Pires, E.; Reiser, O.; Roldán, M.; Villalba, I. *Chem.-Eur. J.* **2007**, *13*, 8830.

2. García, J. I.; López-Sánchez, B.; Mayoral, J. A.; Pires, E.; Villalba, I. *J. Catal.* **2008**, *258*, 378.

3. Hansen, J.; Davies, H. M. L. *Coord. Chem. Rev.* **2008**, *252*, 545.

4. Boruta, D. T.; Dmitrenko, O.; Yap, G. P. A.; Fox, J. M. *Chem. Sci.* **2012**, *3*, 1589.

5. Lindsay, V. N. G.; Charette, A. B. *ACS Catalysis* **2012**, *2*, 1221.

6. Lou, Y.; Horikawa, M.; Kloster, R. A.; Hawryluk, N. A.; Corey, E. J. *J. Am. Chem. Soc.* **2004**, *126*, 8916.

7. Nichols, J. M.; Liu, Y.; Zavalij, P.; Isaacs, L.; Doyle, M. P. *Inorg. Chim. Acta* **2008**, *361*, 3309.

8. Müller, P.; Ghanem, A. *Org. Lett.* **2004**, *6*, 4347.

9. Ghanem, A.; Gardiner, M. G.; Williamson, R. M.; Müller, P. *Chem.-Eur. J.* **2010**, *16*, 3291.

10. Ghanem, A.; Aboul-Enein, H. Y.; Müller, P. *Chirality* **2005**, *17*, 44.

11. Mattiza, J. T.; Fohrer, J. G. G.; Duddeck, H.; Gardiner, M. G.; Ghanem, A. *Org. Biomol. Chem.* **2011**, *9*, 6542.

12. Tsutsui, H.; Abe, T.; Nakamura, S.; Anada, M.; Hashimoto, S. *Chem. Pharm. Bull.* **2005**, *53*, 1366.

13. Kitagaki, S.; Anada, M.; Kataoka, O.; Matsuno, K.; Umeda, C.; Watanabe, N.; Hashimoto, S. *J. Am. Chem. Soc.* **1999**, *121*, 1417.

14. Yao, G.; Dai, W.; Ye, M.; Huang, R.; Pan, Y.-M.; Liao, Z.-X.; Wang, H.-S. *Med. Chem. Res.* **2014**, *23*, 5031.

15. Meyer, V. R. *Practical High Performance Liquid Chormatography, Fifth Edition*; Wiley: Weinheim, Germany, 2010.

16. Ghanem, A.; Lacrampe, F.; Aboul-Enein, H. Y.; Schurig, V. *Monatsh. Chem.* **2005**, *136*, 1205.

17. Hah, J. H.; Gil, J. M.; Oh, D. Y. *Tetrahedron Lett.* **1999**, *40*, 8235.

18. Midura, W. H.; Krysiak, J. A.; Mikołajczyk, M. *Tetrahedron: Asymmetry* **2003**, *14*, 1245.

19. Reid, J. R.; Marmor, R. S. *J. Org. Chem.* **1978**, *43*, 999.

20. Diel, P. J.; Maier, L. *Phosphorus, Sulfur Silicon Relat. Elem.* **1984**, *20*, 313.

21. Duquenne, C.; Goumain, S.; Jubault, P.; Feasson, C.; Quirion, J.-C. *Org. Lett.* **2000**, *2*, 453.

22. Devreux, V.; Wiesner, J.; Goeman, J. L.; Van der Eycken, J.; Jomaa, H.; Van Calenbergh, S. *J. Med. Chem.* **2006**, *49*, 2656.

23. Hercouet, A.; Le Corre, M.; Carboni, B. *Tetrahedron Lett.* **2000**, *41*, 197.

24. Yamazaki, S.; Takada, T.; Imanishi, T.; Moriguchi, Y.; Yamabe, S. *J. Org. Chem.* **1998**, *63*, 5919.

25. Hanessian, S.; Cantin, L.-D.; Roy, S.; Andretti, D.; Gomtsyan, A. *Tetrahedron Lett.* **1997**, *38*, 1103.

26. Midura, W. H.; Krysiak, J.; Rzewnicka, A.; Supeł, A.; Łyżwa, P.; Ewas, A. M. *Tetrahedron* **2013**, *69*, 730.

27. Dappen, M. S.; Pellicciari, J. R.; Natalini, B.; Monahan, J. B.; Chiorri, C.; Cordis, A. A. *J. Med. Chem.* **1991**, *34*, 161.

28. Pyun, H.-J.; Clarke, M. O.; Cho, A.; Casarez, A.; Ji, M.; Fardis, M.; Pastor, R.; Sheng, X. C.; Kim, C. U. *Tetrahedron Lett.* **2012**, *53*, 2360.

29. Erion, M. D.; Walsh, C. T. *Biochemistry* **1987**, *26*, 3417.

30. Groth, U.; Lehmann, L.; Richter, L.; Schollkopf, U. *Liebigs Ann. Chem.* **1993**, 427.

31. Hatse, S.; Naesens, L.; Clercq, E. D.; Balzarini, J. *Biochem. Pharmacol.* **1999**, *58*, 311.

32. Zidek, Z.; Potmesil, P.; Kmoniekova, E.; Holy, A. *Eur. J. Pharmacol.* **2003**, *475*, 149.

33. Van Poelje, P. D.; Erion, M. D.; Fujiwara, T. In PCT/US2001/021557, 2002

34. Naesens, L.; Hatse, S.; Segers, C.; Verbeken, E.; De Clereq, E.; Waer, M.; Balzarini, J. *Oncol. Res.* **1999**, *11*, 195.

35. Choi, J. R.; Cho, D. G.; Roh, K. Y.; Hwang, J. T.; Anh, S.; Jang, H. S.; Cho, W. Y.; Kim, K. W.; Cho, Y. G.; Kim, J. *J. Med. Chem.* **2004**, *47*, 2864.

36. Zidek, Z.; Potmesil, P.; Holy, A. *Toxicol. Appl. Pharmacol.* **2003**, *192*, 246.

37. Hockova, D.; Holy, A.; Masojidkova, M.; Andrei, G.; Snoeck, R. T.; De Clereq, E. *J. Med. Chem.* **2003**, *46*, 5064.

38. Lewis, R. T.; Motherwell, W. B.; Shipman, M.; Slawin, A. M. Z.; Williams, D. J. *Tetrahedron* **1995**, *51*, 3289.

39. Lewis, R. T.; Motherwell, W. B. *Tetrahedron Lett.* **1988**, *29*, 5033.

40. Quntar, A. A. A. A.; Dembitsky, V. M.; Srebnik, M. *Org. Prep. Proced. Int.* **2008**, *40*, 505.

41. Hirao, T.; Hagihara, M.; Agawa, T. *Bull. Chem. Soc. Jpn.* **1985**, *58*, 3104.

42. Pudovik, A. N.; Gareev, R. D.; Kuznetsva, L. I. *Zh. Obshch. Khim.* **1969**, *39*, 1536.

43. Dolhaine, V. H.; Hägele, G. *Phosphorus, Sulfur Silicon Relat. Elem.* **1978**, *4*, 123.

44. Goumain, S.; Jubault, P.; Feasson, C.; Quirion, J.-C. *Tetrahedron Lett.* **1999**, *40*, 8099.

45. Jubault, P.; Goumain, S.; Feasson, C.; Collignon, N. *Tetrahedron* **1998**, *54*, 14767.

46. Guliev, A. N.; Ismailov, V. M.; Nasibov, S. S. *Kimya Problemläri Jurnali* **2004**, 19.

47. Fadel, A.; Tesson, N. *Eur. J. Org. Chem.* **2000**, 2153.

48. Swamy, K. C. K.; Kumar, K. V. P. P.; Suresh, R. R.; Kumar, N. S. *Synthesis* **2007**, 1485.

49. Griffin, C. E.; Kraas, E.; Terasawa, H.; Griffin, G. W.; Lankin, D. C. *J. Heterocycl. Chem.* **1978**, *15*, 523.

50. Nasser, J.; About-Jaudet, E.; Collignon, N. *Phosphorus, Sulfur Silicon Relat. Elem.* **1990**, *54*, 171.

51. Kondo, K.; Liu, Y.; Tunemoto, D. *J. Chem. Soc., Perkin Trans. 1* **1974**, *11*, 1279.

52. Ferrand, Y.; Maux, P. L.; Simonneaux, G. *Org. Lett.* **2004**, *6*, 3211.

53. Maux, P. L.; Abrunhosa, I.; Berchel, M.; Simonneaux, G.; Gulea, M.; Masson, S. *Tetrahedron: Asymmetry* **2004**, *15*, 2569.

54. Chanthamath, S.; Ozaki, S.; Shibatomi, K.; Iwasa, S. *Org. Lett.* **2014**, *16*, 3012.

55. Charette, A. B.; Bouchard, J.-E. *Can. J. Chem.* **2005**, *83*, 533.

56. Lindsay, V. N. G.; Fiset, D.; Gritsch, P. J.; Azzi, S.; Charette, A. B. *J. Am. Chem. Soc.* **2013**, *135*, 1463.

57. Davies, H. M. L.; Lee, G. H. *Org. Lett.* **2004**, *6*, 2117.

58. Reddy, R. P.; Lee, G. H.; Davies, H. M. L. *Org. Lett.* **2006**, *8*, 3437.

59. Tsutsui, H.; Matsuura, M.; Makino, K.; Nakamura, S.; Nakajima, M.; Kitagaki, S.; Hashimoto, S. *Isr. J. Chem.* **2001**, *41*, 283.

60. Hashimoto, S.; Watanabe, N.; Sato, T.; Shiro, M.; Ikegami, S. *Tetrahedron Lett.* **1993**, *34*, 5109.

61. Anada, M.; Kitagaki, S.; Hashimoto, S. *Heterocycles* **2000**, *52*, 875.

62. Nadeau, E.; Ventura, D. L.; Brekan, J. A.; Davies, H. M. L. *J. Org. Chem.* **2010**, *75*, 1927.

63. DeAngelis, A.; Dmitrenko, O.; Yap, G. P. A.; Fox, J. M. *J. Am. Chem. Soc.* **2009**, *131*, 7230.

64. DeAngelis, A.; Boruta, D. T.; Lubin, J.-B.; Plampin, J. N.; Yap, G. P. A.; Fox, J. M. *Chem. Commun.* **2010**, *46*, 4541.

65. Lindsay, V. N. G.; Nicolas, C.; Charette, A. B. *J. Am. Chem. Soc.* **2011**, *133*, 8972.

66. Lindsay, V. N. G.; Lin, W.; Charette, A. B. *J. Am. Chem. Soc.* **2009**, *131*, 16383.

67. Goto, T.; Takada, K.; Shimada, N.; Nambu, H.; Anada, M.; Shiro, M.; Ando, K.; Hashimoto, S. *Angew. Chem., Int. Ed.* **2011**, *50*, 6803.

68. Qin, C.; Boyarskikh, V.; Hansen, J. H.; Hardcastle, K. I.; Musaev, D. G.; Davies, H. M. L. *J. Am. Chem. Soc.* **2011**, *133*, 19198.

69. Kang, Y.-B.; Tang, Y.; Sun, X.-L. *Org. Biomol. Chem.* **2006**, *4*, 299.

70. Christie, S. D.; Davoile, R. J.; Jones, R. C. *Org. Biomol. Chem.* **2006**, *4*, 2683.

71. Carson, C. A.; Kerr, M. A. *J. Org. Chem.* **2005**, *70*, 8242.

72. Kang, Y. B.; Sun, X. L.; Tang, Y. *Angew. Chem., Int. Ed.* **2007**, *46*, 3918.

73. Cardona, F.; Goti, A. *Angew. Chem., Int. Ed.* **2005**, *44*, 7832.

74. Sibi, M. P.; Ma, Z.; Jasperse, C. P. *J. Am. Chem. Soc.* **2005**, *127*, 5764.

75. Ganton, M. D.; Kerr, M. A. *J. Org. Chem.* **2004**, *69*, 8554.

76. Young, I. S.; Kerr, M. A. *Org. Lett.* **2004**, *6*, 139.

77. Young, I. S.; Kerr, M. A. *Angew. Chem., Int. Ed.* **2003**, *42*, 3023.

78. Pohlhaus, P. D.; Johnson, J. S. *J. Am. Chem. Soc.* **2005**, *127*, 16014.

79. Pohlhaus, P. D.; Johnson, J. S. *J. Org. Chem.* **2005**, *70*, 1057.

80. Shi, M.; Yang, Y.-H.; Xu, B. *Tetrahedron* **2005**, *61*, 1893.

81. Bernard, A. M.; Frongia, A.; Piras, P. P.; Secci, F.; Spiga, M. *Org. Lett.* **2005**, *7*, 4565.

82. Fuchibe, K.; Aoki, Y.; Akiyama, T. *Chem. Lett.* **2005**, *34*, 538.

83. Pohlhaus, P. D.; Sanders, S. D.; Parsons, A. T.; Li, W.; Johnson, J. S. *J. Am. Chem. Soc.* **2008**, *130*, 8642.

84. Parsons, A. T.; Johnson, J. S. *J. Am. Chem. Soc.* **2009**, *131*, 3122.

85. Perreault, C.; Goudreau, S. R.; Zimmer, L. E.; Charette, A. B. *Org. Lett.* **2008**, *10*, 689.

86. Ivanova, O. A.; Budynina, E. M.; Grishin, Y. K.; Trushkov, I. V.; Verteletskii, P. V. *Eur. J. Org. Chem.* **2008**, 5329.

87. Jackson, S. K.; Karadeolian, A.; Driega, A. B.; Kerr, M. A. *J. Am. Chem. Soc.* **2008**, *130*, 4196.

88. Dias, D. A.; Kerr, M. A. *Org. Lett.* **2009**, *11*, 3694.

89. Lebold, T. P.; Leduc, A. B.; Kerr, M. A. *Org. Lett.* **2009**, *11*, 3770.

90. Lebold, T. P.; Kerr, M. A. *Org. Lett.* **2009**, *11*, 4354.

91. Marcoux, D.; Goudreau, S. R.; Charette, A. B. *J. Org. Chem.* **2009**, *74*, 8939.

92. Ghanem, A.; Lacrampe, F.; Schurig, V. *Helv. Chim. Acta* **2005**, *88*, 216.

93. Yoon, T. P.; Jacobsen, E. N. *Science* **2003**, *299*, 1691.

94. Bertilsson, S. K.; Andersson, P. G. *J. Organomet. Chem.* **2000**, *603*, 13.

95. Verma, M.; Luxami, V.; Paul, K. *Eur. J. Med. Chem.* **2013**, *68*, 352.

96. Denton, J. R.; Sukumaran, D.; Davies, H. M. L. *Org. Lett.* **2007**, *9*, 2625.

97. Filler, R.; Kobayashi, Y. *Biomedical Aspects of Fluorine Chemistry*; Elsevier Biomedical: Amsterdam, 1982.

98. Welch, J. T.; Eswarakrishnan, S. *Fluorine in Bioorganic Chemistry*; Wiley: New York, 1990.

99. Hiyama, T. *Organofluorine Compounds. Chemistry and Applications*; Springer: New York, 2000.

100. O'Hagan, D.; Harper, D. B. *J. Fluorine Chem.* **1999**, *100*, 127.

101. Chambers, R. D. *Fluorine in Organic Chemistry*; Blackwell: BocaRaton, Fl, 2004.

102. Shimizu, M.; Hiyama, T. *Angew. Chem., Int. Ed.* **2005**, *44*, 214.

103. Park, B. K.; Kitteringham, N. R.; O'Niel, P. M. *Annu. Rev. Pharmacol. Toxicol.* **2001**, *41*, 443.

104. Smart, B. E. *J. Fluorine Chem.* **2001**, *109*, 3.

105. Chepiga, K. M.; Qin, C.; Alford, J. S.; Chennamadhavuni, S.; Gregg, T. M.; Olson, J. P.; Davies, H. M. L. *Tetrahedron* **2013**, *69*, 5765.

106. Denton, J. R.; Cheng, K.; Davies, H. M. L. *Chem. Commun.* **2008**, 1238.

107. Teall, M.; Oakley, P.; Harrison, T.; Shaw, D.; Kay, E.; Elliott, J.; Gerhard, U.; Castro, J. L.; Shearman, M.; Ball, R. G.; Tsou, N. N. *Bioorg. Med. Chem. Lett.* **2005**, *15*, 2685.

108. Harrak, Y.; Casula, G.; Basset, J.; Rosell, G.; Plescia, S.; Raffa, D.; Cusimano, M. G.; Pouplana, R.; Pujol, M. D. *J. Med. Chem.* **2010**, *53*, 6560.

109. Smith, D. A.; Jones, R. M. *Curr. Opin. Drug Discovery Dev.* **2008**, *11*, 72.

110. Xu, W.-M.; Han, F.-F.; He, M.; Hu, D.-Y.; He, J.; Yang, S.; Song, B.-A. *J. Agric. Food Chem.* **2012**, *60*, 1036.

111. Noutoshi, Y.; Ikeda, M.; Saito, T.; Osada, H.; Shirasu, K. *Front. Plant Sci.* **2012**, *3*, 245.

112. In *Modern Crop Protection Compounds*; Kramer, W.; Schirmer, U. Eds.; Wiley-VCH: Weinheim, 2007; pp. 93.

113. Simpkins, N. S. *Sulphones in Organic Synthesis*; Pergamon Press: Oxford, 1993.

114. Ager, D. J.; Pantaleone, D. P.; Henderson, S. A.; Katritzky, A. R.; Prakash, I.; Walters, D. E. *Angew. Chem., Int. Ed.* **1998**, *37*, 1802.

115. Emmett, E. J.; Hayter, B. R.; Willis, M. C. *Angew. Chem., Int. Ed.* **2014**, *53*, 10204.

116. Berkessel, A.; Voges, M. *Chem. Ber.* **1989**, *122*, 1147.

117. Betnev, A. F.; Obuchova, T. A.; Betnev, S. A.; Klynev, I. V.; Pronin, S. V. *Russ. J. Org. Chem.* **2000**, *36*, 399.

118. Krasnikov, S. V.; Obuchova, T. A.; Yasinskii, O. A.; Balakin, K. V. *Tetrahedron Lett.* **2004**, *45*, 711.

119. Benessere, V.; Lega, M.; Ruffo, F. *J. Organomet. Chem.* **2014**, *771*, 105.

120. Steinborn, D.; Junicke, H. *Chem. Rev.* **2000**, *100*, 4283.

121. Benessere, V.; Del Litto, R.; De Roma, A.; Ruffo, F. *Coord. Chem. Rev.* **2010**, *254*, 390.

122. Woodward, S.; Diéguez, M.; Pàmies, O. *Coord. Chem. Rev.* **2010**, *254*, 2007.

123. Diéguez, M.; Pamies, O.; Claver, C. *Chem. Rev.* **2004**, *104*, 3189.

124. Castillón, S.; Claver, C.; Díaz, Y. *Chem. Soc. Rev.* **2005**, *34*, 702.

125. Diéguez, M.; Pàmies, O.; Ruiz, A.; Díaz, Y.; Castillón, S.; Claver, C. *Coord. Chem. Rev.* **2004**, *248*, 2165.

126. Boysen, M. M. *Chem.-Eur. J.* **2007**, *13*, 8648.

127. Descotes, G.; Lafont, D.; Sinou, D. *J. Organomet. Chem.* **1978**, *150*, C14.

128. El-Nezhawy, A. O. H.; Adly, F. G.; Eweas, A. F.; Hanna, A. G.; El-Kholy, Y. M.; El-Sayed, S. H.; El-Naggar, T. B. A. *Arch. Pharm.* **2011**, *344*, 648.

129. El-Nezhawy, A. O. H.; Adly, F. G.; Eweas, A. F.; Hanna, A. G.; El-Kholy, Y. M.; El-Sayed, S. H.; El-Naggar, T. B. A. *Med. Chem.* **2011**, *7*, 624.

130. Roos, G. H. P. *Synth. Commun.* **1992**, *22*, 1751.

131. Mikula, H.; Matscheko, D.; Schwarz, M.; Hametner, C.; Fröhlich, J. *Carbohydr. Res.* **2013**, *370*, 19.

132. Timmers, C. M.; Leeuwenburgh, M. A.; Verheijen, J. C.; van der Marel, G. A.; van Boom, J. H. *Tetrahedron: Asymmetry* **1996**, *7*, 49.

133. McPhillips, T. M.; McPhillips, S. E.; Chiu, H.-J.; Cohen, A. E.; Deacon, A. M.; Ellis, P. J.; Garman, E.; Gonzalez, A.; Sauter, N. K.; Phizackerley, R. P.; Soltis, S. M.; Kuhn, P. *J. Synchrotron Radiat.* **2002**, *9*, 401.

134. Kabsch, W. *J. Appl. Crystallogr.* **1993**, *26*, 795.

135. Sheldrick, G. M. *Shelx-97, Programs for Crystal Structure Analysis*; Universität Göttingen: Germany, 1998.

136. Barbour, L. J. *J. Supramol. Chem.* **2001**, *1*, 189.

137. UrRehman, S.; Li, P.; Zhou, H.; Zhao, X.; Dang, G.; Chen, C. *Polym. Degrad. Stab.* **2012**, *97*, 1581.

138. Spek, A. *J. Appl. Crystallogr.* **2003**, *36*, 7.

139. Huang, Y.; Berthiol, F.; Stegink, B.; Pollard, M. M.; Minnaard, A. J. *Adv. Synth. Catal.* **2009**, *351*, 1423.

140. Seyferth, D.; Marmor, R. S.; Hilbert, P. *J. Org. Chem.* **1971**, *36*, 1379.

141. Regitz, M.; Anschütz, W.; Liedhegener, A. *Chem. Ber.* **1968**, *101*, 3734.

142. Boulch, R.; Scheurer, A.; Mosset, P.; Saalfrank, R. W. *Tetrahedron Lett.* **2000**, *41*, 1023.

143. Tomioka, H.; Miyagawa, H. *J. Chem. Soc., Chem. Commun.* **1988**, 1183.

144. Shepard, R. A.; Wentworth, S. E. *J. Org. Chem.* **1967**, *32*, 3197.

145. Hrdina, R.; Guenee, L.; Moraleda, D. *Organometallics* **2013**, *32*, 473.

146. Zhao, W. J.; Yan, M.; Huang, D.; Ji, S.-J. *Tetrahedron* **2005**, *61*, 5585.

147. Hoye, T. R.; Richardson, W. S. *J. Org. Chem.* **1989**, *54*, 688.

148. Baum, J. S.; Shook, D. A.; Davies, H. M. L.; Smith, H. D. *Synth. Commun.* **1987**, *17*, 1709.

149. Davies, H. M. L.; Panaro, S. A. *Tetrahedron Lett.* **1999**, *40*, 5287.

150. Davies, H. M. L.; Bruzinski, P. R.; Lake, D. H.; Kong, N.; Fall, M. J. *J. Am. Chem. Soc.* **1996**, *118*, 6897.

151. Breslow, R.; Yuan, C. *J. Am. Chem. Soc.* **1958**, *80*, 5991.

152. Nowlan, D. T.; Gregg, T. M.; Davies, H. M. L.; Singleton, D. A. *J. Am. Chem. Soc.* **2003**, *125*, 15902.

153. Lee, Y. R.; Choi, J. H. *Bull. Korean Chem. Soc.* **2006**, *27*, 503.

CHAPTER 3: POLYMER MONOLITH-SUPPORTED DIRHODIUM(II)-CATALYZED CYCLOPROPANATIONS IN CAPILLARY FORMAT

3.1. INTRODUCTION

As raw chemicals are becoming more limited, it is essential to develop more efficient synthetic procedures with less waste. As a result, a number of new strategies have been introduced in the last decade to advance the sustainability of organic synthesis. These new strategies included the introduction of (1) metrics to analyse reaction efficiency,[1] (2) catalytic reactions instead of using stoichiometric reagents,[2] (3) solid-phase synthesis including loading expensive catalysts on solid supports,[3] (4) one-pot procedures including multicomponent reactions,[4] domino reactions,[5] and all classes of tandem catalysis,[6] and (5) microreaction technology.

Synthetic organic chemists have been employing typically the same equipments for decades. While the use of conventional round-bottom flask synthesis is successful, they are inherently wasteful in terms of the amounts of chemicals used. As a consequence, microreaction technology has received a great deal of attention and is currently having great effect on chemical, pharmaceutical, biological and medical science.[7-9] In its simplest form, a microreactor can be defined as a device that consists of a network of micron-sized channels etched into a solid substrate at which chemical reactions can take place in continuous flow.[8] Microreactor technology was described by Prof. Seeberger, from the Swiss Federal Institute of Technology (ETH), Switzerland, as being "*The chemist's round-bottom flasks of the 21st century*".[10,11,7] In contrast to conventional chemical synthetic procedures, microreactors are able to offer many extra advantages[12] including:

a) Microreactors are inherently much less wasteful.
b) Microreactors have improved surface to volume ratio within their microstructure which offers more uniform mixing and heating.
c) Microreactors are more economic and environmentally friendly through the decreased consumption of starting materials and reagents.
d) Microreactors can employ very small reaction volumes which offers inimitable reaction control (i.e. parameters such as temperature, pressure and residence time can be more easily controlled).

e) Safer operation as the hazard potential related to toxic, exothermic and explosive reactions is drastically reduced.
f) Microreactions are able to proceed more rapidly with improved conversion into products and decreased generation of side products.
g) Microreactor systems are easily amendable to integrated reaction monitoring systems using UV/Vis, IR, NMR, MS and LC/MS.

All in all, this new approach to organic synthesis has the potential to improve drug synthesis and discovery, while reducing the impact on human health and environment.

Most of the research carried out in this field, however, is mostly concerned with engineering aspects with minor attention to the potential of microreactors for improving organic synthesis. This is in addition to that synthetic chemists still did have not fully embrace this new technology. This is either because of the high cost related to building up and maintaining microreactors or may be because they already have strategies that are successful and productive for building molecules. Nevertheless, it is becoming clearer that the conventional methodologies for accomplishing organic synthesis are becoming unsustainable and must be changed.[9]

In the current chapter, investigations were carried out on the miniaturization of the Rh_2(*S*-^{tert}PTTL)$_4$-catalyzed cyclopropanation process. This is through the development of new flow-through cyclopropanation capillary microreactor that is inexpensive and easy to produce. The intention of developing a dirhodium(II) continuous flow catalytic system was previously reported by Hashimoto and co-workers[13] who explored an immobilization strategy for Rh_2(*S*-PTTL)$_4$ and its halogenated analogues.[13-15] In this strategy, one of the original Rh_2(*S*-PTTL)$_4$ ligands was replaced by a hydroxy-functionalized ligand and the generated heteroleptic complex was made to react with 6-(4-vinylbenzyloxy)bromohexane. The obtained monomer was then co-polymerised with styrene and 1,6-bis(4-vinylbenzyloxy)hexane as a cross-linker (Scheme 3.1). Through this methodology, a polymer matrix with uniform distribution of the chiral dirhodium(II) complex was generated. This allowed unrestricted access of substrates to catalytic active sites.

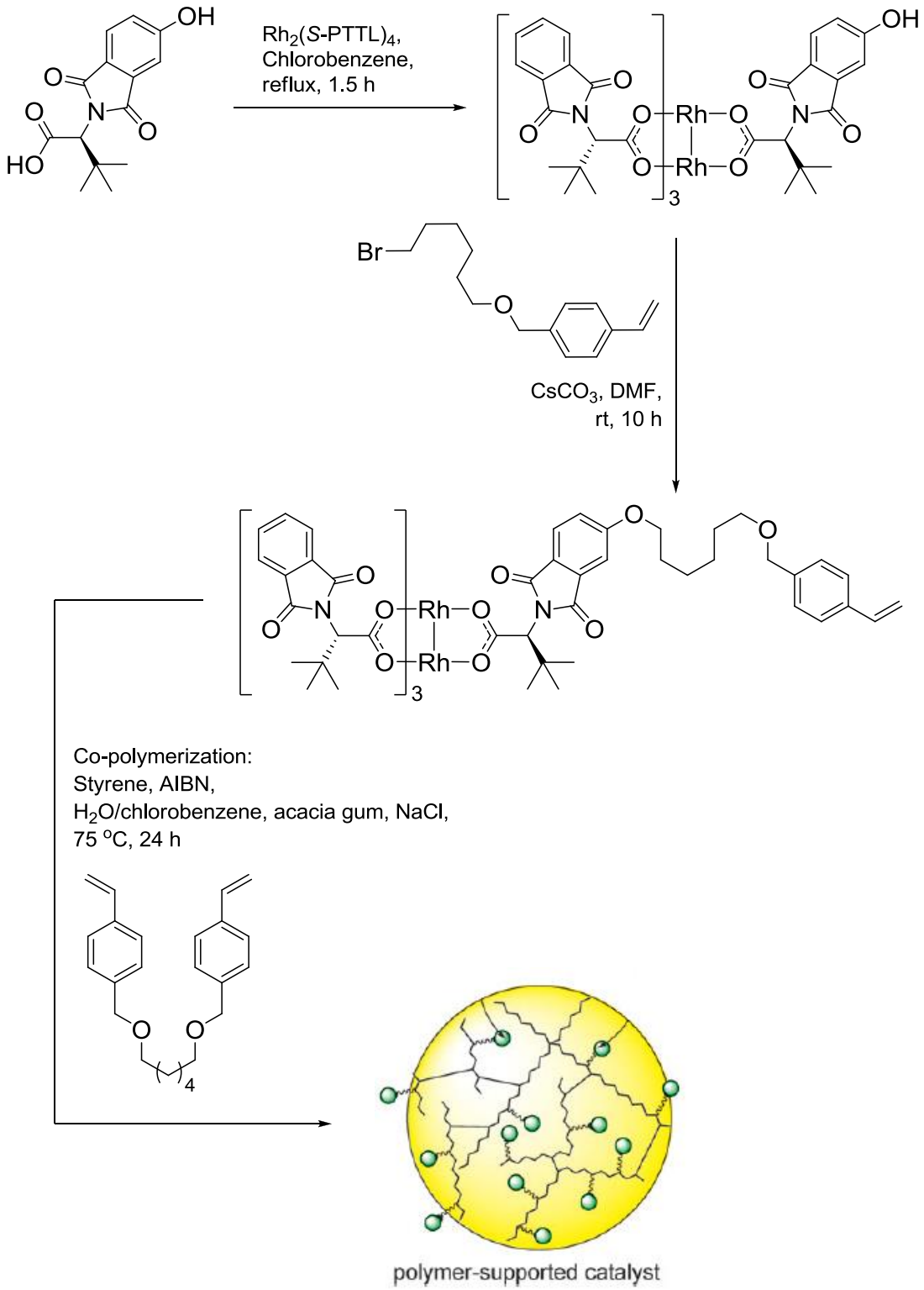

Scheme 3.1. Preparation of polymer-supported Rh_2(*S*-PTTL)$_4$ beads.[13]

The authors also explored the possibility of performing the reaction through the prepared catalytic beads under continuous flow conditions. Toward this goal, a fixed

column housing (80 mm in length and 11 mm in diameter) was packed with a mixture of discrete particle of the prepared catalytic beads and sand (Figure 3.1). A solution containing the reactants (diazodiketoester and styrene) in TFT was passed through the prepared flow reactor under the force of a syringe pump (0.5 $mL.h^{-1}$ for 2 h). Surprisingly, the continuous flow experiments gave higher yields (80%) when compared to the reaction carried out under batch conditions while maintaining the same excellent levels of enantioselectivity (99% *ee*). Tracing the rhodium leaching level by ICP-MS revealed that the reaction mixture contained only 2.1 µg/mL rhodium, which corresponded to only 0.013 *w*% of the initial catalyst charge. The authors also highlighted that the extrusion of nitrogen gas from the reaction had no detrimental effect on the overall continuous flow process. The authors succeeded to make the flow reactor operate for 60 h under steady state.

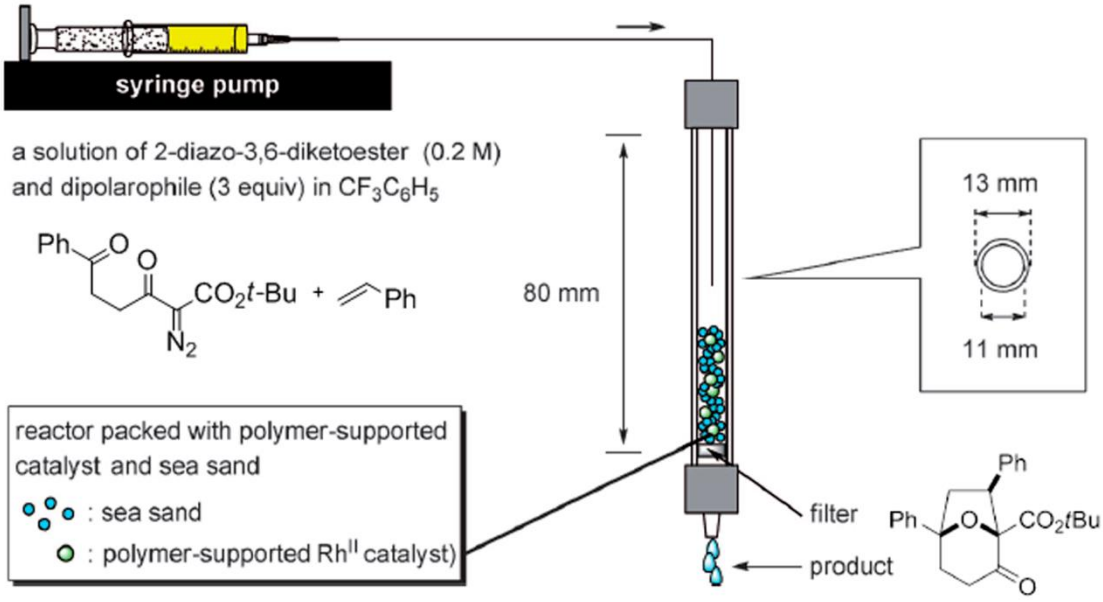

Figure 3.1. Schematic setup for Hashimoto's millilitre continuous flow reactor.[13] (Reprinted from Takeda, K.; Oohara, T.; Shimada, N.; Nambu, H.; Hashimoto, S. *Chem.-Eur. J.* **2011**, *17*, 13992, Copyright 2011, with permission from John Wiley and Sons).

Particle packed reactors, similar to Hashimoto's reactor, are widely used in flow-through processes for a long time. Generally, these reactors will consist of a packed-bed housing randomly filled with the catalytic bodies in the form of grains of particle

size 50-100 mm range. Nevertheless, the use of such reactors may suffer from several drawbacks including the broad variation in residence time and formation of stagnation zones and hot-spots. These drawbacks have the ability to lower the efficiency and the selectivity of the entire process.[16,17] A more efficient alternative to particle packed reactors are the monolithic microreactors.[17] In nature, a monolith is defined as "a single massive block of rock or stone" (Figure 3.2). In chemistry, monolith is defined by IUPAC as being "a shape, fabricated intractable article with a homogeneous microstructure that does not exhibit any structural components distinguishable by optical microscopy".[18] Monolithic materials were originally developed for separation science applications and often perform better than the corresponding particle chromatographic materials. While in microreactors, the use of these type of materials for immobilization of reactive species mostly focused on enzymatic bioreactors, reactive scavengers.[19,20] There has been little interest in the immobilization of homogenous transition metal catalysts on this type of monolithic materials.[21-25]

Figure 3.2. A monolith standing at the entrance of the Summer Palace Park, Beijing, China.[26] (Reprinted from Guiochon, G. *J Chromatogr A* **2007**, *1168*, 101, Copyright 2007, with permssion from Elsevier).

3.1.1. Immobilization of dirhodium(II) catalysts

Immobilization of dirhodium(II) complexes for asymmetric carbenoid transformations has attracted the interest of different research groups.[27,14,28-32] The pioneering work reported by Bergbreiter and co-workers[33,34] on the immobilization of dirhodium(II) complexes on polyethylene polymers (PE) introduced and validated the concept that an immobilized dirhodium(II) complex is still able to catalyze reactions as cyclopropanations and C-H insertions. The catalytic activity of the PE-immobilised dirhodium(II) complex was clearly demonstrated at which the catalyst was successfully re-utilized nine times in the cyclopropanation of 2,5-dimethyl-2,4-butadiene with ethyl diazoacetate (EDA). The cyclopropanation proceeded with better *trans*/*cis* selectivity compared to the homogeneous $Rh_2(OAc)_4$ catalyst. A homogeneous version of that catalyst was later introduced by the same research group using poly*iso*butylene oligomers (PIB) as soluble solid supports (Scheme 3.2).[35]

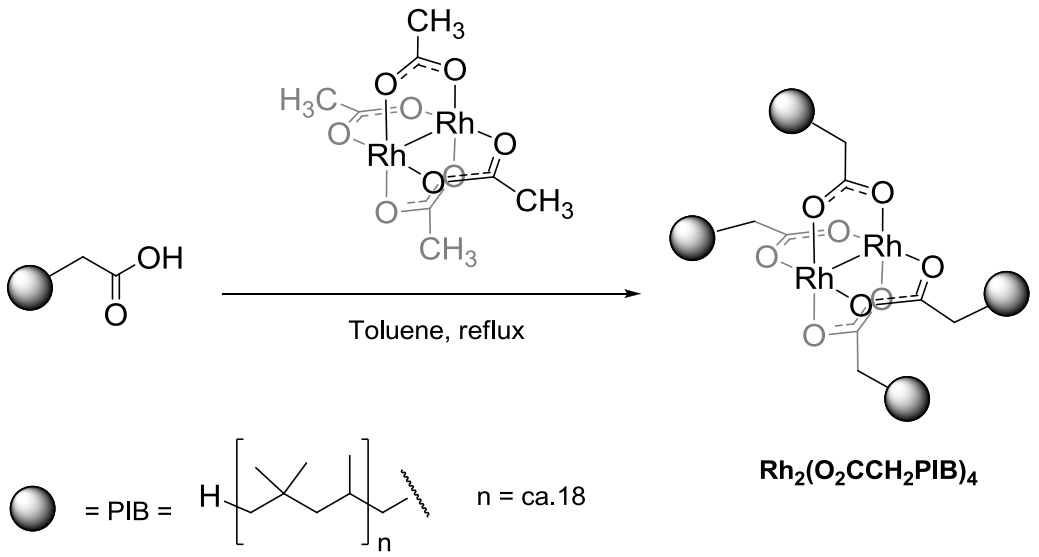

Scheme 3.2. Structure of the PIB-supported dirhodium(II) complex.

This work paved the way for dirhodium(II) complexes immobilization and, from that time, a number of strategies were developed for the immobilization of dirhodium(II) complexes.[36] These strategies included covalent binding of bridging ligand[13-15,37,38] and immobilization by axial coordination.[39,29-32]

3.1.1.1. Immobilization by axial coordination

Recently, Davies and co-workers reported a very general unusual immobilization approach for dirhodium(II) complexes.[29-32] This approach dealt directly with the immobilization of chiral dirhodium(II) tetracarboxylates without any ligand modifications. As axial coordination of dirhodium(II) compounds to basic sites is well-known, the dirhodium(II) molecule is able to coordinate to a pyridine functionalized polymer support at which, the polymer backbone coordinates to one rhodium atom, while the other continue to be an active site available for catalysis (Scheme 3.3).

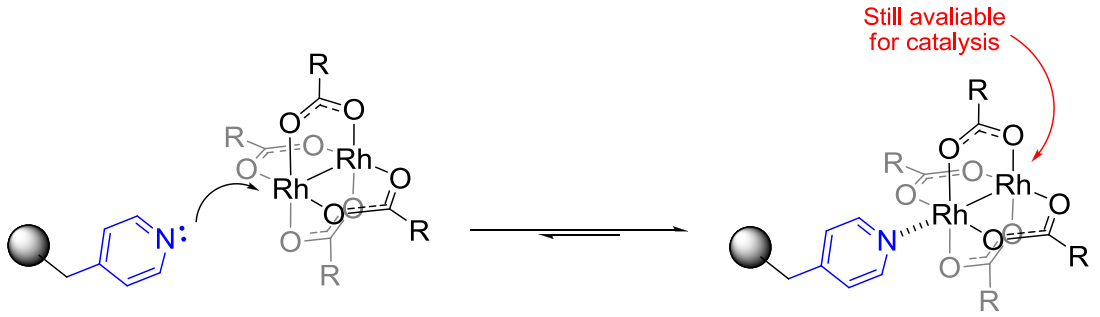

Scheme 3.3. Davies universal strategy for immobilization of dirhodium(II) complexes.

Investigations related to the mode of action for the immobilized catalysts revealed that their reactivity does not arise from a release and capture mechanism. Moreover, the use of a phenyl moiety replacing the pyridine terminal led to the immobilisation of the same complexes in a comparable extent. The immobilized catalysts generated the desired product in similar selectivities when tested in asymmetric cyclopropanation reactions.[29,30] Based on these observations, the authors concluded that, in addition to the axial coordination of the complexes by the pyridine moiety, other factors such as microencapsulation were pointed out as being the foundations of this immobilization methodology.

By applying the same strategy, Rh_2(*S*-DOSP)$_4$ was immobilised on the same resin and the catalytic system was evaluated in asymmetric C-H insertion reactions.[31] The re-utilisation of AWP-Rh_2(*S*-DOSP)$_4$ was possible for ten cycles without a significant drop in the enantioselectivity. The same immobilisation strategy was later

applied to Rh_2(5*S*-MEPY)$_4$, Rh_2(4*S*-MEAZ)$_4$, Rh_2(*S*-PTTL)$_4$ and Rh_2(*R*-BNP)$_4$.[32] These new heterogeneous catalytic systems were utilized in asymmetric intramolecular cyclopropanation and C-H insertion reactions. They generated the products in a comparable selectivity to their homogenous version. Furthermore, these catalytic systems were reused in up to three catalytic cycles without any observable drop in their enantioselectivities.

Also recently, Rh_2(tfa)$_4$ and Rh_2(Opr)$_4$ were immobilised inside nanoporous hosts using the axial coordination strategy.[39] These metal complexes were embedded in a modified mesoporous silica support containing dangling tertiary dimethylamino groups which are suitable for strong Rh-N axial coordinations (Figure 3.3). The immobilized Rh_2(tfa)$_4$ catalytic system was able to be recycled and reused three times in the cyclopropanation of MPDA while maintaining excellent levels of diastereoselectivity.

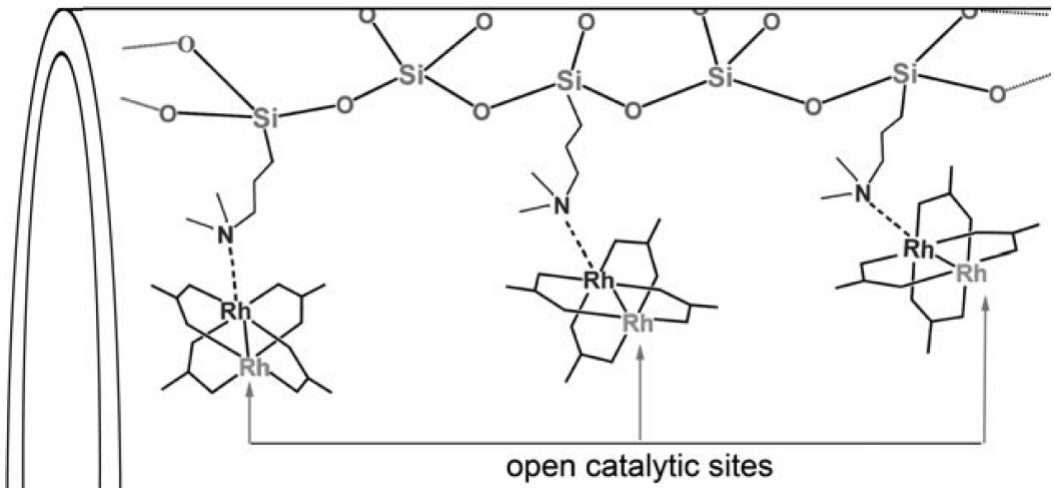

Figure 3.3. Channel of dirhodium(II) immobilized amine-SBA-15 non-porous catalyst.[39] (Reprinted from Dikarev, E. V.; Kumar, D. K.; Filatov, A. S.; Anan, A.; Xie, Y.; Asefa, T.; Petrukhina, M. A. *ChemCatChem* **2010**, *2*, 1461, Copyright 2010, with permission from John Wiley and Sons).

3.2. RESULTS AND DISCUSSION

3.2.1. Preparation of porous polymer monolith

For the supported homogenous catalysis targeted in this project, poly(AA-*co*-VP-*co*-Bis) was chosen as a polymer monolithic support for the microreactor as (1) it is thermally stable at the temperatures used for catalysis, (2) it is chemically inert to reaction solvent, reactants and catalyst, (3) it contain accessible pyridine functional groups suitable for catalyst immobilization and (4) it has high permeability that minimises solvent flow resistance.

First, the internal surface of the glass capillaries was modified to ensure that the synthesized polymer will adhere strongly to it (Scheme 3.4). This is to prevent the solvent from bypassing the polymer network minimizing the interaction with the immobilized catalyst. Furthermore, using such method is able to avert the need for frits or any other equipment to support the monolith in place inside the microreactor. This in turn can simplify its design and effectively diminishes the potential for capillary obstruction.

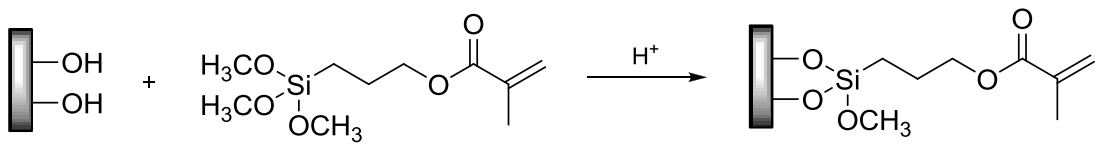

Scheme 3.4. Internal surface modification of glass capillaries.[40]

The surface modification step was followed by the preparation of the poly(AA-*co*-VP-*co*-Bis) monolithic solid support using the concept of "molding" developed by the research group of Fréchet.[41] The preparation was done *in situ* at which a solution of 4-vinylpyridine (VP, 8.0 *wt*%) and acrylamide (AA, 8.0 *wt*%) as selected monomers, *N*,*N*-methylenebisacrylamide (Bis, 9.0 *wt*%) as a crosslinker, DMSO (52.2 *wt*%) and 1-dodecanol (22.7 *wt*%) as porogens and AIBN (0.1 *wt*%) as thermal initiator was prepared. The pre-polymerization mixture was then pumped through the capillary and left to polymerize under the experimental conditions (Scheme 3.5). Porous poly(AA-*co*-VP-*co*-Bis) polymer monolith with both large flow-through

macropores for convection and a connected network of smaller mesopores was obtained.

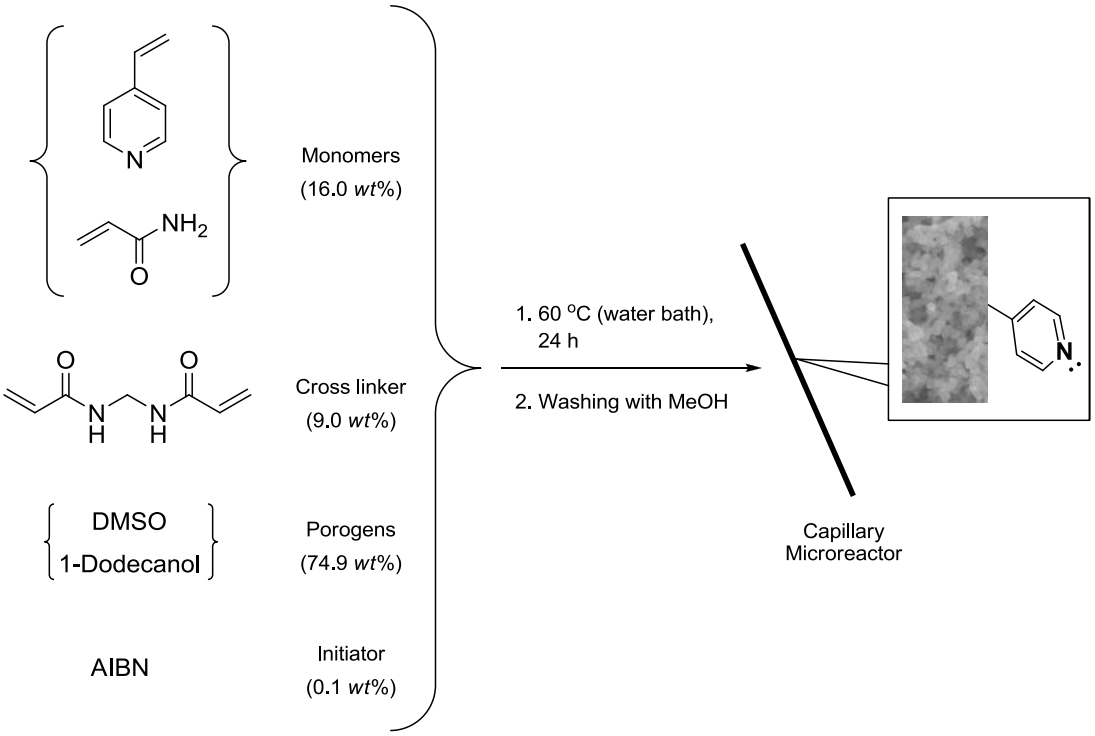

Scheme 3.5. The approach for the preparation of the pyridine-functionalized polymer monolithic support inside the capillary microreactor.

A cross section of the capillary column was imaged by SEM in order to judge the monolith morphology. This involves the monolith's globule size, globule density and interglobular voids. SEM showed homogenous porous structure with interconnecting channels allowing the continuous flow of solvent under low back-pressure (Figure 3.4). The morphology of the prepared polymer monolith was highly reproducible. This was resonated to the relatively slow polymerisation reaction which takes hours to reach completion. As a result, small vacillation in temperature over such long polymerization time will exert negligible effect on the final monolith porous architecture.

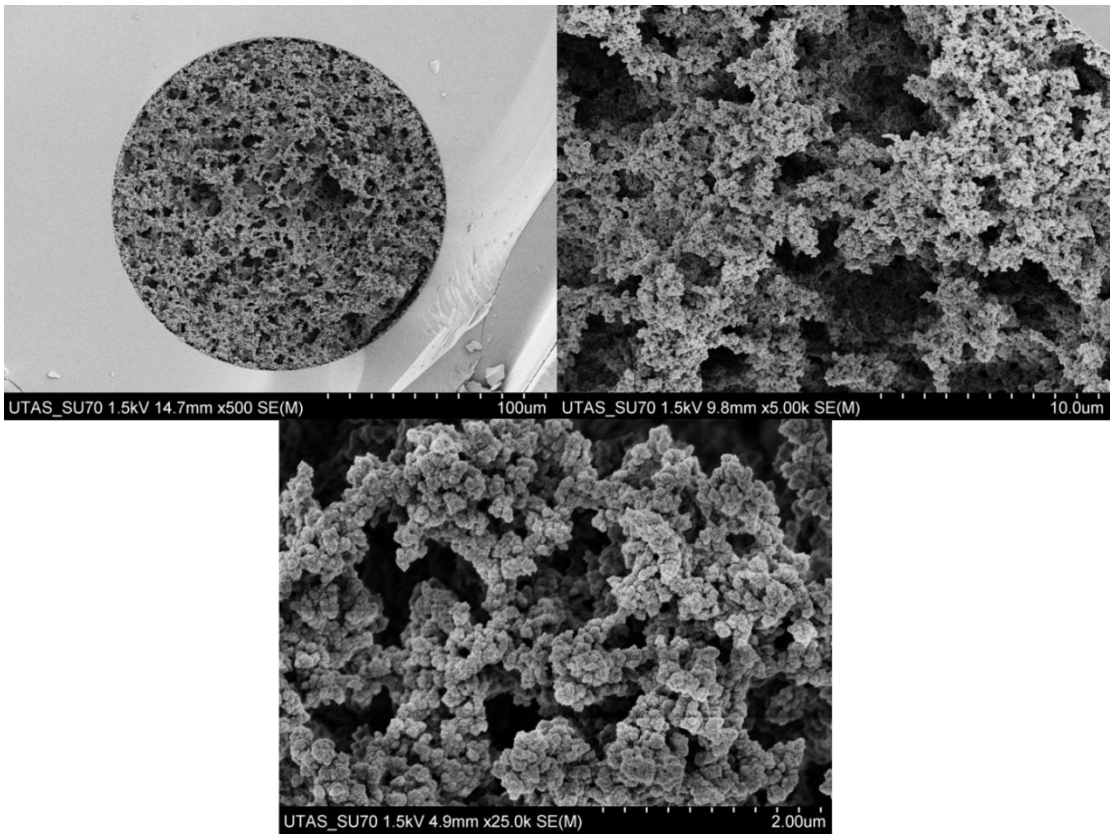

Figure 3.4. SEM image for the prepared poly(AA-*co*-VP-*co*-Bis) monolithic column cross-sections.

Nitrogen content of the prepared monolithic polymer support was also determined by CHN analysis and expressed relative to carbon content. The analysis revealed a carbon to nitrogen ratio of 4.1:1 (*w*/*w*%).

3.2.2. Dirhodium(II) catalyst immobilisation on porous polymer monolith

The pyridyl groups on the monolith were used to coordinately attach Rh_2(*S*-PTTL)$_4$ catalyst to the prepared monolithic support. The immobilization of the catalyst was achieved by simply pumping a solution of Rh_2(*S*-PTTL)$_4$ (2 mg) dissolved in toluene (2 mL) at 0.2 µL.min^{-1} for 18 h at room temperature through the capillary, followed by pumping the same solution in the reverse direction and washing with fresh toluene to get rid of excess catalysts. The capillary microreactors were analyzed for rhodium by ICP-MS and the loading was found to be 43.9 µg rhodium/g of monolithic support. This is much lower than previously found for loadings in conventional

polymer-supported dirhodium(II) complexes which is typically 175 mg rhodium/g support (0.14 mmol/g).[32]

As an attempt to simplify the preparation of the microreactor, another preparation approach was applied at which Rh_2(*S*-PTTL)$_4$ (2 mg) was added as a component to the pre-polymerization mixture. ICP-MS analysis of the prepared capillary microreactor revealed rhodium loading of 17.2 µg rhodium/g of monolithic support which is less than half of the previous strategy. Cross section SEM imaging revealed a dramatic deformation in the morphology at which it showed far finer structure with clusters of interconnected globules (Figure 3.6). This microreactor restricted the flow of the reaction solvent through and hence, it was excluded from further investigations.

This deformation in the monolith morphology was returned to the formation of bis(4-vinylpyridine) adduct when the catalyst was added to the pre-polymerization mixture (Figure 3.5). This species acted as an extra crosslinker. With a higher crosslinker concentration, there was significantly more crosslinking within the formed polymeric material. This led to a far smaller pore size within the formed polymer structure and, in turn, to the observed very poor solvent permeability.

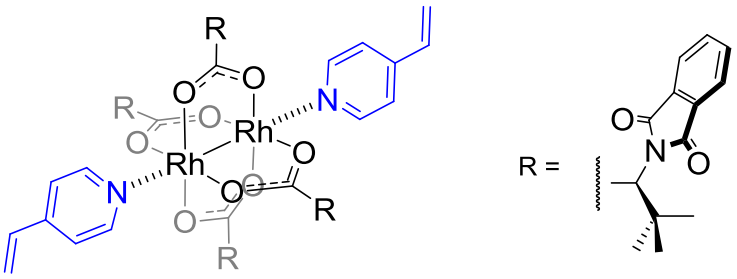

Figure 3.5. Structure of bis(4-vinylpyridine) adduct of Rh_2(*S*-PTTL)$_4$.

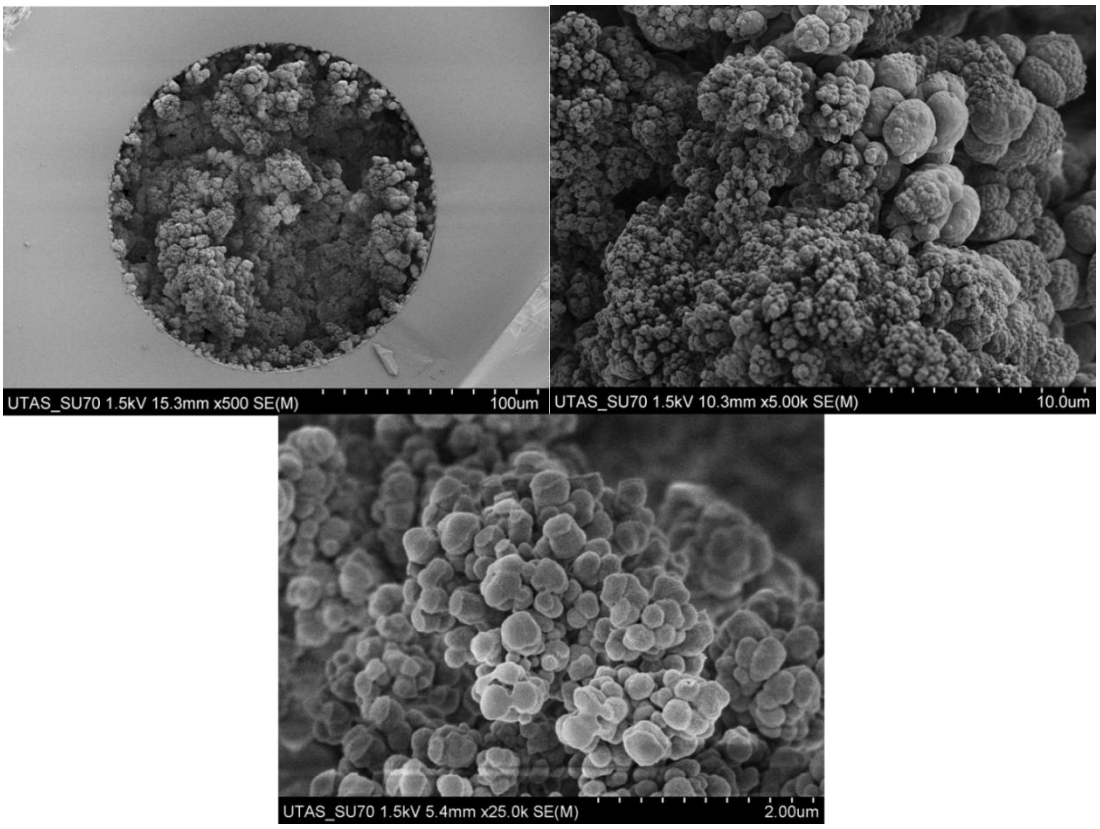

Figure 3.6. SEM imaging for the prepared poly(AA-*co*-VP-*co*-Bis) monolithic column cross section with Rh_2(*S*-PTTL)$_4$ added to the initial pre-polymerization mixture.

3.2.3. Flow-through dirhodium(II)-catalyzed cyclopropanation microreaction

A Rh_2(*S*-^{tert}PTTL)$_4$ microreactor was prepared using the same described procedure used for the preparation of Rh_2(*S*-PTTL)$_4$ microreactor, except in the catalyst immobilization step, at which a solution of 50 mg Rh_2(*S*-^{tert}PTTL)$_4$ per 2.5 mL toluene was employed. The Rh_2(*S*-^{tert}PTTL)$_4$ microreactor was evaluated in the standard cyclopropanation reaction of styrene with dimethyl *α*-diazobenzylphosphonate (Scheme 3.6 and Figure 3.7). The capillary microreactor of 22 cm length was flushed with a solution of dimethyl *α*-diazobenzylphosphonate (1 equiv.) and styrene (5 equiv.) at rate 5 µL.min^{-1} for 45 h at room temperature. The cyclopropane product was collected in a vial from the other side of the reactor (total collected volume of 226 µL). Toluene was chosen as reaction solvent instead of 2,2-DMB used earlier in Chapter 2 for the same reaction to ensure complete solubility of all starting materials.

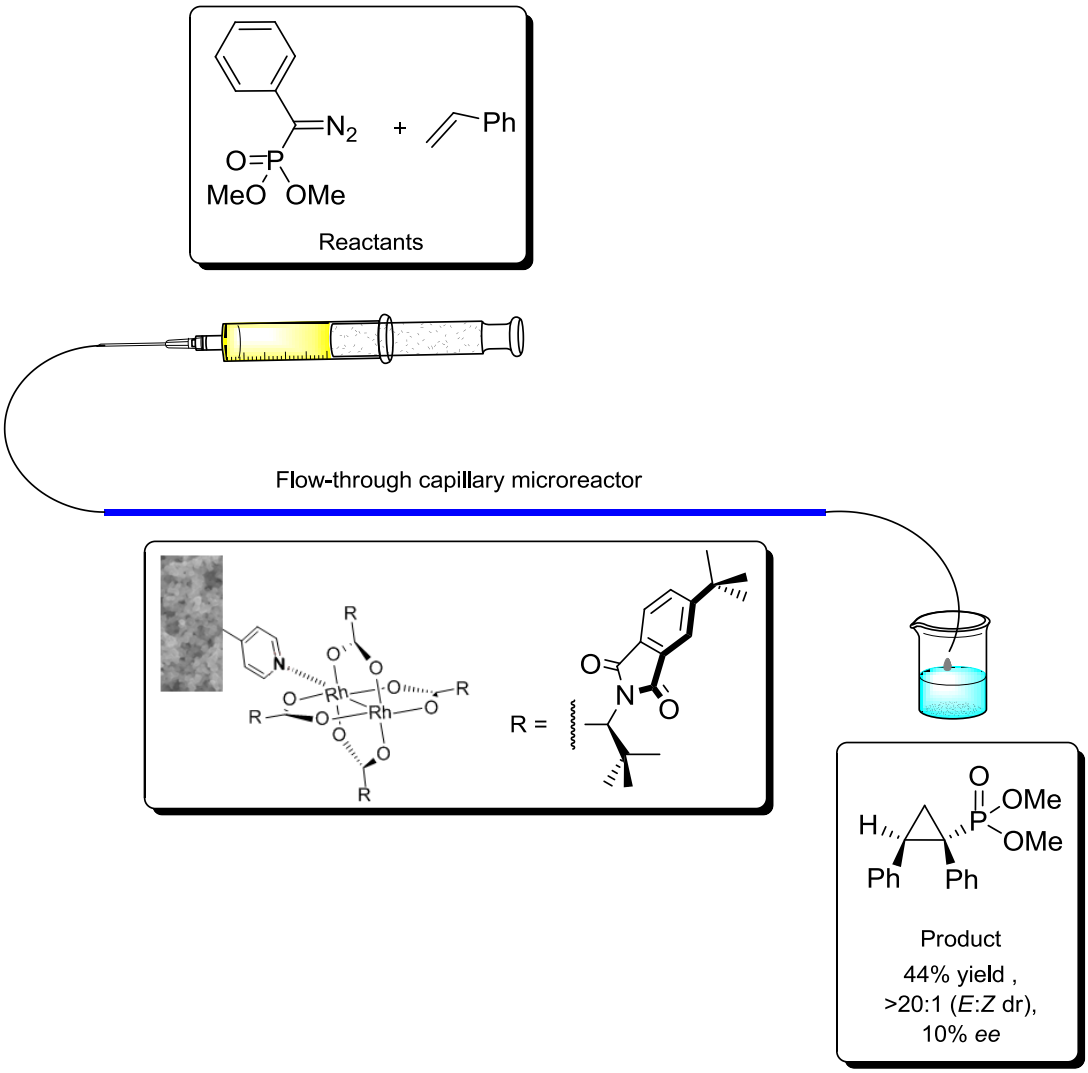

Scheme 3.6. Schematic illustration for the developed flow-through $Rh_2(S\text{-}^{tert}PTTL)_4$-catalyzed cyclopropanation microreactor.

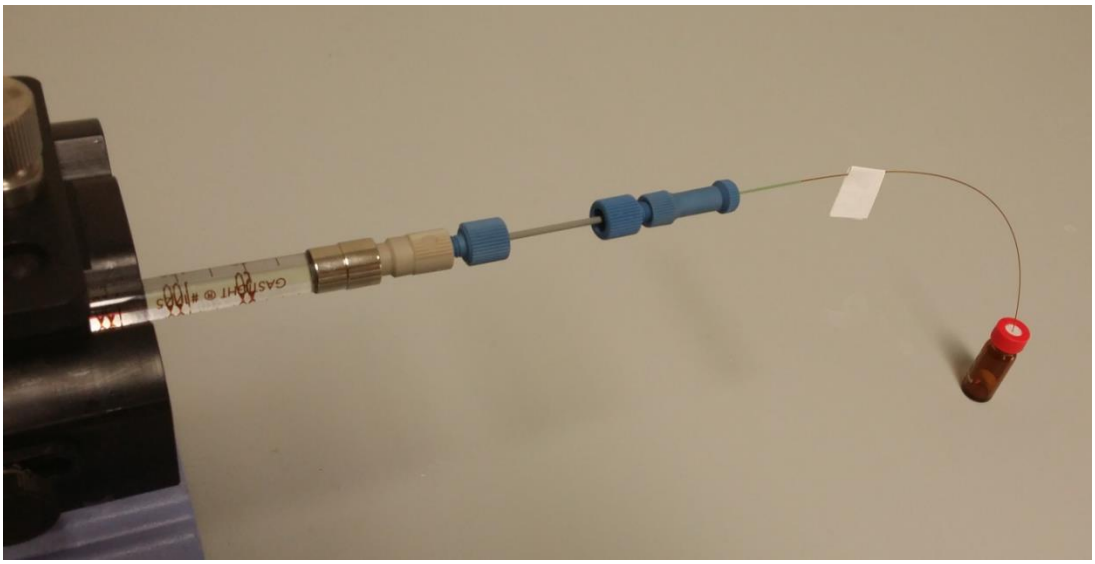

Figure 3.7. Typical flow-through dirhodium(II)-catalyzed cyclopropanation microreaction setup.

To compare the difference between flow-through catalysis and a typical flask reaction under the same conditions, $Rh_2(S\text{-}^{tert}PTTL)_4$-catalyzed cyclopropanation of styrene (5 equiv.) with dimethyl α-diazbenzylphosphonate (1 equiv.) in toluene at room temperature was carried out. The cyclopropane product was generated in excellent yield (92%), diastereoselectivity (>20:1 *E*:*Z* dr) and in 80% enantiomeric excess (Scheme 3.7).

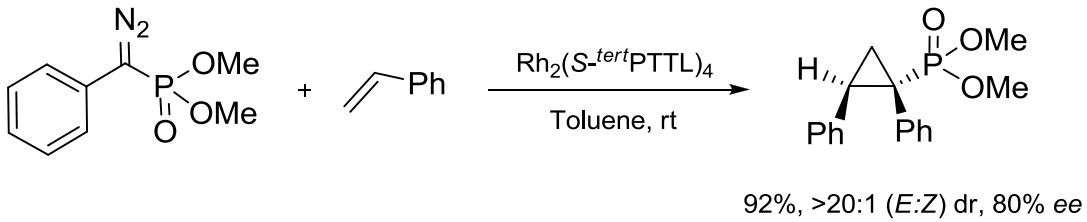

Scheme 3.7. Flask $Rh_2(S\text{-}^{tert}PTTL)_4$-catalyzed cyclopropanation of styrene and dimethyl α-diazobenzylphosphonate in toluene at room temperature.

HPLC analysis of the microreaction product revealed an average yield of 44% (1.5 mg) over the period of 42 h. Further, under the same reaction conditions, It revealed excellent diastereoselectivity (>20:1 *E*:*Z* dr) comparable to the diastereoselectivity of the flask reaction. However, the immobilization of $Rh_2(S\text{-}^{tert}PTTL)_4$ dramatically

affected its enantioinduction. The microreaction product was generated with less enantioselectivity (10% *ee*) compared to the flask reaction product (Figure 3.8). The plain monolith with no rhodium resulted in no catalysis.

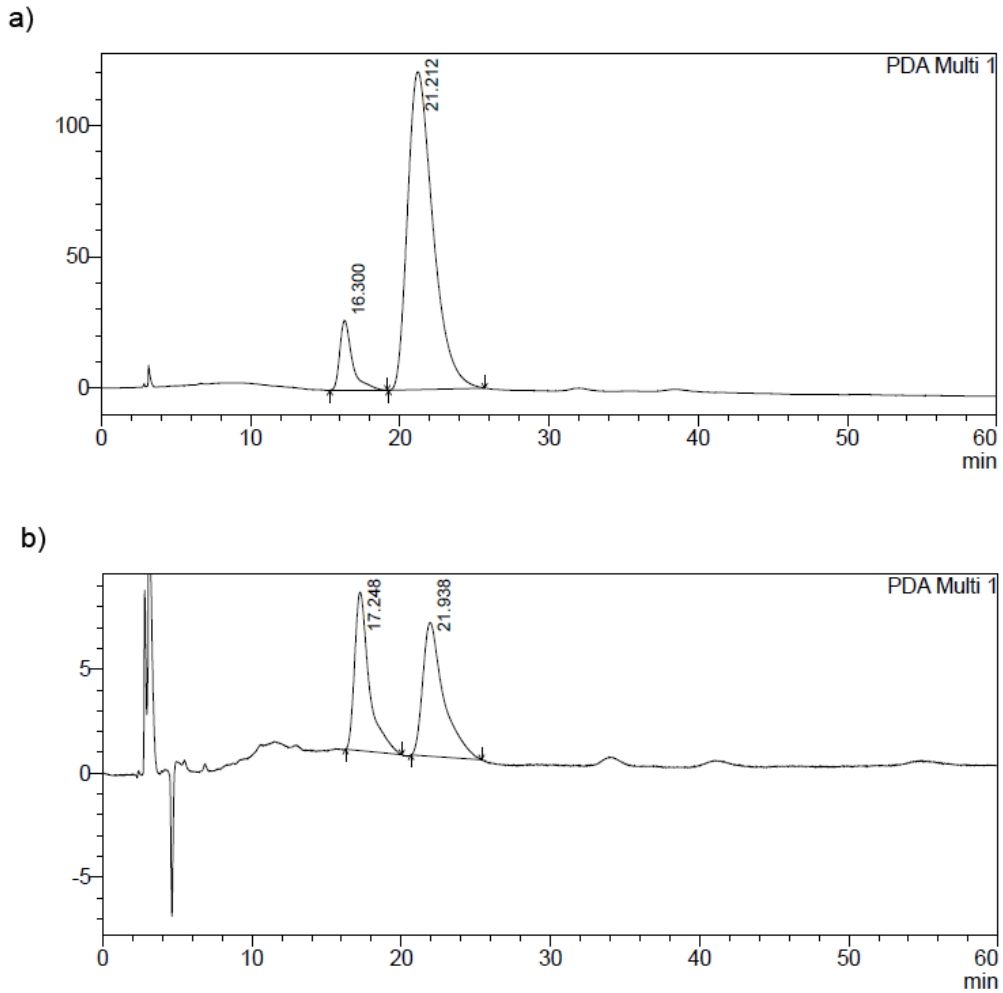

Figure 3.8. Chiral HPLC trace of (1*S*, 2*R*)-dimethyl 1,2-diphenylcyclopropylphosphonate prepared using a) homogenous $Rh_2(S\text{-}^{tert}PTTL)_4$-catalyzed flask reaction, b) polymer-supported $Rh_2(S\text{-}^{tert}PTTL)_4$-catalyzed microreaction. Chromatographic conditions: Chiralcel® OJ column, 2% 2-propanol in *n*-hexane (*v*/*v*%), 1 mL/min, 220 nm.

The leaching level of the dirhodium(II) microreactor was also determined. For that purpose, the capillary microreactor was flushed with the reaction stock mixture for 50 h at which 250 µL of the effluent was collected. The leaching level of rhodium in

the collected effluent was traced by means of ICP-MS to reveal that only 0.296 µg rhodium per millilitre of reaction mixture which is acceptable if compared to the result obtained by Hashimoto for his particle packed flow reactor.[13]

3.3. CONCLUSION

In this chapter, miniaturization of the dirhodium(II)-catalyzed cyclopropanation reaction was carried out through the preparation of asymmetric cyclopropanation capillary microreactor. The solid monolithic support was prepared and characterized using SEM and CHNS analysis. In this microreactor, $Rh_2(S\text{-}^{tert}PTTL)_4$ was immobilized on the surface of the monolithic support and the catalyst loading capacity was determined by ICP-MS analysis. The microreactor was examined for continuous flow asymmetric synthesis of dimethyl 1,2-diphenylcyclopropyl-phosphonate. The results indicated that the cyclopropane product was formed in acceptable yield and diastereoselectivity. However, the enantioselectivity was dramatically less than the value observed for flask synthesis under the same reaction conditions (from 80% to 10% *ee*). The robustness of the microreactor was also investigated by studying the leaching rate of the rhodium catalyst from the microreactor. Generally, the developed microreactor was successful, however, future investigations must focus on improving its enantioselectivity.

3.4. EXPERIMENTAL SECTION

Materials

Acrylamide (AA), 4-vinylpyridine (VP), *N*,*N'*-methylenebisacrylamide (Bis), 1-dodecanol and DMSO were purchased from Sigma-Aldrich Pty. Ltd. AIBN was purchased from Nacalai Tesque, INC. (Japan). Polyimide-coated 150 µm I.D. and 360 µm O.D. fused silica capillaries were obtained from Polymicro Technologies (Phoenix, AZ, USA).

Instruments

Controlled pumping was performed using Harvard Apparatus model Pump 11 Elite (Holliston, Massachusetts, USA) twin syringe pump equipped with 250 µL Hamilton

(Reno, Nevada, USA) Gastight® glass syringes. All capillaries and syringes were connected using Upchurch Scientific (Oak Harbor, Washington, USA) capillary fittings. SEM was done on a Hitachi SU-70 field emission microscope (Hitachi High Technologies, Japan) equipped with Hitachi in-chamber and in-lens scintillation detectors, super ExB filter and beam deceleration. Analysis of samples related to quantitative rhodium loading and leaching determinations was performed on a PerkinElmer NexION® 300D Inductively Coupled Plasma - Mass Spectrometer.

CHN Analysis was achieved using EA3000 CHN analyser. Dynamic Flash Combustion of pressed tin boats containing pre-weighted samples was done in ultra-high purity oxygen gas. Silvered cobaltous/cobaltic oxide and chromium oxide were used as oxidising agents, while reduced copper wires were used as reducing agents. The combustion step is followed by gas chromatographic separation and detection of the resulted gaseous species. The results were calibrated using certified cyclohexanone-2,4-dinitrophenylhydrazone standard.

Vinylization of internal capillary walls[40]

The internal surface of the capillary was treated using a modified literature procedure.[40] A 50 cm length of the fused-silica capillary was rinsed with acetone followed by water. 0.2M NaOH solution was flushed through the capillary until a basic pH was detected at its other end. Flushing with the same solution was continued for 1 h at 0.25 $\mu L.min^{-1}$ flow rate. After this time has elapsed, the capillary was flushed with deionized water until pH 7.0 was detected at its other end. 0.2M HCl solution was flushed through the capillary until an acidic pH was detected at its other end. Flushing with the same solution was continued for 1 h at 0.25 $\mu L.min^{-1}$ flow rate. After this time has elapsed, the capillary was flushed with deionized water until pH 7.0 was detected at its other end. This was followed by flushing the capillary internal surface with ethanol.

A 20% (*w/w*) mixture of 3-(trimethoxysilyl)propyl methacrylate in ethanol was prepared and adjusted with acetic acid to pH 5.0. The mixture was pumped through the capillary at 0.25 $\mu L.min^{-1}$ flow rate for 2 h. The internal surface was finally flushed with acetone and dried with compressed nitrogen gas. The capillary was kept

for at least 24 h to allow the completion of the condensation reaction before proceeding to the next step.

Preparation of solid support of the capillary microreactor

Generic monolith was prepared inside the capillaries using *in situ* polymerization of 4-vinylpyridine (VP, 57 mg, 8.0 *wt*%), acrylamide (AA, 56 mg, 8.0 *wt*%) and *N*,*N*-methylenebisacrylamide (Bis, 63 mg, 9.0 *wt*%) dissolved in binary porogen solvent mixture containing DMSO (370 mg, 52.2 *wt*%) and 1-dodecanol (161 mg, 22.7 *wt*%) and AIBN (2 mg, 0.1 *wt*%) as thermal initiator. The polymerization mixture was degassed with nitrogen gas for 10 min and pumped through the vinylized capillaries at flow rate of 0.25 $\mu L.min^{-1}$ using a syringe pump for at least 2 h. Both capillary terminals were sealed using rubber stoppers and the capillary was placed in pre-adjusted water bath at 60 ^{o}C for 24 h. Both ends were then cut to adjust the length of the capillary and the generated polymer was washed with methanol for another 24 h.

SEM imaging of the polymer monolith

The microreactor capillaries were cut into ~1 cm sections and these sections were mounted perpendicularly on 12 mm pin-type aluminium stub using double face epoxy resin tape (Figure 3.9). High resolution images were collected by coating the capillaries sections with platinum.

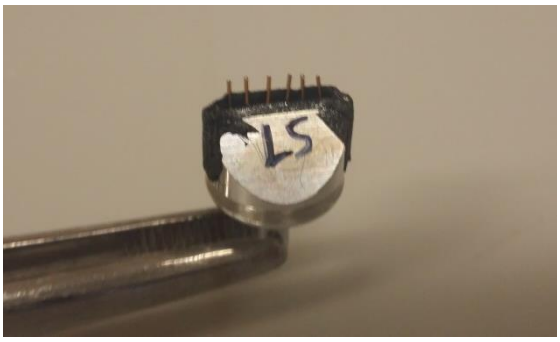

Figure 3.9. Microreactors capillary sections mounted perpendicularly on pin-type aluminium stub using double face epoxy resin tape for high resolution SEM imaging.

Nitrogen content determination through elemental analysis

After blowing air through the capillary reactor overnight using a compressed 10 mL syringe, the external surface of the glass capillary was cleaned with methanol and tissue then left to dry overnight under vacuum. The whole capillary microreactor was finely grinded using a mortar and 0.902 mg sample was weighted into tin boats using a Sartorius SE2 ultra-microbalance (0.2 µg accuracy) and analyzed.

Rh_2(*S*-^{tert}PTTL)$_4$ immobilisation on the porous polymer monolith

A stock solution of Rh_2(*S*-^{tert}PTTL)$_4$ catalyst was prepared by dissolving the catalyst (50 mg) in toluene (2.5 mL), sonicated and filtered through 0.2 µm syringe filter. A 25 cm long 150 µm I.D. poly(AA-*co*-VP-*co*-Bis) monolithic capillary column was prepared as described above. It was flushed with toluene at rate of 0.15 µL.min^{-1} for 3 h using syringe pump, followed by the catalyst stock solution at 0.15 µL.min^{-1} for 24 h. The capillary was then reversed and a second flush with the catalyst stock solution was passed at same flow rate for 8 h. The monolith was then rinsed with toluene at 0.15 µL.min^{-1} flow rate for 4 h to get rid of any excess non-coordinated catalyst molecules.

Rhodium loading determination by ICP-MS

a) Sample preparation

After blowing air through the monolithic capillary reactor overnight using a compressed 10 mL syringe, the external surface of the glass capillary was cleaned with methanol and tissue then left to dry overnight under vacuum. The capillary was cut into ~4 cm portions and grinded with a mortar and pestle. Only the white polymer powder was transferred into a pre-weighed vial and its mass was recorded to 0.05 mg accuracy.

The pre-weighted polymer monolith powder was leached in 1 mL concentrated nitric acid (Aristar, BDH, West Chester, PA, USA) by heating the samples in closed 10 mL polyethylene tubes at 100 °C for 2 h. The tubes were allowed to cool to room temperature before being diluted to 10 mL with deionised water (18.2 mΩ, Millipore, ThermoScientific, Australia) prior to analysis by ICP-MS.

b) Blank preparation

A blank sample was also prepared at which a capillary containing plain polymer monolith and no immobilized rhodium was treated the same way described for the unknown sample. The prepared blank sample was then submitted for ICP-MS analysis.

c) Sample analysis by ICP-MS

Total rhodium (^{103}Rh) concentrations were determined using a PerkinElmer NexION® 300D inductive coupled plasma-mass spectrometer (ICP-MS) with an AS-90 autosampler (PerkinElmer, Waltham, MA, USA). Internal standards (Yttrium [^{89}Y] and Indium [^{115}In]) were added on-line to compensate for any acid effects, instrument drift and changes in the peristaltic pump rate over the course of the analysis. Rhodium (^{103}Rh) has no major interferences so compensation for measured concentrations was based on blank correction and the internal standards listed above. The PerkinElmer NexION® 300D ICP-MS was optimised daily using the automated process built into the NexION (v1.5) software (Table 3.1).

External calibration was performed using single element NIST certified calibration standards from AccuStandard (Merck, Australia). Calibration was performed using five standards in the range of 200 $\mu g.L^{-1}$ to 0.5 $\mu g.L^{-1}$ together with a calibration blank. Quality control consisted of triplicate measurement of one sample, method blank and solvent blank.

Table 3.1. ICP-MS optimised conditions for rhodium analysis in synthetic samples.

Sample flow rate	1.000 mL/min
Plasma RF power	1250 Watts
Nebuliser gas flow rate	0.82 L/min
Plasma gas	18 L/min
Makeup gas (Argon)	1.200 L/min
Sample and skimmer cones	Nickle
Hyper skimmer cone	Aluminium
Scan time	100 ms/element
Scans per replicate	10 scans/element
Replicates	3 replicates/element

The blank sample was analyzed to give 0.1 µg rhodium/g monolith, while the unknown sample was analyzed to give 44 µg rhodium/g monolith.

Reaction mixture preparation

A stock reaction mixture was prepared using dimethyl *α*-diazobenzylphosphonate (0.113 g, 0.5 mmol), styrene (0.286 mL, 2.5 mmol) and toluene (10 mL). The mixture was sonicated for ~5 min, filtered through 0.2 µm syringe filter and used.

Flow-through cyclopropanation reaction in 150 µm ID capillary microreactors

The capillary reactor was flushed with the stock reaction mixture at 5 $\mu L.h^{-1}$ flow rate at room temperature and the effluent was collected from its other terminus into a glass vial. After collecting 225 µL in 45 h, the solvent of collected mixture was evaporated by passing nitrogen gas over its surface and the resulting residue was

purified by means of preparative TLC (refer to Chapter 2 for purification conditions) to afford the pure reaction product.

Determination of product yield and enantiomeric excess (*ee*)

The yield of the product was determined by using the "External Standard Analysis" method. A standard solution of racemic dimethyl 1,2-diphenylcyclopropylphosphonate was prepared by dissolving 6.7 mg of the compound in 1 mL IPA (6.7 $\mu g.\mu L^{-1}$ concentration). The standard solution was injected through the HPLC three times at 1 µL (6.7 µg), 2 µL (13.4 µg) and 4 µL (26.8 µg) injection volumes to generate the calibration curve for each of the enantiomers (Figure 3.10). After the calibration curve was established, the total amount obtained from the purified product was dissolved in 600 µL IPA, filtered through syringe filter and injected through the HPLC at 5 µL injection volume (refer to Chapter 2 for chiral HPLC trace conditions).

ID# : 1
Name : RT17.873
Quantitative Method : External Standard
Function : f(x)=4.14393e-007*x+0.994334
Rr1=0.9998176 Rr2=0.9996352
MeanRF: 5.045239e-007 RFSD: 6.274350e-008 RFRSD: 12.436180
FitType : Linear
ZeroThrough : Not Through
Weighted Regression : None
Detector Name : PDA

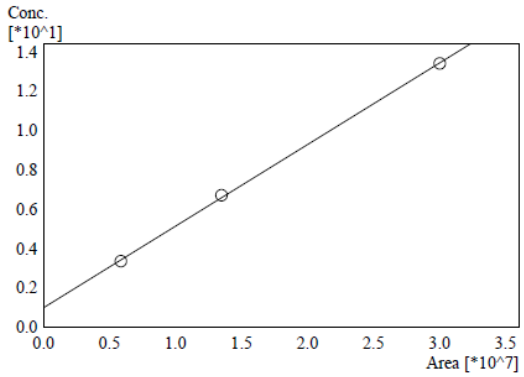

#	Conc.(Ratio)	MeanArea	Area
1	3.35	5866800	5866800
2	6.7	13502342	13502342
3	13.4	30021174	30021174

ID# : 2
Name : RT22.042
Quantitative Method : External Standard
Function : f(x)=4.04101e-007*x+1.03353
Rr1=0.9998040 Rr2=0.9996080
MeanRF: 4.965130e-007 RFSD: 6.479913e-008 RFRSD: 13.050843
FitType : Linear
ZeroThrough : Not Through
Weighted Regression : None
Detector Name : PDA

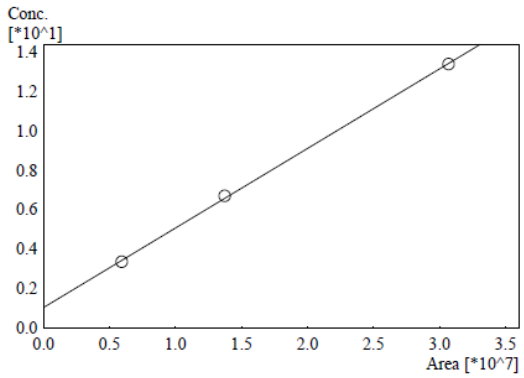

#	Conc.(Ratio)	MeanArea	Area
1	3.35	5926203	5926203
2	6.7	13739269	13739269
3	13.4	30691743	30691743

Figure 3.10. Standard calibration curves for both enantiomers of dimethyl 1,2-diphenylcyclopropylphosphonate generated by injecting different concentrations of a standard sample through the HPLC.

Rhodium leaching rate determination by ICP-MS

a) Sample collection and preparation

The capillary reactor was flushed with the stock reaction mixture at 5 $\mu L.h^{-1}$ flow rate at room temperature for 50 h. The effluent (250 µL) was collected from the other terminus into a glass vial. After the reaction solvent was left to evaporate, the residue was digested with 250 µL of nitric acid (Aristar, BDH, West Chester, PA, USA) by

heating the samples in closed 10 mL polyethylene tubes at 100 °C for 2 h. The tubes were allowed to cool to room temperature before being diluted to 5 mL with deionised water (18.2 mΩ, Millipore, ThermoScientific, Australia) prior to analysis by ICP-MS.

b) Blank preparation

A blank sample was prepared by transferring 1 mL of the reaction stock solution to a glass vial. After leaving the solvent to evaporate, 1 mL of concentrated nitric acid was added to the oily residue, followed by dilution to 10 mL with deionized water. The prepared blank was then submitted for ICP-MS analysis.

c) Sample analysis by ICP-MS

Total rhodium (^{103}Rh) concentrations were determined using the PerkinElmer NexION® 300D ICP-MS instrument and using the same instrument parameters described above.

The blank sample was analyzed to give 0.280 µg rhodium/mL of stock solution, while the unknown sample was analyzed to give 0.576 µg rhodium/mL of stock solution.

3.5. REFERENCES

1. Andraos, J. *Org. Process Res. Dev.* **2005**, *9*, 519.
2. Denmark, S. E.; Jacobsen, E. N. *Acc. Chem. Res.* **2000**, *33*, 324.
3. Dörwald, F. Z. *Organic Synthesis on Solid Phase: Supports, Linkers, Reactions*; Wiley-VCH: Weiheim, Germany, 2003.
4. Zhu, J.; Bienaymé, H. *Multicomponent Reactions*; Wiley-VCH: Weinheim, Germany, 2005.
5. Tietze, L. F.; Brasche, G.; Gericke, K. *Domino Reactions in Organic Synthesis*; Wiley-VCH: Weinheim, Germany, 2006.

6. Behr, A.; Neubert, P. *Applied Homogeneous Catalysis*; Wiley-VCH: Weinheim, Germany, 2012.

7. Wirth, T. *Microreactors in Organic Chemistry and Catalysis*; Wiley-VCH: Weinheim, Germany, 2013.

8. Fletcher, P. D. I.; Haswell, S. J.; -Villar, E. P.; Warrington, B. H.; Watts, P.; Wong, S. Y. F.; Zhang, X. *Tetrahedron* **2002**, *58*, 4735.

9. Mason, B. P.; Price, K. E.; Steinbacher, J. L.; Bogdan, A. R.; McQuade, D. T. *Chem. Rev.* **2007**, *107*, 2300.

10. Geyer, K.; Codee, J. D. C.; Seeberger, P. H. *Chem.-Eur. J.* **2006**, *12*, 8434.

11. Seeberger, P. H. *Chemfiles* **2005**, *5*, 2.

12. Chen, Y.-T.; Chem, K.-H.; Fang, W.-F.; Tsai, S.-H.; Fang, J.-M.; Yang, J.-T. *Chem. Eng. J.* **2011**, *174*, 421.

13. Takeda, K.; Oohara, T.; Shimada, N.; Nambu, H.; Hashimoto, S. *Chem.-Eur. J.* **2011**, *17*, 13992.

14. Takeda, K.; Oohara, T.; Anada, M.; Nambu, H.; Hashimoto, S. *Angew. Chem., Int. Ed.* **2010**, *49*, 6979.

15. Oohara, T.; Nambu, H.; Anada, M.; Takeda, K.; Hashimoto, S. *Adv. Synth. Catal.* **2012**, *354*, 2331.

16. Stankiewicz, A. *Chem. Eng. Sci.* **2001**, *56*, 359.

17. Sachse, A.; Galarneau, A.; Coq, B.; Fajula, F. *New J. Chem.* **2011**, *35*, 259.

18. *IUPAC Recommendations* **2007**, pp. 1812.

19. Svec, F. *Electroanalysis* **2006**, *27*, 947.

20. Buchmeiser, M. R. *Polymer* **2007**, *48*, 2187.

21. Katrina, F. B.; Jeremy, A. J.; Deverell, J. A.; Guijt, R. M.; Hilder, E. F.; Rodemann, T.; Smith, J. A. *Tetrahedron Lett.* **2006**, *47*, 9321.

22. Canty, A. J.; Deverell, J. A.; Gomann, A.; Guijt, R. M.; Rodemann, T.; Smith, J. A. *Aust. J. Chem.* **2008**, *61*, 630.

23. Gomann, A.; Deverell, J. A.; Munting, K. F.; Jones, R. C.; Rodemann, T.; Canty, A. J.; Smith, J. A.; Guijt, R. M. *Tetrahedron* **2009**, *65*, 1450.

24. Jones, R. C.; Canty, A. J.; Deverell, J. A.; Gardiner, M. G.; Guijt, R. M.; Rodemann, T.; Smith, J. A.; Tolhurst, V.-A. *Tetrahedron* **2009**, *65*, 7474.

25. Garcia-Verdugo; Leuis. *Chem. Commun.* **2006**, 3095.

26. Guiochon, G. *J. Chromatogr. A* **2007**, *1168*, 101.

27. Takeda, K.; Oohara, T.; Shimada, N.; Nambu, H.; Hashimoto, S. *Chem. Eur. J.* **2011**, *17*, 13992.

28. Doyle, M. P.; Eismont, M. Y.; Bergbreiter, D. E.; Gray, H. N. *J. Org. Chem.* **1992**, *57*, 6103.

29. Nagashima, T.; Davies, H. M. L. *Org. Lett.* **2002**, *4*, 1989.

30. Davies, H. M. L.; Walji, A. M.; Nagashima, T. *J. Am. Chem. Soc.* **2004**, *126*, 4271.

31. Davies, H. M. L.; Walji, A. M. *Org. Lett.* **2003**, *5*, 479.

32. Davies, H. M. L.; Walji, A. M. *Org. Lett.* **2005**, *7*, 2941.

33. Bergbreiter, D. E.; Morvant, M.; Chen, B. *Tetrahedron Lett.* **1991**, *32*, 2731.

34. Bergbreiter, D. E. *Chem. Rev.* **2002**, *102*, 3345.

35. Bergbreiter, D. E.; Tian, J. *Tetrahedron Lett.* **2007**, *48*, 4499.

36. Candeias, N. R.; Afonso, C. A. M.; Gois, P. M. P. *Org. Biomol. Chem.* **2012**, *10*, 3357.

37. Doyle, M. P.; Yan, M. *Org. Lett.* **2003**, *5*, 561.

38. Chepiga, K. M.; Feng, Y.; Brunelli, N. A.; Jones, C. W.; Davies, H. M. L. *Org. Lett.* **2013**, *15*, 6136.

39. Dikarev, E. V.; Kumar, D. K.; Filatov, A. S.; Anan, A.; Xie, Y.; Asefa, T.; Petrukhina, M. A. *ChemCatChem* **2010**, *2*, 1461.

40. Schaller, D.; Hilder, E. F.; Haddad, P. R. *Anal. Chim. Acta* **2006**, *556*, 104.

41. Peters, E. C.; Svec, F.; Frechet, J. M. *Adv. Mater.* **1999**, *11*, 1169.

CHAPTER 4: GENERAL DISCUSSION, CONCLUSION AND FUTURE PERSPECTIVE

Asymmetric interactions through chiral recognition are believed to be the foundation of the chemistry of life. Hence, the broadest range of natural occurring biologically active molecules abides in the form of single enantiomers. The same principle applies for important synthetic molecules such as pharmaceuticals, agrochemicals, flavours and fragrances. As only one enantiomer can exhibit the desired biological effect, recent FDA regulations stressed the necessity of producing these compounds as single enantiomers and strongly dis-favoured production of racemates.[1,2] From here, the invention and discovery of efficient methodologies for accessing enantiomerically pure molecules has been an extensive challenge for synthetic chemists.

Generally, three strategies are applied for achieving enantiomerically pure compounds. They are all based upon the fact that chiral compounds can be artificially synthesized and/or purified only in a chiral environment. The three strategies are (i) chiral resolution of racemates, (ii) using conventional synthesis starting from commercially available chiral building blocks and (iii) using asymmetric synthesis involving chiral auxiliaries, reagents or catalysts. Enantioselective catalysis is currently considered the most appealing strategy among the different methods employed for the production of enantiomerically pure compounds. This is reflected by the large number of reports related to that field. This is, in addition to, the Nobel Prize that was awarded to Knowles, Noyori and Sharpless in 2001 for their crucial contribution in that field.[3] Typically in this approach, a transition metal complex carrying chiral ligand(s) will catalyze the transformation of the prochiral starting material. During this process, the chiral catalyst will dissymmetrically curve the space surrounding the reaction centre so that only one stereochemical outcome can be favourably obtained. Indeed, the optimization of several parameters is essential when employing this approach for achieving superior levels of reactivity, chemo-, regio- and stereoselectivity. Among these parameters, the design and careful selection of the chiral ligand(s) is perhaps the key step in the field of asymmetric catalysis development.

As illustrated in Chapter 1, chiral dirhodium(II) paddlewheel complexes have been used as effective catalysts for highly stereoselective inter- and intramolecular cyclopropanation reactions. In fact, the evolution in this field has greatly concentrated on varying the ligand's steric profile. Thus, the current project was aiming to investigate the stereoselection in linkage to lowering the symmetry of the ligand's *N*-heterocyclic tether as a possible way for varying ligand sterics. Enantioselection mainly arises from the different preferred reaction channels as a function of the different steric interplay between the carbene and the ligands structures. Accordingly, the introduction of an asymmetry factor to the ligand's *N*-protecting group is able to modify the steric surrounding in the proximity of the rhodium active site. This can lead to two possible electronically equivalent but sterically different substrate orientations within the chiral cavity (Figure 4.1).

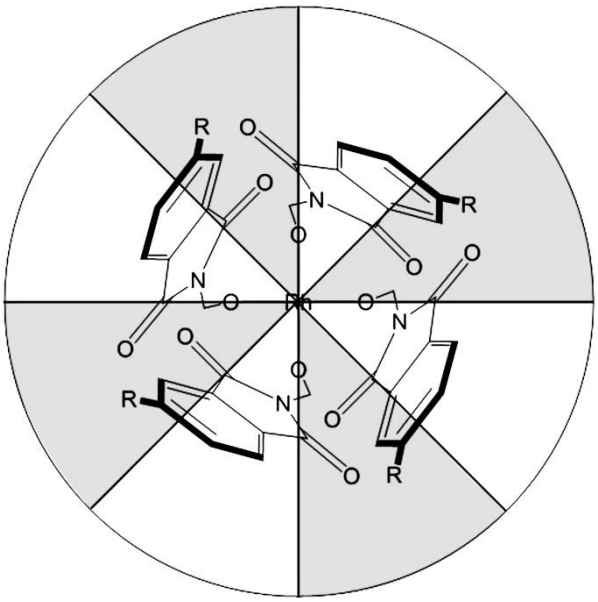

Figure 4.1. The two possible electronically equivalent and sterically different substrate orientations within the chiral cavity (represented in grey and white areas).

The current investigation contributes to the discovery of new chiral dirhodium(II) carboxylates for application in highly enantioselective cyclopropanation reactions. Ten novel dirhodium(II) complexes derived from chiral (*S*)-amino acid ligands were synthesized where each complex features a reduction in symmetry in its *N*-protecting group. In each case, the reduction in symmetry was of different nature and impacts

on the accessibility of binding substrates within the higher order chirally twisted rhodium binding pocket.

Initially, the idea of reducing the ligand's heterocyclic tether symmetry by fusing a ring at only one side of the *N*-protecting group was employed. Primary screening demonstrated that Rh_2(*S*-1,2-NTTL)$_4$ (**3a**) with the larger aromatic surface area was a promising backup catalyst for the cyclopropanation reaction involving *donor-acceptor* phosphonate carbenoids. However, the obtained results did not provide any clear advantage for the aimed "lower symmetry" approach.

Two more ways were investigated as alternative routes for the reduction of the ligand's heterocyclic tether symmetry. The first way was by partial substitution of the *N*-protecting group as in Rh_2(*S*-1-Ph-BPTTL)$_4$ (**11**) and Rh_2(*S*-^{tert}PTTL)$_4$ (**12**). While the second was by possible orientation to either sides of the planar core of the *N*-protecting group as in Rh_2(*S*-BHTL)$_4$ (**13**) and Rh_2(*S*-BOTL)$_4$ (**14**).

Among the prepared complexes, Rh_2(*S*-^{tert}PTTL)$_4$ (**12**) proved to be an exceptional catalyst with extraordinary enantioselectivity (up to 99% *ee*). Screening in a number of different *donor-acceptor* diazo systems revealed that, generally, Rh_2(*S*-^{tert}PTTL)$_4$ (**12**) is a much more enantioselective catalyst than Rh_2(*S*-PTTL)$_4$ and Rh_2(*S*-NTTL)$_4$, with a comparable enantioselectivity to Rh_2(*S*-PTAD)$_4$. This is in addition to overcoming the synthetic limitations associated with Rh_2(*S*-PTAD)$_4$ as being much more synthetically accessible. Rh_2(*S*-^{tert}PTTL)$_4$ (**12**) was achieved in high yield using a two steps procedure, while Rh_2(*S*-PTAD)$_4$ is reported to be prepared in more than thirteen steps taking around two weeks period of time. In the synthesis of cyclopropylphosphonate derivatives, Rh_2(*S*-^{tert}PTTL)$_4$ (**12**) proved to offer an extra advantage than Rh_2(*S*-PTAD)$_4$. For Rh_2(*S*-^{tert}PTTL)$_4$, after stirring at room temperature for 5 h, the corresponding cyclopropane products were generated in high yields, diastereoselectivity and enantioselectivity. Results for similar reactions catalyzed by Rh_2(*S*-PTAD)$_4$ were reported under refluxing conditions for 10 h.[4] My results also demonstrated that, Rh_2(*S*-^{tert}PTTL)$_4$ (**12**) is compatible with some *donor-acceptor* diazaoacetate substrates. This reflected its ability to complement with the currently known flagship catalyst, Rh_2(*S*-DOSP)$_4$ and broadens the range of available catalysts for the asymmetric preparation of chiral cyclopropylcarboxylate derivatives.

Synchrotron X-ray crystallographic studies revealed that both Rh_2(*S*-^{tert}PTTL)$_4$ (**12**) and Rh_2(*S*-PTAD)$_4$ structures were different from Fox's X-ray structure of Rh_2(*S*-PTTL)$_4$. Fox implied that Rh_2(*S*-PTTL)$_4$ and related complexes are in a C_2-symmetric arrangement in solid state.[5,6] From solid state structures comparisons, it was obvious that the extra *tert*-butyl groups introduced in Rh_2(*S*-^{tert}PTTL)$_4$ (**12**) generated similar structural effects generated by increasing the size of the *α*-substituents to adamantyl groups in Rh_2(*S*-PTAD)$_4$. This was further confirmed by the comparable enantioselectivity observed for both Rh_2(*S*-^{tert}PTTL)$_4$ (**12**) and Rh_2(*S*-PTAD)$_4$. Through the study of the halogen bond rigidification effect observed in chlorinated complexes, Charette and co-workers[7,8] previously highlighted the effect of chiral cavity rigidity on enhancement of enantioselectivity. Herein and based on enantioselectivities achieved along with crystallographic observations with the new catalytic systems, it can be confirmed that partial substitution of the ligand's *N*-hetereocyclic tether is another factor towards reinforcing the rigidity of the cavity and enhancing the catalyst stereoselectivity.

As a further development for Rh_2(*S*-^{tert}PTTL)$_4$ (**12**), the synthesis of chiral dirhodium(II) carboxylate complex carrying adamantyl substituents on the heterocyclic tethers was briefly explored, however, achievement of the required *N*-(4-adamantylphthaloyl)-(*S*)-*tert*-leucine ligand was not successful. Future investigations related to the preparation, screening and structural studies for this complex must continue as being a promising extension for the current project.

Chiral dirhodium(II) complex derived from per-*O*-acetylated D-glucuronic acid was also synthesized and fully characterized. Its catalytic selectivity was evaluated through various cyclopropanations and, unfortunately, very low enantioselectivities were obtained. Carbohydrate derivatives are still a very promising class of ligands and future investigations related to using them as chiral ligands in the dirhodium(II) chemistry should carry on to find the optimum ligand that is able to return high levels of enantioselection.

All in all and in the light of the achieved results, it is strongly believed that the introduced "reduction of symmetry" approach is an excellent new way for enhancing the enantioselectivity in asymmetric dirhodium(II)-catalyzed transformations. Further explorations related to this new trend are crucial to further confirm the impact of the lowering the symmetry of the *N*-protecting group on the final

enantioselectivity of the catalyst. Also, although the synthesis of chiral dirhodium(II) carboxylate complex carrying *N*-(4-*tert*-butylnaphthaloyl)-(*S*)-*tert*-leucine ligand was briefly explored, $Rh_2(S\text{-}^{tert}NTTL)_4$ is a very promising catalyst to look at. A suggested alternative synthesis procedure for the ^{tert}NTTL ligand can be by starting form 1-*tert*-butylnaphthalene which is commercially available from Amber Moltech Chemicals company. The proposed synthesis can begin with Friedel-Crafts double acylation of 1-*tert*-butylnaphthalene with oxalyl chloride to generate 4-*tert*-butylacenaphthene dione. This can be followed by oxygen insertion using potassium peroxymonosulfate (Oxone) according to the reported conditions of Loh and co-workers[9] which can lead to the desired dicarboxylic acid anhydride. Suggested reaction of the generated anhydride with L-*tert*-leucine can afford the desired chiral ligand (Scheme 4.1).

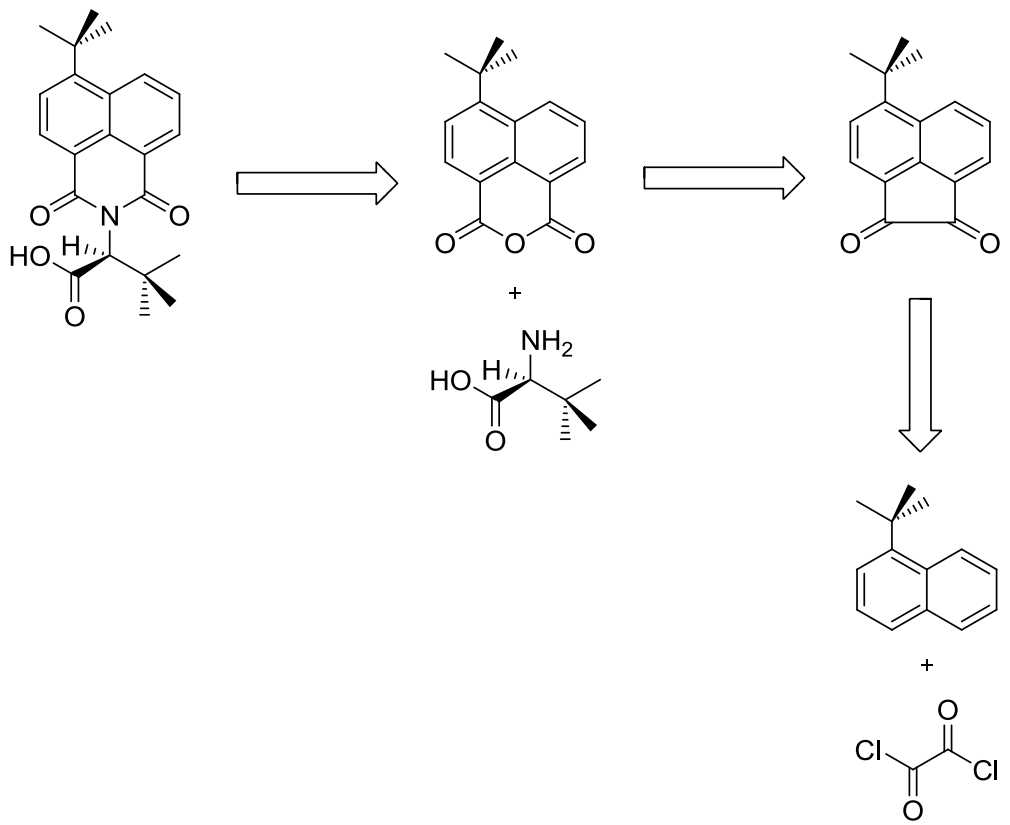

Scheme 4.1. Suggested retro-synthetic route for the preparation of *N*-(4-*tert*-butylnaphthaloyl)-(*S*)-*tert*-leucine ligand, ^{tert}NTTL.

Another interesting observation was, the binding of identical MeOH axial ligands to each Rh centre in Rh_2(*S*-BOTL)$_4$ complex (**14**) has not resulted in a major *α,α,α,α* to *α,α,β,β* or *α,β,α,β* conformational flip. The C_4-symmetry of the chiral cavity, however, were lost while the catalyst's *α,α,α,α* conformation still exists. More extensive structural investigations need to be undertaken before any generalities should be drawn regarding the effects of axial bound ligands on the conformational preference of this class of complexes.

With the fast development in the field of crystallography, computational modelling and solution NMR spectroscopy, future efforts may succeed in uncovering the mystery around the conformations of dirhodium(II) complexes in both solid state and in solution. This, in turn, can ultimately help in the design of new, more universal and highly stereoselective chiral dirhodium(II) systems. Synchrotron single crystal X-ray analysis is an utmost non-destructive technique in the field of chiral dirhodium(II) catalysis that is able to provide a wealth of information from very small amounts of material. By analysing a crystal as small as 0.05 mm^3, the identity of all molecular or ionic species present, their oxidation states, mutual arrangement in the lattice, symmetry, conformations, torsion angles and interatomic distances and angles can be established with high precision.

The current project was further extended by looking at the miniaturization of the cyclopropanation reaction through the preparation of cyclopropanation capillary microreactor. The solid polymeric monolithic support was prepared and characterized using SEM imaging and CHN analysis. In this microreactor, Rh_2(*S*-^{tert}PTTL)$_4$ was immobilized on the surface of the monolithic support, while the catalyst loading capacity was determined by ICP-MS analysis. The microreactor was examined for continuous flow asymmetric synthesis of cyclopropylphosphonates. The results revealed that the cyclopropane product was formed in high yields and diastereoselectivity. In terms of enantioinduction, the enantioselectivity of the catalyst was shown to be deteriorated compared to the same compound obtained through flask synthesis under the same reaction conditions (from 80% to 10% *ee*). Studying the leaching rate of rhodium coming out of the microreactor indicated high levels of robustness.

Although the immobilized dirhodium(II)-catalyzed cyclopropanations was successfully demonstrated in capillary microreactors for the first time satisfying one

of the main objectives of the current project, this "proof of concept" needs deeper investigation for achieving better levels of enantioselectivity. Using the obtained results as a framework, future investigations may include trying different monolith compositions, introduction of spacer moieties and employing other dirhodium(II) complexes for immobilization.

4.1. REFERENCES

1. *Chirality* **1992**, *4*, 338.
2. Branch, S. In *Chiral Separation Techniques. A Practical Approach. 2nd Edition;* Subramanian, G. Ed.; Wiley-VCH: Weinheim, 2001; pp. 319.
3. http://www.nobelprize.org/nobel_prizes/chemistry/laureates/2001/
4. Reddy, R. P.; Lee, G. H.; Davies, H. M. L. *Org. Lett.* **2006**, *8*, 3437.
5. DeAngelis, A.; Dmitrenko, O.; Yap, G. P. A.; Fox, J. M. *J. Am. Chem. Soc.* **2009**, *131*, 7230.
6. DeAngelis, A.; Boruta, D. T.; Lubin, J.-B.; Plampin, J. N.; Yap, G. P. A.; Fox, J. M. *Chem. Commun.* **2010**, *46*, 4541.
7. Lindsay, V. N. G.; Lin, W.; Charette, A. B. *J. Am. Chem. Soc.* **2009**, *131*, 16383.
8. Lindsay, V. N. G.; Charette, A. B. *ACS Catalysis* **2012**, *2*, 1221.
9. Yao, J. H.; Chi, C.; Wu, J.; Loh, K.-P. *Chem.-Eur. J.* **2009**, *15*, 9299.

APPENDICES

2-Dimentional NMR spectral data recorded for 4,4'-binaphthyl-1,1',8,8'-tetracarboxylic dianhydride (**18**)

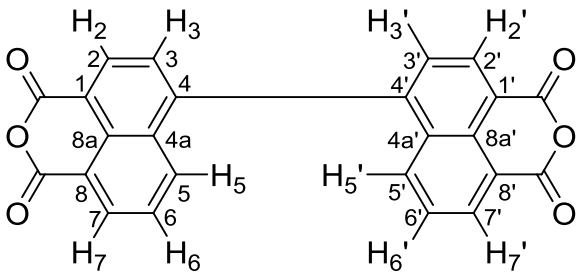

^{1}H-^{13}C HMBC

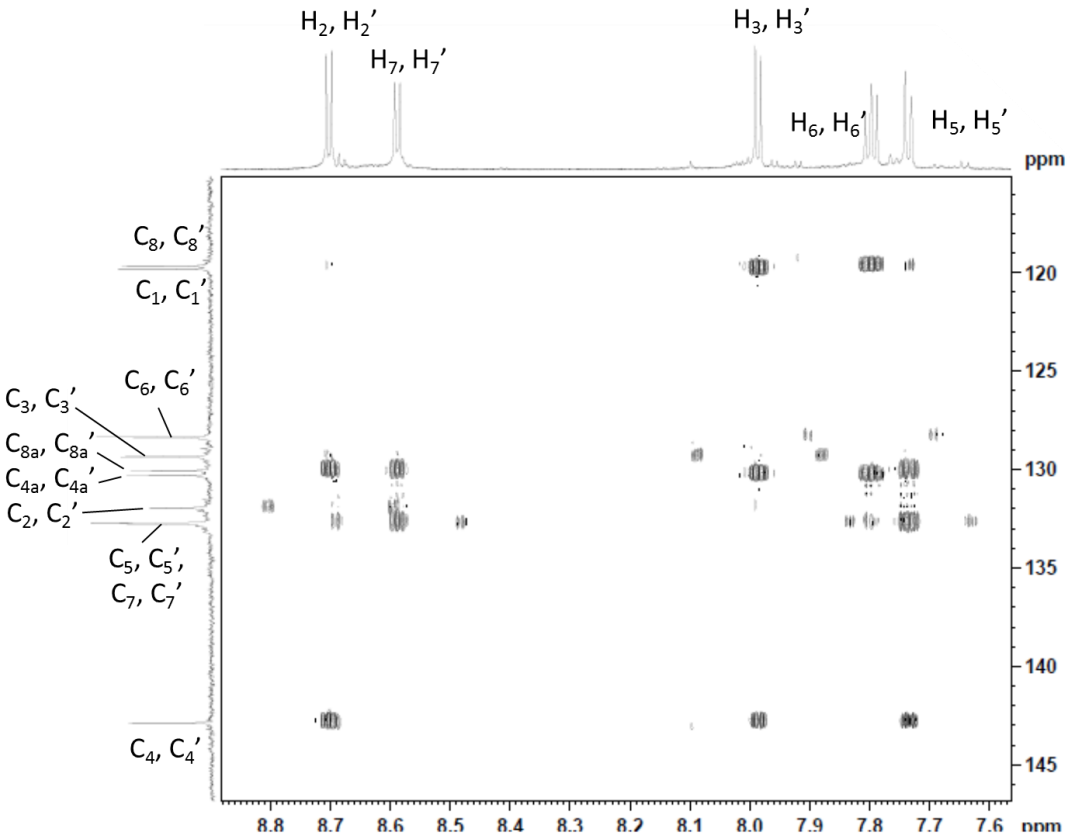

^{1}H-^{13}C HSQC

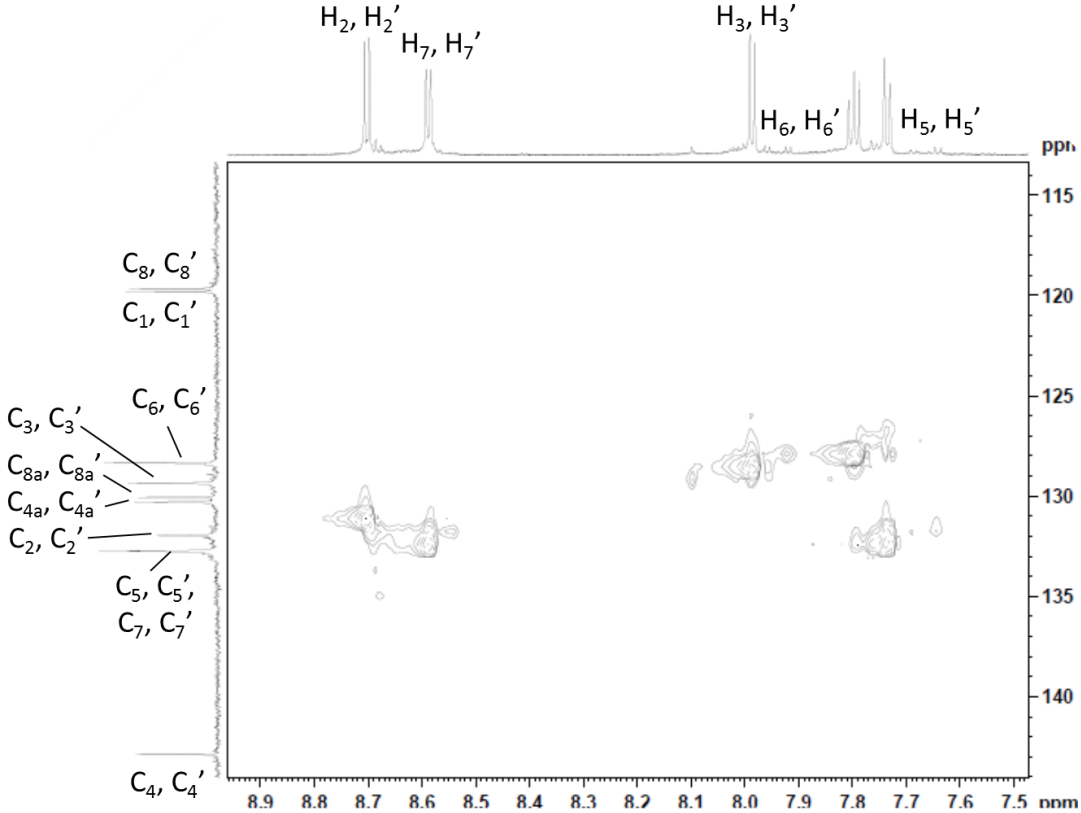
H2, H2'
H7, H7'
H3, H3'
H6, H6'
H5, H5'
ppm
115
120
125
130
135
140
C8, C8'
C1, C1'
C6, C6'
C3, C3'
C8a, C8a'
C4a, C4a'
C2, C2'
C5, C5',
C7, C7'
C4, C4'
8.9
8.8
8.7
8.6
8.5
8.4
8.3
8.2
8.1
8.0
7.9
7.8
7.7
7.6
7.5
ppm

Table S1. Effect of ligand enantiopurity on the enantioselectivity of the final catalyst.

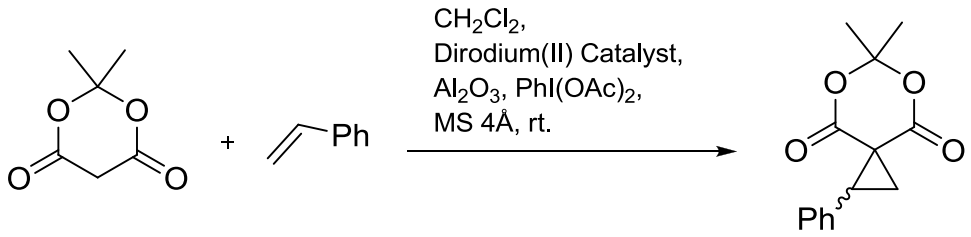

Entry	Complex	Acetic Acid Catalyst		DMF Catalyst		Toluene/TEA Catalyst	
		***ee*% of Ligand**	***ee*% of Cyclopropane**	***ee*% of Ligand**	***ee*% of Cyclopropane**	***ee*% of Ligand**	***ee*% of Cyclopropane**
1	Rh_2(*S*-PTTL)$_4$	86%[a]	32%[a]	78%	20%	99%[a]	37%
2	Rh_2(*S*-1,2-NTTL)$_4$ (**3a**)	84%	28%	74%	26%[a]	>99%	30%
3	Rh_2(*S*-1,2-NTTR)$_4$ (**3d**)	60%	7%	92%	17%[a]	99%	18%
4	Rh_2(*S*-1,2-NTPA)$_4$ (**3b**)	2%	6%	70%	9%[a]	84%	12%[a]

5	Rh_2(*S*-1,2-NTLU)$_4$ (**3c**)	60%	12%	36%	10%[a]	97%	16%[a]
6	Rh_2(*S*-1,2-NTTY)$_4$ (**3e**)	17%	3%	95%	10%[a]	99%	13%

[a]Analyzed as crude mixture.

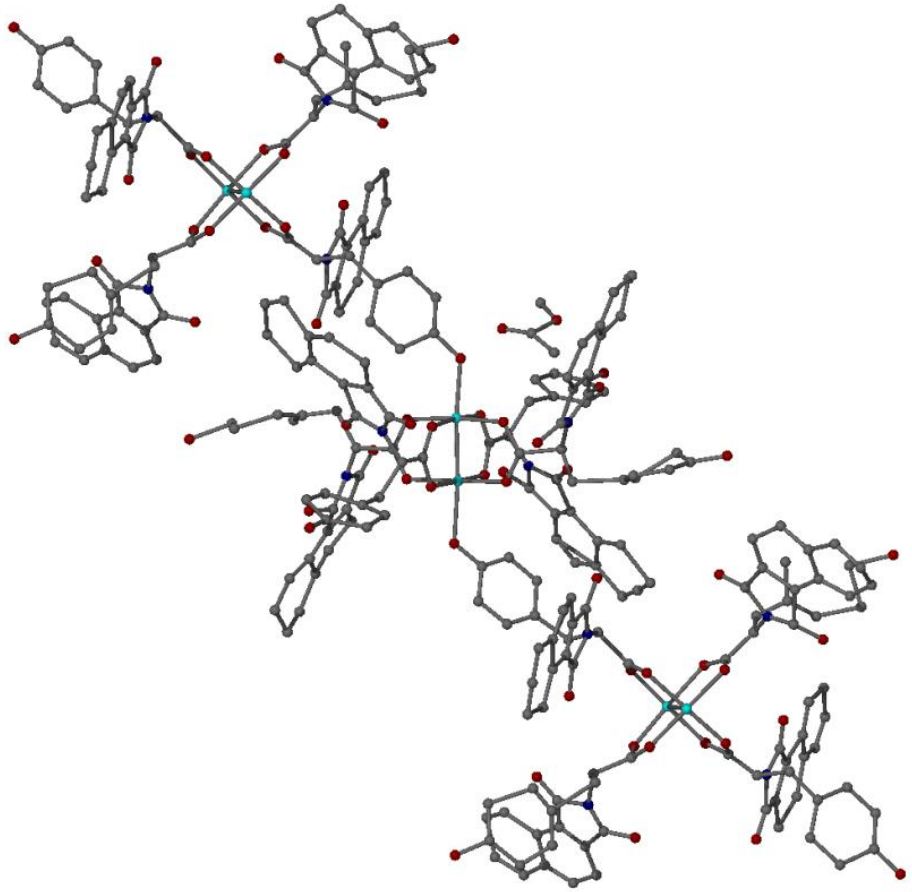

Figure S1. Molecular structure of polymeric Rh_2(*R*,*R*,*S*,*S*-1,2-NTTY)$_4$ (side view). As shown, not all ligand atoms could be located in the structure refinement.

The X-ray structure of a Rh_2(1,2-NTTY)$_4$ (**3e**) crystal grown from a complex prepared using the acetic acid ligands was obtained. The X-ray revealed a polymeric structure where some of the *p*-OH groups of the -$CH_2C_6H_4$-OH substituents of one complex molecule acts as the axial ligands on each Rh centre of adjacent complex molecules (Figure S1). The crystal was for the (*R*,*R*,*S*,*S*)-diastereomer. The catalyst is adopting the *α*,*α*,*β*,*β* conformation which is similar to the obtained structure of Rh_2(*S*-1,2-NTPA)$_4$ (**3b**) and agree with the proposed enantioinduction model discussed earlier in Chapter 2. The two (*S*)-ligands are together on one partial cavity face shrouding the axial site of a Rh-centre and the two (*R*)-ligands were similarly disposed on the other catalyst face.

Table S2 illustrates the results obtained for Rh_2(1,2-NTTY)$_4$-catalyzed cyclopropanations series of olefins with Meldrum's acid when using either

enantiomerically impure Rh_2(1,2-NTTY)$_4$ (from acetic acid) or relatively enantiomerically pure catalyst (from Tol/TEA or DMF ligands).

Table S2. Rh_2(1,2-NTTY)$_4$-catalyzed cyclopropanation of various olefins with Meldrum's acid.

Entry	R	Yield (%)	*ee* of cyclorpropane product (%)	
			Enantio-impure catalyst (Acetic acid) (*S*,*S*,*R*,*R*)-	Enantio-pure catalyst (Tol/TEA or DMF) (*S*,*S*,*S*,*S*)-
1	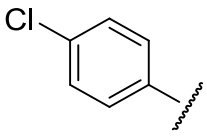	16	>1	14[a]
2	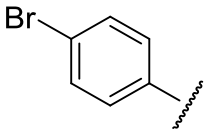	14	4	9[b]
3	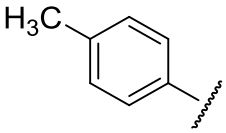	13	9	12[b]
4	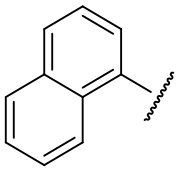	15	5	7[b]

[a]Analyzed as crude mixture, [b]Using DMF catalyst.

Crystal structure of $C_{18}H_{21}O_3P$ — uc1401

Frady Gouany,[a] Ashraf Ghanem[a] and Anthony C. Willis[b]*

[a]Biomedical Sciences, Faculty of Education, Science, Technology and Mathematics, Locked Bag 1, University of Canberra, A. C. T. 2601, Australia, and [b]Research School of Chemistry, Australian National University, Canberra, A. C. T. 0200, Australia

Correspondence email: willis@rsc.anu.edu.au

Abstract

The crystal structure of $C_{18}H_{21}O_3P$ is reported and the absolute configuration established.

1. Comment

The crystallographic asymmetric unit consists of one molecule of $C_{18}H_{21}O_3P$.

The compound is enantiomerically pure. Its absolute configuration has been determined by refinement of the Flack parameter and is in agreement with the configuration expected on the basis of the synthetic precursors. The final value of the Flack parameter is −0.03 (8) and the final value of the Hooft parameter is −0.04 (3).

2. Synthesis and crystallization

The compound was prepared by FG and was recrystallized from ethyl acetate / n-hexane. The sample ID is FGCy.

Related literature

Computing details

Data collection: *COLLECT* (Nonius, 2001).; cell refinement: *DENZO*/*SCALEPACK* (Otwinowski & Minor, 1997); data reduction: *DENZO*/*SCALEPACK* (Otwinowski & Minor, 1997); program(s) used to solve structure: *SIR92* (Altomare *et al.*, 1994); program(s) used to refine structure: *CRYSTALS* (Betteridge *et al.*, 2003); molecular graphics: *ORTEP*-II (Johnson 1976) in *TEXSAN* (MSC, 1992-1997); software used to prepare material for publication: *CRYSTALS* (Betteridge *et al.*, 2003).

Acknowledgements

References

Mackay, S., Gilmore, C. J., Edwards, C., Stewart, N. & Shankland, K. (2000). *maXus* Computer Program for the Solution and Refinement of Crystal Structures. Nonius, The Netherlands, MacScience, Japan & The University of Glasgow.

Coppens, P. (1970). *The Evaluation of Absorption and Extinction in Single-Crystal Structure Analysis. Crystallographic Computing. F. R. Ahmed, S. R. Hall and C.* P. Huber, eds., Munksgaard. Copenhagen. pp 255-270.

Altomare, A., Cascarano, G., Giacovazzo, G., Guagliardi, A., Burla, M. C., Polidori, G. & Camalli, M. (1994). J. Appl. Cryst. 27, 435.

Betteridge, P. W., Carruthers, J. R., Cooper, R. I., Prout, K. & Watkin, D. J. (2003). J. Appl. Cryst. 36, 1487.

Nonius (1997–2001). *COLLECT*. Nonius BV, Delft, The Netherlands.

Otwinowski, Z. & Minor, W. (1997). *Methods in Enzymology*, Vol. 276, edited by C. W. Carter Jr & R. M. Sweet, pp. 307–326. New York: Academic Press.

Molecular Structure Corporation. (1992–1997). *TEXSAN*. Single Crystal Structure Analysis Software. Version 1.8. MSC, 3200 Research Forest Drive, The Woodlands, TX 77381, USA.

Johnson, C. K. (1976). *ORTEP*II, A Fortran Thermal-Ellipsoid Plot Program, Report ORNL-5138, Oak Ridge National Laboratory, Oak Ridge, Tennessee, USA.

Flack, H. D. (1983). Acta Cryst. A39, 876-881.

Hooft, R. W. W., Straver, L. H. & Spek, A. L. (2008). J. Appl. Crystallogr., 41, 96-103.

(uc1401)

Crystal data

$C_{18}H_{21}O_3P$
M_r = 316.34
Orthorhombic, $P2_12_12_1$
Hall symbol: P 2ac 2ab
a = 6.6766 (1) Å
b = 15.6794 (3) Å
c = 16.3174 (3) Å
V = 1708.19 (5) Å^3
Z = 4
F(000) = 672
D_x = 1.230 Mg m^{-3}
Mo $K\alpha$ radiation, λ = 0.71073 Å
Cell parameters from 18470 reflections
θ = 3–27.5°
μ = 0.17 mm^{-1}
T = 200 K
Plate, colourless
0.30 × 0.26 × 0.09 mm

Data collection

Nonius KappaCCD diffractometer
Graphite monochromator
φ & ω scans
Absorption correction: integration via Gaussian method (Coppens, 1970) implemented in *maXus* (2000)
T_{min} = 0.956, T_{max} = 0.986
30661 measured reflections
3918 independent reflections
3605 reflections with $I > 2.0\sigma(I)$
R_{int} = 0.034
θ_{max} = 27.5°, θ_{min} = 2.6°
h = −8→8
k = −20→20
l = −21→19

Refinement

Refinement on F^2
Least-squares matrix: full
$R[F^2 > 2\sigma(F^2)]$ = 0.035
$wR(F^2)$ = 0.092
S = 1.00
3918 reflections
263 parameters
27 restraints
Primary atom site location: structure-invariant direct methods
Hydrogen site location: difference Fourier map
Only H-atom coordinates refined
Method = Modified Sheldrick $w = 1/[\sigma^2(F^2) + (0.06P)^2 + 0.24P]$, where $P = (\max(F_o^2,0) + 2F_c^2)/3$
$(\Delta/\sigma)_{max}$ = 0.014
$\Delta\rho_{max}$ = 0.15 e Å^{-3}
$\Delta\rho_{min}$ = −0.31 e Å^{-3}
Absolute structure: Flack (1983), 1661 Friedel-pairs
Absolute structure parameter: −0.03 (8)

Special details

Refinement

Hydrogen atoms were observed in a difference electron density map and included at calculated positions. They were initially refined with soft restraints on the bond lengths and angles to regularize their geometry (C—H in the range 0.93–0.98) and on U_{iso}(H) (in the range 1.2–1.5 times U_{eq} of the parent atom). Subsequently, H atom positional parameters were refined freely, but with restraints on distances and angles for the methyl groups, and the displacement parameters were held fixed.

The largest peaks in the final difference electron density map are located randomly through the structure.

Fractional atomic coordinates and isotropic or equivalent isotropic displacement parameters (Å^2)

	x	y	z	U_{iso}*/U_{eq}
P1	0.30617 (6)	0.23364 (2)	0.35647 (2)	0.0342
O1	0.2768 (2)	0.19601 (8)	0.43782 (8)	0.0470
O2	0.16110 (19)	0.20173 (7)	0.28739 (8)	0.0445
O3	0.51727 (18)	0.21496 (7)	0.31753 (8)	0.0422
C1	0.2676 (2)	0.34609 (9)	0.35308 (10)	0.0326

C2	0.1168 (3)	0.38110 (12)	0.41386 (11)	0.0405
C3	0.3352 (2)	0.39419 (10)	0.43124 (9)	0.0351
C4	0.2903 (2)	0.38671 (9)	0.27028 (9)	0.0329
C5	0.4791 (3)	0.40732 (12)	0.23995 (11)	0.0438
C6	0.5007 (4)	0.44330 (14)	0.16280 (11)	0.0545
C7	0.3341 (4)	0.45821 (13)	0.11454 (11)	0.0543
C8	0.1476 (3)	0.43693 (12)	0.14316 (12)	0.0527
C9	0.1247 (3)	0.40171 (11)	0.22105 (11)	0.0435
C10	0.4347 (2)	0.47914 (10)	0.42623 (9)	0.0343
C11	0.6262 (3)	0.48791 (11)	0.45888 (10)	0.0384
C12	0.7235 (3)	0.56648 (12)	0.45749 (11)	0.0454
C13	0.6336 (3)	0.63822 (11)	0.42400 (11)	0.0479
C14	0.4438 (3)	0.62879 (12)	0.39079 (13)	0.0517
C15	0.3459 (3)	0.55104 (11)	0.39183 (11)	0.0446
C16	0.7384 (5)	0.72345 (15)	0.42338 (16)	0.0727
C17	0.1383 (4)	0.11130 (13)	0.27304 (16)	0.0631
C18	0.6942 (3)	0.21563 (17)	0.36801 (16)	0.0665
H21	0.043 (3)	0.4296 (13)	0.3976 (13)	0.0459*
H22	0.039 (3)	0.3442 (12)	0.4522 (13)	0.0480*
H31	0.390 (3)	0.3567 (13)	0.4771 (12)	0.0430*
H51	0.594 (3)	0.4022 (13)	0.2716 (14)	0.0523*
H61	0.633 (4)	0.4576 (16)	0.1435 (15)	0.0653*
H71	0.351 (4)	0.4906 (15)	0.0582 (15)	0.0655*
H81	0.033 (4)	0.4449 (15)	0.1105 (15)	0.0641*
H91	−0.009 (4)	0.3880 (14)	0.2413 (13)	0.0492*
H111	0.690 (3)	0.4357 (12)	0.4848 (12)	0.0454*
H121	0.865 (4)	0.5749 (13)	0.4839 (13)	0.0530*
H141	0.386 (4)	0.6769 (15)	0.3674 (16)	0.0641*
H151	0.207 (3)	0.5498 (14)	0.3683 (13)	0.0541*
H161	0.687 (4)	0.7631 (14)	0.3823 (14)	0.1100*
H162	0.732 (4)	0.7533 (15)	0.4753 (12)	0.1103*
H163	0.878 (3)	0.7173 (14)	0.4079 (16)	0.1098*
H171	0.032 (3)	0.1046 (13)	0.2341 (13)	0.0939*
H172	0.099 (3)	0.0829 (13)	0.3241 (12)	0.0942*
H173	0.267 (3)	0.0860 (13)	0.2550 (14)	0.0936*
H181	0.812 (3)	0.2283 (16)	0.3324 (12)	0.1000*
H182	0.679 (3)	0.2556 (14)	0.4149 (13)	0.0996*
H183	0.714 (3)	0.1575 (12)	0.3914 (14)	0.0992*

Atomic displacement parameters (Å²)

	U^{11}	U^{22}	U^{33}	U^{12}	U^{13}	U^{23}
P1	0.03396 (18)	0.03164 (17)	0.03692 (19)	−0.00145 (15)	0.00160 (15)	0.00440 (16)
O1	0.0570 (7)	0.0398 (6)	0.0441 (7)	−0.0030 (5)	0.0067 (6)	0.0127 (5)
O2	0.0448 (6)	0.0347 (5)	0.0541 (7)	−0.0063 (5)	−0.0083 (6)	−0.0011 (5)
O3	0.0372 (6)	0.0441 (6)	0.0452 (6)	0.0061 (5)	0.0023 (5)	0.0010 (5)
C1	0.0312 (7)	0.0336 (7)	0.0330 (7)	−0.0009 (5)	0.0022 (6)	0.0021 (6)
C2	0.0366 (8)	0.0416 (9)	0.0432 (9)	0.0007 (7)	0.0103 (7)	0.0019 (7)
C3	0.0398 (8)	0.0347 (7)	0.0309 (7)	0.0003 (6)	0.0034 (6)	0.0025 (6)
C4	0.0385 (8)	0.0279 (6)	0.0325 (7)	0.0008 (6)	−0.0018 (6)	0.0009 (5)
C5	0.0429 (9)	0.0543 (10)	0.0343 (8)	−0.0093 (8)	−0.0014 (7)	0.0057 (7)
C6	0.0657 (12)	0.0609 (11)	0.0368 (9)	−0.0158 (10)	0.0068 (8)	0.0040 (8)
C7	0.0852 (14)	0.0462 (9)	0.0316 (8)	0.0085 (10)	0.0010 (9)	0.0052 (7)
C8	0.0672 (12)	0.0512 (10)	0.0396 (8)	0.0220 (9)	−0.0102 (9)	0.0005 (8)

C9	0.0436 (9)	0.0448 (9)	0.0422 (9)	0.0117 (7)	−0.0043 (7)	−0.0001 (7)
C10	0.0418 (8)	0.0335 (7)	0.0276 (7)	0.0019 (6)	0.0028 (6)	−0.0002 (6)
C11	0.0417 (8)	0.0404 (8)	0.0332 (7)	0.0020 (7)	0.0024 (6)	0.0015 (6)
C12	0.0508 (10)	0.0472 (9)	0.0383 (8)	−0.0085 (8)	0.0003 (7)	0.0005 (7)
C13	0.0651 (12)	0.0385 (8)	0.0400 (9)	−0.0089 (8)	0.0038 (8)	−0.0019 (7)
C14	0.0701 (13)	0.0352 (8)	0.0499 (10)	0.0022 (9)	−0.0046 (9)	0.0062 (8)
C15	0.0518 (10)	0.0382 (8)	0.0438 (8)	0.0035 (8)	−0.0067 (8)	0.0047 (7)
C16	0.0983 (19)	0.0491 (12)	0.0706 (14)	−0.0254 (12)	−0.0017 (13)	0.0003 (10)
C17	0.0731 (14)	0.0391 (9)	0.0769 (14)	−0.0113 (10)	−0.0062 (12)	−0.0092 (10)
C18	0.0368 (9)	0.0910 (16)	0.0716 (13)	0.0046 (10)	−0.0067 (10)	0.0018 (12)

Geometric parameters (Å, º)

P1—O1	1.4659 (12)	C8—H81	0.94 (3)
P1—O2	1.5681 (13)	C9—H91	0.98 (2)
P1—O3	1.5735 (12)	C10—C11	1.392 (2)
P1—C1	1.7827 (15)	C10—C15	1.392 (2)
O2—C17	1.445 (2)	C11—C12	1.393 (2)
O3—C18	1.440 (2)	C11—H111	1.01 (2)
C1—C2	1.516 (2)	C12—C13	1.387 (3)
C1—C3	1.549 (2)	C12—H121	1.05 (2)
C1—C4	1.501 (2)	C13—C14	1.387 (3)
C2—C3	1.499 (2)	C13—C16	1.508 (3)
C2—H21	0.94 (2)	C14—C15	1.383 (3)
C2—H22	1.00 (2)	C14—H141	0.93 (2)
C3—C10	1.491 (2)	C15—H151	1.00 (2)
C3—H31	1.02 (2)	C16—H161	0.977 (18)
C4—C5	1.392 (2)	C16—H162	0.969 (18)
C4—C9	1.387 (2)	C16—H163	0.968 (18)
C5—C6	1.387 (2)	C17—H171	0.956 (17)
C5—H51	0.93 (2)	C17—H172	0.980 (17)
C6—C7	1.383 (3)	C17—H173	0.991 (17)
C6—H61	0.97 (3)	C18—H181	0.996 (17)
C7—C8	1.371 (3)	C18—H182	0.994 (17)
C7—H71	1.06 (2)	C18—H183	0.998 (17)
C8—C9	1.394 (3)		
O1···C11^{i}	3.488 (2)	O2···C18^{iii}	3.391 (2)
O1···C18^{i}	3.502 (3)	O2···C16^{iv}	3.521 (3)
O1···C2^{ii}	3.532 (2)	C13···C17^{v}	3.583 (3)
O1—P1—O2	116.09 (8)	C9—C8—H81	118.8 (15)
O1—P1—O3	114.24 (7)	C8—C9—C4	120.54 (18)
O2—P1—O3	101.74 (7)	C8—C9—H91	119.7 (13)
O1—P1—C1	114.01 (8)	C4—C9—H91	119.8 (13)
O2—P1—C1	101.78 (7)	C3—C10—C11	118.46 (14)
O3—P1—C1	107.51 (6)	C3—C10—C15	123.78 (15)
P1—O2—C17	119.64 (13)	C11—C10—C15	117.75 (15)
P1—O3—C18	120.15 (12)	C10—C11—C12	120.64 (16)
P1—C1—C2	115.70 (11)	C10—C11—H111	117.6 (12)
P1—C1—C3	114.46 (11)	C12—C11—H111	121.8 (12)
C2—C1—C3	58.56 (11)	C11—C12—C13	121.45 (17)
P1—C1—C4	115.65 (11)	C11—C12—H121	121.8 (12)
C2—C1—C4	120.13 (13)	C13—C12—H121	116.7 (12)

C3—C1—C4	120.34 (12)	C12—C13—C14	117.58 (17)
C1—C2—C3	61.80 (10)	C12—C13—C16	121.4 (2)
C1—C2—H21	117.0 (13)	C14—C13—C16	121.06 (19)
C3—C2—H21	116.7 (12)	C13—C14—C15	121.41 (18)
C1—C2—H22	123.1 (11)	C13—C14—H141	117.0 (15)
C3—C2—H22	117.9 (12)	C15—C14—H141	121.6 (15)
H21—C2—H22	111.9 (17)	C10—C15—C14	121.16 (18)
C1—C3—C2	59.64 (10)	C10—C15—H151	122.2 (12)
C1—C3—C10	121.31 (13)	C14—C15—H151	116.7 (12)
C2—C3—C10	123.04 (15)	C13—C16—H161	113.9 (13)
C1—C3—H31	115.4 (11)	C13—C16—H162	113.8 (14)
C2—C3—H31	114.2 (11)	H161—C16—H162	106.1 (15)
C10—C3—H31	113.3 (11)	C13—C16—H163	111.0 (13)
C1—C4—C5	120.64 (14)	H161—C16—H163	102.8 (16)
C1—C4—C9	120.86 (14)	H162—C16—H163	108.5 (15)
C5—C4—C9	118.46 (14)	O2—C17—H171	107.0 (13)
C4—C5—C6	120.73 (18)	O2—C17—H172	109.6 (13)
C4—C5—H51	122.1 (13)	H171—C17—H172	108.5 (15)
C6—C5—H51	117.0 (13)	O2—C17—H173	110.4 (13)
C5—C6—C7	120.1 (2)	H171—C17—H173	113.6 (15)
C5—C6—H61	119.0 (15)	H172—C17—H173	107.6 (15)
C7—C6—H61	120.8 (14)	O3—C18—H181	108.3 (13)
C6—C7—C8	119.70 (16)	O3—C18—H182	111.3 (13)
C6—C7—H71	119.5 (14)	H181—C18—H182	113.8 (15)
C8—C7—H71	120.6 (14)	O3—C18—H183	108.8 (13)
C7—C8—C9	120.41 (18)	H181—C18—H183	107.4 (15)
C7—C8—H81	120.8 (15)	H182—C18—H183	107.1 (15)

P1—C1—C2—C3	104.1 (1)	C2—C1—C4—C5	131.6 (2)
P1—C1—C3—C2	−106.3 (1)	C2—C1—C4—C9	−50.8 (2)
P1—C1—C3—C10	141.2 (1)	C2—C3—C1—C4	108.9 (1)
P1—C1—C4—C5	−81.8 (2)	C2—C3—C10—C11	167.4 (2)
P1—C1—C4—C9	95.9 (2)	C2—C3—C10—C15	−11.5 (2)
O1—P1—O2—C17	−52.1 (2)	C3—C1—C4—C5	62.6 (2)
O1—P1—O3—C18	−39.1 (2)	C3—C1—C4—C9	−119.8 (2)
O1—P1—C1—C2	−30.1 (1)	C3—C2—C1—C4	−109.2 (1)
O1—P1—C1—C3	35.2 (1)	C3—C10—C11—C12	−178.4 (2)
O1—P1—C1—C4	−178.3 (1)	C3—C10—C15—C14	178.3 (2)
O2—P1—O3—C18	−165.0 (1)	C4—C1—C3—C10	−3.6 (2)
O2—P1—C1—C2	95.7 (1)	C4—C5—C6—C7	−0.8 (3)
O2—P1—C1—C3	161.0 (1)	C4—C9—C8—C7	−0.8 (3)
O2—P1—C1—C4	−52.5 (1)	C5—C4—C9—C8	−0.2 (2)
O3—P1—O2—C17	72.6 (2)	C5—C6—C7—C8	−0.3 (3)
O3—P1—C1—C2	−157.8 (1)	C6—C5—C4—C9	1.0 (3)
O3—P1—C1—C3	−92.5 (1)	C6—C7—C8—C9	1.1 (3)
O3—P1—C1—C4	54.0 (1)	C10—C11—C12—C13	0.2 (3)
C1—P1—O2—C17	−176.5 (2)	C10—C15—C14—C13	−0.1 (3)
C1—P1—O3—C18	88.5 (2)	C11—C10—C15—C14	−0.6 (3)
C1—C2—C3—C10	109.7 (2)	C11—C12—C13—C14	−0.9 (3)
C1—C3—C10—C11	−120.7 (2)	C11—C12—C13—C16	179.3 (2)
C1—C3—C10—C15	60.4 (2)	C12—C11—C10—C15	0.6 (2)
C1—C4—C5—C6	178.7 (2)	C12—C13—C14—C15	0.8 (3)

C1—C4—C9—C8	−177.9 (2)	C15—C14—C13—C16	−179.4 (2)
C2—C1—C3—C10	−112.5 (2)		

Symmetry codes: (i) $x-1/2, -y+1/2, -z+1$; (ii) $x+1/2, -y+1/2, -z+1$; (iii) $x-1, y, z$; (iv) $-x+1, y-1/2, -z+1/2$; (v) $-x+1, y+1/2, -z+1/2$.

Crystal structure of $C_{16}H_{13}F_3$ — uc1402SN

Frady Gouany,[a] Ashraf Ghanem[a] and Anthony C. Willis[b]*

[a]Biomedical Sciences, Faculty of Education, Science, Technology and Mathematics, Locked Bag 1, University of Canberra, A. C. T. 2601, Australia, and [b]Research School of Chemistry, Australian National University, Canberra, A. C. T. 0200, Australia

Correspondence email: willis@rsc.anu.edu.au

Abstract

The crystal structure of $C_{16}H_{13}F_3$ is reported and the absolute configuration established.

1. Comment

The crystallographic asymmetric unit consists of one molecule of $C_{16}H_{13}F_3$.

The compound is enantiomerically pure. Its absolute configuration has been determined by refinement of the Flack parameter and is in agreement with the configuration expected on the basis of the synthetic precursors. The final value of the Flack parameter is −0.14 (18) and the final value of the Hooft parameter is −0.33 (13).

2. Synthesis and crystallization

The compound was prepared by FG and was recrystallized from 2-propanol. The sample ID is CyCF3.

Related literature

Computing details

Data collection: *CrysAlis PRO*, Agilent Technologies, Version 1.171.37.21t (release 24-10-2013 CrysAlis171 .NET) (compiled Oct 24 2013,16:12:21); cell refinement: *CrysAlis PRO*; data reduction: *CrysAlis PRO*; program(s) used to solve structure: *SIR92* (Altomare *et al.*, 1994); program(s) used to refine structure: *CRYSTALS* (Betteridge *et al.*, 2003); molecular graphics: *PLATON* (Spek, 2008); software used to prepare material for publication: *CRYSTALS* (Betteridge *et al.*, 2003).

Acknowledgements

References

Altomare, A., Cascarano, G., Giacovazzo, G., Guagliardi, A., Burla, M. C., Polidori, G. & Camalli, M. (1994). J. Appl. Cryst. 27, 435.

Betteridge, P. W., Carruthers, J. R., Cooper, R. I., Prout, K. & Watkin, D. J. (2003). J. Appl. Cryst. 36, 1487.

Flack, H. D. (1983). Acta Cryst. A39, 876-881.

Hooft, R. W. W., Straver, L. H. & Spek, A. L. (2008). J. Appl. Crystallogr., 41, 96-103.

CrysAlis PRO, Agilent Technologies, Version 1.171.37.21t (release 24-10-2013 CrysAlis171 .NET) (compiled Oct 24 2013,16:12:21)

Spek, A. L. (2008). *PLATON*, A Multipurpose Crystallographic Tool, Utrecht University, Utrecht, The Netherlands.

(uc1402SN)

Crystal data

$C_{16}H_{13}F_3$
M_r = 262.27
Monoclinic, $P2_1$
Hall symbol: P 2yb
a = 9.2411 (3) Å
b = 5.7885 (2) Å
c = 12.0746 (5) Å
β = 94.319 (3)°
V = 644.06 (4) Å^3
Z = 2
$F(000)$ = 272
D_x = 1.352 Mg m^{-3}
Cu $K\alpha$ radiation, λ = 1.54180 Å
Cell parameters from 8024 reflections
θ = 4–72°
μ = 0.91 mm^{-1}
T = 150 K
Block, colourless
0.44 × 0.31 × 0.20 mm

Data collection

SuperNova, Dual, Cu at zero, Sapphire3 diffractometer
Mirror monochromator
ω scans
Absorption correction: multi-scan *CrysAlis PRO*, Agilent Technologies, Version 1.171.37.21t (release 24-10-2013 CrysAlis171 .NET) (compiled Oct 24 2013,16:12:21) Empirical absorption correction using spherical harmonics, implemented in SCALE3 ABSPACK scaling algorithm.
T_{min} = 0.55, T_{max} = 0.83
11761 measured reflections
2538 independent reflections
2502 reflections with $I > 2.0\sigma(I)$
R_{int} = 0.066
θ_{max} = 72.6°, θ_{min} = 3.7°
$h = -11 \rightarrow 11$
$k = -7 \rightarrow 7$
$l = -14 \rightarrow 14$

Refinement

Refinement on F^2
Least-squares matrix: full
$R[F^2 > 2\sigma(F^2)]$ = 0.081
$wR(F^2)$ = 0.201
S = 1.02
2530 reflections
173 parameters
1 restraint
Primary atom site location: structure-invariant direct methods
Hydrogen site location: difference Fourier map
H-atom parameters constrained
Method = Modified Sheldrick $w = 1/[\sigma^2(F^2) + (0.19P)^2 + 0.03P]$, where $P = (\max(F_o^2,0) + 2F_c^2)/3$
$(\Delta/\sigma)_{max}$ = 0.010
$\Delta\rho_{max}$ = 1.01 e Å^{-3}
$\Delta\rho_{min}$ = −0.41 e Å^{-3}
Absolute structure: Flack (1983), 1128 Friedel-pairs
Absolute structure parameter: −0.14 (18)

Special details

Refinement
Data were not of high quality and several outlier reflections needed to be removed from the refinement.
Hydrogen atoms were included at calculated positions and ride on the atoms to which they are bonded.
The largest peaks in the final difference electron density map are generally located midway between atoms.

Fractional atomic coordinates and isotropic or equivalent isotropic displacement parameters (Å^2)

	x	y	z	U_{iso}*/U_{eq}
F1	0.85512 (14)	0.7626 (3)	0.11129 (13)	0.0376
F2	0.88252 (17)	0.4472 (4)	0.02260 (13)	0.0481
F3	1.04708 (14)	0.5616 (4)	0.14599 (15)	0.0491
C1	0.8295 (2)	0.4156 (4)	0.20965 (19)	0.0265
C2	0.9135 (3)	0.2207 (5)	0.2667 (2)	0.0346
C3	0.8968 (2)	0.4439 (4)	0.32937 (19)	0.0280
C4	0.6684 (2)	0.3921 (4)	0.18415 (17)	0.0231
C5	0.5736 (2)	0.5672 (4)	0.21135 (19)	0.0251
C6	0.4259 (2)	0.5462 (4)	0.18274 (18)	0.0268
C7	0.3719 (2)	0.3533 (5)	0.12518 (18)	0.0271
C8	0.4654 (2)	0.1786 (4)	0.0971 (2)	0.0278

C9	0.6133 (2)	0.1990 (4)	0.12721 (19)	0.0269
C10	0.8072 (2)	0.4646 (4)	0.42591 (19)	0.0277
C11	0.8228 (2)	0.6633 (4)	0.4914 (2)	0.0296
C12	0.7431 (2)	0.6934 (5)	0.5835 (2)	0.0315
C13	0.6467 (2)	0.5249 (5)	0.61196 (19)	0.0329
C14	0.6297 (3)	0.3273 (5)	0.5475 (2)	0.0354
C15	0.7098 (3)	0.2979 (4)	0.45513 (19)	0.0329
C16	0.9048 (2)	0.5472 (5)	0.1238 (2)	0.0311
H21	1.0057	0.1788	0.2430	0.0415*
H22	0.8640	0.0860	0.2880	0.0415*
H31	0.9820	0.5364	0.3352	0.0336*
H51	0.6101	0.7009	0.2495	0.0302*
H61	0.3614	0.6644	0.2027	0.0323*
H71	0.2709	0.3408	0.1049	0.0326*
H81	0.4288	0.0463	0.0578	0.0333*
H91	0.6774	0.0792	0.1085	0.0323*
H111	0.8889	0.7800	0.4725	0.0355*
H121	0.7551	0.8298	0.6270	0.0379*
H131	0.5925	0.5443	0.6751	0.0395*
H141	0.5631	0.2112	0.5662	0.0425*
H151	0.6974	0.1615	0.4117	0.0396*

Atomic displacement parameters (Å²)

	U^{11}	U^{22}	U^{33}	U^{12}	U^{13}	U^{23}
F1	0.0387 (8)	0.0402 (8)	0.0355 (9)	0.0084 (6)	0.0124 (6)	0.0065 (7)
F2	0.0627 (10)	0.0651 (12)	0.0184 (8)	0.0035 (9)	0.0143 (6)	−0.0093 (8)
F3	0.0292 (7)	0.0746 (13)	0.0444 (10)	0.0106 (8)	0.0090 (6)	0.0093 (10)
C1	0.0285 (10)	0.0342 (12)	0.0162 (11)	0.0092 (9)	−0.0010 (8)	−0.0010 (9)
C2	0.0373 (11)	0.0400 (14)	0.0253 (12)	0.0155 (10)	−0.0046 (9)	−0.0017 (11)
C3	0.0278 (10)	0.0379 (12)	0.0173 (11)	0.0035 (9)	−0.0048 (8)	−0.0020 (9)
C4	0.0291 (10)	0.0300 (11)	0.0099 (10)	0.0065 (8)	−0.0007 (7)	0.0002 (8)
C5	0.0328 (10)	0.0275 (10)	0.0148 (10)	0.0050 (9)	0.0007 (8)	−0.0035 (8)
C6	0.0342 (11)	0.0308 (11)	0.0160 (11)	0.0102 (9)	0.0044 (8)	0.0002 (8)
C7	0.0276 (9)	0.0400 (12)	0.0137 (10)	−0.0007 (9)	0.0007 (8)	0.0011 (9)
C8	0.0378 (12)	0.0308 (11)	0.0143 (11)	0.0007 (9)	−0.0005 (8)	−0.0005 (8)
C9	0.0356 (11)	0.0297 (11)	0.0153 (11)	0.0096 (9)	0.0016 (8)	−0.0020 (8)
C10	0.0304 (10)	0.0348 (12)	0.0162 (11)	0.0048 (9)	−0.0086 (8)	−0.0008 (9)
C11	0.0316 (11)	0.0345 (12)	0.0214 (12)	−0.0016 (9)	−0.0059 (9)	−0.0019 (9)
C12	0.0371 (12)	0.0406 (13)	0.0159 (11)	0.0023 (10)	−0.0045 (8)	−0.0078 (9)
C13	0.0412 (12)	0.0437 (14)	0.0131 (12)	0.0041 (10)	−0.0032 (9)	0.0004 (10)
C14	0.0461 (13)	0.0394 (13)	0.0200 (12)	−0.0070 (11)	−0.0018 (10)	0.0028 (10)
C15	0.0484 (13)	0.0327 (12)	0.0168 (12)	−0.0038 (10)	−0.0040 (9)	−0.0008 (9)
C16	0.0315 (11)	0.0414 (13)	0.0208 (12)	0.0099 (10)	0.0052 (8)	−0.0026 (10)

Geometric parameters (Å, º)

F1—C16	1.334 (3)	C6—H61	0.950
F2—C16	1.354 (3)	C7—C8	1.388 (4)
F3—C16	1.324 (2)	C7—H71	0.950
C1—C2	1.506 (3)	C8—C9	1.393 (3)
C1—C3	1.539 (3)	C8—H81	0.950
C1—C4	1.504 (3)	C9—H91	0.950
C1—C16	1.499 (3)	C10—C11	1.397 (3)

C2—C3	1.511 (4)	C10—C15	1.383 (3)
C2—H21	0.950	C11—C12	1.390 (4)
C2—H22	0.950	C11—H111	0.950
C3—C10	1.485 (3)	C12—C13	1.382 (4)
C3—H31	0.950	C12—H121	0.950
C4—C5	1.395 (3)	C13—C14	1.386 (4)
C4—C9	1.389 (3)	C13—H131	0.950
C5—C6	1.388 (3)	C14—C15	1.394 (4)
C5—H51	0.950	C14—H141	0.950
C6—C7	1.388 (3)	C15—H151	0.950

F1···C2^{i}	3.270 (3)	C5···F1	3.159 (2)
F1···C5	3.159 (2)	C5···C10	3.299 (3)
F2···C9	3.213 (3)	C7···F3^{vii}	3.262 (3)
F2···F3^{ii}	3.122 (3)	C9···F2	3.213 (3)
F3···F2^{iii}	3.122 (3)	C10···C5	3.299 (3)
F3···C7^{iv}	3.262 (3)	C12···C2^{viii}	3.536 (3)
C2···F1^{v}	3.270 (3)	C13···C14^{ix}	3.543 (4)
C2···C12^{vi}	3.536 (3)	C14···C13^{x}	3.543 (4)
C4···C15	3.311 (3)	C15···C5	3.482 (3)
C5···C15	3.482 (3)	C15···C4	3.311 (3)

C2—C1—C3	59.50 (15)	C7—C8—C9	119.4 (2)
C2—C1—C4	119.6 (2)	C7—C8—H81	120.3
C3—C1—C4	121.72 (18)	C9—C8—H81	120.3
C2—C1—C16	116.52 (19)	C8—C9—C4	120.9 (2)
C3—C1—C16	114.8 (2)	C8—C9—H91	119.6
C4—C1—C16	114.11 (18)	C4—C9—H91	119.6
C1—C2—C3	61.33 (16)	C3—C10—C11	118.1 (2)
C1—C2—H21	119.8	C3—C10—C15	123.8 (2)
C3—C2—H21	119.8	C11—C10—C15	118.1 (2)
C1—C2—H22	119.8	C10—C11—C12	121.2 (2)
C3—C2—H22	119.8	C10—C11—H111	119.4
H21—C2—H22	109.5	C12—C11—H111	119.4
C1—C3—C2	59.18 (15)	C11—C12—C13	120.0 (2)
C1—C3—C10	122.41 (18)	C11—C12—H121	120.0
C2—C3—C10	123.1 (2)	C13—C12—H121	120.0
C1—C3—H31	113.8	C12—C13—C14	119.4 (2)
C2—C3—H31	113.8	C12—C13—H131	120.3
C10—C3—H31	113.8	C14—C13—H131	120.3
C1—C4—C5	121.06 (19)	C13—C14—C15	120.4 (2)
C1—C4—C9	119.63 (18)	C13—C14—H141	119.8
C5—C4—C9	119.21 (18)	C15—C14—H141	119.8
C4—C5—C6	120.09 (19)	C14—C15—C10	120.9 (2)
C4—C5—H51	120.0	C14—C15—H151	119.6
C6—C5—H51	119.9	C10—C15—H151	119.5
C5—C6—C7	120.30 (19)	C1—C16—F2	111.1 (2)
C5—C6—H61	119.9	C1—C16—F1	112.29 (19)
C7—C6—H61	119.8	F2—C16—F1	105.7 (2)
C6—C7—C8	120.09 (18)	C1—C16—F3	113.4 (2)
C6—C7—H71	120.0	F2—C16—F3	106.93 (19)
C8—C7—H71	119.9	F1—C16—F3	107.0 (2)

C4—C1—C2—C3	−111.5 (2)	C1—C2—C3—C10	110.9 (2)

C16—C1—C2—C3	104.5 (2)	C1—C3—C10—C11	−121.0 (2)
C2—C1—C3—C10	−112.0 (3)	C1—C3—C10—C15	59.4 (3)
C4—C1—C3—C2	108.1 (2)	C2—C3—C10—C11	167.0 (2)
C4—C1—C3—C10	−4.0 (3)	C2—C3—C10—C15	−12.6 (3)
C16—C1—C3—C2	−107.4 (2)	C1—C4—C5—C6	177.2 (2)
C16—C1—C3—C10	140.6 (2)	C9—C4—C5—C6	0.8 (3)
C2—C1—C4—C5	131.4 (2)	C1—C4—C9—C8	−176.4 (2)
C2—C1—C4—C9	−52.1 (3)	C5—C4—C9—C8	0.1 (3)
C3—C1—C4—C5	61.0 (3)	C4—C5—C6—C7	−1.2 (3)
C3—C1—C4—C9	−122.6 (2)	C5—C6—C7—C8	0.8 (3)
C16—C1—C4—C5	−83.8 (3)	C6—C7—C8—C9	0.0 (3)
C16—C1—C4—C9	92.7 (3)	C7—C8—C9—C4	−0.4 (3)
C2—C1—C16—F1	−154.0 (2)	C3—C10—C11—C12	−179.6 (2)
C2—C1—C16—F2	87.9 (2)	C15—C10—C11—C12	0.1 (3)
C2—C1—C16—F3	−32.5 (3)	C3—C10—C15—C14	179.5 (2)
C3—C1—C16—F1	−87.2 (2)	C11—C10—C15—C14	−0.1 (3)
C3—C1—C16—F2	154.70 (19)	C10—C11—C12—C13	0.2 (3)
C3—C1—C16—F3	34.3 (3)	C11—C12—C13—C14	−0.5 (3)
C4—C1—C16—F1	60.1 (3)	C12—C13—C14—C15	0.4 (4)
C4—C1—C16—F2	−58.0 (3)	C13—C14—C15—C10	−0.1 (4)
C4—C1—C16—F3	−178.4 (2)		

Symmetry codes: (i) *x*, *y*+1, *z*; (ii) −*x*+2, *y*−1/2, −*z*; (iii) −*x*+2, *y*+1/2, −*z*; (iv) *x*+1, *y*, *z*; (v) *x*, *y*−1, *z*; (vi) −*x*+2, *y*−1/2, −*z*+1; (vii) *x*−1, *y*, *z*; (viii) −*x*+2, *y*+1/2, −*z*+1; (ix) −*x*+1, *y*+1/2, −*z*+1; (x) −*x*+1, *y*−1/2, −*z*+1.